UNIVERSITY OF MINNESOTA
ST. ANTHONY FALLS HYDRAULIC LABORATORY

Project Report No. 318

MIXING OF TEMPERATURE-STRATIFIED LAKES, RESERVOIRS OR PONDS BY SUBMERGED JETS

by

Ruochuan Gu and Heinz G. Stefan

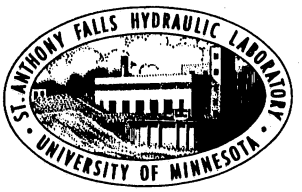

Prepared for

LEGISLATIVE COMMISSION ON MINNESOTA RESOURCES
State of Minnesota
St. Paul, Minnesota

July 1991

Minneapolis, Minnesota

ABSTRACT

In water quality management and environmental protection of lakes or reservoirs, techniques such as artificial destratification and aeration for water quality improvement and fishkill prevention are used with increasing frequency. The disposal of waste water and heat are major problems in environmental engineering. In both cases the interaction of jet flows and weakly density–stratified ambients including the mixing is currently not well understood and difficult to predict. In this study 1–D and 2–D numerical simulation models and laboratory measurements are employed to provide information on jet flows and mixing in density–stratified waters. Flow and thermal fields and their evolution are simulated. Jet trajectories are predicted and analyzed especially in low temperature water where strong nonlinearity between water density and temperature exists. Mixing processes which result in destratification and dilution are simulated and analyzed.

Laboratory experiments are designed and conducted to observe and measure the basic features of buoyant water jet flows and mixing in a stratified basin. Experiments are conducted with different initial conditions and governing parameters. Data of temperature profiles are analyzed and used to verify the 1–D jet–mixing model.

The one–dimensional numerical simulation model is developed to describe the gross behavior of jet flows and mixing. The integral 1–D model is incorporated into an existing multi–purpose dynamic lake water quality model (MINLAKE) for practical application. This incorporation makes it possible to evaluate effects of jet flows on mixing and water quality of aquatic environments. The temperature submodel in MINLAKE is also extended to winter conditions so that a warm water discharge into an ice–covered lake can be investigated. The model developed for winter predicts the growth and decay of ice and snow covers and thermal structures of a lake in a cold climate. Based on numerical analysis and experimental data, information on design and operation of artificial mixing (destratification) devices is also provided.

Details of flow fields, which would be too complicated to measure in the laboratory and are omitted in the 1–D simulation model, are studied in a two–dimensional numerical simulation model. The Reynolds equations are solved with a buoyancy–extended k–ϵ turbulence model as a closure. The flow and thermal fields are modeled as an unsteady phenomenon. The 2–D model is verified against existing data for a vertical jet impinging on a plate and data for offset jets. This 2–D model is applied to simulate the details of flow and mixing of a warm water discharges into a cold lake with ice cover. Buoyancy reversal results in dramatic changes in jet flow behavior.

ACKNOWLEDGEMENTS

Special thanks are expressed to those who have provided information, constructive comments and field data, especially C. Ellis and M. Riley. T. Johnson assisted in carrying out the laboratory experiments. Laboratory studies were supported by grants from the Legislative Commission on Minnesota Resources. The numerical computation was made possible by grants from the Minnesota Supercomputer Institute and the Computer Center, University of Minnesota.

TABLE OF CONTENTS

LIST OF TABLES

LIST OF FIGURES

List of symbols:

A	area
A_b	lake bottom area
b	measure of half width of the jet
B	buoyancy flux
b_l	lake specific coefficient
B_r	Bowen's ratio
c	heat capacity
C	concentration
c_b	heat capacity of sediment
C_M	concentration in jet at the maximum centerline rise
C_N	minimum value of N at which K_{max} occurs
C_p	specific heat of water
d	depth from the surface
D	jet diameter
D_j	jet diameter at the origin
D_o	discharge jet diameter
E	entrainment rate
ΔE	increase in potential energy
Fr	densimetric Froude number
Fr_c	critical densimetric Froude number for surface overshooting
Fr_L	system Froude number
g	acceleration of gravity
h	enthalpy
H	distance between discharge and water surface
H_e	depth of the region below diffuser
H_i	thickness of spreading layer of a surface impinging jet
H_q	$= H - H_i$
h_a	turbulent convective heat transfer coefficient

h_{ia}	bulk heat transfer coefficient (ice/air interface)
h_{sa}	bulk heat transfer coefficient (snow/air interface)
I_g	total groundwater inflow
k	thermal conductivity
k_φ	diffusivity for temperature or concentration
K	thermal diffusivity
K_m	molecular diffusivity
K_{max}	maximum hypolimnetic diffusivity
L	distance between the jet discharge and withdrawal
ℓ_b	characteristic length scale
ℓ_Q	characteristic length scale
ℓ_M	characteristic length scale
ℓ_m	Characteristic length scale
ℓ'_b	characteristic length scale
m	percent mixed
M	momentum flux
N	Brunt–Vaisala buoyancy frequency
p	pressure
P	power of jet
p_d	dynamic pressure
p_h	hydrostatic pressure
Pr	Prandtle number
q	entrainment flow rate from an individual layer
q_e	transport flow rate per unit depth
Q	discharge, volume flux
Q_a	convective heat transfer rate
Q_e	entrainment flow rate
Q_g	heat transfer rate from groundwater
Q_{ia}	heat transfer rate through the ice/air interface
Q_j	jet discharge flowrate at the origin
Q_p	flowrate of interflow
Q_{rl}	heat flux due to longwave radiation
Q_{sa}	heat transfer rate through the snow/air interface

Q_{sw}	sensible heat supplied from sediment to lake water
Q_t	total volume flux, $Q_e + Q_j$
Q_{wi}	heat flux from water to ice
r	radial coordinate, distance from jet centerline
R	net solar radiation
R_a	net absorbed solar radiation
Re	Reynolds number
Ri	Richardson number
Ri_l	local Richardson number
Ri_o	discharge Richardson number
R_{iw}	solar radiation penetrating into the lake water
R_s	total incoming solar radiation reaching lake surface
s	streamwise coordinate, distance along the jet axis
S	heat source or sink per unit volume
Sc	Schmidt number
S_M	dilution = C_o/C_M
St	stratification number
t	time
T	temperature
T_1	mean annual temperature of hypolimnetic water
T_a	air temperature
T_b	water temperature at lake bottom
T_i	temperature at the top of ice layer
T_j	jet discharge temperature
T_m	temperature at the bottom of ice layer
T_p	temperature of interflow
T_s	temperature at the top of snow layer
t*	dimensionless time = $t \frac{Q}{V}$
ΔT	temperature difference
U	mean velocity in x direction
U_j	jet velocity at the origin
U'	velocity fluctuation
u	component of velocity in x direction

u'	velocity fluctuation
u_e	entrainment velocity
u_m	centerline velocity of the jet
v	component of velocity in y direction
v'	velocity fluctuation
V	volume
v_{eb}	entrainment velocity at interface near injection
v_w	wind velocity
V_t	total volume of a basin
ΔV	volume of control volume
W	mean longitudinal velocity component
W_f	wind function
W_o	discharge jet width
x	coordinate
y	coordinate
z	vertical coordinate, depth
z^*	dimensionless vertical coordinate = z/L
z_m	elevation of jet centerline where $u_m = 0$
z_n	elevation of jet centerline where $\Delta T_m = 0$
z_t	top of the jet = $z_m + b$

Greek symbols:

α	entrainment coefficient
α_e	effective diffusivity, $\mu_t/\sigma_t + k_\varphi$
β	surface reflectivity (albedo)
β_e	thermal coefficient of volumetric expansion
Γ_ϕ	generalized diffusion coefficient
δ	thickness of withdrawal layer
δ_i	ice thickness
δ_s	snow thickness
ϵ	turbulent energy dissipation
η	efficiency of a destratification system

θ	angle between jet centerline and horizontal
θ_o	discharge angle, θ at s = 0
κ	turbulent kinetic energy
λ	dispersion ratio
μ	dynamic viscosity
μ_e	effective viscosity, $\mu + \mu_t$
μ_t	eddy (turbulent) viscosity
ν	kinematic viscosity
ρ	density
$\Delta\rho$	density difference
σ	standard deviation
σ_t	turbulent Prandtle number
τ	shear stress
ϕ	angle coordinate (chapter 3)
ϕ	generalized dependent variable, u, v, T, C, k, ϵ
φ	temperature or concentration

Subscripts

$( )_a$	ambient value
$( )_b$	sediment (chapter 5)
$( )_i$	ice (chapter 5)
$( )_j$	jet
$( )_m$	at the jet centerline (chapter 3)
$( )_o$	at the jet origin
$( )_p$	plume (chapter 3)
$( )_r$	round (chapter 3); rainfall (chapter 5); reference (chapter 8)
$( )_s$	slot (chapter 3); snow (chapter 5)
$( )_w$	water (chapter 5)

Chapter 1 Introduction

1.1 Buoyant jets in stratified basins

In the area of water quality management and environmental protection of lakes or reservoirs, techniques such as summer artificial destratification (Fig. 1.1b) and winter aeration (Fig. 1.1d) for water quality improvement and fishkill prevention are used with increased frequency. Buoyant jet flows and their mixing effects are also involved in the disposal of waste water and heat from power plants in summer or winter (Fig. 1.1a, Fig. 1.1c and Fig. 1.1e). In addition, impingement of waste water jet discharge on boundaries and the melting of ice covers induced by jet flows are of practical interest (Fig. 1.1f).

Thermal density stratification occurs in most lakes or reservoirs as a result of heating and wind mixing of surface water. A general deterioration of water quality is often associated with this stratification (Price, 1989; Burns and Powling, 1981; Henderson–Seller, 1984). Artificially forced vertical mixing has been shown to be an efficient and economic technique to improve water quality in a lake or reservoir by eliminating the thermal summer stratification (Burns and Powling, 1981). Mixing of stratified water basins by jets is a common practice to improve water quality but based primarily on years of trial–and–error experience rather than a clear understanding of underlying physical processes and mechanism (Irwin, et al, 1966; Dortch, 1979). As shown in Fig. 1.1 the hydraulic destratification system, i.e. a mechanical recirculating pump system, withdraws water from one elevation in the basin and discharges it vertically or horizontally at another elevation in the form of a buoyant jet to producing mixing of water at various levels.

The most common method for the disposal of waste water and heat during summer or winter is to discharge it horizontally into a large ambient body of water such as a lake or reservoir (Margeta, et al, 1990; Lee, 1980; Lee and Jirka, 1981). The outfalls may be designed as a single port outlet or a multi–port pipeline diffuser (Hino, et al, 1975). A multi–port disposal system is one practical method of producing a plane jet. A series of equally spaced identical, axisymmetric (round) jets are aligned along an axis with each jet issuing into a common plane. At a sufficient distance downstream of the multi–port nozzles, their discharges blend to form a plane jet (Blevins, 1984). It was found (Blevins, 1984) that the axial distance from the multi–port nozzle exit required for nearly uniform merging of the nozzle discharges was in the range of 40 to 60 nozzle radii.

Stabilization ponds are an economical and efficient method of waste treatment in small communities (Luck and Stefan, 1990). Wastewater is pumped underground through a pipe and discharged vertically into a pond. The jet may overshoot the water surface of a shallow pond and collapse or impinge on the surface. This is a special case of a submerged jet and a practical example of a vertical jet in shallow water.

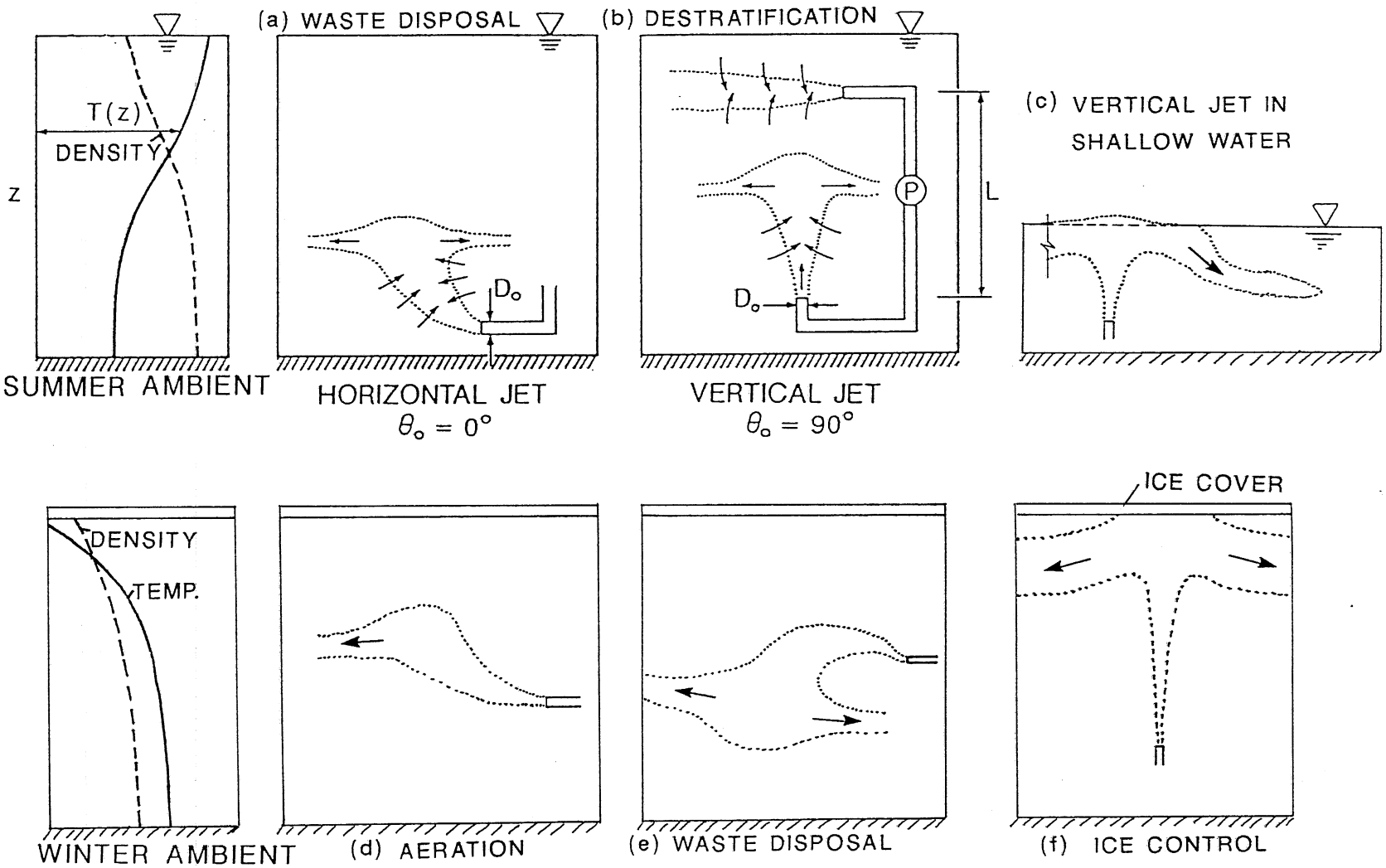

Fig. 1.1 Buoyant jets in stratified lakes, reservoirs and ponds

Winter lake aeration to prevent fishkill due to oxygen depletion under ice is often accomplished with a "pump and baffle" system (Ellis and Stefan, 1990). In this case oxygen is added to the pumped water and the water is then discharged into the lake (Wirth, 1970). This produces a horizontal water jet into a nonlinearly stratified lake at low temperatures (0–4° C) with an ice cover. Effects of the jet flow on the ice cover are of great concern because of the safety of people on the ice cover.

On other situations, submerged pumps have been used intentionally for ice control to suppress ice covers by delivering warm water vertically against the ice in a river or reservoir (Ashton, 1983).

1.2 Review of previous work

Most previous work by other investigators has dealt only with the jet itself, i.e. the jet portion of the flow field (nearfield). The integral analysis approach has been followed by a number of investigators (Abraham, 1972, Brooks, 1980, Fox, 1970, Fischer et al., 1979, Koh and Brooks, 1975, Hart, 1961, Lee and Jirka, 1981, Sotil, 1971, Hirst, 1971, Wright, 1979, and Lee, 1986) in their studies of buoyant jets in linearly stratified ambients. The integral approach has been widely used to analyze and formulate the mechanics of jet flows and to calculate trajectories, velocity and temperature decay and dilution. The scope of these previous studies differed in terms of jet geometry, shape and orientation. These previous attempts to describe the global behavior of buoyant jet flows in (linearly) stratified ambients have had some success. The basic elements of jet theory are followed and extended in this study to the development of a general 1–D integral numerical simulation model for both the nearfield and the farfield. The conventional assumptions of hydrostatic pressure in the jet and constant entrainment rate from the ambient water are modified in this study.

Little attention has previously been paid to jet mixing in the farfield (jet–mixing region). Mixing of stratified water in a pond or reservoir can improve water quality significantly but such practice has to rely on years of trial–and–error experience rather than a clear understanding of underlying physical process and mechanism. Very little research has been done to study the interaction of jets and ambient water, effects of buoyancy and density stratification on flow patterns and the processes of mixing induced by buoyant jets. In previous studies of lake destratification techniques, Hydraulic mixing by water jets, has received limited attention (Dortch and Holland, 1980, Dortch, 1979 and Irwin et al., 1969, Ditmars, 1972). Besides his laboratory work, Ditmars conducted both theoretical studies and numerical simulations (1–D) of destratification by a pumping system. His basic methods and assumptions are followed and extended in the development of the farfield jet–mixing model.

Multidimensional numerical analysis of flow fields has become increasingly popular in the recent decade. Among other investigators, Rodi (1984), working on the well known k–ϵ turbulence model, proposed an

extension to account for buoyancy effects and applied the model to vertical turbulent buoyant jets (Hossain and Rodi, 1986). This buoyancy–extended k–ϵ model has been followed by Sini and Dekeyser (1986) and Li and Chen (1984) for vertical plane jets in stratified fluid, and by Glekas et al. (1986) for negatively buoyant axisymmetric jet flows into a cavity. In this study, the turbulent model as described by Rodi, is used to develop a two–dimensional numerical simulation model for unsteady turbulent buoyant jet flows in stratified basins.

Very little effort has been spent previously to study horizontal discharges into a nonlinearly stratified lake at low temperatures (0–4° C) with an ice cover. Previous research was limited to uniform ambients and to the description of jet trajectories through the indirect calculation of turbulence and entrainment with an integral method (Robillard and Vassur, 1978, Jain and Rena, 1975). Investigation on jet impingement, spreading and entrainment related to buoyancy and stratification, effects of buoyancy and stratification on turbulent transport, and on the pattern of flow circulation are needed. There is no experimental data available for jet discharge into low temperature ambient water (0–4° C).

1.3 Objective scope and methodology of study

The practical problems mentioned in section 1.1 have a common denominator. They deal with buoyant jet flows and mixing effects in stratified lakes, reservoirs or ponds. Evolution of flow and thermal fields, jet mixing effects, jet trajectories, dilution of concentration and effects of jet flows on an ice cover are the major aspects of this study. Buoyant jets considered in this study differ in orientation, typically horizontal and vertical, and dimension or shape, typically axisymmetric and plane. A plane jet can be generated by a discharge from a slot or by a multi–port system as described in section 1.1. Ambient water is stratified strongly or weakly. Uniform ambient is a special case. Lakes and ponds studied here are with ice covers during winter or free surface during summer.

The objectives of the this study are to apply basic physical laws to the study of buoyant water jet flows and mixing in temperature–stratified basins such as lakes, ponds or reservoirs, to simulate and describe the process and behavior of the jet mixing, to predict the physical feature of the flow and thermal fields, and to provide design and operation information for use of artificial mixing devices in practice with less uncertainty.

The study is carried out by theoretical analysis, numerical simulation and experimental investigation. Theoretical analysis is based on available theories of jets, lake and reservoir hydrodynamics, heat transfer, and limnology. The 1–D and 2–D numerical simulation models predict flows and mixing by extracting solutions of the equations of momentum, continuity and heat transfer. Experimental investigation is carried out to observe basic features of jet flows and mixing and to provide data to verify theories and numerical models.

This research started out with the integral method and development of 1–D models. An integral model is developed for steady and turbulent jets in infinite ambients. A mixing model for the interaction of jet and ambient is developed to deal with convective–transport of thermal energy and mass in unsteady situations.

Laboratory experiments are then designed to model the basic features of buoyant water jet flows and mixing in a stratified basin in open water situations. Flow rates and temperature profiles over depth are measured. Multiple experiments are conducted with different initial conditions and governing parameters.

In order to make it possible to evaluate effects of jet flows and mixing on water quality and environments in lakes or reservoirs and ponds, the integral 1–D jet–mixing model is incorporated into a existing dynamic lake water quality simulation model, MINLAKE. The MINLAKE model was originally for summer season and is extended to accomplish year–round temperature simulation in this study.

The details of the flow field, which would be too complicated to measure in the laboratory or to simulate with the 1–D models, are studied in a 2–D numerical simulation model. The two–dimensional model solves the Reynolds equations with a k–ϵ turbulence model as a closure. The details of the flow and thermal fields during the mixing process, which is analyzed as an unsteady phenomenon, are modeled numerically. Since large memory and computational time are required, computations have to be performed on the CRAY2 computer.

1.4 Outline of study

Chapter one introduces the problem and objectives of this study.

Chapter two gives theoretical background including concepts and basic equations. Three flow regions or fields are introduced and characterized. Some characterizing dimensionless parameters are defined.

The development of the 1–D jet–mixing model for a submerged buoyant jet in stratified ambient with the integral method is presented in chapter three. Sensitivity of the model to empirical coefficients is analyzed. A simple mixing model for a vertical jet in shallow water is also provided.

Laboratory experiments on jet mixing are described in chapter four. Results are presented and analyzed. The 1–D jet–mixing simulation model is verified against experimental data.

Chapter five deals with the region which is not disturbed by the jet but is affected by meteorological conditions and hydrological processes. An existing simulation model for the summer season is extended to year–round simulation of hydrothermal processes of a lake including winter when an ice cover forms. A winter cover simulation model (ice and snow) and sediment heat transfer model is developed and linked to the main model (MINLAKE).

Application of the 1–D jet–mixing simulation model is made to a stratified lake and a stabilization pond. Chapter six summarizes the incorporation of the jet–mixing model into the year–round MINLAKE model and presents numerically simulated results.

Design information for hydraulic destratification systems are provided in chapter seven. Different mixing systems are discussed in terms of efficiency. Effects of jet orientation and jet momentum on mixing are analyzed. The method and procedure of conceptual design are outlined.

In chapter eight the 2–D simulation model is developed for the direct simulation of detailed jet flow fields and mixing in a stratified water basin (combination of jet region and mixing region). This model is especially for the complex situation, i.e. a horizontal buoyant jet into low temperature water with an ice cover.

Chapter 2

Theoretical Background—Concepts and Basic Equations

2.1 Characteristics of flow fields

A schematic representation of buoyant jet flows in a stratified lake is shown in Fig. 2.1 The lake is divided into three fields or regions for convenience of analysis and numerical modeling: a nearfield or jet region, a farfield or mixing region and a natural field or region undisturbed by the jet. The nearfield is characterized by entrainment, dilution and turbulent mixing processes in the jet portion of flow. The farfield includes the spreading of flows, ambient water mixing, re–entrainment and circulation due to entrainment and deliverance of water by the jet. The nearfield and farfield can be, as far as mixing is considered, unified to one so called jet–mixing region. The natural field, outside of the jet–mixing region and covering a much larger area (remainder of the lake), is characterized by the hydrothermal and dynamic processes in the natural state. This region is not disturbed by the jet. In the natural filed the distribution of temperature and dissolved materials are determined by external factors other than artificial mixing.

2.2 Flow behavior and mixing mechanism

The jet considered in this study is generated by discharging water into stagnant stratified ambients and can be characterized as a turbulent shear flow increasing in size with a boundary between it and ambient fluid (Fig. 2.2). At the point of discharge the jet has not only kinetic energy but also potential energy due to buoyancy. Both kinds of energy are dissipated in the turbulent mixing of the jet with the surrounding fluid while the jet is driven by initial momentum and buoyancy force during penetration. The jet transits to buoyancy–dominated flow (plume–like) from inertia–dominated flow (jet–like). Due to the stratification of the ambient, the turbulent mixing and the dilution resulting from entrainment, the jet reaches a "neutral" level. Beyond this level the jet becomes negatively buoyant.

The negative buoyancy interacts with the initial momentum and the momentum generated by the positive buoyancy. The jet flow may overshoot its neutral buoyancy depth (Figs. 2.1 and 2.2) due to inertial effects. After reaching its maximum height or ceiling level, because of the negative buoyancy force, the jet falls down and intrudes into the lower layer of ambient water and spreads horizontally out at the equilibrium level.

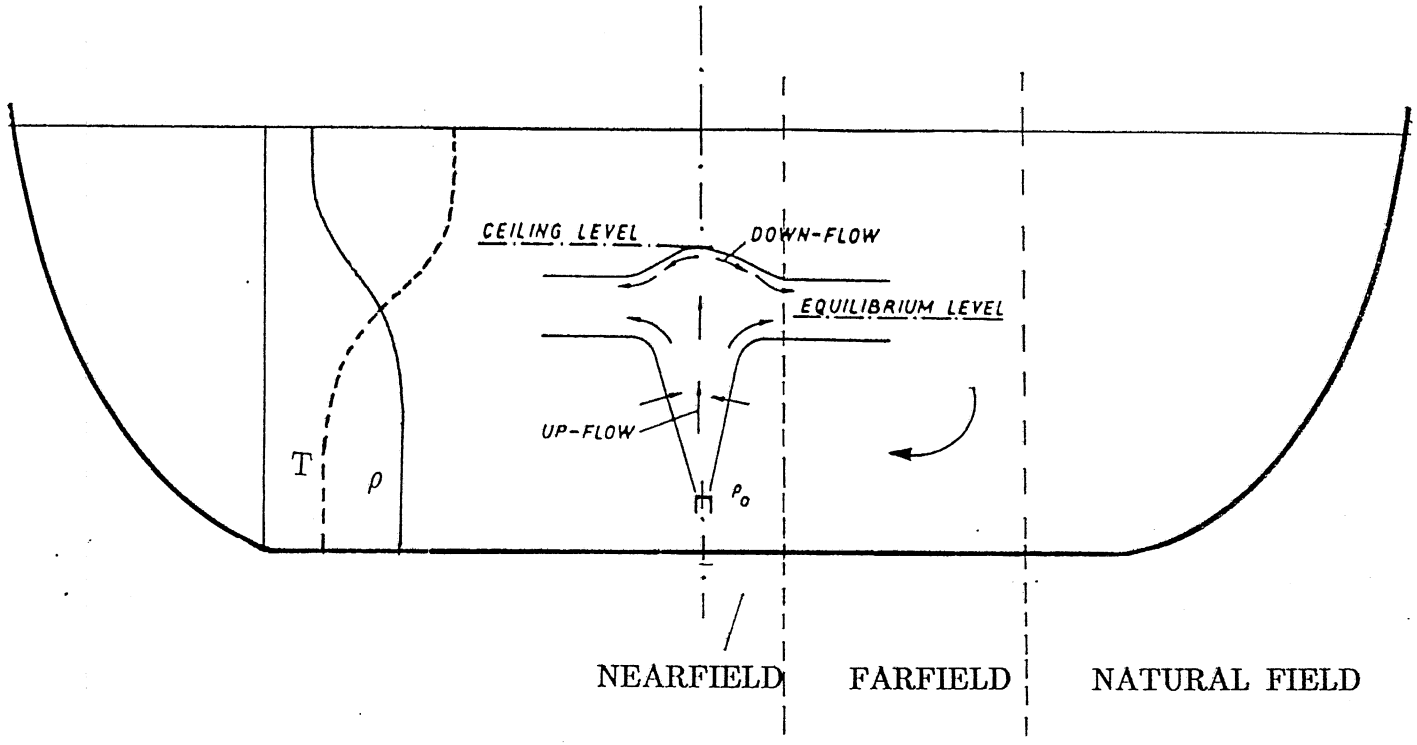

Fig. 2.1 Schematic diagram of a vertical buoyant jet in a stratified basin

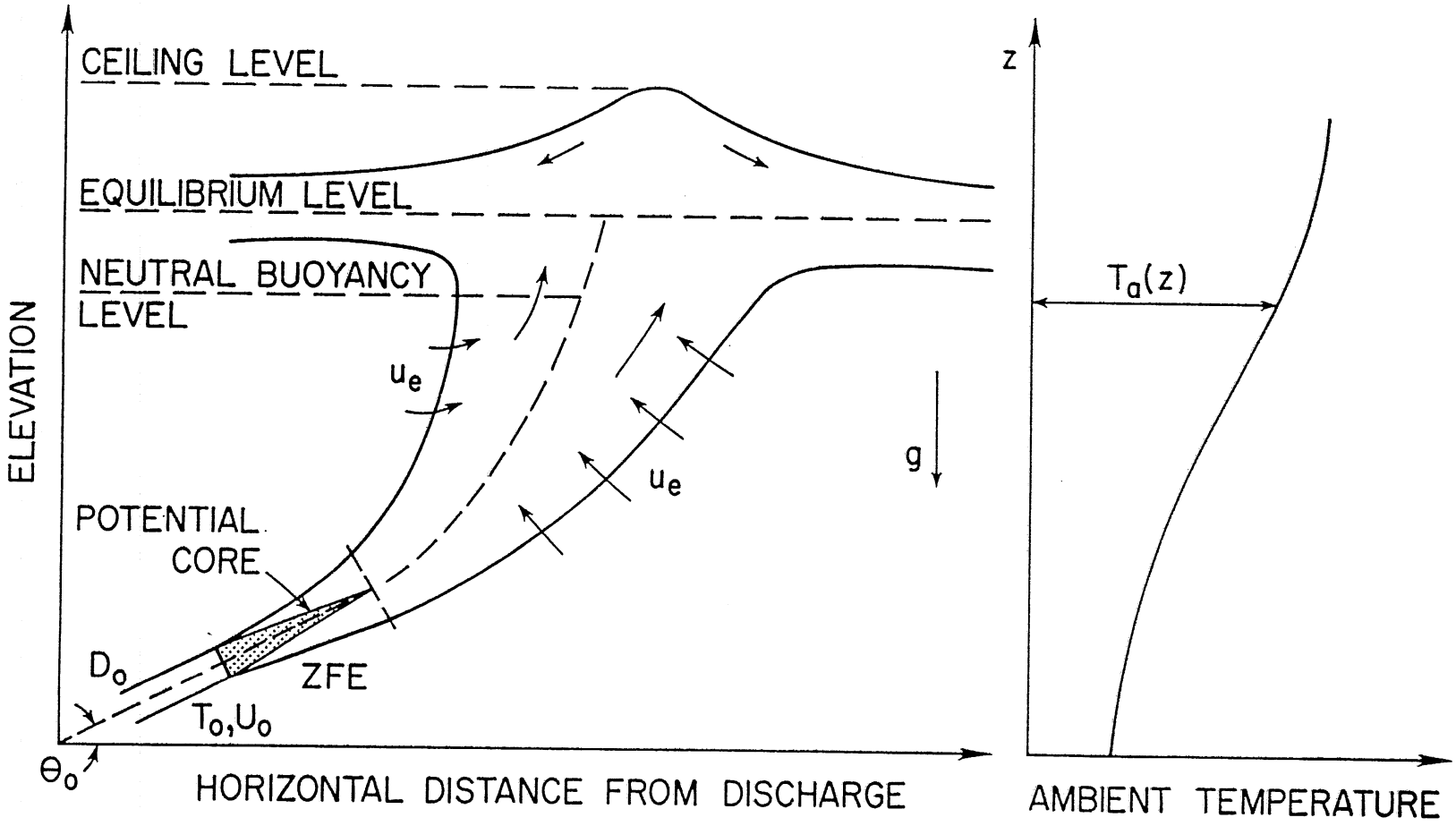

Fig. 2.2 Schematic representation of flow behavior of a buoyant jet in a stratified ambient water body

In the case of very small discharge angle, typically a horizontal jet, and high initial momentum, the jet flow is gradually deflected from an inclined direction to a horizontal flow in one direction at the ceiling level (Fig. 1.1d). The deflected flow finally extends to its equilibrium level. The behavior of the horizontal jet is different from the case of large discharge angle, typically a vertical jet, which falls down upon the succeeding fluid and spreads out at both sides of the jet.

Inertial forces which drive the jet flow upward and negative buoyancy forces which drive the flow downward may cause the jet flow to oscillate around the equilibrium level. The amplitude of oscillation decreases with increasing distance from the discharge point.

Depending on its initial momentum the jet may not extend to the surface of a stratified water. If a jet reaches the surface it collapses or impinges on the surface. A horizontal spreading flow, driven by excess pressure, may form either at the surface or at a deeper layer after possibly plunging from the surface to its equilibrium level. This occurs when the jet has either sufficient kinetic energy or the ambient has a weak stratification. An example of the overshooting jet flow is a vertical jet in shallow water, e.g. a pond, as shown in Fig. 1.1c. After the jet plunges down, it intrudes into its equilibrium layer, delivering water entrained from other layers to the equilibrium layer.

Mixing in the nearfield is induced by the jet through turbulent convection and diffusion of mass, momentum and energy due to shear stress and vortices. Entrainment from the ambient to the jet must satisfy conservation of mass, resulting in dilution of the jet flow. Flow in the ambient water surrounding the jet is induced. Circulation patterns in the farfield are then established with deliverance of fluid by the spreading flows. The shear at the interface of the intruding or spreading layer and the ambient fluid at the equilibrium level induces re–entrainment and enhances the turbulent mixing in the farfield. On the other hand, stable stratification in the ambient has a strong damping effect on the turbulence and therefore inhibits spreading and mixing. The turbulent mixing in the farfield is not as strong as in the nearfield and therefore the circulation pattern of flows may play a more important role in mixing of that region.

2.3 Basic equations and solution methods

Flow (laminar and turbulent) obeys the laws of conservation of mass, momentum, thermal energy and species concentration. The basic equations describing the general flow are the unsteady Navier–Stokes equations, continuity, and thermal energy equations and the state equation.

$$\frac{d\rho}{dt} + \rho\frac{\partial U_j}{\partial x_j} = 0 \tag{2.1}$$

$$\rho\frac{dU_i}{dt} = -\frac{\partial p}{\partial x_i} + \rho g_i + \frac{\partial \tau_{ij}}{\partial x_j} \tag{2.2}$$

$$\rho\frac{d\varphi}{dt} = \frac{\partial}{\partial x_j} k_\varphi \frac{\partial \varphi}{\partial x_j} + S_\varphi \tag{2.3}$$

$$\rho = \rho(T, C) \tag{2.4}$$

in which stresses are

$$\tau_{ij} = \mu\left[\left(\frac{\partial U_i}{\partial x_j} + \frac{\partial U_j}{\partial x_i}\right) - \frac{2}{3}\delta_{ij}\frac{\partial U_k}{\partial x_k}\right] \tag{2.5}$$

and $k_\varphi \frac{\partial \varphi}{\partial x_j}$ = molecular diffusion fluxes of heat or chemical species. U, ρ, φ, p, x and t are velocity, density, temperature (T) or species concentration (C), pressure, coordinate and time, respectively. S_φ is a source or sink of heat and masses, μ is molecular viscosity and k is molecular diffusivity, $k_T = \frac{\mu}{Pr}$ for heat (φ = T) and $k_C = \frac{\mu}{Sc}$ for mass (φ = C) where Pr and Sc are Prandtl and Schmidt numbers, respectively.

Concentration C can represent dissolved material or neutrally buoyant solid suspended material. When dissolved material is contained in the flow the effect of C on density is herein assumed to be negligible, and then the state equation becomes

$$\rho = \rho(T) \tag{2.6}$$

The basic equations are averaged with respect to time by the Reynolds approach for turbulent flows by which the instantaneous values of the variables are separated into mean and fluctuating quantities. Using the same symbols for mean variables as those for instantaneous variables for convenience, the time–averaged mean flow (Reynolds) equations are

$$\frac{\partial \rho}{\partial t} + \rho\frac{\partial(\rho U_j)}{\partial x_j} = 0 \tag{2.7}$$

$$\frac{\partial(\rho U_i)}{\partial t} + \frac{\partial}{\partial x_j}(\rho U_i U_j) = -\frac{\partial p}{\partial x_i} + \rho g_i + \frac{\partial}{\partial x_j}(\tau_{ij} - \rho\overline{U_i' U_j'}) \tag{2.8}$$

$$\frac{\partial(\rho\varphi)}{\partial t} + \frac{\partial}{\partial x_j}(\rho U_i \varphi) = \frac{\partial}{\partial x_j}\left(k_\varphi \frac{\partial \varphi}{\partial x_j} - \rho \overline{U_j' \varphi'}\right) + S_\varphi \tag{2.9}$$

$$\rho = \rho(T, C) \tag{2.10}$$

where the superscript "′" denotes fluctuation, $-\rho\overline{U_i' U_j'}$ is the turbulent or Reynolds stresses and $-\rho\overline{U_j' \varphi'}$ is the turbulent diffusion flux of heat or chemical species.

Two methods are used in this study to solve numerically the Reynolds equations, i.e. mean flow equations, for the problem of turbulent buoyant jet flows: (1) the integral method and (2) the differential (field) method. The integral method reduces the multidimensional partial differential equations to one–dimensional ordinary ones by integration. An integral jet model for the nearfield and a one–dimensional mixing model for the farfield is developed in this study, using the integral approach. Coupling the nearfield model and farfield model gives a 1–D model for the jet–mixing region, which is the combination of nearfield and farfield. The 1–D jet–mixing model is incorporated into an existing multi–purpose dynamic lake water quality model (MINLAKE) for the natural field so that solutions for all three regions are possible.

In the differential (field) method the governing equations are solved directly with a closure by a turbulence model. The differential method was also called field method since variables such as velocities and temperature are determined for each point in the field as direct solutions of the governing equations. The field method does not require a similarity hypothesis, an empirical entrainment relation, and simplification from 2–D to 1–D and from partial differential to ordinary differential equations as is necessary for the integral method. A two–dimensional simulation model is developed for the jet–mixing field as a whole rather than dividing it into the nearfield and farfield.

The 1–D model is simpler in analysis and calculation than the 2–D model and more suitable for incorporation to MINLAKE. It can also provide more direct design information for practical applications than the 2–D model. The 2–D model gives more insight into the flow field induced by the water jet and gets closer to the real situation with less assumptions than the 1–D model.

2.4 Dimensionless characterizing parameters

The initial characteristics of the water jet are described by two dimensionless independent parameters, Reynolds number, Re, and densimetric Froude number, Fr, which are defined as

$$Re = \frac{U_0 D_0}{\nu} \qquad \text{and} \tag{2.11}$$

$$Fr = \frac{U_0}{\left[g\, D_0\, \frac{\Delta\rho_0}{\rho_0}\right]^{1/2}} \tag{2.12}$$

where $\Delta\rho_0$, ρ_0, D_0, and U_0 are the density difference between the jet and the ambient, the jet density, the jet diameter, and the mean jet velocity, respectively, all at the jet origin, g is acceleration of gravity and ν is viscosity of water. Reynolds number, Re, is used to express the level of turbulence in the flow field. Fr expresses the strength of initial jet momentum relative to buoyancy of the jet.

A bulk Richardson number, Ri, defined for buoyant jets as

$$Ri = \frac{g D_0 \Delta\rho_0}{\rho_0 U_0^2} \tag{2.13}$$

is also used in large measure by investigators. The Richardson number is the combination of the kinematic momentum flux, the volume flux and the buoyancy flux. The two numbers, Fr and Ri, are related to each other by

$$Ri = \frac{1}{Fr^2} \tag{2.14}$$

The sign of Ri indicates whether the jet is positively buoyant or negatively buoyant.

The initial stratification of the ambient water is expressed by a stratification number, St, defined as

$$St = \left[\frac{\Delta\rho_0}{D_0}\right]\left[\frac{d\rho_a}{dz}\right]^{-1} = \left[\frac{\Delta\rho_0}{D_0}\right]\left[\frac{1}{\rho_0 \epsilon}\right] \tag{2.15}$$

where ρ_a is ambient water density, and z is a vertical coordinate. The stratification number, St, is related to a stratification parameter, ϵ, defined as

$$\epsilon = \frac{1}{\rho_o} \frac{d\rho_a}{dz} \tag{2.16}$$

A non–linear vertical distribution of the ambient density is not described by St which represents the overall strength of ambient stratification.

Time, t, used as one of the independent variables in this study, is normalized by the jet flowrate, Q, and the lake volume, V, as

$$t^* = \frac{Q}{V} t \tag{2.17}$$

The progression of the mixing process is analyzed and presented with respect to the dimensionless time, t^*.

Chapter 3 Integral Method and 1–D Models

3.1 Jet model for the nearfield

In this section a turbulent buoyant jet issuing into quiescent stratified ambient fluid and the application to the artificial mixing of a lake, reservoir or pond is investigated by following the basic elements of jet theory. The theoretical integral analysis approach is used and extended. A general model is devised to predict the development of turbulent buoyant jets discharged at arbitrary angles to infinite, quiescent and stratified ambients. The model is developed by using the integral conservation equations with a similarity hypothesis for velocity and temperature profiles and an entrainment function. The integral model developed here is capable of predicting jet trajectories, jet width, centerline temperature or density and velocity decay, centerline dilution, point of neutral buoyancy, and maximum height of rise for buoyant jets discharged at arbitrary angles to stratified or uniform ambients.

The behavior of turbulent buoyant jets in stratified ambients is quite complex. As found by several previous investigators, the conservation equations of mass, momentum, and energy, which describe all the details of the turbulent buoyant jet motion, are rather complicated, even after various simplifying assumptions. For practical problems integral methods were developed in which the partial differential equations are integrated over the jet cross–section area and a set of coupled ordinary differential equations is obtained by introducing empirical similarity profiles for velocity, temperature difference in the lateral direction and an entrainment principle. The resulting ordinary differential equations describe the axial variation of the velocity, excess temperature or concentration scales, and the characteristic shear–layer width. The solution to the resulting equations yields results for the centerline trajectory of the jet and gives useful results about jet centerline dilution and jet width. The main purpose of the integral approach is to describe the gross behavior of the jet for practical problems and to avoid the specification of turbulent transport terms in the conservation equations.

3.1.1 Governing equations

The governing equations are formulated from the Reynolds mean flow equations with the following assumptions: 1) the fluid is incompressible; 2) the motion is two–dimensional (or axisymmetric) and steady in the mean; 3) the ordinary free shear boundary–layer approximation of fluid dynamics can be evoked; 4) the flow in jets is effectively turbulent; 5) the Boussinesq approximation is applied and 6) the pressure term is divided into two components, dynamic and hydrostatic.

The resulting system of governing equations for conservation of mass, momentum, and mechanical and internal energy can be written in either an axisymmetric or a two–dimensional natural coordinate system (s, y) in the form of partial differential equations of continuity, s–momentum, y–momentum, mechanical energy, thermal energy and state

$$\frac{\partial(uy^k)}{\partial s} + \frac{\partial(vy^k)}{\partial y} = 0 \tag{3.1}$$

$$u\frac{\partial u}{\partial s} + v\frac{\partial u}{\partial y} = -\frac{1}{\rho_o}\frac{\partial p_d}{\partial s} - \frac{1}{y^k}\frac{\partial(y^k\overline{u'v'})}{\partial y} - \frac{\partial\overline{u'^2}}{\partial s} - \frac{\Delta\rho}{\rho_o} g \sin\theta \tag{3.2}$$

$$u\frac{\partial v}{\partial s} + v\frac{\partial v}{\partial y} = -\frac{1}{\rho_o}\frac{\partial p_d}{\partial y} - \frac{1}{y^k}\frac{\partial(y^k\overline{v'^2})}{\partial y} - \left[\frac{\Delta\rho}{\rho_o} g \cos\theta + u^2\frac{\partial\theta}{\partial s}\right](\sin\phi)^k \tag{3.3}$$

$$u\frac{\partial(\frac{u^2}{2})}{\partial s} + v\frac{\partial(\frac{u^2}{2})}{\partial y} = -\frac{u}{\rho_o}\frac{\partial p_d}{\partial s} - \frac{u}{y^k}\frac{\partial(y^k\overline{u'v'})}{\partial y} - u\frac{\partial\overline{u'^2}}{\partial s} - u\frac{\Delta\rho}{\rho_o} g \sin\theta \tag{3.4}$$

$$u\frac{\partial T}{\partial s} + v\frac{\partial T}{\partial y} = -\frac{1}{y^k}\frac{\partial(y^k\overline{u'T'})}{\partial y} \tag{3.5}$$

$$\rho = \rho(T, C) \tag{3.6}$$

where the s–coordinate follows tangentially the jet trajectory, i.e. the axis of the jet, and the y–coordinate is normal to the s–coordinate. In the equations $\Delta\rho$ = the difference between the jet density and the ambient density $(\rho - \rho_a)$, T = jet temperature, T′ = fluctuating component of T, u = the velocity in the main flow direction (s), u′ = fluctuating component of u, v = the velocity in the transverse direction (y), v' = fluctuating component of v, p_d = pressure due to the change of density and the curvature of jet $(p - p_h)$, in which p_h = hydrostatic pressure, θ = jet angle, ϕ = angle coordinate in the cylindrical polar coordinates, $_k$ = 0 for a two–dimensional jet discharged from a slot source, and $_k$ = 1, y = r for a three–dimensional jet discharged from a round source. The s–coordinate shown in Fig. 3.1 follows the jet trajectory. The jet centerline is taken as the s–coordinate and measures the distance from the discharge or jet origin. For the case of a circular jet cylindrical polar coordinates (s, r, ϕ) are used.

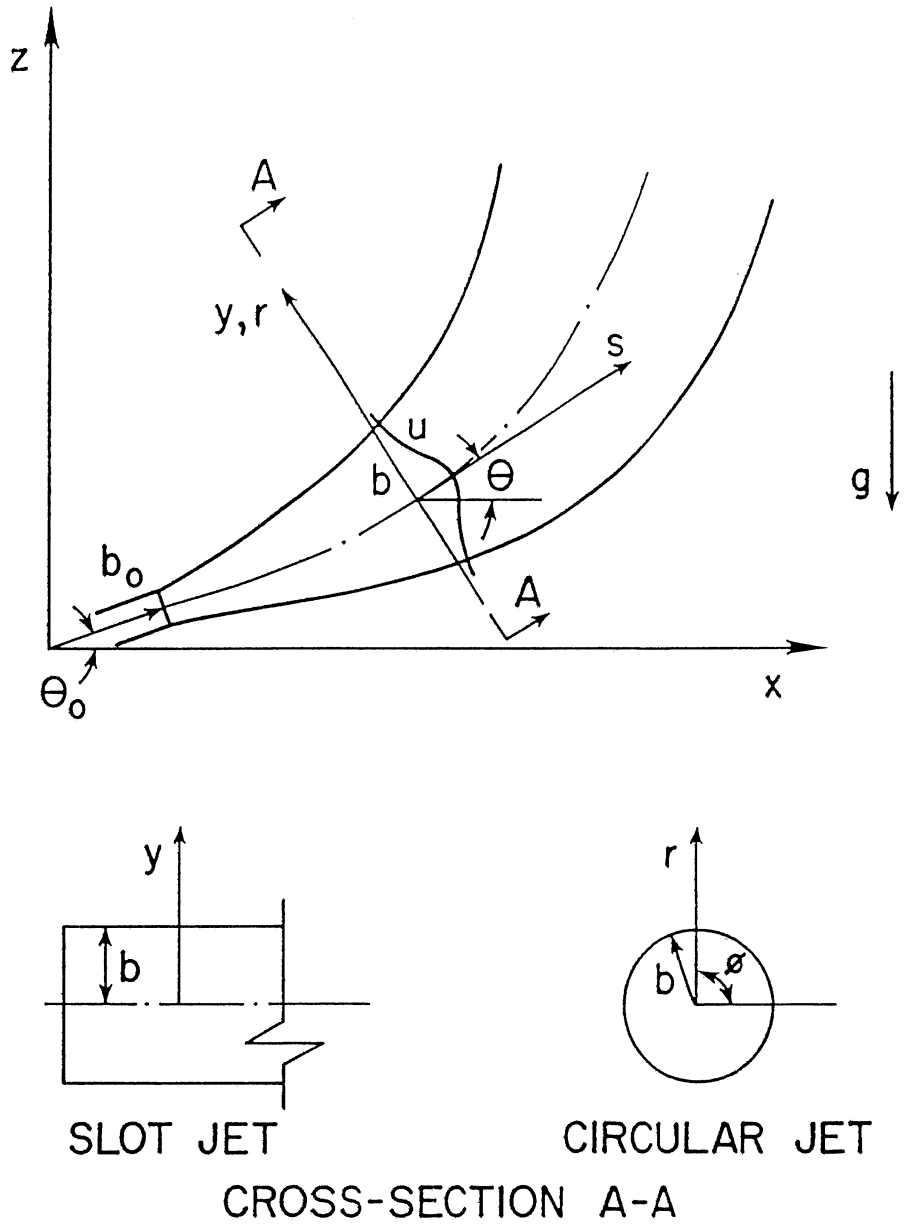

Fig. 3.1 Coordinate system used for buoyant jet analysis

If the jet fluid does not contain dissolved or suspended material the density is only related to the fluid temperature. When this condition is not satisfied, an equation for dissolved or suspended material concentration C, which is similar to the thermal energy equation, is added to the governing equations and consequently the equation of state becomes $\rho = \rho(T, C)$. A linear equation of state is assumed by some investigators. This is represented by the Oberbeek–Boussinesq equation $\rho = \rho_1(1 - \beta_e(T - T_1))$ where β_e is the thermal coefficient of volumetric expansion of the fluid, sometimes assumed constant for cases with limited temperature ranges. The thermal coefficient for volumetric expansion for water, a is actually a strong function of temperature in the range 5° C – 40° C. Tatom (1985) studied errors from using a constant β_e which is equivalent to a conservation of buoyancy approach. He concluded that any jets predicted by models based on the conservation of buoyancy principle will tend to overestimate the effect of buoyancy. It is therefore proposed that the use of the conservation of buoyancy principle should be avoided wherever possible, especially for cases involving low water temperatures. In this study, a non–linear function of state for pure water is adopted.

3.1.2 Integral method

The general integral approach is used and extended in this study by introducing a pressure term due to jet curvature and density difference where previous models used only a hydrostatic pressure assumption. Furthermore the entrainment coefficient is derived from the energy equation, instead of being treated as constant as done in previous models.

The y–momentum equation (Eq. 3.3) is integrated from y to 1 to obtain the expression for the pressure p_d which is then substituted into the axis–momentum equation (Eq. 3.2) and the mechanical energy equation (Eq. 3.4). The partial differential equations (Eqs. 3.1, 3.2, 3.4 and 3.5) are integrated over the jet cross–section area with respect to y from 0 to 1 by employing the Leibnitz rule. Then a set of coupled ordinary differential equations are obtained by assuming empirical similarity profiles for velocity and temperature difference in the lateral direction of the jet and by introducing an entrainment principle. The Gaussian profile is used here.

3.1.3 Set of differential equations for jet variables

The governing equations are integrated, simplified and combined to get the following set of first order differential equations for the main jet variables: the centerline velocity, u_m, jet width, b, and centerline temperature difference, ΔT_m (Gu and Stefan, 1988a). The jet width, b, is arbitrarily

defined as the characteristic width of the jet–velocity profile. Here, for Gaussian form, the normal half–width of the jet is $b = 2^{0.5}\,\sigma$, where σ is the standard deviation of the Gaussian profile defined by $\sigma^2 = \int_0^\infty r^2 u dr / \int_0^\infty u dr$. For round jets one obtains

$$\frac{du_m}{ds} = 2(\alpha - \frac{db}{ds})\frac{u_m}{b} \tag{3.7}$$

$$\frac{db}{ds} = \frac{\pi(\alpha + \frac{1}{4}Ri_1\lambda^2\sin\theta) + A\,(\frac{d\Delta\rho_m}{ds}\cos\theta - \frac{d\theta}{ds}\Delta\rho_m\sin\theta) + 4\frac{d\theta}{ds}\alpha I_5 b}{0.5\pi - 3\lambda^3 I_6\, Ri_1\cos\theta + 2\frac{d\theta}{ds}I_5\, b} \tag{3.8}$$

$$\frac{d\Delta T_m}{ds} = -(\frac{1+\lambda^2}{\lambda^2}\sin\theta\,\frac{dT_a}{dz} + \frac{2\alpha\Delta T_m}{b}) \tag{3.9}$$

where $A = 2\lambda^3 g b^2 I_6/(u_m^2\,\rho_o)$, λ = dispersion ratio, Ri_1 = local Richardson number, defined as $Ri_1 = \Delta\rho_m g 2b/\rho_o u_m^2$, I_5 and I_6 = integral constants of Gaussian distribution.

The $\rho(T)$ relationship (Eq. 3.6) and the entrainment function, α, are required to solve the equations for the jet variables.

$$\alpha = -\frac{\lambda^2 Ri_1 \sin\theta}{2} + \frac{Ri_1\sin\theta\,\frac{2\lambda^2 - \lambda^4}{1+\lambda^2} + 12I}{2 + 8(I_6\lambda^3 - 2I_5\lambda^2)\frac{Ri_1\cos\theta}{\pi}} \tag{3.10}$$

where I = shear–stress integral coefficient, defined as

$$I = \frac{1}{u_m^3 b}\int_0^\infty u\,\frac{\partial[r\overline{(u'v')}]}{\partial r}dr$$

Also required is an expression for the jet trajectory angle θ. This expression has to be derived from the momentum equations. This can be done most easily by consideration of the momentum equations in the s and z directions (Fig. 3.1) rather than the previously used s and y–direction. Combination of the integral s–momentum and z–momentum equations gives

$$\frac{d\theta}{ds} = -\frac{2\lambda^2 \Delta\rho_m g \cos\theta}{u_m^2 \rho_o} \tag{3.11}$$

The geometry of the jet centerline gives

$$\frac{dx}{ds} = \cos\theta \tag{3.12}$$

and

$$\frac{dz}{ds} = \sin\theta \tag{3.13}$$

When the jet fluid contains some contaminants, equations for tracer concentration derived from the conservation equation of tracer mass, have to be added

$$Cu_M b = C_o u_o b_o \tag{3.14}$$

where subscript "o" denotes an initial value.

The eight variables u_m, b, ΔT_m, α, θ, x, y and C are functions of s only. These variables can be determined by solving the above set of equations, given initial values at the jet origin for the jet parameters.

Examination of the set of final equations shows that they are valid either for buoyant jets as well as for a sinking (negatively buoyant) jets. They reduce to the proper forms in case of a uniform ambient temperature environment $dT_a/ds = 0$, and for the case of a simple momentum jet (no buoyancy flux: $dT_a/ds = 0$ and $\Delta T = 0$.

The similarities between axisymmetric and plane jets are significant; however, the equations describing each are dissimilar enough to establish certain quantitative differences in the motion. The experimental data of Kotsovinos (1977) show that velocity and temperature–difference distributions of slot jets also can be adequately represented by Gaussian profiles. Applying the same integral approach as used for round jets to the governing equations for slot jets yields similarly a set of first–order ordinary differential equations.

In order to determine the entrainment coefficient one must decide upon the values of the dispersion ratio, λ, and the shear–stress integral, I. It is difficult to specify the shear stress profile $(\overline{u'v'})$. The integral, I, was determined empirically by several investigators. Koh and Brooks (1975) suggested I = 0.0095 and 0.0138 for turbulent round jets and plumes and I = 0.0182 and 0.046 for slot jets and plumes, respectively. Blevins (1984) gave a range of $0.0052 \leq I \leq 0.0068$ for round jets and plumes and $0.0153 \leq I \leq 0.029$ for slot jets. A value of 0.0095 for round jets was recommended by

Abraham (1972) and 0.018 for slot jets by Fan (1966) and Koh and Brooks (1975). The dispersion ratio, λ, was found in the range of 1.08 to 1.16 (Fostal and Gaylord, 1955) for round jets which corresponds to the turbulent Schmidt number, $0.75 \leq Sc \leq 0.85$. The commonly used value is 1.16 suggested by Koh and Brooks (1975). For slot jets various values, $0.89 < \lambda < 1.40$, are chosen by a number of investigators (Wright, 1980, Brooks, 1980 and Sotil, 1971). Experiments by Rouse et al. (1952) found $\lambda = 0.9$ for slot jets.

The equations outlined above describing the gross behavior are, however, valid only in the zone of established flow where Gaussian profiles may be used. The initial values for jet trajectory (x, y), jet width and centerline temperature difference can be corrected to account for the zone of flow establishment following the methods presented by Shirazi and Davis (1972), Sotil (1971) and Singh (1976). This correction has been incorporated into the solution. Details are given by Gu and Stefan (1987).

3.1.4 Model validation with experimental data

The model equations are solved by a 4th order Runge–Kutta method and the results compared with experimental data from Fan (1967) as given by Hirst (1971) and from Wright and Wallace (1979) and Lee and Cheang (1986).

Fig. 3.2 shows comparisons between numerical calculations and experimental measurements of the centerline trajectory for several round buoyant jets discharged at various angles into stably stratified ambients (Hirst, 1971). The quality of prediction is quite good for these flows. The calculations and measurements in horizontal and vertical projections of the jet axis and along the jet axis are in substantial agreement.

Approximate solutions for the maximum height of rise of slot vertical jets and the centerline dilution at the terminal height are developed with a length scale analysis and experimental results by Wright and Walance (1979). Roberts and Matthews (1987) applied the dimensionless length scale to the study of low–buoyancy jets in a linearly stratified fluid. The numerical calculations for z_t with the integral model presented are compared with Wright's experimental data for slot jets in Fig. 3.3, where $z_t = z_m + b$, z_m is the maximum centerline height of rise and b is the jet width. The numerical and experimental results are in fairly good agreement.

Figs. 3.4 and 3.5 show the comparison of numerical calculations with Lee's experimental results (Lee and Cheung, 1986) for z_t and S_M, where S_M is the dilution in a jet at its maximum centerline rise, i.e. C_o/C_M, for slot jets discharged at an angle of 45°.

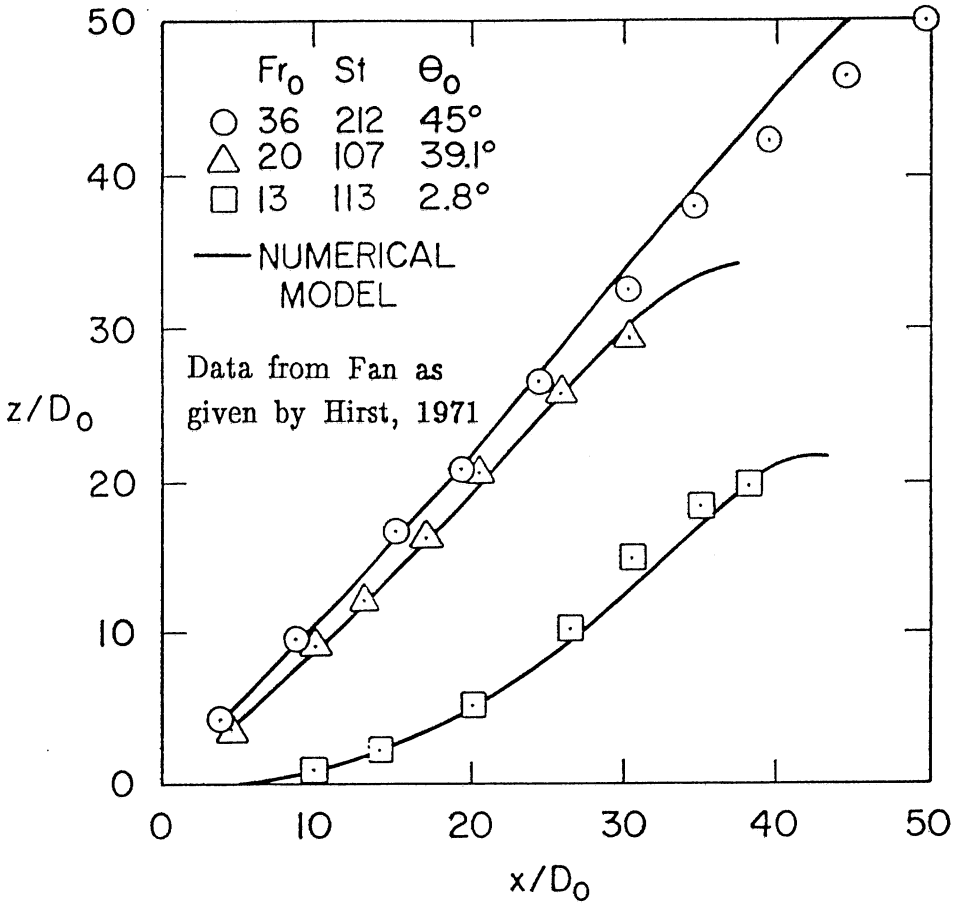

Fig. 3.2 Trajectory for round buoyant jets in stratified ambients

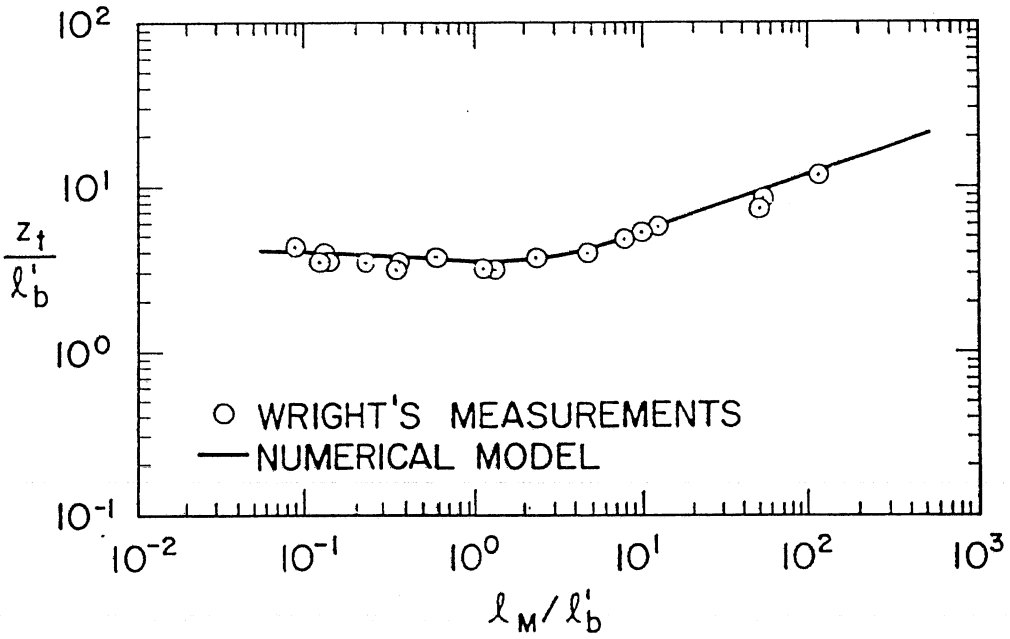

Fig. 3.3 Maximum height of rise for slot jets discharged vertically

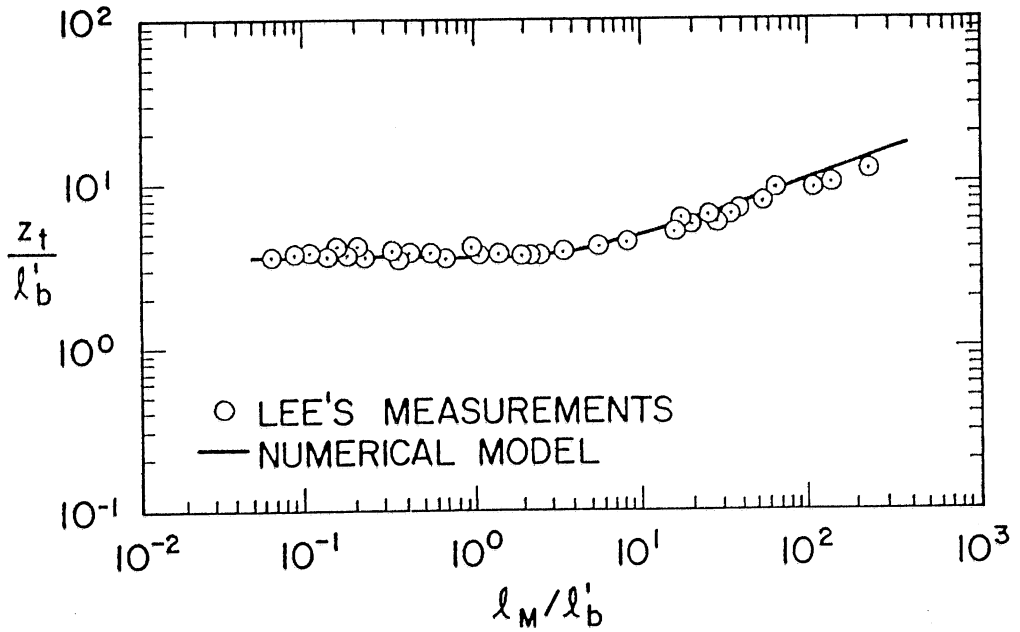

Fig. 3.4 Maximum height of rise z_m for slot jets with $\theta_o = 45^o$

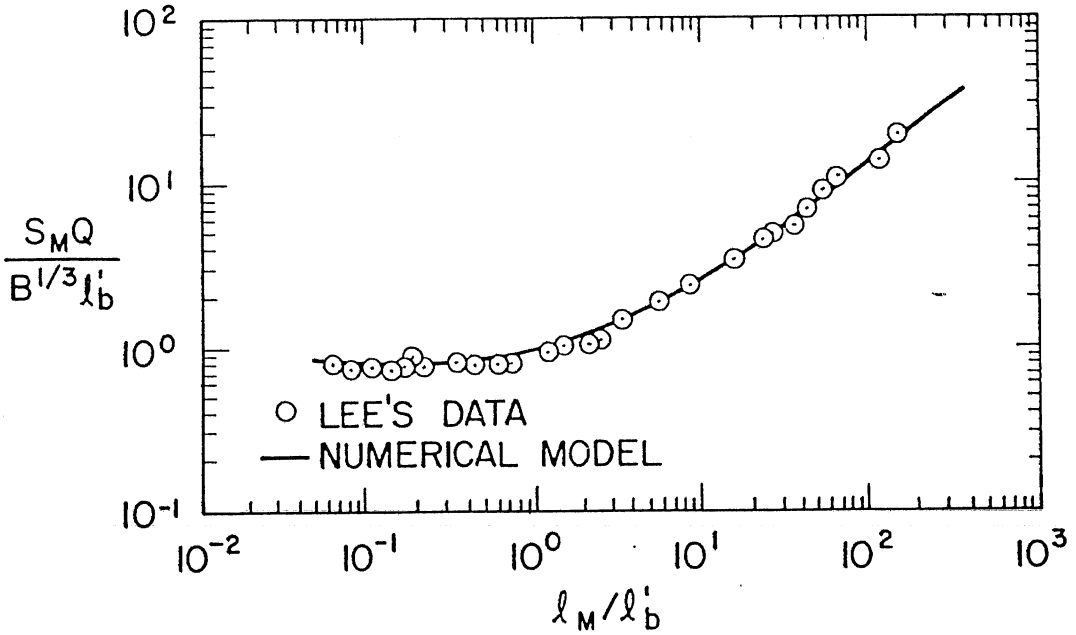

Fig. 3.5 Dilution in spreading layer for slot jets with $\theta_o = 45^o$

Characteristic length scales used in Fig. 3.3 to 3.5 are defined as $\ell_Q = Q/M^{1/2}$, $\ell_M = M^{3/4}/B^{1/2}$, and $\ell_b' = B^{1/4}/\epsilon_g^{3/8}$ in which Q, M and B are the source volume, momentum and buoyancy flux of the source, respectively ($Q = \pi D_0^2 U_0/4$, $M = QU_0$, $B = Qg\Delta\rho_0/\rho_0$ and $\epsilon_g = (g/\rho_0)(\Delta\rho/\Delta z)$).

3.2 Mixing model

Thermal or density stratification often causes a deterioration of water quality. Mixing of temperature–stratified lakes or reservoirs using recirculating pumping systems can counteract the deterioration of water quality through jet mixing. Various destratification devices are used in lakes and reservoirs. However, the mechanical pumping systems for mixing are considered to provide more efficient mixing and to be better suited for mixing of impoundments (Ditmars, 1970). Dortch and Holland (1980) reviewed methods of total lake destratification. Hooper, et al. (1952) broke the stratification by pumping cold water from the bottom to the top. A series of reservoir mixing experiments with pumping systems was performed by Irwin and Symons (1966). In this section the physical aspects of the mixing processes are investigated, the development of a simulation model predicting the process of temperature destratification is presented. This model is validated in chapter 4 with laboratory experimental data. Application is made to a lake in chapter 6 to simulate jet mixing processes. Effectivenesses and efficiencies of water jet mixing (destratification) systems and a design method and procedure will to be discussed in chapter 7.

3.2.1 Basic consideration

The pumping system considered in this study withdraws water from one elevation in a temperature–stratified lake or reservoir and discharges it to another elevation in the form of a buoyant jet as shown in Fig. 3.6. The fluid motion created by the pumping system is essentially a buoyant jet generated at the discharge and a selective withdrawal layer in a stratified environment at the intake. The pumping system is characterized by its properties of transport to and from the stratified ambient water. The buoyancy of the jet, positive or negative with respect to the surrounding fluid, causes it to move upward or downward.

In a temperature–stratified environment, a buoyant jet does not always extend to the surface (Gu and Stefan, 1987). After reaching the maximum height of rise, the jet flow spreads horizontally and intrudes into the ambient fluid at its equilibrium level. Essentially, the buoyant jet entrains fluid from the ambient along its trajectory and delivers this fluid to a different elevation in the ambient. In addition, the shear at the interface of the intruding layer and the ambient fluid at the equilibrium level will enhance the turbulent mixing in this region. Moreover, circulation patterns may be established by the entrainment of fluid and deliverance of fluid by the jet.

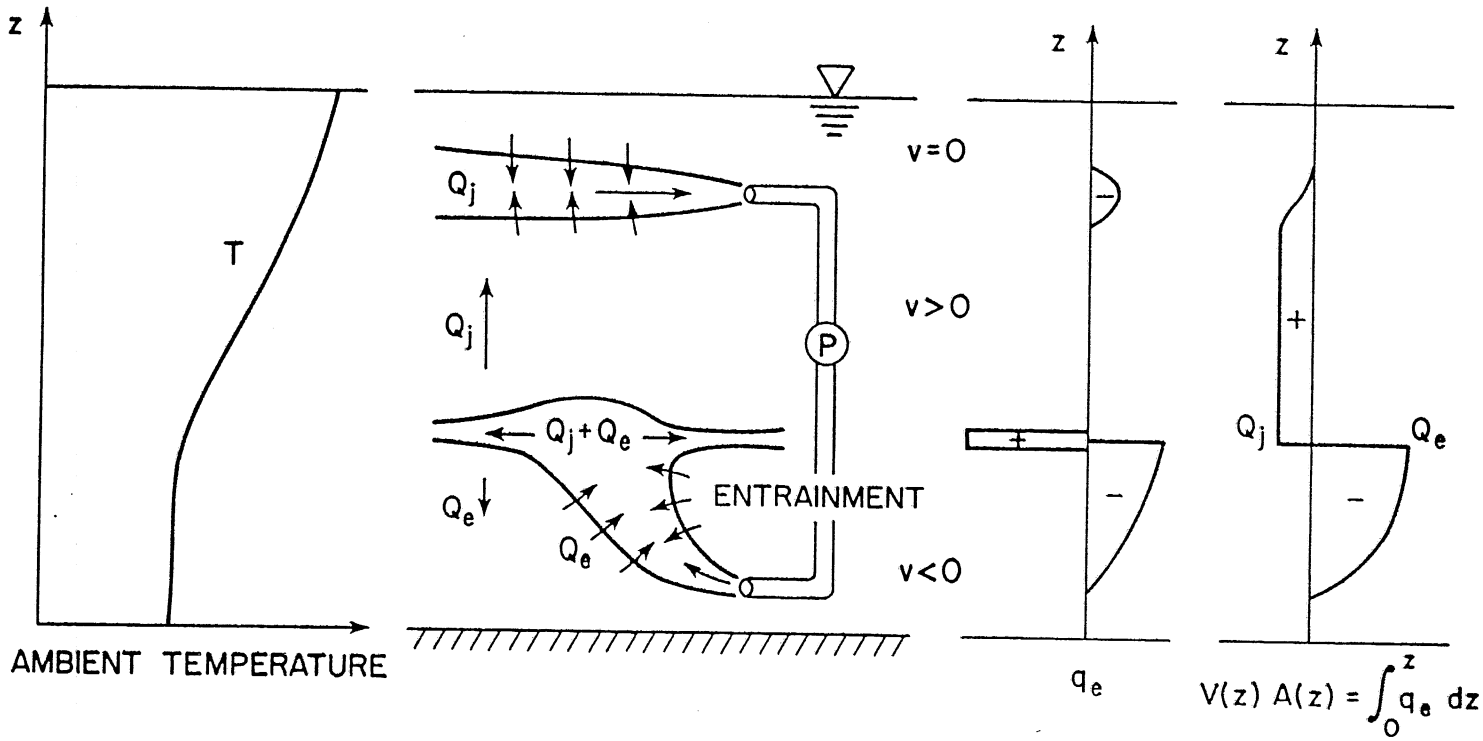

Fig. 3.6 Schematic diagram of a pumping system in a temperature–stratified lake with vertical distributions of q_e and v

3.2.2 Governing equations

A one–dimensional simulation model is developed to predict the global behavior of mixing which is reflected by the changes in temperature stratification during the mixing process. For the simulation model several assumptions are made:

1) A closed system for the stratified lake or reservoir is assumed. Mass in the system is conserved. There is no energy exchange through the boundaries, except those required by the pumping system.

2) The surfaces of constant temperature (or isothermal surfaces) of the stratified water are assumed to be horizontal planes.

3) The buoyant jet and withdrawal layer are the only components of the mixing process that require simulation (Fig. 3.6). The natural mixing induced by external factors (heat and wind) is considered to be small.

For the simulation a stratified lake or reservoir is viewed as a one–dimensional system with the only space coordinate, z, in the vertical direction. The horizontal cross–sectional area, A, is a function of z, the vertical elevation. The relationship between A and z is assumed to be known. The pumping system removes fluid from the surrounding water body at the withdrawal elevations and then injects it back into the ambient at other elevations. The volume rate of flow per unit depth into or from the ambient water body at a given elevation is $q_e(z,t)$. It is positive for fluid delivered into the ambient and negative for fluid entrained from the ambient. An effective transport velocity $v(z,t)$ is introduced to characterize the vertical movement of fluid at a given elevation.

The governing partial differential equations are derived from the basic equations, continuity and thermal energy equations, with consideration of above assumptions. Conservation of mass leads to continuity equation

$$\frac{\partial u}{\partial x} + \frac{1}{A}\frac{\partial (Av)}{\partial z} = 0 \tag{3.15}$$

Conservation of heat requires that

$$\frac{\partial T}{\partial t} + v\frac{\partial T}{\partial z} = 0 \tag{3.16}$$

Integration of the continuity equation gives

$$v(z) = -\frac{1}{A}\int_0^z q_e(\xi)\, d\xi \tag{3.17}$$

where q_e is entrainment flow rate which is calculated in nearfield model.

The entrainment into the jet, q_e, is the change in volume flux along distance. The boundary conditions at upper and lower boundaries are the heat fluxes equal to zero, i.e., $\frac{\partial T}{\partial z} = 0$.

The determination of q_e as a function of z at a given time requires the knowledge of the behavior of the buoyant jet and withdrawal layer. The farfield 1–D mixing model developed here is coupled with the nearfield integral jet model to give an 1–D jet–mixing simulation model.

3.2.3 Buoyant jet mechanics

The analysis of buoyant jets in stratified ambients follows the classical concepts of integral modelling presented by Hirst (1971), Kotsovinos (1977) and Fox (1970). An expanded version described in section 3.1 is used here and combined with the mixing model. The integral model predicts the main jet variables, specifically jet centerline velocity, u_m, half width of the jet, b, and centerline temperature dufference, ΔT_m. From the jet flow analysis the entrainment q_e can be calculated as a function of elevation z.

The buoyant jet reaches a maximum height of rise at which the fluid in the jet is negatively buoyant with respect to the ambient fluid at that elevation. This is the elevation of zero vertical momentum. The fluid sinks back slightly to its eqilibrium level and spreads horizontally into the ambient. It can be seen that the transport velocity v is positive above the equilibrium level and negative below.

The calculation of trajectory and the neutral point, i.e. the elevation at which $\Delta T_m = 0$, and the maximum height, provides information for locating the elevation over which fluid is discharged back into the ambient, the equilibrium level. Ditmars (1970) suggested that the location of the equilibrium level for the buoyant jet could be approximated by the elevation at which the centerline temperature of the jet equals to the temperature of the fluid in the ambient, i.e., neutral buoyancy ($\Delta T_m = 0$). However, the "real" jet continues above this elevation due to vertical momentum before coming down to spread out at the equilibrium level. Mixing due to entrainment occurs as the fluid reaches this level from the elevation of neutral buoyancy, changing direction at the jet top. The equilibrium level is difficult to predict as the similarity analysis breaks down here and the mixing that occurs is complicated. An elevation somewhere between the point of neutral buoyancy and the maximum height of rise may be more representative of the equilibrium level

$$z_e = C_z(z_m - z_n) + z_n \tag{3.18}$$

where C_z is a coefficient and $0.0 \leq C_z \leq 1.0$. Coefficient C_z is equal to 0 if the neutral point is chosen as the equilibrium level, and 1.0 for $z_e = z_m$.

Integration of the continuity equation for a round jet gives

$$\frac{d(\pi u_m b^2)}{ds} = 2\pi\alpha u_m b \tag{3.19}$$

From the entrainment principle, it follows that

$$q_e = -2\pi\alpha u_m b \tag{3.20}$$

The integral, $\int_0^z q_e(\xi)d\xi$ in Eq. 3.17 is the summation of all the jet entrainment up to the elevation z. This is simply the volume flux at z minus the initial fluid discharge, i.e.

$$\int_0^z q_e(\xi)d\xi = -\pi u_m(z)b^2(z) + Q_j \tag{3.21}$$

where Q_j = the jet discharge at the origin. Then

$$v(z) = -\frac{\pi u_m(z)b^2(z) - Q_j}{A(z)} \tag{3.22}$$

over the trajectory of the buoyant jet only. Outside the jet region, between the (equilibrium) level of neutral buoyancy of the jet and the bottom of the withdrawal layer, there is no transport of fluid between the ambient and the jet or withdrawal layer. The integration of q_e from $z = 0$ to any elevation in this zone equals Q_j. The vertical transport velocity in this zone is therefore

$$v(z) = \frac{Q_j}{A(z)} \tag{3.23}$$

There is no fluid transport between the top of the withdrawal and the water surface. The integral of q_e from $z = 0$ to the top of the withdrawal layer equals zero, therefore v is zero above the top.

3.2.4 Selective withdrawal from stratified fluids

The thickness of the selective withdrawal layer and the distribution of velocity cross the layer are required to determine q_e in this region. Brooks and Koh (1969) gave detailed information on the development of theoretical models for selective withdrawal in stratified impoundments. More recently a summary of existing methods was given by Smith et al. (1987). Smith et al. presented improved description of selective withdrawal through point sinks and developed a more general expression which generalizes the established equations by using the concepts of "withdrawal angle" and symmetry.

The flow is considered to be steady and 2–dimensional. Following experiments performed by Debler and Yih (1958) the inviscid and nondiffusive withdrawal layer for a linearly stratified lake or reservoir were expressed as the function of discharge per unit width, q, and density gradient, $d\rho_a/dz$, which is essentially a near–sink solution. Since q is involved, this may be applicable only for a line sink. The expression for the thickness of withdrawal layer for a point sink is based on the general equation given by Smith et al. (1987)

Selective withdrawal layers in lakes or reservoirs are likely to be turbulent due to their large scale or large Reynolds numbers. The solution for turbulent, diffusive flow presented by Brooks and Koh (1969) is used for the calculation of thickness of a turbulent withdrawal layer at the great distance from the sink.

Expressions for the vertical transport velocity in the withdrawal layer, v, were derived by Ditmars (1970) using Koh's similarity solution for velocity distribution.

3.2.5 Solution of the governing equations

The temperature profiles at any time during mixing for a given pumping system and initial profile can be obtained by a numerical solution of the governing equations (Eqs. 3.17 and 3.18), employing the mechanics of buoyant jets and withdrawal. A finite difference technique is adopted for the numerical solution.

The vertical transport velocity, v, is a function of time and must be calculated numerically in the buoyant jet region for a given temperature profile. Because the temperature profile must be known for v, an explicit scheme for the finite difference form of Eq. 3.17 is required.

The time step was chosen arbitrarily about or less 0.001 V/Q_j. The space step was selected according to the Courant stability criterion.

3.3 Sensitivity analysis

Sensitivity of the jet model and mixing model is studied to provide information on the magnitude of change in the simulated value of a jet variable or a mixing parameter, for a given change in an empirical coefficient. In the sensitivity analysis, each empirical coefficient is changed over some range of values which were suggested previously based on theoretical studies and laboratory experiments. The values of empirical coefficients are adjusted to a certain percent of the standard values which are fixed. Standard values of dispersion ratio, λ and shear–stress integral, I were set equal to 1.16 and 0.009 for round jets and 1.2 and 0.025 for slot jets, respectively. A value of 0.5 was chosen for the standard equilibrium level coefficient, C_z. In the sensitivity analysis, λ and I were adjusted to 60 to 140 percent of the standard values and C_z varied from 0.0 to 1.0. The relative perturbation is expressed as

$$P^* = \frac{P - P_0}{P_0} \tag{3.24}$$

where P = adjusted value of a empirical coefficient and P_0 = standard value of P. The difference between the standard simulation and the perturbed result is expressed in a deviance function

$$F^* = \frac{F - F_0}{F_0} \tag{3.25}$$

where F^* = deviation estimate, F = perturbed value of a jet or mixing parameter corresponding to P and F_0 = value from standard simulation. The deviance function used here is simply a measure of relative deviation.

In this study, sensitivity of the jet mixing model to the choice of empirical coefficient values is represented by the ratio of the relative deviation of the solution for a dependant variable, i.e. the jet and mixing parameter, to the relative variation of the empirical coefficient, F^*/P^*. Analyzed were jet trajectories including the maximum height, z_m, the neutral point, z_n, and the equilibrium level, z_e, the total volume of entrainment, E, temperature profiles and mixing process (percent mixed). Horizontal ($\theta = 0°$), vertical ($\theta = 90°$) and incline ($\theta = 45°$) jets with $2 \leq Fr \leq 50$ and $20 \leq St \leq 200$ were considered.

Generalized results from the sensitivity analysis for z_e and E responding to changes in λ are presented in Fig. 3.7. The sensitivity plotted in the figure is an averaged value over the range of variation of the empirical coefficient. It is shown that the sensitivity ratio is from 0.22 to 0.4 for E and from –0.15 to –0.42 for z_e. The relative deviation of solutions for the jet and mixing parameters, z_e and E, is within 16%. The sensitivity analysis indicated that the jet model is more sensitive to the shear–stress integral, I, with respect to E, than to the dispersion ratio, λ. Fig. 3.8 suggested that the sensitivity ratio for E to I is from 0.2 to 0.6. The relative deviation of E is in the range of 0 to 25%. It can also be seen from Fig. 3.7 and Fig. 3.8 that the jet model is more sensitive to λ and I for round jets than for slot jets. The variation of sensitivity ratio with densimetric Froude number, Fr, and stratification number, St, for $\theta = 0°$ and $\theta = 45°$ are shown in Figs. 3.9 and 3.10, respectively. The effects of Fr on model sensitivity is significant as indicated. It is obvious that model sensitivity in z_e to λ increases with larger St (weaker stratification). The sensitivity to I does not change considerably for different St.

Figs. 3.11–3.14 show the detailed results from the sensitivity analysis of the jet model for a round jet with $\theta = 2.8°$, Fr = 13 and St = 113. Numerical simulations with the jet model were performed to investigate variations of the distribution of dimensionless entrainment, q_e/U_oB_o, and jet centerline trajectory with different λ and I. Figs. 3.11 and 3.12 suggested that entrainment distribution is quite sensitive to both λ and I but the

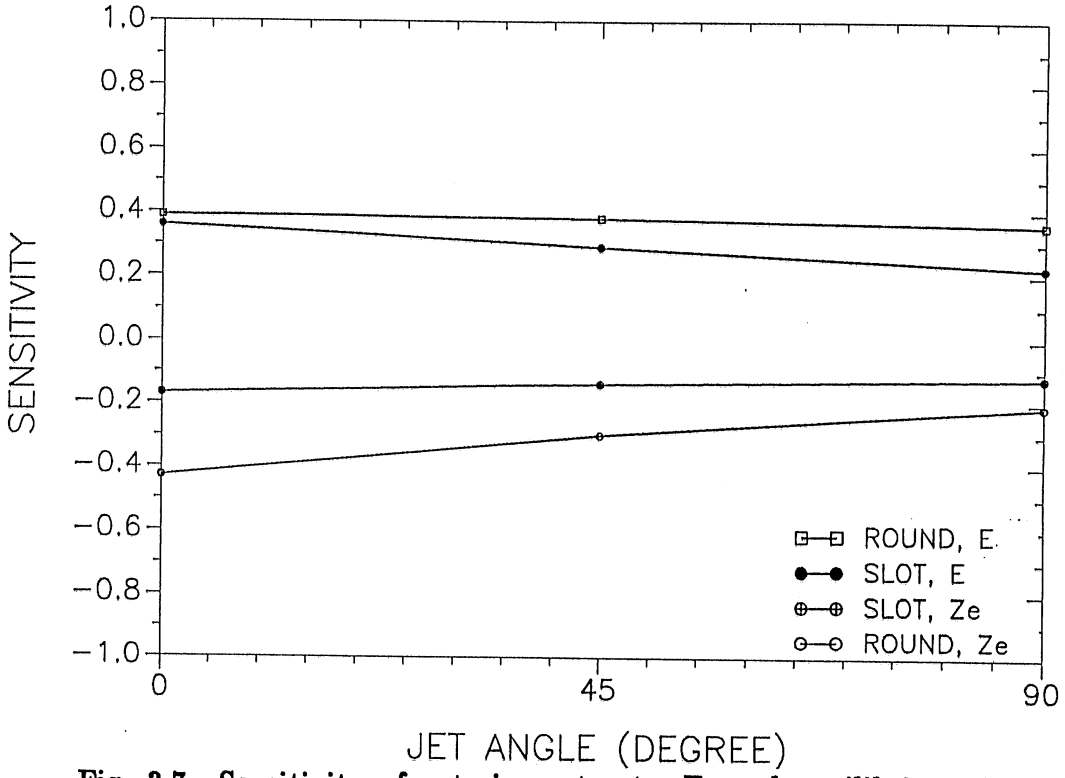

Fig. 3.7 Sensitivity of entrainment rate, E, and equilibrium depth, z_e, to dispersion ratio, λ

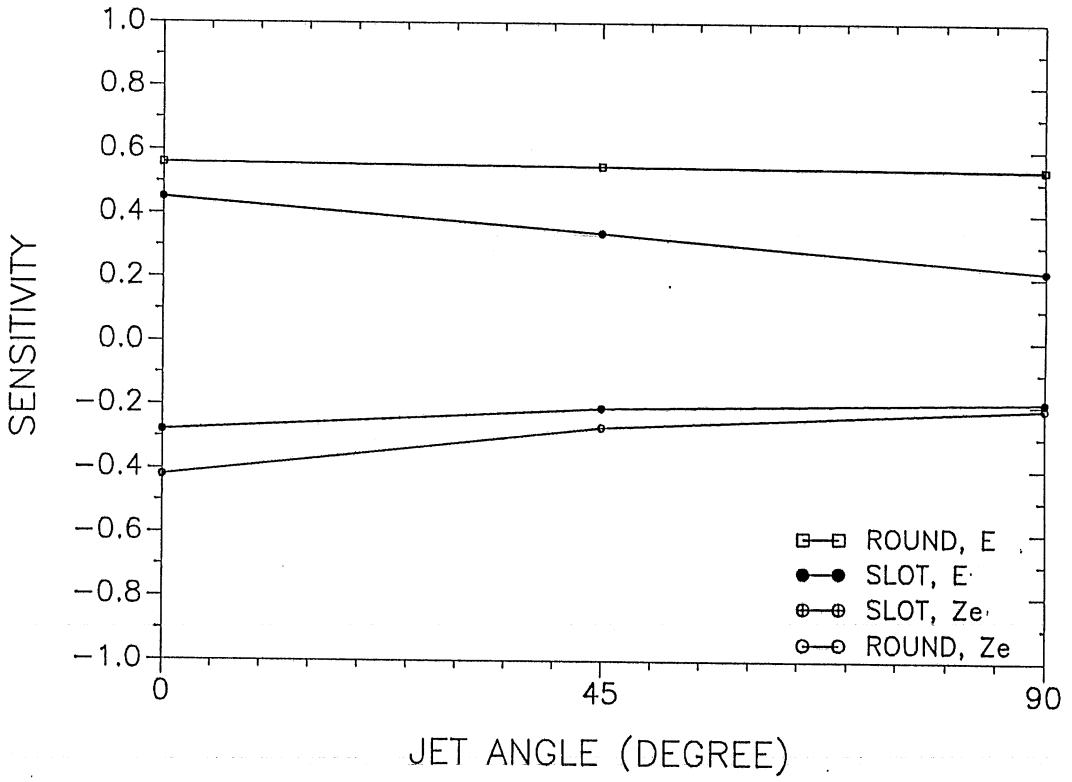

Fig. 3.8 Sensitivity of entrainment rate, E, and equilibrium depth, z_e, to shear–stress integral, I

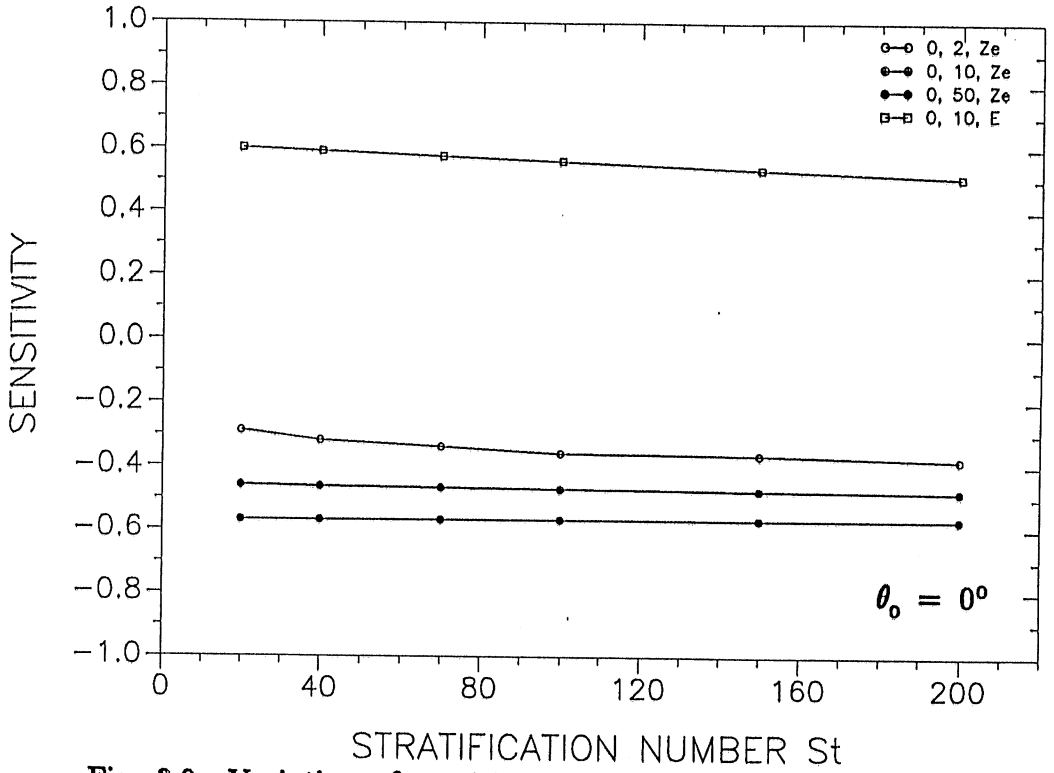

Fig. 3.9 Variation of sensitivity of z_e and E to I with Fr and St

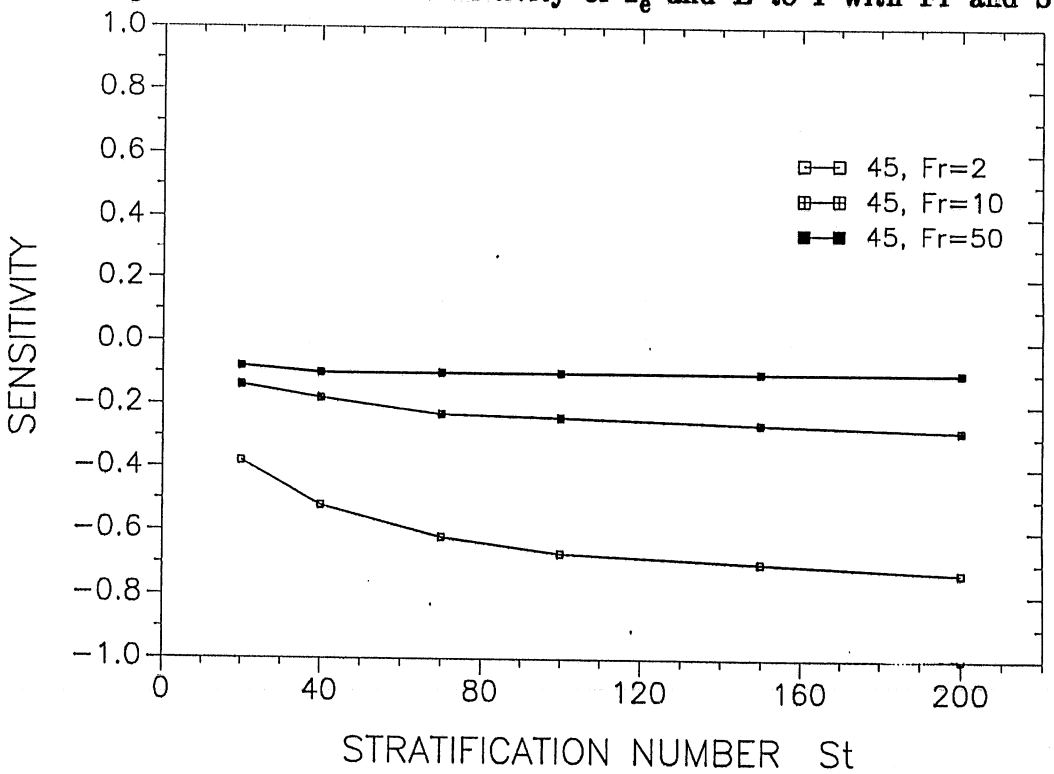

Fig. 3.10 Variation of sensitivity of z_e to λ with Fr and St: round jets, $\theta_o = 45^o$

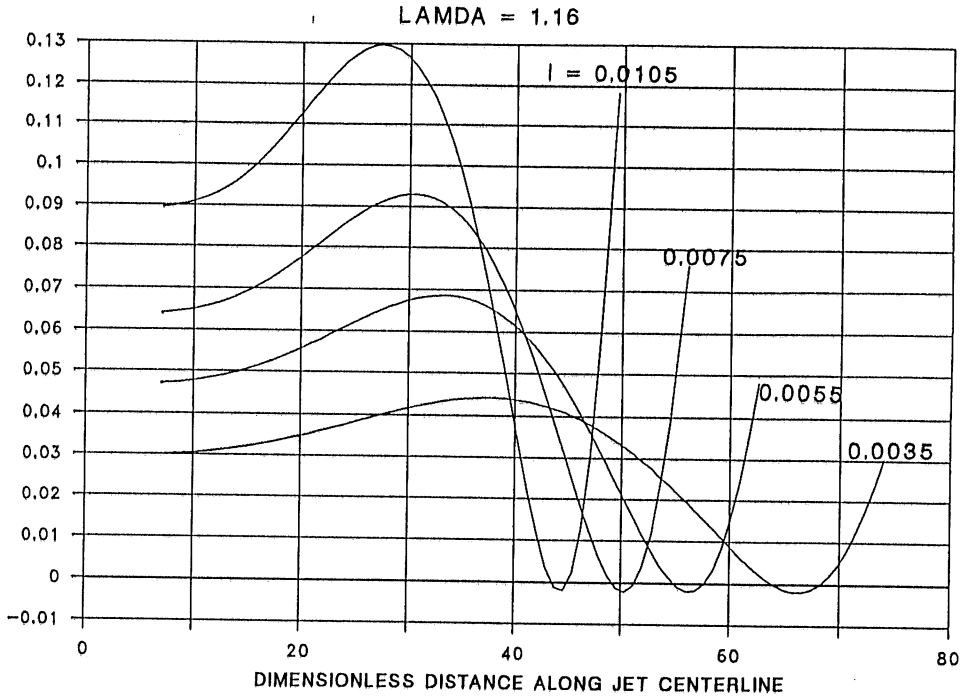

Fig. 3.11 Variation of distribution of entrainment rate along centerline of a round jet with I: $\lambda = 1.16$, $\theta_0 = 2.8^\circ$, Fr = 13, St = 113

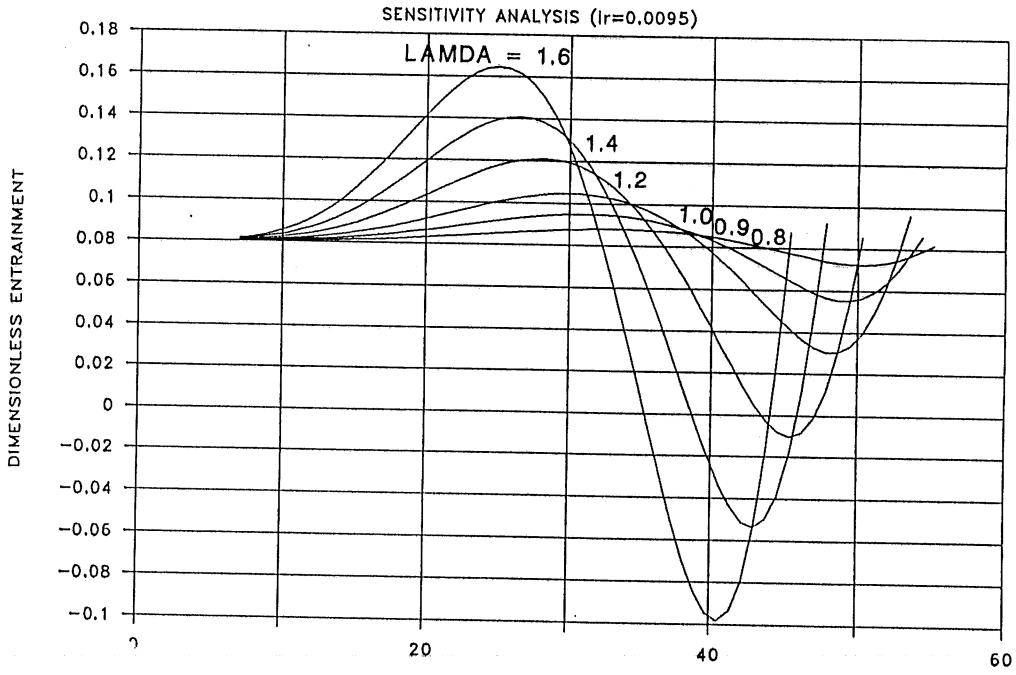

Fig. 3.12 Variation of distribution of entrainment rate along centerline of a round jet with λ: I = .0095, $\theta_0 = 2.8^\circ$, Fr = 13, St = 113

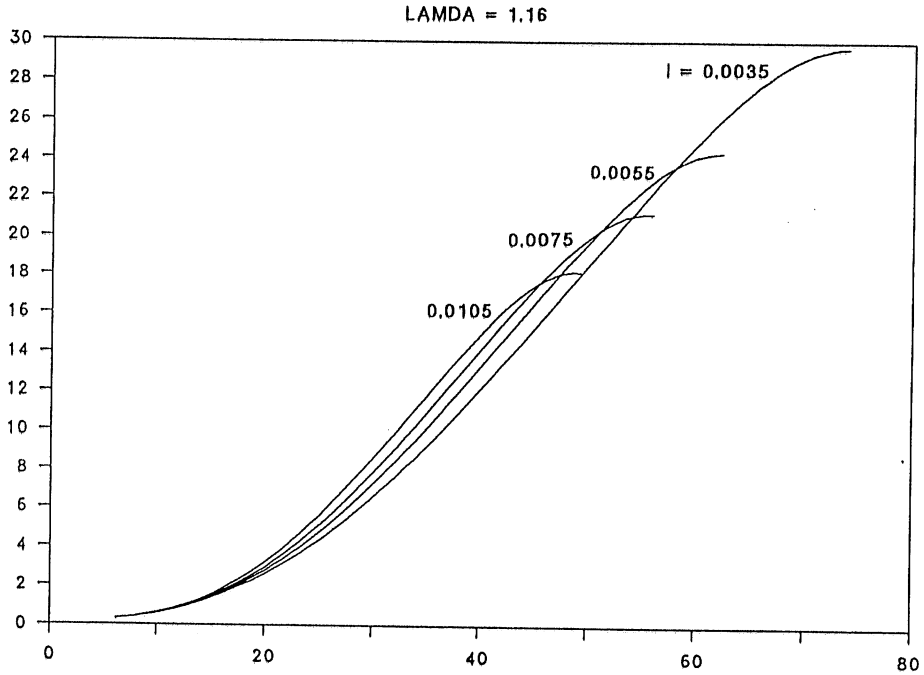

Fig. 3.13 Variation of jet centerline of a round jet with I: $\lambda = 1.16$, $\theta_0 = 2.8^0$, Fr = 13, St = 113

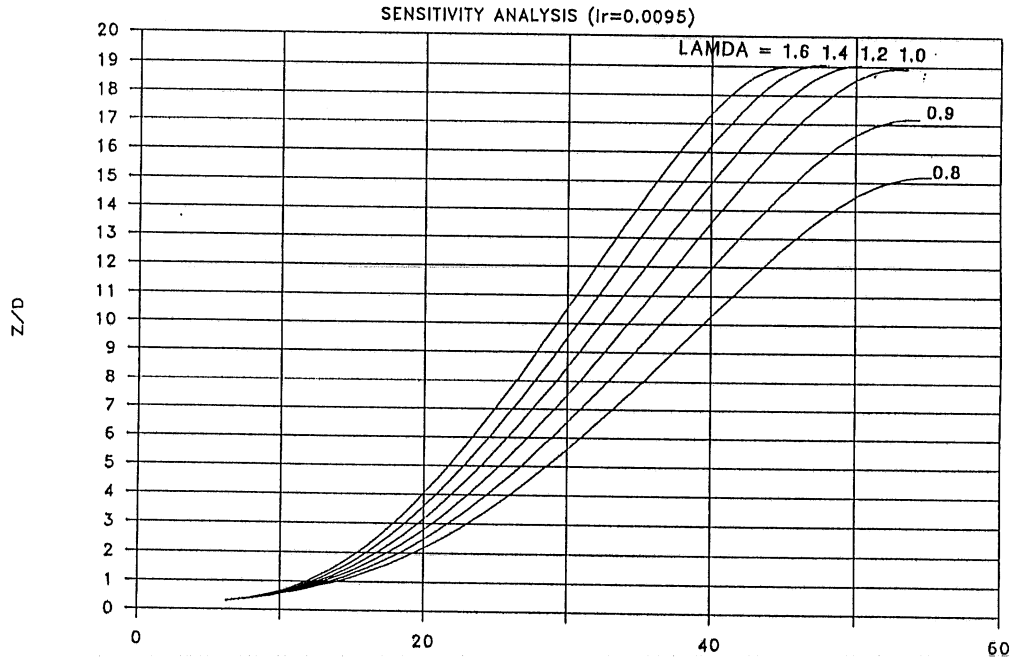

Fig. 3.14 Variation of jet centerline of a round jet with λ: I = 0.0095, $\theta_0 = 2.8^0$, Fr = 13, St = 113

deviation of total entrainment, i.e the integration along jet centerline, is smaller than the change in distribution. The jet centerline trajectory is insensitive to I (Fig. 3.13). However, the maximum height is quite sensitive to I. Fig. 3.14 indicates that the change in λ results in a large shift of the jet centerline and a small difference in z_m.

Mixing by a jet is dependent on the total amount of entrainment, E, and the equilibrium level, z_e (Eq. 3.18). Effects of λ and I on E and z_e had been investigated through the sensitivity analysis described above. Since the equilibrium level coefficient is arbitrarily selected (0.0 to 1.0), the sensitivity of the mixing model to C_z was examined using Vesuvius Lake data, Ohio (Irwin, et al., 1966). Initial values of Fr, St and θ are 26, 30 and 0°, respectively. Temperature profiles measured during the field experiments and predicted by the simulation model for different values of C_z, 0.1, 0.25 and 0.5, are shown in Fig. 3.15. It can be seen that an increase of C_z from 0.1 to 0.25 results in considerably more mixing, but the model is insensitive to large C_z (e.g. 0.5 to 1.0). A value of 0.25 for C_z is considered as giving the best match.

Effects of λ, I and C_z on the jet mixing process reflected by variation of the "percent mixed" value with time (see chapter 6 for definition) are investigated for a horizontal jet with Fr = 5.7 and St = 52 as shown in Figs. 3.16–3.18. Fig. 3.19 presents variations of $(z_m - z_n)/z_m$ with Fr and St. The sensitivity analysis indicated that the mixing process is not very sensitive to the empirical coefficients. The maximum deviation of the solution is within 15%.

Based on the sensitivity analysis it was found that previously suggested ranges of values for empirical coefficients could be used for the jet mixing simulation model with a maximum solution deviation of 20% for jet trajectory, 25% for entrainment and 15% for the mixing process. If the model is applied without available data for calibration of the model to determine λ and I, the commonly used values are recommended. They are λ = 1.16 and 0.9 and I = 0.01 and 0.02 for round jets and slot jets, respectively. In general, a value of 0.25 for C_z is suggested if a fitting technique is not used for practical application of the mixing model.

3.4 Vertical jets in shallow water

3.4.1 Analysis of overshooting

A vertical jet can reach the water surface of a shallow lake or pond, and then a spreading and possibly plunging layer is formed where the typical jet flow pattern is lost. This is illustrated in Fig. 3.20 schematically. The integral jet–mixng model developed in Section 3.1 and 3.2 does not simulate the surface impingement and plunging flow because similarity assumptions doesd not hold in this region. There is added entrainment and mixing in the stratified water body that is not simulated by an integral jet model.

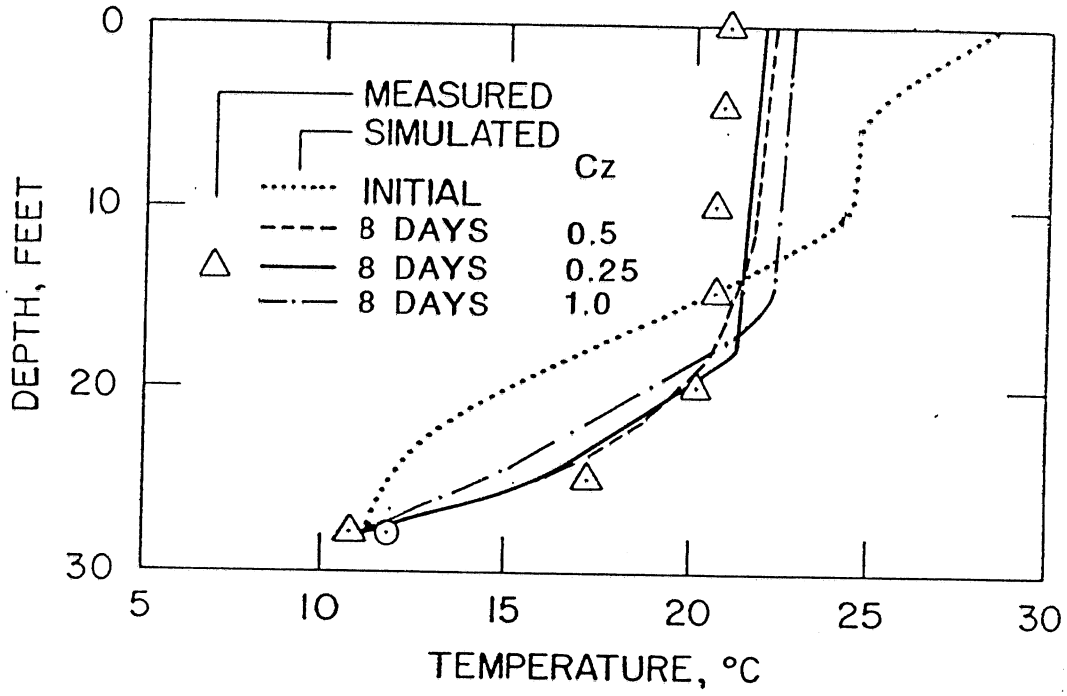

Fig. 3.15 Temperature profiles with jet mixing measured in Versuvius Lake, Ohio, by Irwin, et al (1986) and presently predicted by the 1–D mixing model using different values of C_z

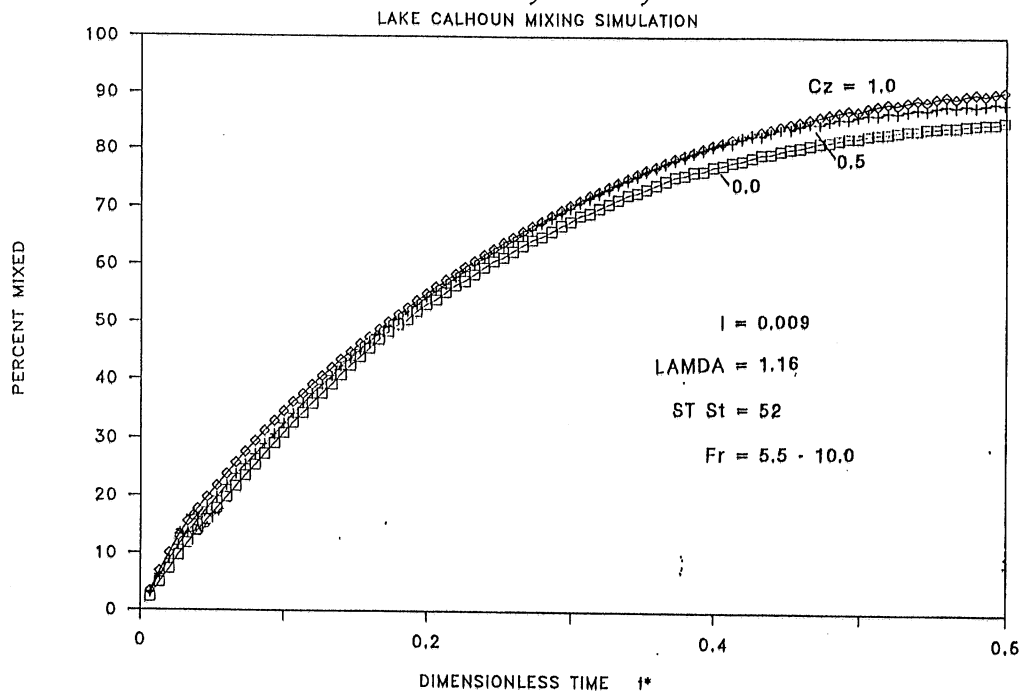

Fig. 3.16 Effects of C_z on jet mixing process

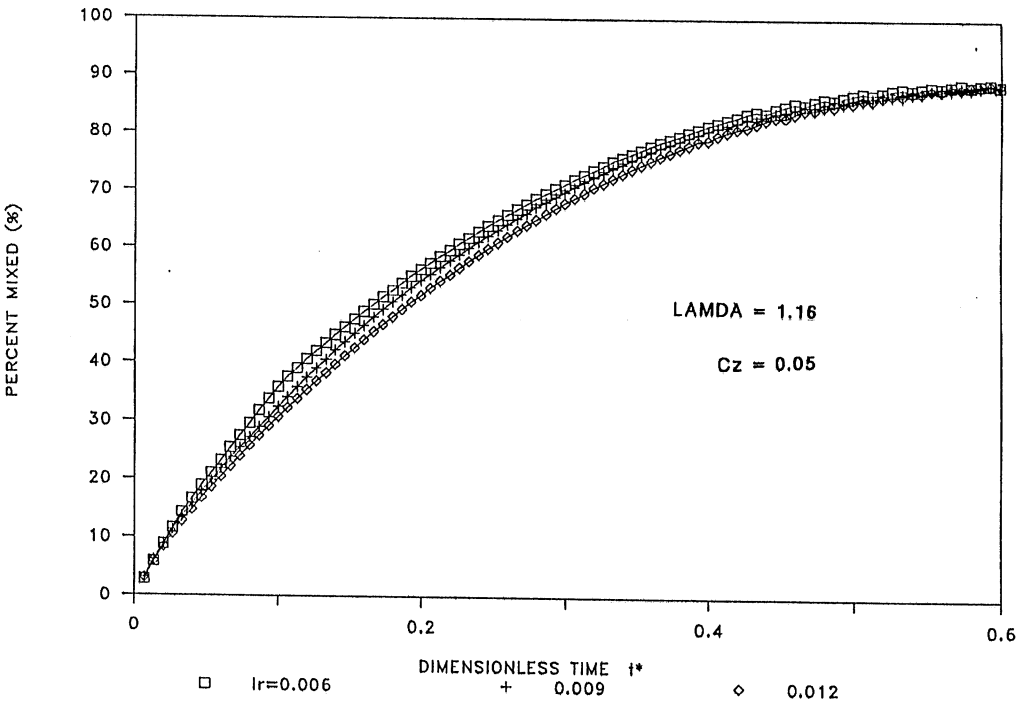

Fig. 3.17 Effects of I on jet mixing process

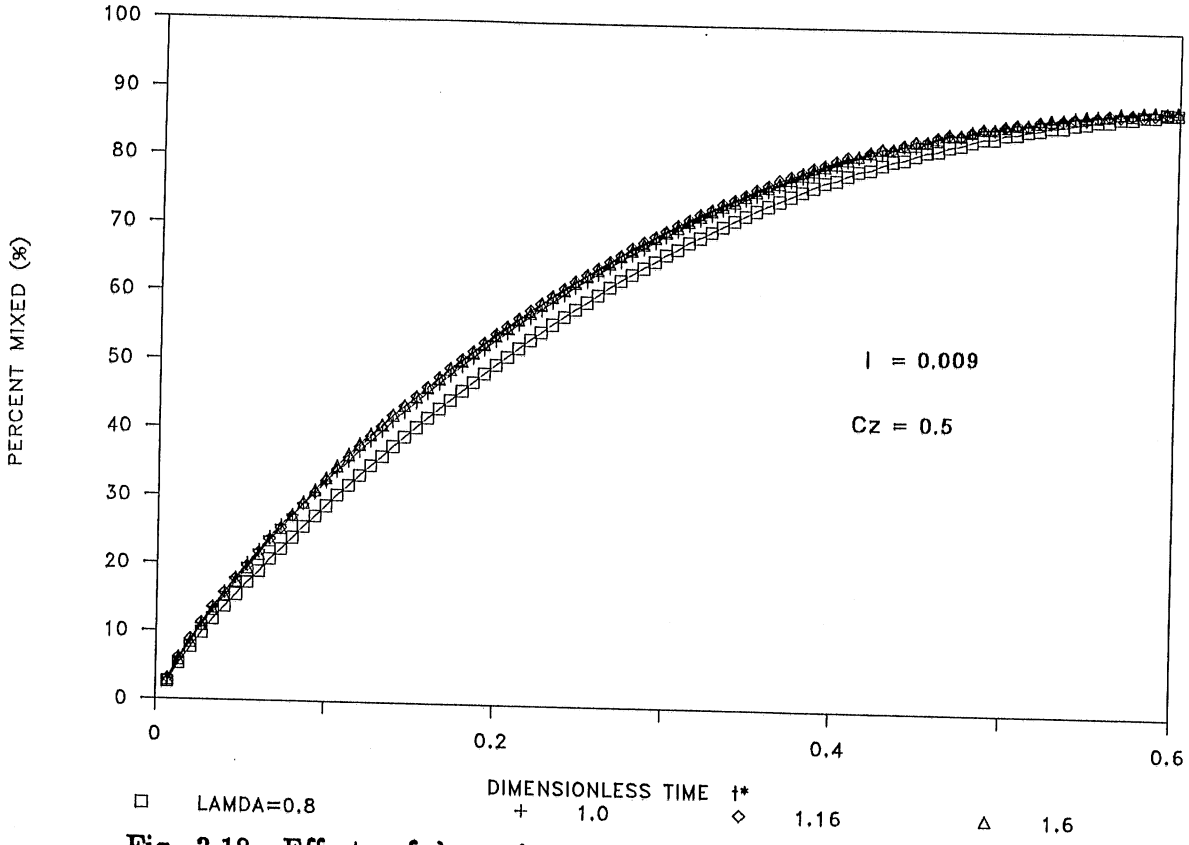

Fig. 3.18 Effects of λ on jet mixing process

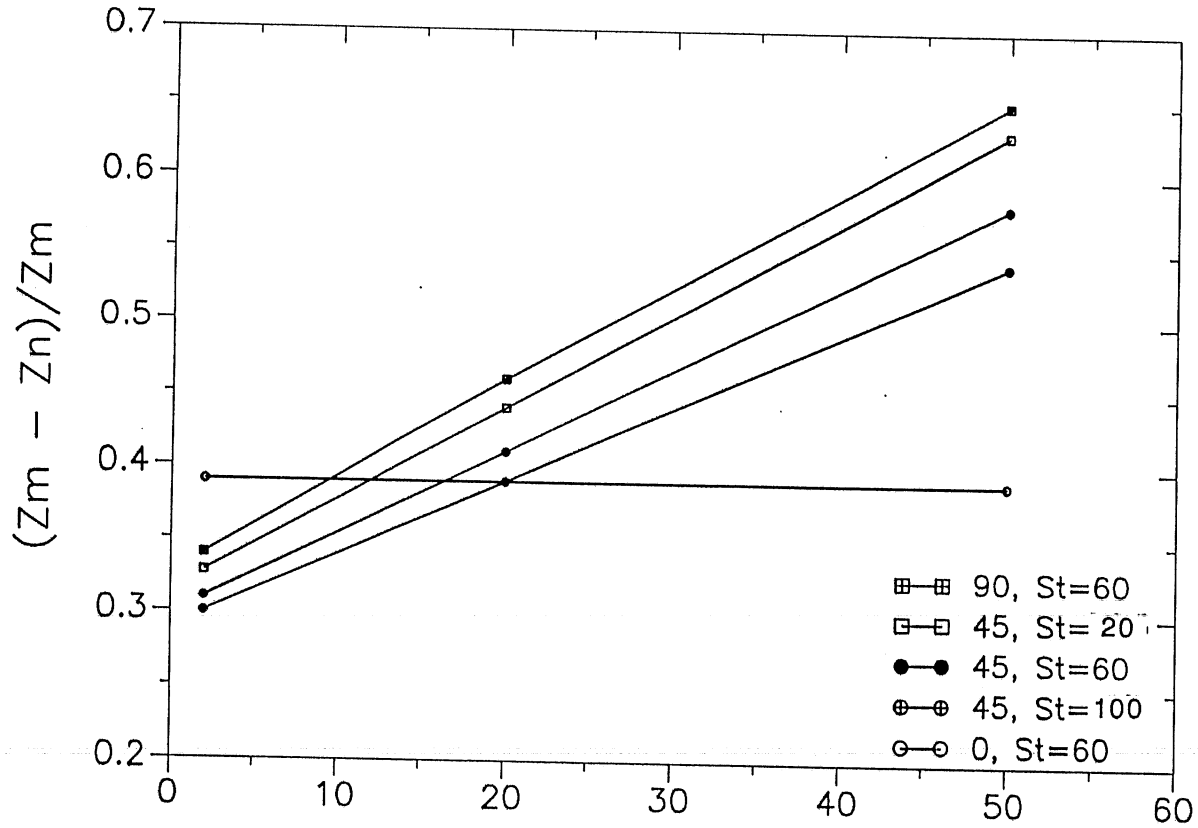

Fig. 3.19 Variation of $(z_m - z_n)/z_m$ with Fr and St for round jets

The requirement for the application of the integral jet model is that the jet remain submerged, i.e., $z_t < H$, where z_t denotes the distance between the discharge and the jet top and H denotes the distance between the discharge and the water surface. Low densimetric Froude numbers are required since higher Fr gives rise to larger z_t, if the jet is vertical (Fig. 3.21). A critical densimetric Froude number Fr_c is introduced here which satisfies the condition $z_t = H$ at $Fr = Fr_c$. Fr_c can be estimated by applying the experimentally determined equations for the terminal height of jet rise. Experimental results (Wong and Wright, 1988) for vertical round buoyant jets give the following empirical equations:

For plume–like discharge ($\ell_M/\ell_b < 1$):

$$\frac{z_t}{\ell_b} = 4.5 \tag{3.26}$$

For jet–like discharge ($\ell_M/\ell_b > 2$):

$$\frac{z_t}{\ell_m} = 3.6 \tag{3.27}$$

where ℓ_M, ℓ_b, and ℓ_m are characteristic length scales. They are defined by $\ell_M = M^{3/4}/B^{1/2}$, $\ell_b = B^{1/4}/\epsilon_g^{3/8}$ and $\ell_m = (M\epsilon_g)^{1/4}$, in which Q, M, and B are the source volume, momentum and buoyancy flux of the source, respectively ($Q = \pi D_o^2 U_o/4$, $M = QU_o$ and $B = Q\ g\ \Delta\rho_o/\rho_o$).

The critical densimetric Froude number Fr_c is, therefore obtained as follows:

$$Fr_c = 0.0031\ H^4/(D_o^{5/2}\ L^{3/2}) \tag{3.28}$$

for plume–like flow;

$$Fr_c = 0.087\ H^2/(D_o^{3/2}\ L^{1/2}) \tag{3.29}$$

and for jet–like flow. Eqs. 3.28 and 3.29 are for a pumping system with a jet outlet diameter D_o and a distance between the discharge and the withdrawal L in a linearly stratified fluid (lake or pond) with a depth H.

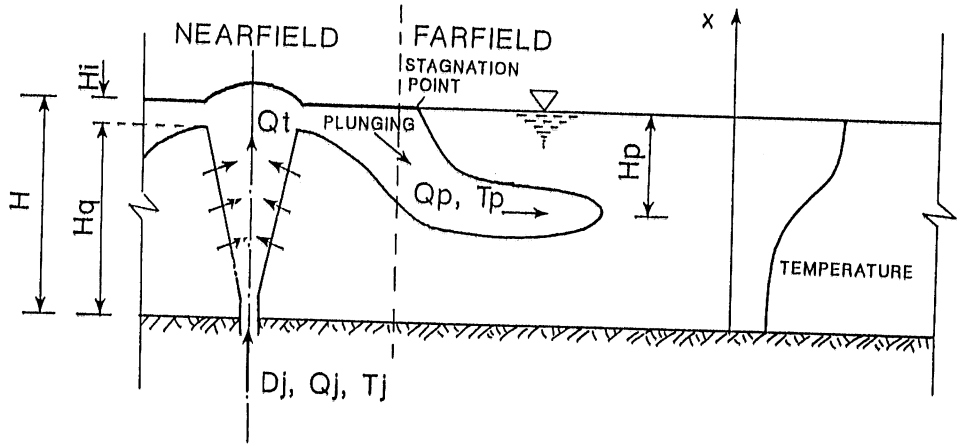

Fig. 3.20 Flow pattern and jet behavior of a wastewater discharge in a shallow pond

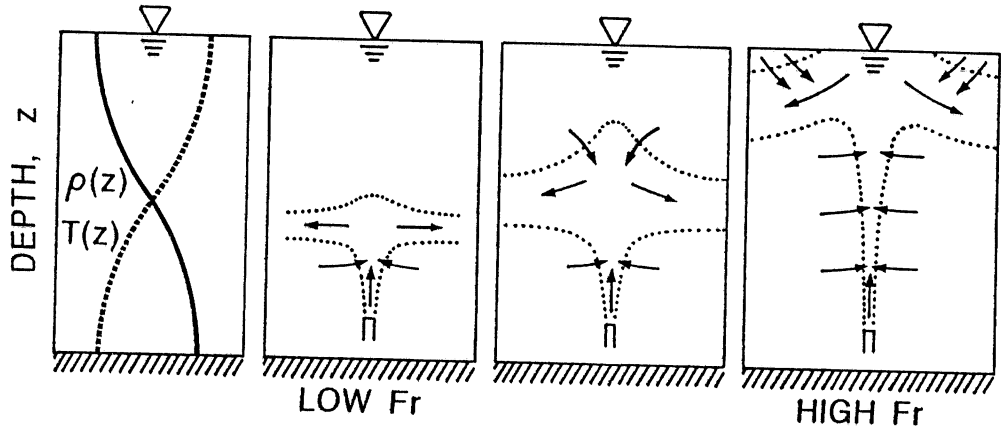

Fig. 3.21 Schematic diagram of vertical jet flow regimes in temperature stratified water.

3.4.2 Stability of the flow

After the jet reaches and overshoots the water surface due to shallow water and high initial momentum, it collapses on the water surface. Following impingement and radial spreading on the water surface, the much diluted inflow sinks (plunges) into the pond (Fig. 3.20). A horizontal intruding–spreading interflow is formed in the layer where buoyancy is neutral, i.e. where inflow density is identical to ambient water density (equilibrium layer). This discharge configuration is termed stable because the discharged water is not recirculated (re–entrained) into the buoyant jet near the jet discharge (Lee, 1980). Based on theoretical and experimental studies of an axisymmetric (round) turbulent buoyant jet discharged vertically into a stagnant shallow water body, Lee (1980) indicated that there would be no recirculation if the jet densimetric Froude number Fr is less than the value

$$Fr_s = 4.6 \frac{H}{D_j} \tag{3.30}$$

If Fr is greater than Fr_s due to either shallow water (H) or low buoyancy ($\Delta\rho$) or high initial momentum (U_j), an unstable discharge configuration is formed. In this situation, recirculation cells are set up near the jet discharge, leading to re–entrainment into the discharge. It was also suggested by Lee (1980) that in deep water and mider stable discharge conditions, the spreading layer thickness, H_i, on the surface was about one tenth of the total depth (0.1H). Therefore the depth over which jet entrainment contributes to dilution of the jet, H_q, is estimated to be on the order of 0.9H.

3.4.3 The jet entrainment and mixing model

A simplified model for jet entrainment in the nearfield and mixing in the farfield is formulated for incorporation into the pond temperature stratification simulation model. The entrainment rate of ambient water by the vertical jet is determined from the jet flowrate as a function of vertical distance from the orifice (Albertson et al, 1948)

$$\frac{Q}{Q_j} = 1 + 1.0133C_2 \frac{z}{D_j} + 1.9735C_2^2\left(\frac{z}{D_j}\right)^2 \tag{3.31}$$

in which Q = volume flux at height z above the efflux, Q_j = jet discharge, C_2 = coefficient, in the range from 0.081 to 0.111. The total entrainment by the jet over height 0.9H is estimated as

$$Q_e = Q_t - Q_j \tag{3.32}$$

or

$$Q_e = Q_j\left[1.0133C_2 \frac{0.9H}{D_j} + 1.9735C_2^2\left(\frac{0.9H}{D_j}\right)^2\right] \tag{3.33}$$

where Q_t is the total volume flux at $z = 0.9H$. Entrainment from an individual horizontal water layer of thickness Δz is

$$q = \frac{dQ_e}{dz}\,\Delta z \tag{3.34}$$

or in numerical form

$$q_i = Q(z_i + \tfrac{1}{2}\Delta z_i) - Q(z_i - \tfrac{1}{2}\Delta z_i), \qquad i = 1, 2, \ldots, N \tag{3.35}$$

where N = total number of layers contributing to entrainment. It is assumed that there is no entrainment into the plunging–intruding–spreading flow beyond the jet region (nearfield). Flowrate and temperature of the interflow are therefore approximated, respectively, as

$$Q_p = Q_t \tag{3.36}$$

and

$$T_p = \frac{\sum_{i=1}^{N}(q_i\, T_i) + T_j Q_j}{Q_e + Q_j} \tag{3.37}$$

Densities of the interflow and ambinet water are calculated to determine the depth of the interflow layer, H_p, by neutral buoyancy. Generally, density of water in the lake or pond is a function of temperature and concentration of suspended and dissolved solids.

Mixing effects of the inflow jet on the lake or pond stratification are represented by changes in volume and in temperature of each layer due to jet entrainment and interflow deliverance. The volume of each layer in the lake or pond is modified in each timestep by subtracting the water entrained from the layer and adding the interflow to the equilibrium layer. The temperature in the equilibrium layer is modified using temperature of the incoming water weighted by its volume over a computational timestep.

3.5 Summary

A turbulent buoyant jet in a, linearly stratified, stagnant ambient fluid was systematically investigated by the integral–analysis approach, and a general nearfield (1–D) numerical simulation model was developed to predict the jet trajectories, centerline temperature or density and velocity decay, and dilution on the axis of a axisymmetric or plane jet discharged at an arbitrary angle. The basic jet theory and existing knowledge were followed and extended in several ways: 1) effect of density change (buoyancy) and jet curvature on dynamic pressure was considered; 2) an entrainment function was derived from the continuity, tangential momentum and mechanical energy equations; 3) the conservation equation for heat was used in place of conservation of buoyancy and 4) a nonlinear $\rho(T)$ relationship is used. Predictions obtained with the jet model were compared with experimental data.

The mixing effect of a buoyant jet which was created by a pumping system in a stratified basin was examined. Mixing leads to thermal destratification. A farfield mixing model was devised and coupled with the nearfield jet model, and an unsteady 1–D jet–mixing simulation model was developed to predict the mixing processes reflected by changes in the temperature–depth profiles with time. Effects of jet orientation and jet momentum on mixing processes was investigated.

Sensitivity of the jet model and mixing model to empirical coefficients was analyzed. Based on the sensitivity study, values of empirical coefficients are suggested for the situation without data for model calibration.

A special case, a vertical jet in shallow water, was studied. The jet is characterized by its overshooting of the water surface, plunging into depth, and spreading and intruding into an equilibrium layer. A critical jet densimetric Froude number, Fr_c, for determining overshooting or submergence is derived. A simple integral model was developed to simulate mixing produced by the jet in a lake or a pond. Application is made to a wastewater stabilization pond in chapter 6.

To sum up, the main purpose of the integral approach and 1–D models is to describe the gross behavior of the jet flow and mixing for basic understanding and practical application.

Chapter 4 Laboratory Experiments and Verification of 1–D Jet–Mixing Model

4.1 Purpose

Laboratory experiments of the mixing of stratified water by buoyant jets were conducted at St. Anthony Falls Hydraulic Laboratory, University of Minnesota. The laboratory experiments served two main objectives: to verify the validity of the simulation model which predicts the bulk behavior of the mixing process with buoyant jets and to identify those phenomena associated with the mixing process which are not simulated by the model.

Withdrawing water from one level of a temperature–stratified reservoir, pond or lake and reinjection at another elevation (Fig. 1.1) is one of several available methods for artificial destratification (Irwin et al., 1966; Ditmars, 1970; Garton, 1980, Price, 1989, Dortch 1979). By this method, which may be called hydraulic or mechanical destratification, water quality can be significantly influenced.

The physical aspects of the mixing processes created by a single round jet in a stratified ambient were theoretically and investigated in chapter 2 and chapter 3 following earlier work by Ditmars (1970). A simulation model predicting the progression of the temperature profiles in time was developed in chapter 3. Dortch and Holland (1980) conducted laboratory experiments with both horizontal and vertical jets in density–stratified ambients. Their experiments were conducted with jets of high densimetric Froude numbers ($30 < Fr < 1000$).

Experiments for both horizontal and vertical jets of low Froude number ($1 < Fr < 10$) were conducted in this study. The information to be presented in this chapter will emphasize low momentum jets. Experimental results are presented and compared with those predicted by the 1–D jet mixing simulation model. The model predicts only the bulk behavior of the jet flow and mixing process. The main objective of the experiments is to provide data for model validation. The other purpose is to investigate the physical features associated with the jet flow and mixing so as to understand the interaction of water jets with the stratified ambient under various conditions, i.e. different Fr and St numbers. An example of the phenomenon not simulated by the model is the deepening of the thermocline below the diffuser during the mixing process. A dye–flow–visualization study was carried out to investigate the growth of mixing layers and the global behavior of the jet flow. The effects of the discharge Froude number Fr, which was adjusted by varying the flow rate and the temperature difference, ΔT_o, were studied in the visualization.

4.2 Equipment

Experiments were carried out in a rectangular tank with dimensions 1.12 x 1.12 x 1.42 m^3. Main components of the experimental set–up are shown in Fig. 4.1. The tank is glass–walled and insulated . The experimental arrangement included a water pump, hot and cold water sources, a rotameter, temperature probes (thermisters), tubes providing an intake and a discharge, a dye injection apparatus and a computer recording, in five minutes time interval, the temperature profiles.

For horizontal jet experiments the nozzle was located near one wall to get significant distance to the other side of the tank, for vertical jets it was in the center of the tank. The sizes of the discharge tubes and the flowrates of the system for an experiment are selected based on the desired range of Froude number Fr and turbulence level (Re). Since flowrates were restricted by the pump capacity and the tank size, tubes of various diameters were prepared for the experiments. The position of the withdrawal and jet discharge in the tank were varied. A vertical array of temperature probes were calibrated, with a standard deviation of 0.05° C, against a thermometer placed in a constant temperature bath.

4.3 Procedure

Temperature stratification was produced in the tank by using hot and cold water sources. Flow was generated by using a laboratory pump connected to the withdrawal and discharge tube in the tank. Temperature profiles were recorded at regular time intervals (5 minutes) during the mixing process by using an Apple computer connected to the temperature probes. The data were stored immediately on disk.

Temperature–stratified environments were created in the tank by filling with hot water and cold water to produce vertical temperature gradients. The shape of the temperature–depth profile was dependent on the manner in which the tank was filled. The water taken from the source was discharged into the bottom of the tank by using a radial spreader, that dissipates the water jet and minimizes the mixing during spreading. The filling started with the hot water and ended with the cold water. Floating insulate material were spread on the surface of the tank water to reduce heat loss through the surface. The temperature at the water surface tends to move toward the equilibrium temperature if there is no insulate materials on the surface. After a suitable temperature profile was created, the water was then left undisturbed to allow turbulent mixing to die out and hydrostatic equilibrium to be reached before recording the initial temperature profile.

The equilibrium temperature, the air temperature, the initial temperature profile, and the location and size of the withdrawal tube and discharge nozzle were recorded before initiating circulation. Measurements were initiated at the beginning of pumping. The temperature probes were

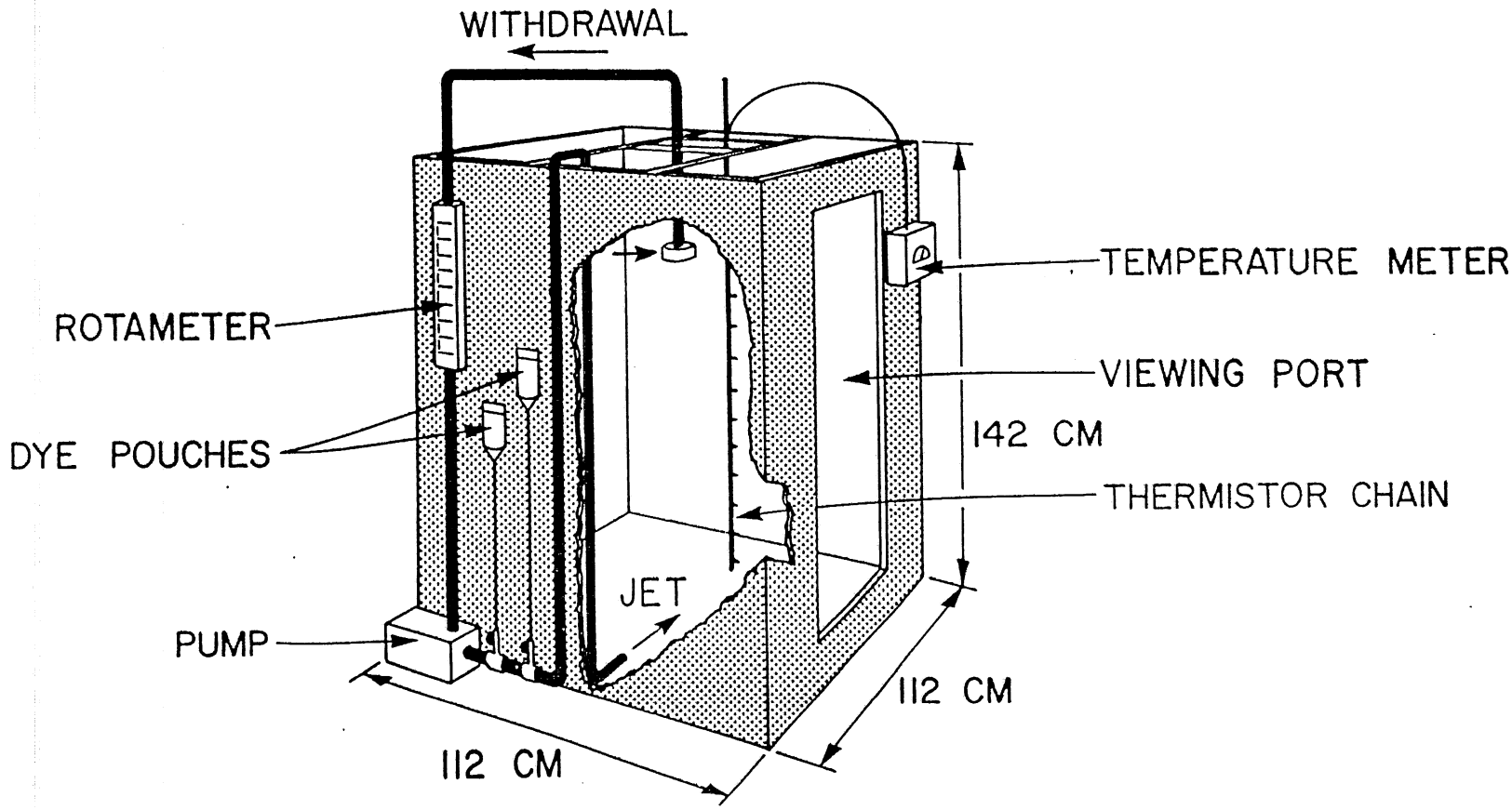

Fig. 4.1 Major equipment components

located near a corner of the tank approximately 25 cm from the insulated wall and far away from the jet. The temperature profiles recorded were considered representative of the farfield.

The development of the mixing layer could be seen in the temperature profiles. Observations of jet trajectories and withdrawal layer were made using dye injection during experiments.

4.4 Experimental results and comparisons with simulations

The independent variables, including location of jet discharge and withdrawal, initial stratification conditions, hydraulic and other characteristic parameters are listed for each experiment in Table 4.1. The experimental data for temperature profiles were taken at time intervals of 5 minutes. Only a few profiles at selected times are presented in the figures. Measured and simulated water temperature profiles after the beginning of the jet discharge are presented and plotted against normalized elevation $z^* = z/L$, where z is the elevation above the centerline of the discharge tube and L is the distance between the discharge and withdrawal tubes. The dimensionless time is defined as $t^* = tQ/(LA)$, where $Q/(LA)$ is the characteristic (residence) time for the system defined as the time required to pump the volume of water, $V = AL$, between the planes of the jet discharge and withdrawal layer.

4.4.1 Horizontal Jets

Sample results from several experiments and numerical simulations for horizontal jets are presented in Figs. 4.2 and 4.3 in the form of elevation–temperature profiles at various times of mixing. More can be found in Gu and Stefan (1987). The model predicts reasonably well the change in the temperature structure of the tank during the mixing process for the experiments performed. Some disagreement is shown at both the water surface and near the discharge level. Discrepancies between the experimental results and those predicted can be explained mostly by simplified nature of the simulation model. In addition, maintaining a closed system during the experiments is difficult. Heat loss at the water surface, despite insulation, contributes to the disagreement between experimental and simulated profiles in the surface region, and at the final stages of mixing when changes due to the pumping system are small but the cumulative heat loss with the environment is significant.

The effect of the walls cannot be ignored when Fr is very large since the jet axis becomes nearly horizontal and the jet impinges on the walls (see Fig. 4.4). It is obvious that the larger the tank and the smaller the Froude number Fr, the less the effect of walls and the better the agreement between the prediction and measurements.

Table 4.1 Summary of experiments with horizontal and vertical jets

Exp. No.	Total depth	Distance between jet and intake	Jet disch. rate	Nozzle (jet) dia-meter	Initial temp. differ-ence	Strati-fication No.	Jet Froude No.	Jet Rey-nolds No.	Jet nozzle length	
	d	L	$Qx10^5$	D_o	ΔT_o	St	Fr	Re	l	V/Q
	(m)	(m)	(m^3/s)	(m)	(°C)				(m)	(h)
1	1.27	1.10	2.60	0.0095	10.7	116	29.1	3500	0.17	15
2	1.27	0.52	0.85	0.0095	14.5	55	8.4	1100	0.17	21
3	1.27	0.72	1.00	0.0095	9.8	76	11.5	1340	0.17	25
4	1.27	0.80	2.95	0.0254	18.3	32	2.0	1500	0.17	8.0
5	1.27	0.80	6.20	0.0254	17.2	32	4.2	3100	0.17	4.5
6	1.27	1.04	4.40	0.0191	14.0	55	7.0	2200	0.19	8.2
7	1.27	0.72	2.75	0.0191	6.3	48	6.4	1800	0.38	9.1
8	1.27	0.72	5.60	0.0191	9.8	48	10.0	3700	0.38	4.5
8L	1.27	0.72	5.60	0.0191	9.8	48	10.0	3700	0.38	4.5
Area of tank $A = 1.12 \times 1.12 = 1.254\ m^2$ Volume $V = A \times L$										

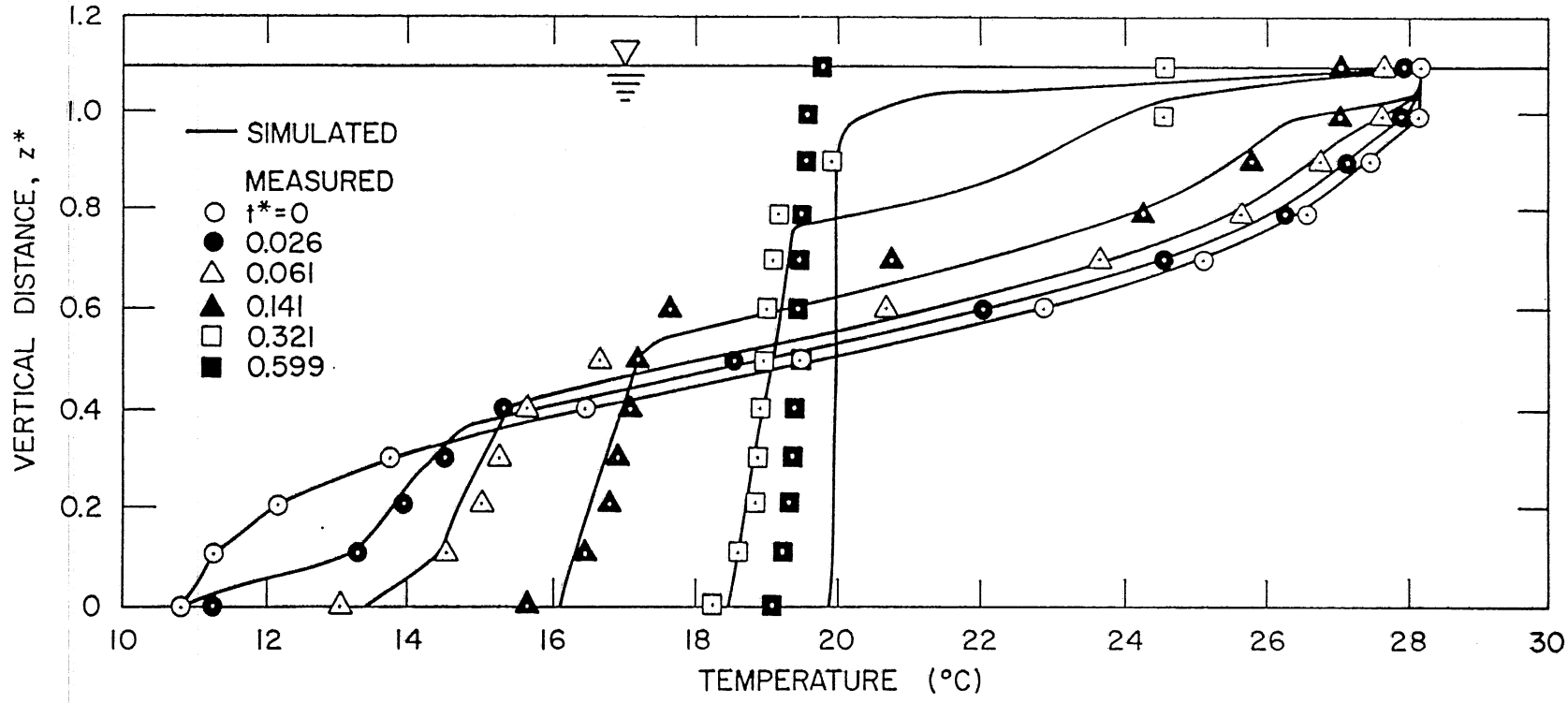

Fig. 4.2 Measured and simulated temperature profiles: Exp. No. 5, $\theta_0 = 0^\circ$

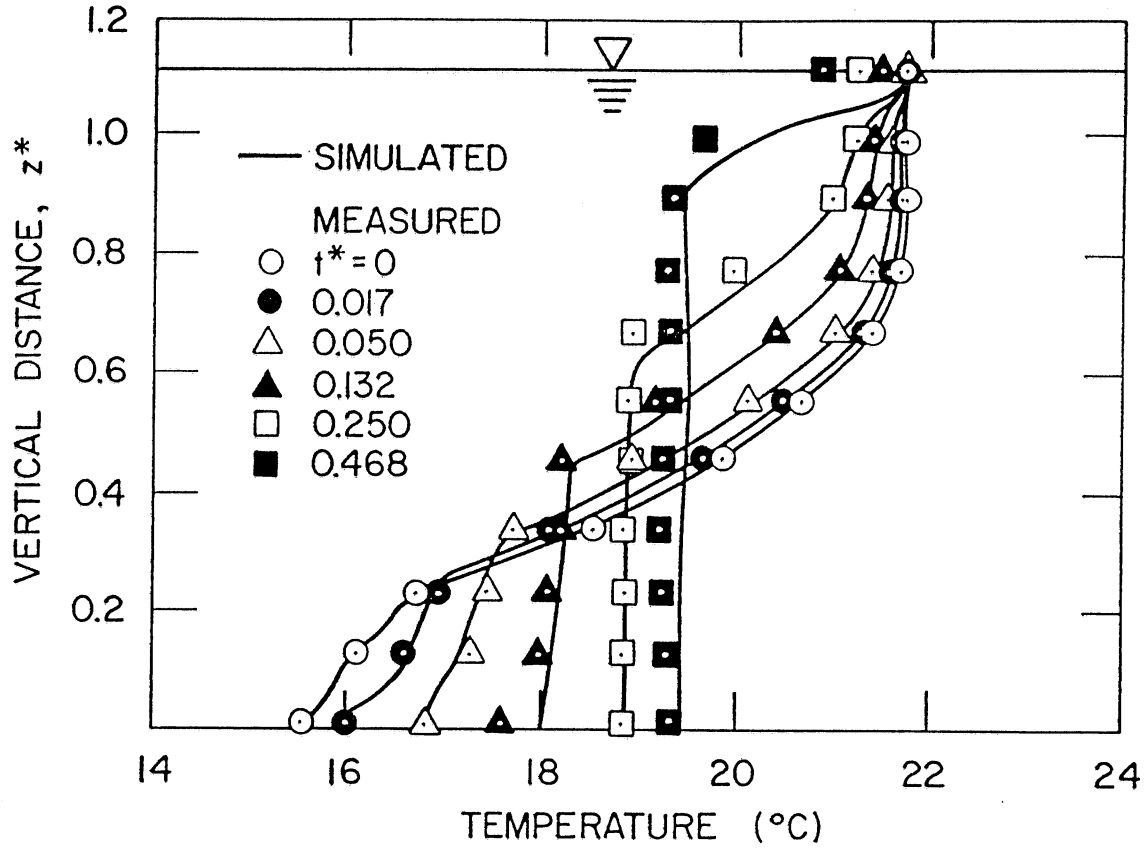

Fig. 4.3 Measured and simulated temperature profiles: Exp. No. 7, $\theta_0 = 0^\circ$

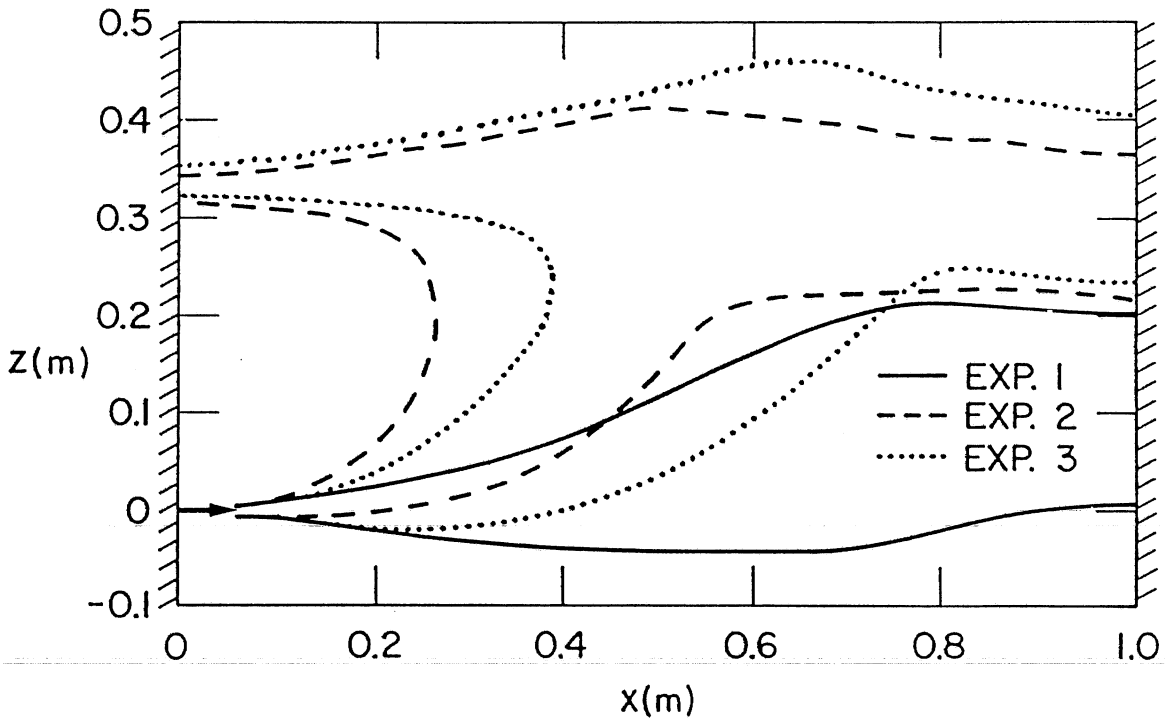

Fig. 4.4 Flow visualization—jet boundaries: $\theta_0 = 0^\circ$

Experiments show that horizontal jets do erode and mix the region below their origin as shown in Fig. 4.5. The visible upper and lower boundaries of the mixing layer made visible by dye move with time during he mixing process as shown in Fig. 4.6. The simulation model predicts no change in the temperature profile below the jet origin. This is the cause for the disagreement of temperature profiles between experimental and simulated results in the discharge region. Therefore, the heat balance made with the measured water temperatures from the discharge level to the surface does not agree with that made for the simulated profiles. This could contribute to some of the disagreement between experimental and simulated profiles in the final stages of mixing. However, this effect is not significant for small Fr values (in the range from 2 to 10) for which the jet trajectory is strongly deflected to a vertical direction (see Fig. 4.4).

The elevation at which the centerline temperature of the jet equals the temperature of the fluid in the tank i.e. neutral buoyancy ($\Delta T = 0$) was chosen as the location of equilibrium level. However, the "real" jet continues above this elevation due to vertical momentum before coming down to spread out at the equilibrium level (Gu and Stefan, 1987).

In addition, a horizontal jet with a large initial densimetric Froude number Fr may impinge on the bottom. This effect is also not included in the integral jet model and can cause incorrect predictions. This is an additional reason why the model is limited to small densimetric Froude number applications ($Fr < 10$). This does not make the model less practical since higher densimetric Fr number jets have larger power requirements and lower efficiency, as will be shown in Chapter 7, and the tendency would be to select low Fr number jets.

4.4.2 Vertical Jets

Temperature profiles measured after the beginning of the vertical jet discharge are shown in Fig. 4.7 and Fig. 4.8. It can be seen that measurements and simulations agree very well in the lower part of the tank, but not well in the upper region, especially for the high Froude number discharge. The actual (measured) mixing of the upper part of the stratified water body is faster than the simulated one. The discrepancies can be explained by some special features, not presented in the horizontal jets, of the vertical jet and the spreading layer. A vertical jet can reach the water surface, and then a spreading and possibly plunging layer is formed where the typical jet flow pattern is lost. This was illustrated in Fig. 3.20 and Fig. 3.21 schematically. The model did not simulate the surface impingement and plunging flow because similarity assumptions did not hold in this region. There is added entrainment and mixing in the stratified water body that is not simulated by an integral jet model. The simulated results (Fig. 4.7 and Fig. 4.8) indicate that the one–dimensional simulation model gives a better prediction of mixing if the jet densimetric Froude number Fr is small ($Fr = 2$) rather than large ($Fr = 10$).

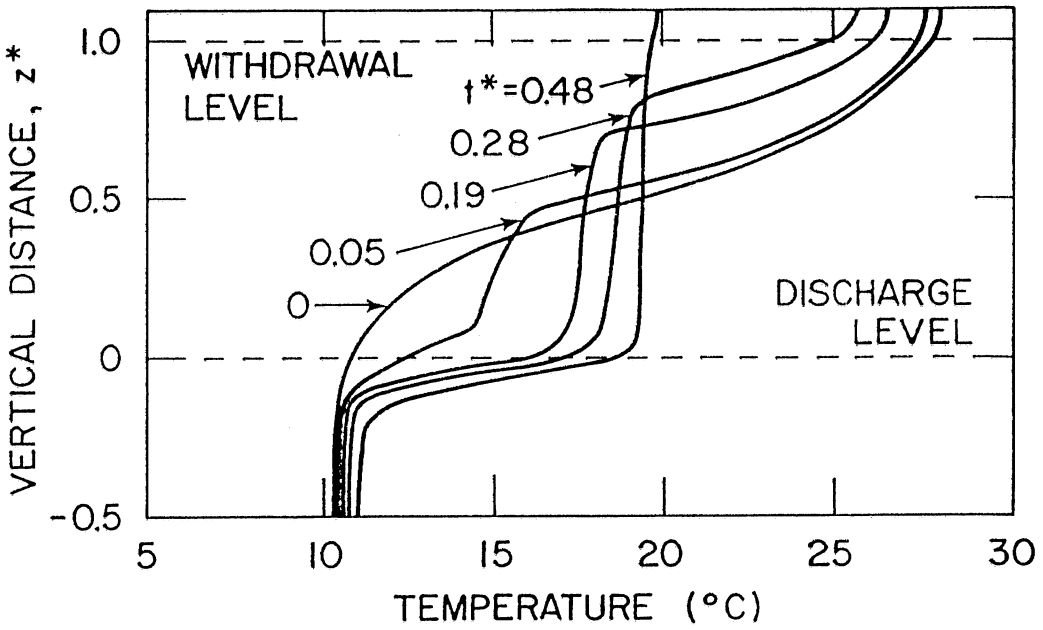

Fig. 4.5 Measured temperature profiles: Exp. No. 5, $\theta_0 = 0^\circ$

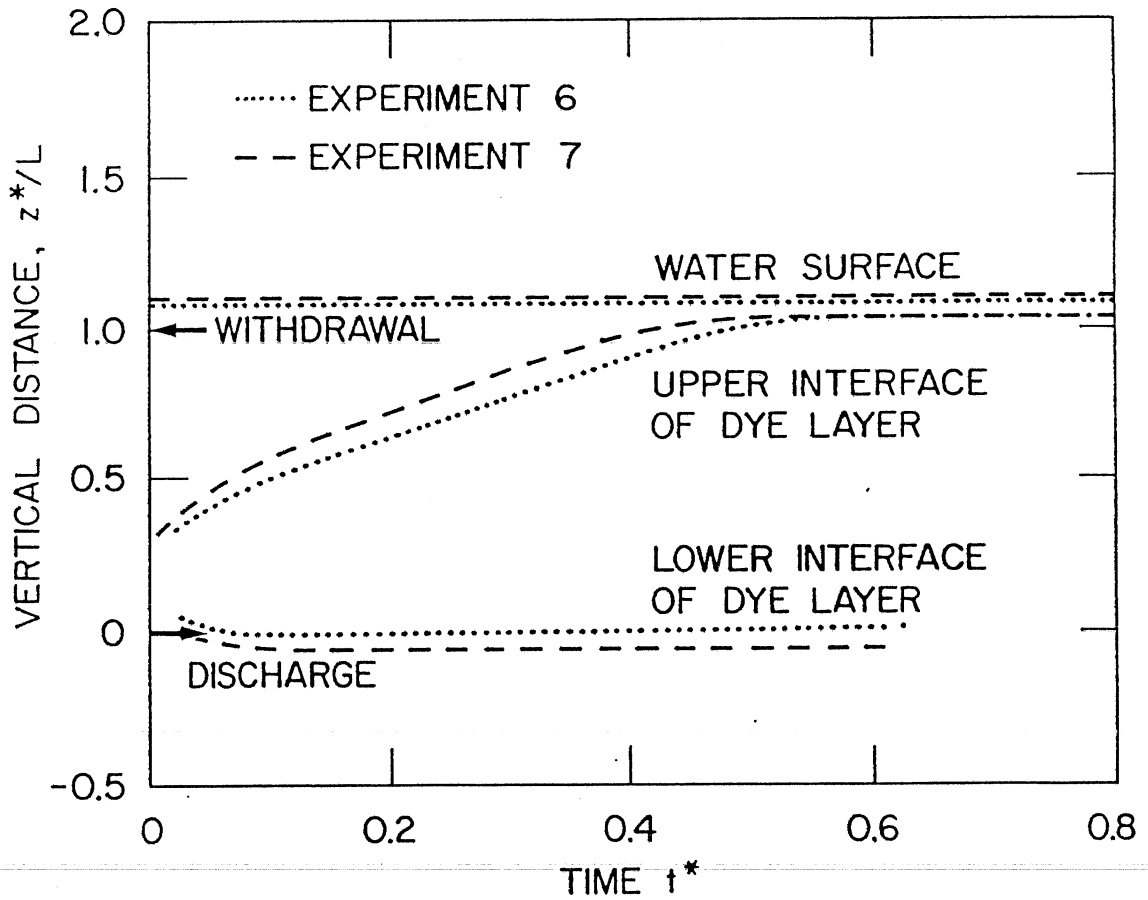

Fig. 4.6 Development of mixing layers: $\theta_0 = 0^\circ$

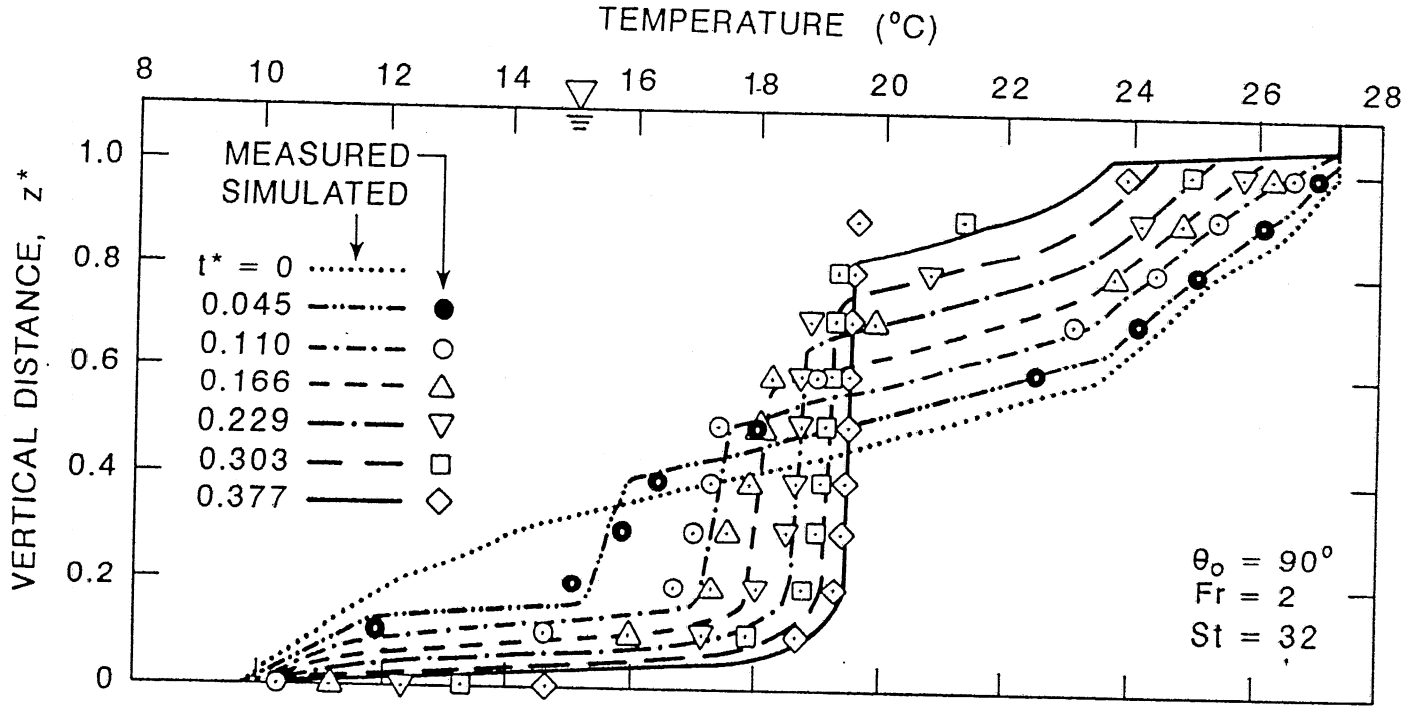

Fig. 4.7 Measured and simulated temperature profiles: Exp. No. 4, $\theta_0 = 90^\circ$

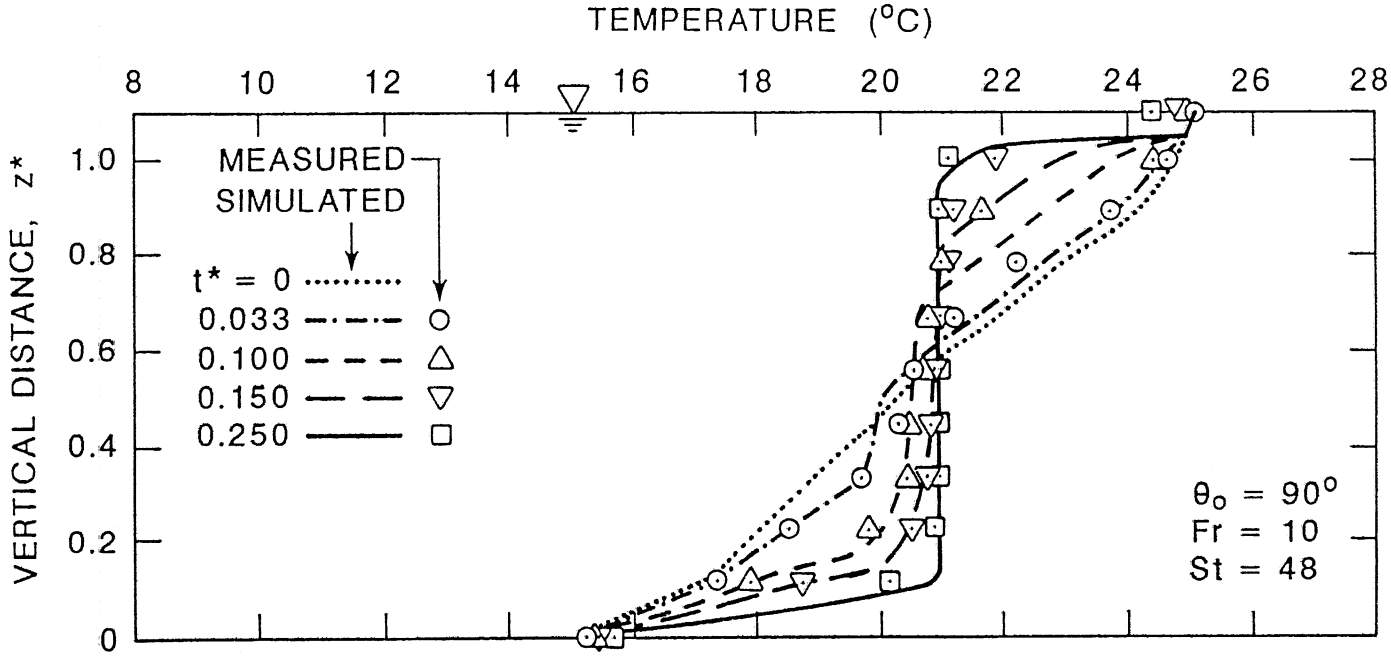

Fig. 4.8 Measured and simulated temperature profiles: Exp. No. 8L, θ_0=90°

4.4.3 Entrainment from the region below the injection level

The deepening of thermocline below the diffuser was measured in the laboratory experiments (Fig. 4.5). The region below diffuser is outside the computational domain of the 1–D jet–mixing simulation model. Therefore a 2–D model to be discussed in chapter 8 is required to simulate mixing in this region. The deepening process may be characterized by jet entrainment from the below–diffuser region mainly due to shear at the interface, i.e. at the level of injection (Fig. 4.9). Water in the region below diffuser is moved upwards to the region above diffuser by the jet. The removed water is replenished by the water coming from the above–diffuser region through recirculation to satisfy the continuity of the flow field. Mixing in the region below diffuser is generated by the recirculation.

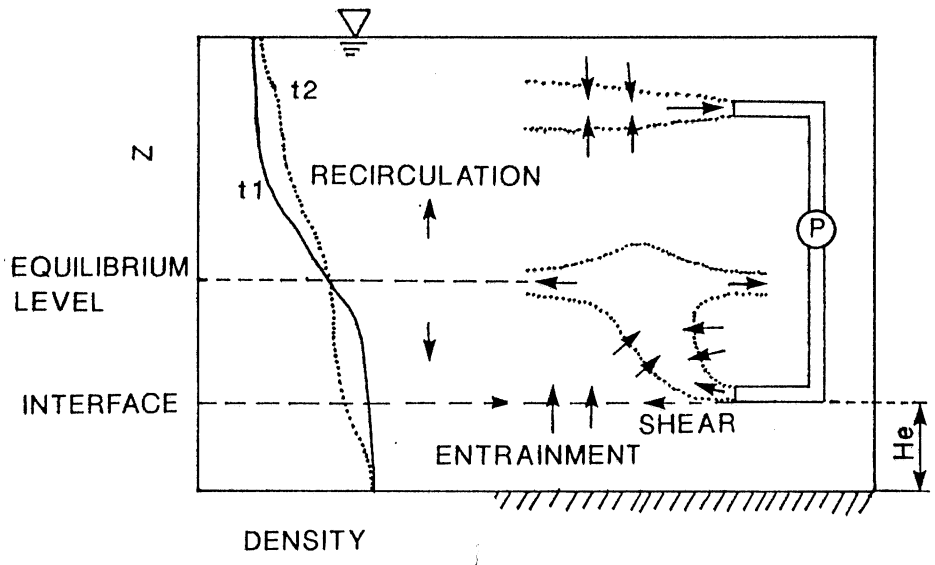

Fig. 4.9 Schematic diagram of deepening process in the region below diffuser

The mixing process is described by the change in potential energy, which increases in the upper region and decreases in the lower. The change represents the stability of stratification in the tank. The potential energy, which leads to deepening of the thermocline below injection, comes from the lifting work consuming some of kinetic energy provided by the jet.

The analysis of entrainment from below the injection level is made in a way similar to that used in deepening of surface mixed layers by wind in lakes. The lifting power of the jet and the change in potential energy of water in the below–diffuser region are herein considered. The kinetic energy available for entrainment provided by the jet is expressed as

$$KE = \Delta t \int_A \rho v_{eb}^3 dA \tag{4.1}$$

where v_{eb} is the entrainment velocity at the interface. The lifting work required to move the mass, $\Delta\rho\Delta V$, from the center of mass in the below–diffuser region to its position at the interface is described by

$$LW = \int_0^{H_e} A\Delta\rho g z dz \tag{4.2}$$

where H_e is depth of the below–diffuser region and z is vertical distance.

The entrainment velocity is assumed to be a linear function of shear stress, τ, which depends on the jet velocity, U_j. Let $v_{eb}^3 = C_k U_j^3$ and substitute into Eq. 4.1, then

$$KE = C_k \Delta t \rho A U_j^3 \tag{4.3}$$

where C_k is called the entrainment coefficient for the below–diffuser region. Since the entrainment velocity is also related to buoyancy force, C_k is a function of Richardson number, Ri, or densimetric Froude number, Fr. C_k is determined by energy balance. Let KE = LW and then

$$C_k = \frac{LW}{\rho A \Delta\, t\, U_j^3} \tag{4.4}$$

This relation is consistent with the previously discussed entrainment coefficient, α, for the jet region (Eq. 3.10), which is expressed as a function of Ri. The physical meaning of Ri is the ratio of lifting work to kinetic energy of the jet.

Fig. 4.10 shows the decrease of C_k with increasing Fr, based on laboratory measurements for both vertical and horizontal jets. It is obvious that horizontal jets entrain more water from the below–diffuser region than vertical jets do. This is mainly contributed by stronger shear at the interface created by horizontal jets than by vertical jets. Variation of the entrainment coefficient with the mixing time is presented in Fig. 4.11. It can be seen that C_k does not change significantly with time when $t^* > 0.10$.

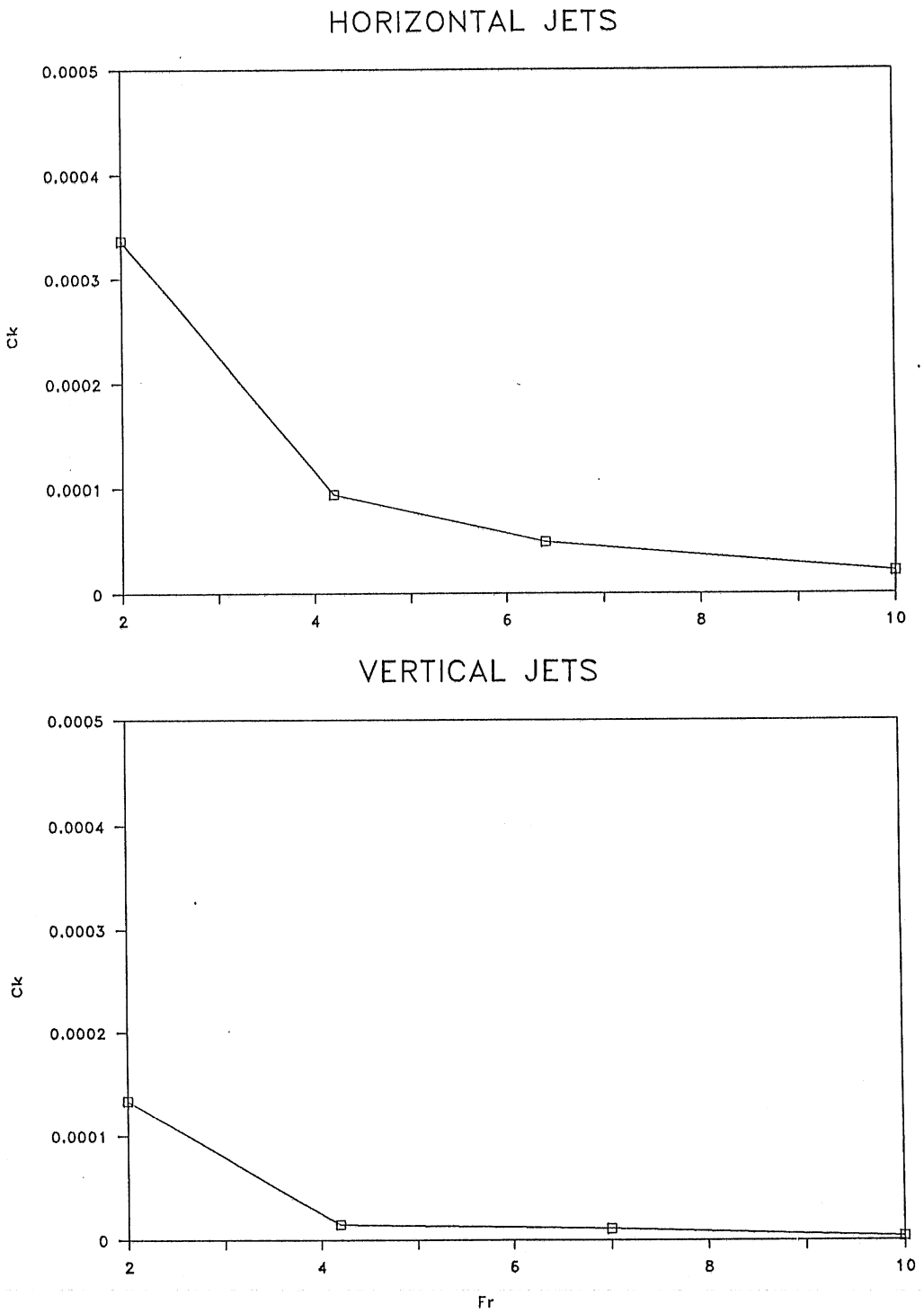

Fig. 4.10 Variation of entrainment coefficient in the region below diffuser, C_k, with Fr

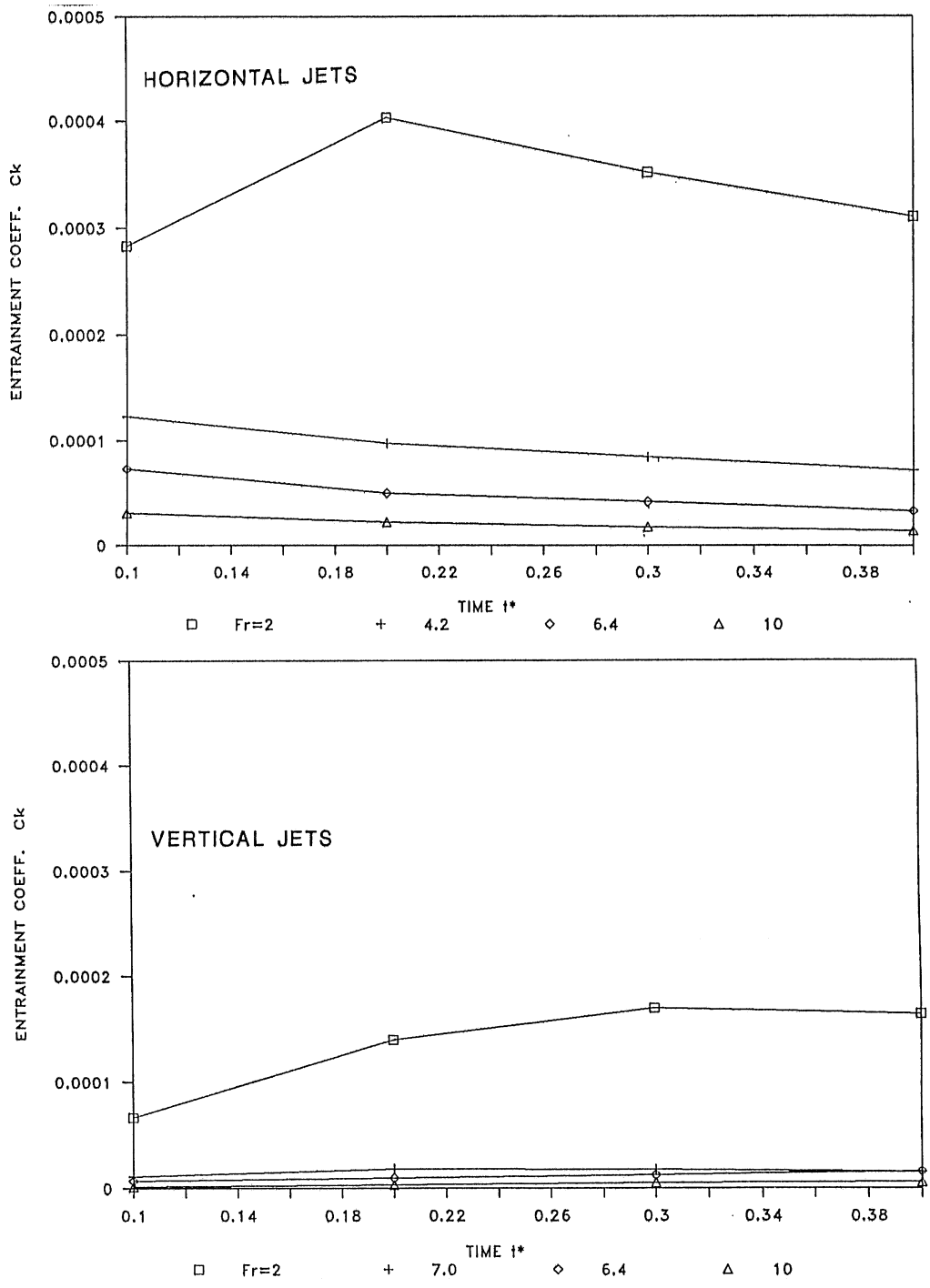

Fig. 4.11 Variation of C_k with time

4.5 Summary of experimental results

The main physical features which have been studied experimentally were jet behavior and mixing processes. Phenomena associated with the mixing process which are not simulated by the model, e.g. the entrainment from region below the injection were identified and described. The results for both horizontal and vertical jets are presented and compared with those predicted by the 1–D jet–mixing simulation model. The validity of the model is verified against experimental data.

The laboratory experiments analyzed herein suggest that hydraulic destratification systems using selective withdrawal and jet reinjection have the potential to destratify sections of temperature stratified water bodies or entire water bodies very effectively. When Fr is large, the vertical jet collapses on the water surface and the horizontal jet impinges on the bottom.

It has been noticed that there is better agreement between measured and simulated mixing of vertical jets for small Fr than for large Fr. Comparison of data for horizontal and vertical jets suggest that the simulation model better predicts the horizontal jet mixing than the vertical jet mixing. More results supporting these remarks can be seen in chapter 7, in which the measured and simulated effectivenesses and efficiencies of jet mixing systems are analyzed.

Chapter 5 Year–round Temperature Simulation of Cold Climate Lakes Without Artificial Mixing

5.1 Introduction

A dynamic lake water temperature simulation model developed for summer conditions is extended to accomplish the year–round one–dimensional, unsteady simulation of hydrothermal processes in a lake located in the temperate region. New submodels for the winter cover and for the heat exchange with lake bottom sediments are added to the existing summer stratification model. This extension enhances the applicability of the model. Numerical results were obtained with the expanded simulation model for Lake Calhoun and Ryan Lake, Minnesota, and compared with some field data for model validation.

The thermal structure of a lake is determined by the absorption of solar radiant energy, heat exchange through the boundaries (surface and bottom), and heat transfer in the water by turbulent mixing and advection. Because of changing features in the formation of the thermal structure in a cold climate lake during different seasons, two main periods are distinguished: the summer period and the ice cover period.

A dynamic lake water quality model MINLAKE (Minnesota Lake Model) was developed earlier to simulate the principal hydrothermal and kinetic processes in a lake on a daily time scale (Riley and Stefan, 1988). The model is one–dimensional and unsteady. The water quality parameters (as state variables or dependent variables), including water temperature, dissolved oxygen, phosphate, chlorophyll–a, and suspended solids, are simulated as a function of depth and time over a summer season (several months). Governing equations are the basic conservation equations of mass (expressed by concentration) and thermal energy (expressed by temperature) in one–D form. The bottom boundary condition is zero heat flux through the water/sediment interface. Local lake and weather data and limnological field investigations are required for calibration and verification of the model. The MINLAKE model was initially developed to simulate lake water quality in the main growth season (summer) and the effect of the frequently applied abatement techniques. The simulation typically starts with isothermal conditions at 4° C at time of ice–out and ends in late fall. In order to extend the MINLAKE model to the year–round simulation, analysis and numerical simulation of thermal processes during the ice cover period had to be added to the model.

The formation of a continuous ice cover, and later a snow cover on the surface of the water, greatly changes the conditions of heat exchange with the atmosphere. The heat loss from the water to the atmosphere is reduced by the insulating effect of the cover. Water underneath an ice cover receives heat from two sources: solar radiation penetrating through the ice and heat being released from the bottom sediments. While the latter is important in early winter, the former dominates toward spring (Ashton, 1986). On the lower face of the ice cover the process of ice formation stabilizes the temperature, which equals that of freezing water (0° C). The dynamic effect of the atmosphere is almost completely eliminated, and thermal effects find expression mainly by changes in the thickness of the ice and snow cover. These features make it possible to predict the temperature field in the water underneath the ice cover during the entire ice period using information on the initial temperature distribution in the water and bottom sediment at the time of freezing, the characteristics of turbulent heat exchange in the water, and the thermal characteristic of the bottom.

The importance of sediment heat storage is its effect on water temperatures during the winter. Due to the low thermal conductivity of the bottom sediment, the spring and summer heat reserves cannot be expended during fall cooling, and they are partly retained. Heat exchange with bottom sediment becomes the main external source for heating the water after freezing. The amount of heat stored in sediments depends strongly on the lake depth (Ashton, 1986). A shallow lake in which the entire volume of water is heated will transfer more heat to the sediment than a deep one with a cool hypolimnion.

The effort to extend the model to a year–long time cycle was made not only because of interest in the winter thermal regime of lakes in a cold climate but also to solve practical winter lake problems. One example is the water discharge into an ice–covered lake, including effects of jet mixing on the ice cover.

To extend the simulation period of the MINLAKE model to a whole year, submodels to simulate the most significant hydrothermal features of the winter cover and the lake bottom were developed. The submodel SNOWICE simulates the growth and decay of the winter cover (ice and snow) and computes the heat exchange through the upper boundary (interface of the water surface and winter cover). The submodel SEDIMENT predicts heat conduction in the lake sediments and calculates heat flux through the bottom boundary. These submodels are added to the MINLAKE model.

The winter cover model is similar to the one by Patterson and Hamblin (1988) who linked a two–component (ice and snow) model based on the Maykut and Untersteiner formulation to the reservoir model DYRESM. They used a minimum ice thickness to incorporate the two–dimensional effects of partial ice cover into the one–dimensional framework. The development of the submodels SNOWICE and SEDIMENT (Gu and Stefan, 1990a) is related to previous work of Ashton (1986), Billello (1968), Greene (1981), Fertuck et al. (1971), Pivovarov (1972), Rumer (1983) and Shen (1984 and 1983).

This chapter summarizes the extension of the MINLAKE simulation model with the following two objectives: (1) to complete the year–round simulation of hydrothermal processes of a lake and (2) to develop a winter cover simulation model and a sediment heat transfer model, and to incorporate these in the main model (MINLAKE). The versatility of this revised MINLAKE simulation model is shown by application to Lake Calhoun, Minneapolis, Minnesota. Direct model validation is made with field data for Ryan Lake, Minneapolis, Minnesota.

5.2 The heat transport equation

The thermal state of a lake can be determined by application of the law of conservation and conversion of energy, in the form of the one–dimensional heat transfer equation

$$\frac{\partial T}{\partial t} = \frac{1}{A}\frac{\partial}{\partial z}\left(KA\frac{\partial T}{\partial z}\right) + \frac{S}{\rho c} \tag{5.1}$$

where A = horizontal area of lake at depth z
T = temperature
t = time
K = turbulent diffusion coefficient
S = strength of heat source or sink per unit volume
z = vertical coordinate

The source or sink term consists essentially of internal absorption of solar radiation. The heat exchange with the atmosphere changes with the presence or absence of a continuous ice cover on the surface of the water body. The total heat exchange with the atmosphere is by turbulent convection, evaporation and effective radiation during the open water season, and by conduction through the ice and snow cover in winter. Some radiation effects remain. The thermal effect of the atmosphere is mainly in the buildup or thawing of the ice cover during the winter, and only slightly affects the water temperature.

Heat transfer with the bottom sediments also becomes an important external factor for the temperature structure of ice–covered lakes.

The winter thermal structure of an ice–covered lake can therefore be analyzed as a one–dimensional unsteady heat transfer problem in a four–layer medium consisting of snow, ice, water and sediment (Figs. 5.1 and 5.2). The heat source term (S) in Eq. 5.1 for the ice period is written as

$$S = R_a \frac{A}{\Delta V} \tag{5.2}$$

where R_a = net absorbed solar radiation and ΔV = volume of a horizontal layer of thickness Δz. R_a is equal to the difference of incoming radiation and outgoing radiation.

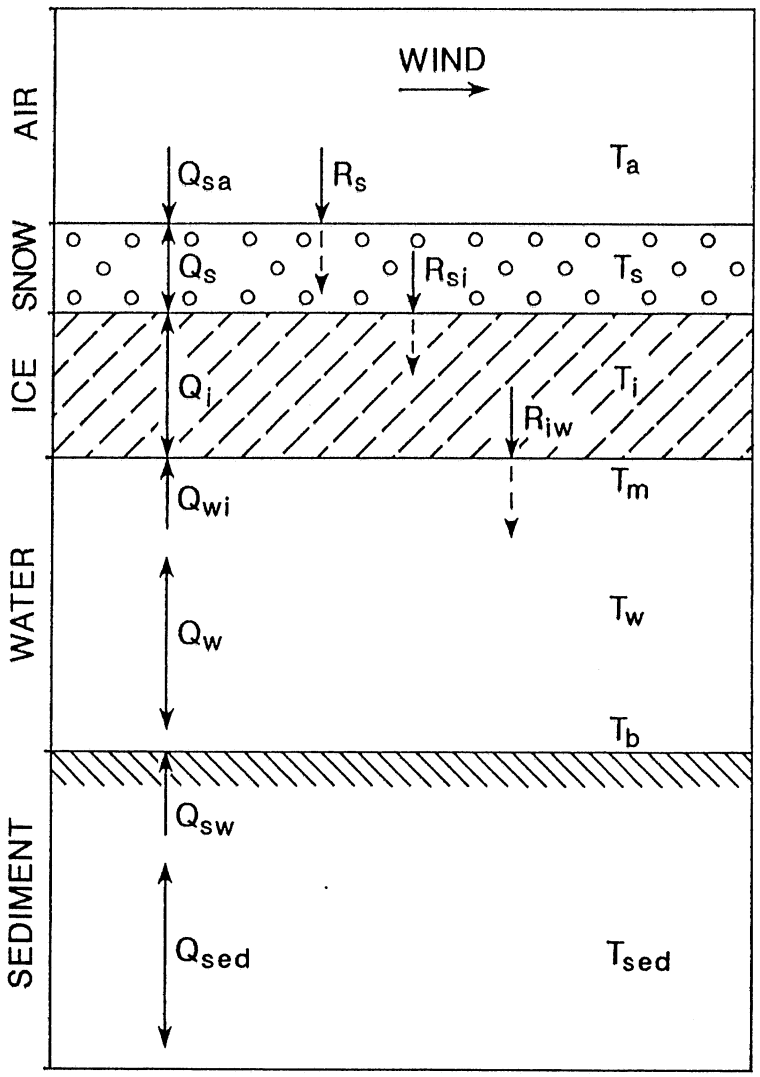

Fig. 5.1 Schematic vertical section through a lake with ice cover and snow cover

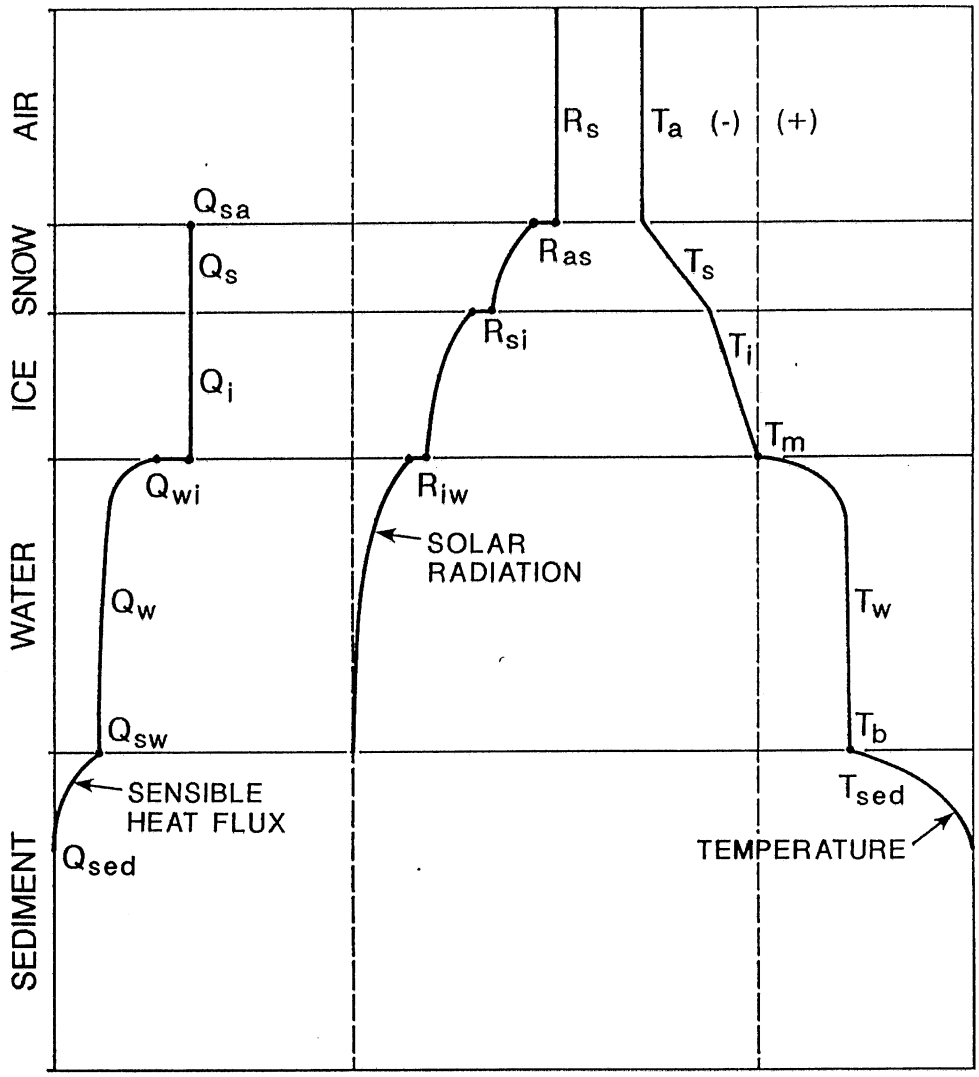

Fig. 5.2 Distribution of sensible heat flux (Q), solar radiation (R) and temperature (T) with depth

$$R_a = -(\Delta z)\,\frac{dR(z)}{dz} \tag{5.3}$$

where R(z) = the radiation flux at depth z. The vertical radiation distribution is (Dake and Harleman, 1969)

$$R(z) = R_{iw}\,(1-\beta_w)(1-\alpha_w)\exp(-z\eta_w) \tag{5.4}$$

where R_{iw} = solar radiation penetrating into the lake water below the ice. It is expressed as

$$R_{iw} = R_s\,(1-\beta_s)(1-\alpha_s)(1-\beta_i)(1-\alpha_i)\exp(-\eta_s\delta_s)\exp(-\eta_i\delta_i) \tag{5.5}$$

where

β_s, β_i, β_w = surface reflectivity (albedo) for snow, ice and water respectively;

α_s, α_i, α_w = surface absorption coefficients for snow, ice and water, respectively;

η_s, η_i, η_w = attenuation (extinction) coefficients in snow, ice and water, respectively;

R_s = total incoming solar radiation flux reaching the snow surface in winter or water surface in summer and

δ_s, δ_i = snow thickness and ice thickness, respectively.

The surface reflectivities and surface absorption coefficients vary with medium properties at both sides of the interface. Values of these parameters listed in Table 5.1 are for (medium) surfaces exposed to air.

The problem becomes the simultaneous solution of the system of equations 1 to 5 for the water, with additional equations for snow, ice and sediment as given in the following section. The boundary conditions for Eq. 5.1 are: (1) 0° C (melting point) at the ice/water interface; (2) heat balance including ice formation on the lower face of the ice and full heat flux balance at the air/snow and snow/ice interfaces; (3) continuous heat flux at the water/sediment interface. This heat flux is taken into account in the source term for the lake bottom layer.

$$S = (R_a + Q_{sw})\,\frac{A}{\Delta V} \tag{5.6}$$

where Q_{sw} = sensible heat supplied from bottom sediment to lake water (Fig. 5.1).

Table 5.1 Material properties used in simulation

	Snow	Ice	Water	Sediment
density (kg m^{-3})	350[a]	920[b]	1000[b]	2500[b]
Heat capacity (kJ kg^{-1} $^oC^{-1}$)	2.1[b]	2.1[b]	4.2[b]	1.0[b]
Thermal Conductivity (W m^{-1} $^oC^{-1}$)	0.27[a]	2.6[c]	0.55[b]	0.55[c]
Albedo	0.4–0.8[d]	0.55[f]		
Absorption coefficient	0.17–0.34[d]	0.17–0.32[e]	0.4[g]	
Extinction coefficient(m^{-1})	20–40[d]	7[e] 1.6[h]		
Latent Heat of fusion (kJ kg^{-1})		335[c]		
Latent Heat of vaporization (kJ kg^{-1})			2500[c]	

[a]Greene (1981)

[b]Carslaw & Jaeger (1971)

[c]Ashton (1986)

[d]Scott (1964)

[e]Wake and Rumer (1979)

[f]Bolsenga (1977)

[g]Riley and Stefan (1988)

[h]Pivovarov (1972)

The vertical turbulent heat exchange coefficient K in Eq. 5.1 is substantially smaller in winter than during other times of the year because the continuous ice cover excludes vertical mixing by wind. Pivovarov (1972) stated that processes such as currents and uneven depth were the main causes of turbulent mixing under the ice cover. Patterson and Hamblin (1988) explained that mixing resulted from surface cooling, wind stirring in partially ice covered lakes, seiche–induced shear at the thermocline, and billowing at the thermocline resulting from shear instability. In general the eddy diffusivity K depends on the rate of dissipation of turbulent kinetic energy as well as the local density gradient. However, the mechanisms of turbulent mixing in an actual lake with ice cover are so far not clearly verified.

The turbulent exchange coefficient, K, in Eq. 5.1 can be obtained from field data. In the MINLAKE simulation model, K is computed separately for epilimnion and hypolimnion in open water. It was given as a function of wind speed for the epilimnion. The effect of density stratification on the hypolimnetic diffusion coefficient is taken into account by relating the coefficient to the Brunt–Vaisala frequency given by

$$N = \left(\frac{g}{\rho}\frac{d\rho}{dz}\right)^{1/2} \tag{5.7}$$

The K–N relationship is characterized by a maximum hypolimnetic diffusion coefficient K_{max} which occurs at N equal to a certain value C_N. The turbulent exchange coefficients K decreases in layers of high stability (strongest stratification) approximately inversely to N. In the model the hypolimnetic diffusion coefficient is determined from

$$K = \min[K_{max},\ K_{max}C_N N^{-1}] \tag{5.8}$$

where K_{max} = maximum hypolimnetic diffusion coefficient and C_N = minimum value of N at which the K_{max} occurs (taken to be 8.66×10^{-3} sec^{-1} from Jassby and Powell, 1975).

In winter the K value near the ice cover is equal to the molecular diffusivity because of the solid wall effect. K_{max} for the ice period is much smaller than in the summer but larger than the molecular diffusion coefficient K_m.

$$K_{max} = b_\ell K_m \tag{5.9}$$

where b_ℓ = lake specific coefficient, in the range of one to ten. Pivovarov assumed K = 0.005 cm^2/sec for the Klyazma reservoir (USSR) with ice cover. This estimate corresponds to $b_\ell = 5.0$.

5.3 Winter cover simulation

The ice–cover growth and decay is a complicated problem because of the moving interface separating water and ice. Fig. 5.1 presents a five layer system including an ice layer and a snow layer. Each layer is considered to be a homogeneous material with uniform properties. Energy fluxes are considered only in the vertical direction. Energy is assumed to be absorbed at idealized boundaries which are flat and have no thickness. Energy is balanced at each interface, air/snow, snow/ice and ice/water by taking account of heat fluxes and latent heat of fusion and vaporization. The transfer of heat from the ice to the snow is continuous. At the snow surface, snowfall can occur as well as the melting of snow and ice. At the lower boundary, ice growth and thaw will occur and the temperature at the ice/water interface, T_m, is equal to 0° C.

The simulation model takes account of the following processes to determine the snow thickness: snow accumulation due to precipitation accompanied by a compaction process, melting on the snow surface due to conduction or convection, longwave radiation and rainfall and melting in the snow layer due to absorption of shortwave solar radiation. Similarly, processes that affect the ice cover include ice growth and decay on the underside of the ice cover, ice melting on the top (after the snow cover has melted) due to sensible heat fluxes, longwave radiation and rainfall and internal melting due to absorption of solar radiation.

The main equation governing the growth or decay of ice on its underside in contact with water is given by the energy balance at the water/ice interface

$$Q_i - Q_{wi} = \rho_i \lambda_i \frac{d\delta_i}{dt} \tag{5.10}$$

where Q^i = the heat flux through ice into the snow and from there into the atmosphere, Q_{wi} = the heat flux from water to ice, λ_i = latent heat of fusion of ice. The heat flux Q_i is by conduction through the ice–snow system with a total heat balance on the snow surface as boundary condition in order to express the effect of the atmosphere. To calculate Q_i, it is assumed that the thermal conditions in ice and snow covers are quasi–steady.

The energy balance equation at the ice/snow boundary is

$$Q_i = Q_s \tag{5.11}$$

where Q_i and Q_s are heat flux in ice and snow, respectively. The energy balance at the snow/air interface under equilibrium conditions (Greene, 1981) can be written as

$$Q_{sa} = Q_s \tag{5.12}$$

where Q_{sa} is the sum of the fluxes from net longwave radiation, Q_{rl}, sensible (conductive or convective) heat flux to the air, Q_a, and latent (evaporative) heat flux, Q_e, through the snow/air interface.

The net longwave radiation, Q_{rl}, is expressed as the product of the emissivity coefficient, a Stefan–Boltzman constant and a fourth power of the snow temperature. The evaporative heat flux, Q_e, and the convective heat flux, Q_a, are determined by using a wind function and the vapor pressure difference between air and snow surface for the former and the temperature difference between air and snow for the latter (Ashton, 1986; Shen, 1984; Greene, 1981; Light, 1941). Ashton suggested that sensible heat transfer rate, Q_a, and evaporative (latent) heat transfer rate, Q_e, were related through Bowen's ratio, B_r, as B_rQ_e, such that $Q_a = B_rQ_r$.

One simplified approach (Greene, 1981; Fertuck, 1971) is to express the heat leaving the surface, Q_{sa}, in the energy balance as

$$Q_{sa} = h_{sa} (T_s - T_a) \tag{5.13}$$

where h_{sa} = (snow/air interface) bulk heat transfer coefficient which is a function of wind speed (Fertuck, 1971), T_s = temperature at the top of snow layer. In Eq. 5.11 and 12,

$$Q_i = -k_i \left(\frac{dT}{dz}\right)_i \tag{5.14}$$

$$Q_s = -k_s \left(\frac{dT}{dz}\right)_s \tag{5.15}$$

where k_i and k_s represent thermal conductivity of ice and snow, respectively.

If the concept of serial heat conductors is applied,

$$Q_i = \frac{T_m - T_a}{\frac{\delta_i}{k_i} + \frac{\delta_s}{k_s} + \frac{1}{h_{sa}}} \tag{5.16}$$

where T_m is the temperature at the bottom of the ice layer. Then

$$Q_i = Q_s = Q_{sa} \tag{5.17}$$

The heat flow from water to ice (Q_{wi}) also plays a role during ice melting. Determination of Q_{wi} requires knowledge of the temperature profile in the water. After the lake freezes, a boundary layer forms through which the transition from the melting temperature (on the bottom of the ice) to the temperature of warm water deeper in the lake occurs. The heat flux from water to ice depends on the temperature profile in the water boundary layer.

$$Q_{wa} = -k_w \left(\frac{dT}{dz}\right)_{z = 0} \tag{5.18}$$

where k_w = turbulent conductive heat transfer coefficient.

Greene (1981) related the turbulent heat transfer (Q_{wi}) to the Reynolds and Prandtl numbers. Patterson and Hamblin (1988) assumed that Q_{wi} consisted of laminar (molecular conduction) and turbulent (same as Greene's) components. The velocity of flow in the uppermost layer under the ice must be known in both Greene's and Patterson's model. If a lake with a river inflow underneath the ice is considered, it would be appropriate to apply the above mentioned models. In a lake without inflow known, the flow component is unknown and very small.

Substitution of Eqs. 5.16 and 18 in Eq. 5.9 gives the basic balance equation of ice formation on the underside of the ice cover

$$\rho_i \lambda_i \frac{d\delta_i}{dt} = \frac{T_m - T_a}{\frac{\delta_i}{k_i} + \frac{\delta_s}{k_s} + \frac{1}{h_{sa}}} + k_w \left(\frac{dT}{dz}\right)_{z = 0} \tag{5.19}$$

Eq. 5.19 is used to calculate the growth or decay of ice at the bottom of the ice layer.

Ice can decay not only from the bottom but also from the top, or from within. Ice decay begins on its top after the snow cover melts. Rains have a considerable effect on upper surface melt, even though the thermal effects of a given rainfall may be minimal. Rainfall causes significant change in the snow and ice cover texture, which in turn speeds up other processes of decay. Rainfall increases snow density, causes loss of internal ice strength and mechanical destruction, and decreases the albedo due to water pools forming on the ice surface. The ice decay rate at the top of the ice layer taking account of the effect of rainfall and neglecting the heat conduction in the ice layer during ice melting is evaluated from

$$\rho_i \lambda_i \frac{d\delta_i}{dt} = Q_{ia} - Q_r \tag{5.20}$$

where Q_r is the rate of energy from rainfall per unit area and Q_{ia} can be determined by Eq. 5.13 with the ice/air interface heat transfer coefficient, h_{ia} (Fertuck, 1971), and the temperature at the top of ice, T_i, replacing h_{sa} and T_s, respectively.

Internal melting in the ice layer results from the low surface albedo and the internal absorption of solar radiation. Deterioration of ice occurs when heat losses by long–wave radiation, and sensible and latent heat transfer are unable to remove the internal energy resulting from short–wave radiation

absorption. Once deterioration begins, further energy absorption results in internal melting and the ice becomes porous. Ashton (1983) introduced a melt fraction ϕ_i (porosity) which is calculated by integration of

$$\frac{d\phi_i}{dt} = \frac{q_i}{\rho_i \lambda_i} \tag{5.21}$$

where q_i is the rate of energy absorption per unit volume of ice.

The snow cover forming on the ice surface of the lake is likely to be thinner than direct accumulation of snowfall. To account for compaction, the cumulative snow depth is found by multiplying the snowfall by a compacting factor (0.2 to 0.4) before adding it to the existing snow depth (Adams, 1981).

The snow melting on the snow surface in contact with air is evaluated by the energy balance equation at the snow/air interface:

$$\rho_s \lambda_s \frac{d\delta_s}{dt} = Q_{sa} - Q_r - Q_s \tag{5.22a}$$

The concept of serial heat conductors (Eqs. 5.16 and 17) may not be applied to obtain Q_s in Eq. 5.22a since it is based on the assumption of equilibrium conditions of snow cover, i.e., $d\delta_s/dt = 0$. However it is found that for high snow melting rates the heat contributed by convection (or conduction) and condensation of moisture through turbulent diffusion of warm moist air are important heat–sources (Light, 1941). By neglecting the heat conduction in snow, Q_s, and the longwave radiation flux, Q_{rl}, previously included in Q_{sa}, Eq. 5.22a can be approximated by

$$\rho_s \lambda_s \frac{d\delta_s}{dt} = Q_a + Q_e - Q_r \tag{5.22b}$$

in which Q_a is empirically expressed as

$$Q_a = h_a(T_s - T_a) \tag{5.23a}$$

where h_a is a turbulent convective heat transfer coefficient, which depends on the wind function, W_f (Ashton, 1986; Shen, 1984; Light, 1941; Greene, 1981). By applying a logarithmic law for wind velocity (Greene, 1981, Light, 1941), h_a is approximately evaluated as

$$h_a = 1.74 \rho_s \lambda_s v_w \, 10^{-0.0000047 z_{msl}} \, 10^{-9} \tag{5.23b}$$

where v_w = average wind velocity (m/s) and z_{msl} = elevation above MSL (m).

The internal melting in the snow layer resulting from the absorption of solar radiation, ϕ_s, can be expressed as Eq. 5.21 with ρ_s and the rate of energy absorption per unit volume of snow, q_s, replacing ρ_i and q_i, respectively.

The ice thickness and snow depth calculation uses quasi–steady state assumptions. This means that the heat fluxes in the snow and ice take instantaneously their steady–state values dictated by the temperature gradients calculated in the previous time–step (usually one day). During each time step the thicknesses of snow and ice are kept constant and equal to the thicknesses they had at the end of the previous time step. At the end of a time step the thicknesses of snow and ice are adjusted for growth or decay according to snowfalls and the heat loss or gain that occurred during the timestep.

5.4 Simulation of heat exchange with lake sediments

Thermal conditions in lakes, before and during the ice cover period, can be significantly influenced by heat exchange between lake water and bottom sediments. The amount of heat stored in and released from sediments during an annual cycle depends strongly on the lake depth. A shallow lake in which the entire volume of water is heated will transfer more heat to the sediments than a deep one with a cool hypolimnion (Ashton, 1986). The magnitude of this heat exchange is mainly determined by two processes: heat transfer in the bottom sediments by heat conduction and heat transfer by groundwater. Michel (1971) expressed the heat transfer from groundwater Q_g as a function of the total groundwater inflow I_g, the temperature difference between lake water and groundwater T_g and the lake bottom area A_b, i.e., Q_g is proportional to $I_g\ T_g/A_b$. For lakes that are relatively large in area and of about constant depth it may be assumed that heat transfer by groundwater is insignificant except in parts close to the shores.

The conductive heat flux between the sediment and the lake water is

$$Q_{sw} = -k_b \left(\frac{dT}{dz}\right)_{sw} \tag{5.24}$$

where k_b is the thermal conductivity of the sediment and "sw" denotes the sediment temperature gradient at the interface of water and sediment (the lake bottom). The temperature distribution in the sediments is determined from the solution of the one–dimensional, unsteady heat conduction equation

$$\frac{\partial T}{\partial t} = K_b \frac{\partial^2 T}{\partial z^2} \tag{5.25}$$

where K_b is the thermal diffusivity of the sediment,

$$K_b = \frac{k_b}{\rho_b c_b}$$

with $\rho_b c_b$ = specific heat of sediment (per unit volume).

The boundary condition at the lake bottom is

$$T = T_b \tag{5.26}$$

where T_b is a known (water) temperature. The boundary condition at some depth below the bottom (taking the bottom as a semi-infinite medium) is

$$\frac{\partial T}{\partial z} = 0$$

or

$$T = T_1 = \text{constant} \tag{5.27}$$

The second boundary condition reflects the observation that the temperature waves of the annual period propagating from the surface downward penetrate only to a certain depth, beneath which the temperature remains practically constant and equal to the mean long-term temperature T_1. That temperature is a priori unknown. It will be close to the mean annual temperature of the hypolimnetic water. As a first approximation it is chosen to be the water temperature at ice-out. When the ice cover melts, the deviation in the sediment temperature distribution from its long-term mean can be assumed to be small.

$$T = T_1 \qquad \text{at} \quad t=0 \tag{5.28}$$

In practice this initial condition can be replaced by a better estimate of an annual average after several years of water temperatures have been calculated.

A finite difference technique is employed for the numerical solution of Eq. 5.25. An implicit scheme is used. The stability criterion is $\Delta z^2/(\Delta t\ K_b) \geq 2.0$. Due to the lake bottom water temperature fluctuations which respond to weather conditions, the coupling of the sediment conduction with the water temperature calculations can result in oscillations due to the numerical coupling. To avoid the unrealistic oscillations, the time and space steps should be made sufficiently small, provided that they satisfy the stability criterion.

5.5 Application and model validation

5.5.1 Lake Calhoun simulation

The dynamic lake water temperature simulation model by Ford and Stefan (1980) and Stefan and Ford (1975), which was developed for the summer period and is now contained in MINLAKE (Riley and Stefan, 1988) is extended to year–round simulation by incorporation of submodels SNOWICE and SEDIMENT which simulate winter cover and sediment heat transfer, respectively. The subroutines SNOWICE and SEDIMENT are linked to the main program MINLAKE by the lake specific subroutine USER. The main program may call the two subroutines whenever it needs them from USER.

To demonstrate the applicability of the year–round simulation model, temperature profiles in Lake Calhoun were simulated for the years 1971 and 1972. The lake is located in south Minneapolis, Minnesota. It has a surface area of 1.71 km^2, a volume of 1.71 x 10^7 m^3 and a mean depth of 10 m. Maximum depth is 27 m. The meteorological data and limnological data for the years 1971 and 1972 are available. The simulation started with isothermal conditions of 4° C at the time of ice–out (April 24, 1971) and ended on the same date of the following year (1972).

The important difference between the year–round simulation and the main season (summer) simulation is that some coefficients which are determined by calibration cannot be set constant in the year–round simulation. The calibration coefficients to which the temperature model is sensitive are the maximum hypolimnetic vertical diffusion coefficient (HKMAX), the wind sheltering coefficient (WSTR) and the wind function coefficient (WCOEF). These coefficients are defined by Riley and Stefan (1988).

Variations of the physical lake conditions between seasons are much more significant than within a season. Coefficient values which are determined from lake and weather data therefore give reasonably good simulation results for each season separately but not for the year–round simulation. During the ice period WSTR and WCOEF were set to zero and HKMAX to 0.023; summer values were respectively 0.3, 22.0 and 0.35. A change of the coefficients occurs at the time of freeze–up in fall and ice melting in spring.

The ice thickness is calculated by the submodel SNOWICE. Wind mixing will delay the formation of ice (freeze–up of lake) because it creates heat exchange between the water surface and the internal layers (warmer region). Ashton (Harleman, 1986) introduced the following "threshold conditions" to be met before an intact ice cover is established: a) volume average water temperature is less than 2° C; b) average wind speed over a day is less than 5 m/s; and c) average daily air temperature is less than –5 ° C. He explained that criterion (a) requires that the water mass be cooled below the 4° C neutral stability point. This implicitly includes the effect of

wind mixing. The choice of (b) is based on his experience that strong winds prevent continuous ice formation. The requirement (c) is a subjective one that allows the ice sheet to attain a thickness sufficient to resist breakup. Patterson and Hamblin (1988) assumed a minimum thickness at which ice can persist on the surface and chose a fixed value of 0.1 m. It should be pointed that the criteria for determining the time of an intact ice cover are critical to ice cover period simulations since the cooling rate of the water at the time of freezeover is generally very rapid and missing the freezeover date by even a few days may result in temperature differences far greater than errors in the simulation of the subsequent evolution of the water temperature. Conditions (a) with 2.65° C of average water temperature, (b) with 5 m/s of average wind speed and (c) with –2.0 °C of average air temperature are found to be appropriate for Lake Calhoun in the year–round simulation to determine the freeze–up date.

Simulated and measured temperature profiles in Lake Calhoun for 1971–1972 are shown in Fig. 5.3. The annual variations of simulated and measured temperatures at the surface, bottom and middle of the lake are shown in Fig. 5.4. Even though water temperature data for the winter (ice period) are available only for two days, the annual temperature cycles were simulated reasonably well. The difference in temperature scales in Fig. 5.4 should be noted. Fig. 5.5 presents the annual course of net (solar) radiation entering the water. The annual temperature variations in Fig. 5.4 are strongly related to the annual course of solar radiation in Fig. 5.5 as to be expected.

Ice and snow thicknesses for 1971–1972 are shown in Fig. 5.6. Pivovarov (1972) indicates that the thickness of the snow cover that the ice can support is limited. In the equilibrium state the ratio between the thickness of ice and snow is

$$\frac{\delta_s}{\delta_i} = \frac{\rho_w - \rho_i}{\rho_s} \tag{5.29}$$

For an estimate, ρ_w = 1000 kg/m^3, ρ_i = 920 kg/m^3 and ρ_s = 200 kg/m^3, then δ_s/δ_i = 0.40. If there is abundant snowfall, δ_s may exceed the value in the equilibrium state. In this case the stresses induced cause cracks to appear in the ice cover. The results shown in Fig. 5.6 give ratios less than 0.4. Comparison with data for other lakes and rivers in the area (Wei and Hamblin, 1986; Greene, 1981; Bates, 1980; Hill, 1967) indicates that maximum ice thickness is within a "typical" range (0.5 – 0.7 m). The simulation shows that the ice cover would form in early December and a total melt–out would occur in early or mid–April.

Coefficients to which the ice cover thickness computation was found to be very sensitive are the compacting factor of snow, the turbulent convective heat transfer coefficient at the air/snow interface (h_{sa}), and the conductive heat transfer coefficient at the ice/water interface (k_w).

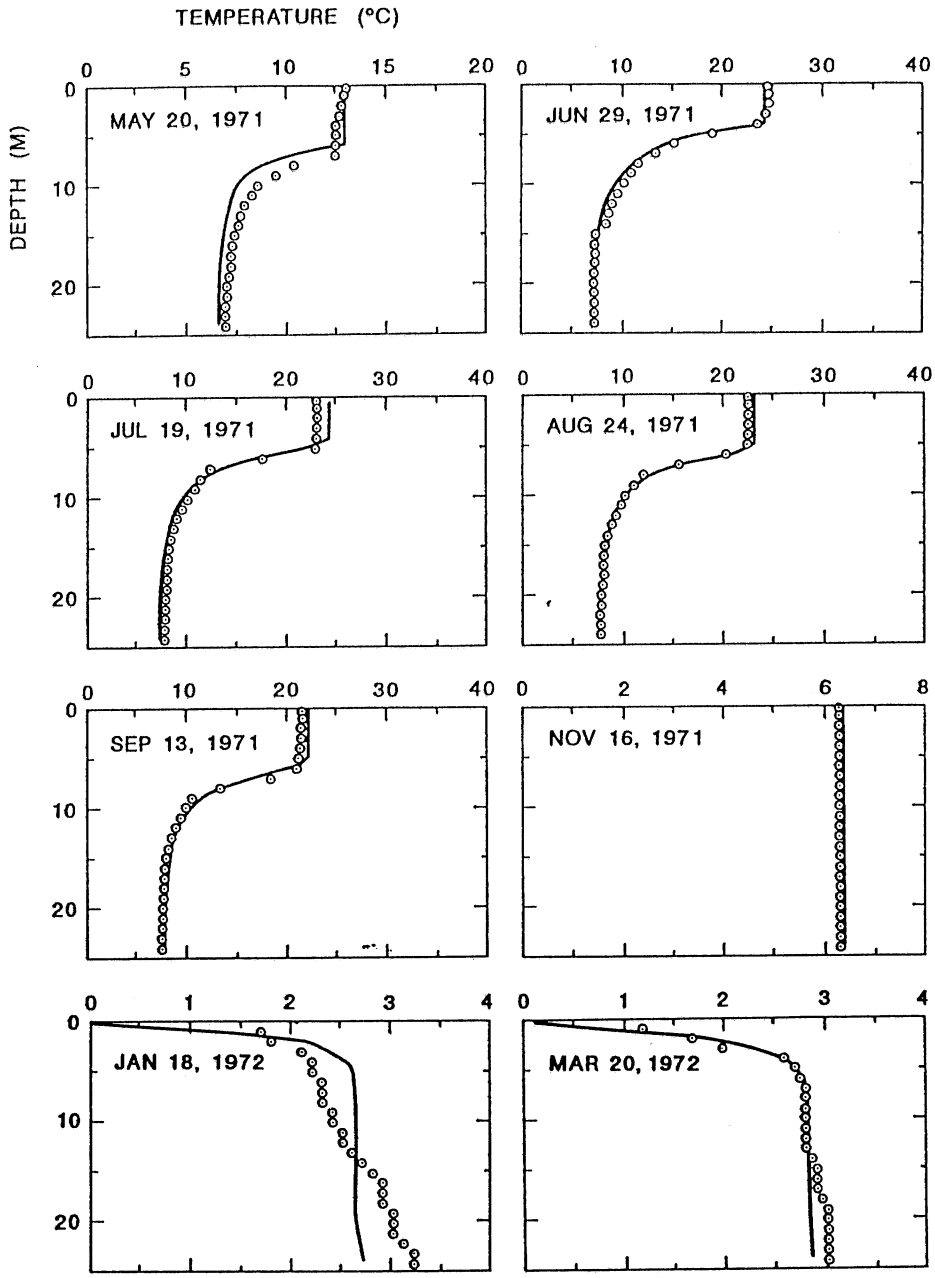

Fig. 5.3 Measured and simulated temperature profiles, Lake Calhoun, 1971–1972

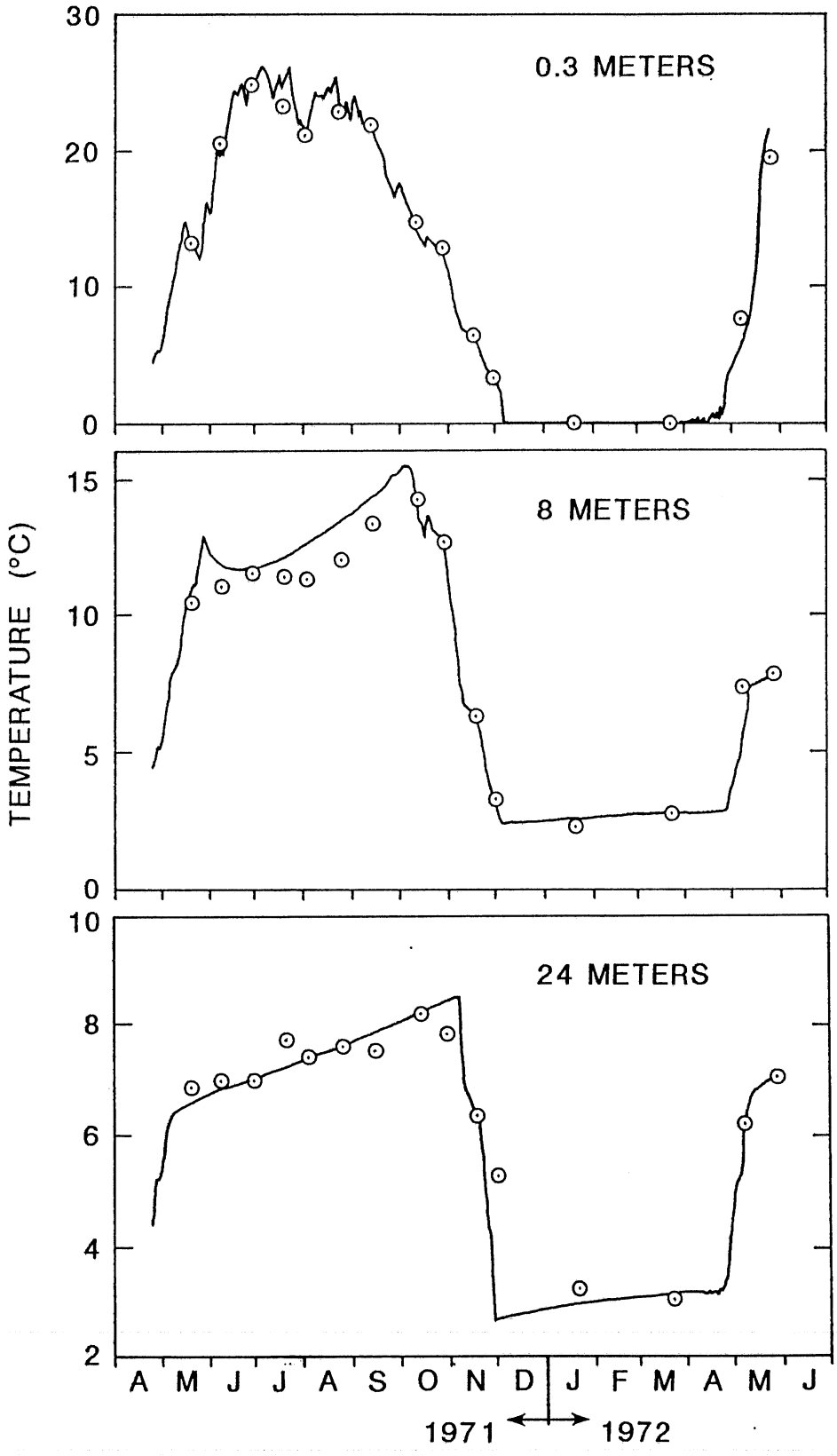

Fig. 5.4 Annual course of lake temperature at (a) 0.3 m, (b) 8.0 m and (c) 24.0 m (bottom)

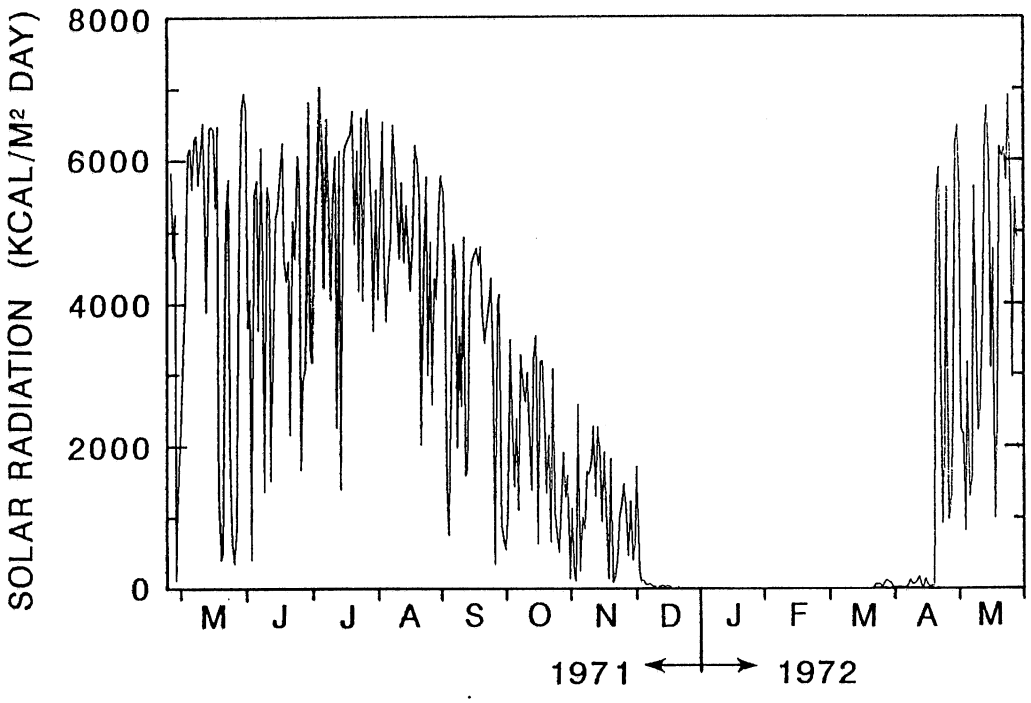

Fig. 5.5 Annual course of computed net solar radiation entering lake water

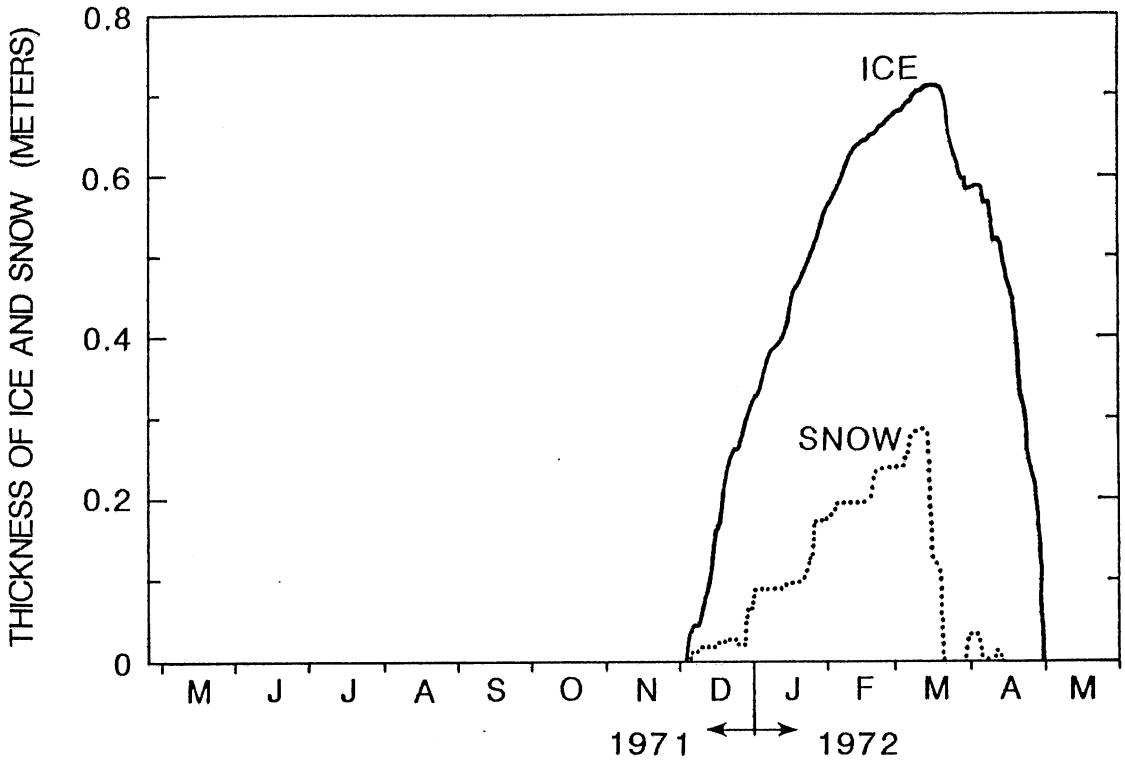

Fig. 5.6 Computed ice and snow thicknesses for Lake Calhoun, 1971–1972

Fig. 5.7 presents the simulated heat transfer rate from ice to snow to air and from water to ice. The difference of these two heat transfer rates is the latent heat of the ice associated with ice growth (positive) and decay (negative). The heat transfer from water to ice changes gradually and is quite small compared to the heat exchanged between the atmosphere and snow. The largest rates of heat transfer from the water to the ice occur at the beginning of ice formation. The major effect of the heat transfer from water to ice occurs during ice melting. Fig. 5.7 also shows that the cumulative heat flux from water to ice is only about 9% of the cumulative heat flux from snow (ice) to air.

The annual temperature envelope in the lake sediment (Fig. 5.8) was drawn by using the calculated temperature profiles at different times of the year. Fig. 5.8 displays the behavior described by Falkenmark's data (Ashton, 1986). From January 30 to April 10 (before the ice melting) the sediment–temperature profiles seem not strongly affected because the lake water temperature near the bottom does not change much.

The annual course of heat exchange between water and sediment is shown in Fig. 5.9. The heat flux is strongly related to the bottom water temperature (Fig. 5.4). The heat flux changes its direction during fall overturn when the bottom water temperature drops rapidly. Fig. 5.9 also shows the cumulative heat flux through the water/sediment interface and the heat balance in a one year cycle. Direct measurements of the temperatures in the sediments of Lake Calhoun have not been made. Temperature measurements by Falkenmark in the bottom sediments of Lake Velen in southern Sweden (Ashton, 1986) have shown an average heat flux of 1.0 to 2.0 W m^{-2} and a maximum heat flux of 4.0 W m^{-2}. These are consistent with a theoretical calculation of heat flux by O'Neil and Ashton (1981) based on a sinusoidal annual water temperature approximation. The average and maximum heat flux from sediments to water calculated here for lake Calhoun are approximately 1.6 and 6.0 W m^{-2}, respectively. The maximum heat flux was at the beginning of the ice cover period. The actual "crash" of the water temperature just prior to freezeup may result in a higher heat flux at the beginning of the ice cover period and the average water temperature of 2.0 to 3.0 °C may lead to a lower heat flux from sediments to water in the rest of the period than the analytical value based on the sinusoidal annual water temperature cycle truncated at 0° C.

5.5.2 Ryan Lake simulation

Field data for Ryan Lake, Minnesota, collected by Ellis et al (1990) were used to validate further the year–round temperature simulation model and its submodels SNOWICE and SEDIMENT. Simulated were ice thickness, snow thickness, vertical water temperature profiles and temperature distribution in the bottom sediment. These results were compared with field measurements.

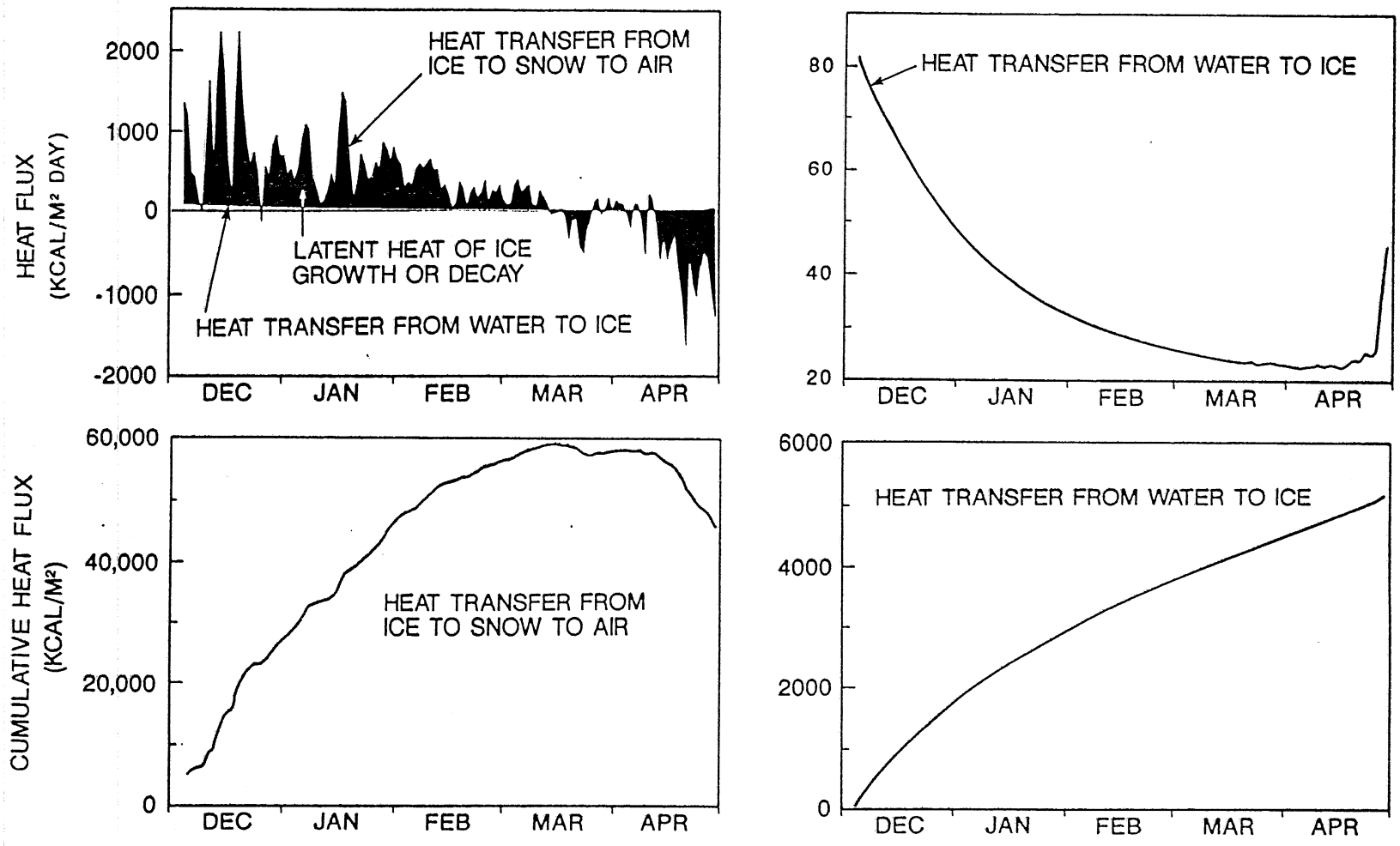

Fig. 5.7 Heat transfer rates and cumulative heat fluxes from ice to snow to air and from water to ice

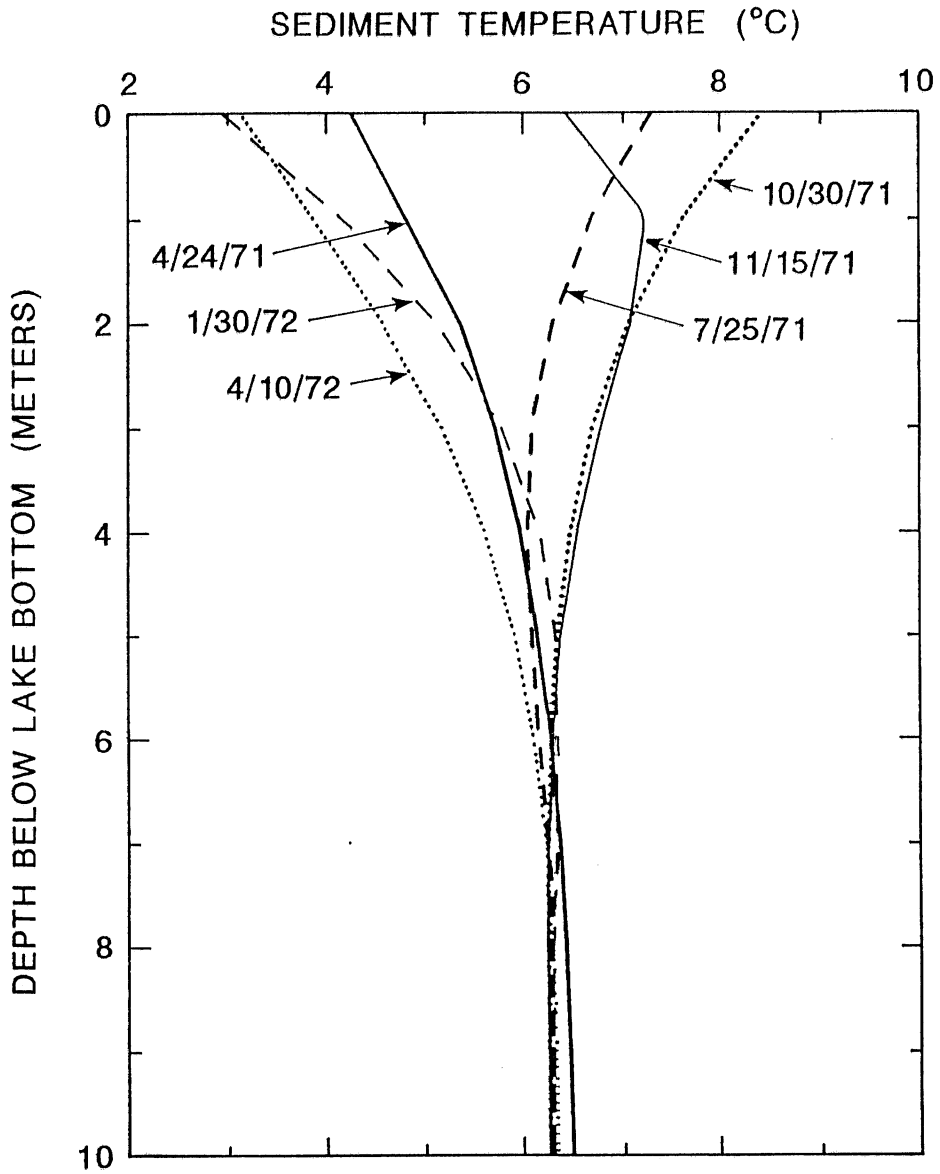

Fig. 5.8 Annual sediment temperature envelope

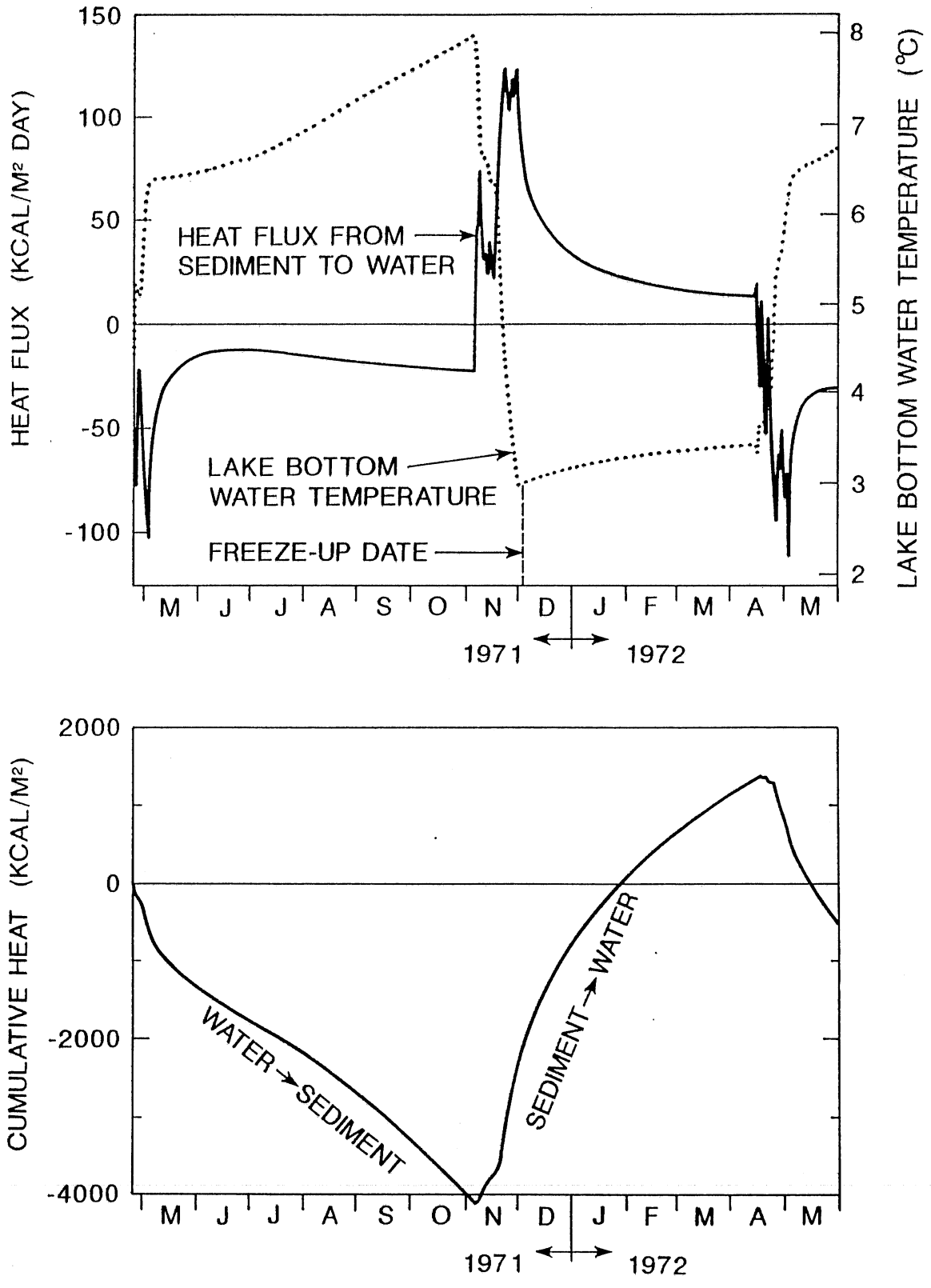

Fig. 5.9 Annual course of heat exchange through the water/sediment interface

Ryan Lake has a surface area of 6.1 hectares, a mean depth of 5.0 meters and a maximum depth of 11.0 meters (Ellis et al., 1990). The thermisters were placed 0.0, 2.0, 3.0, 4.0, 5.0, 6.0, 7.0, 8.0, 8., 9.0, 9.5, 9.75, 10.0, 10.2, 10.4, 10.6, 10.8, 11.0, 11.1, 11.2, and 12.2 meters above the lake bottom and 0.5, 1.0 and 1.5 meters into the sediments to measure temperatures of air, snow and/or ice, water and sediments. Measurement of the 24 temperatures was made every 2 minutes and averaged and stored every 20 minutes. Data was collected from Nov. 15, 1989 to Apr. 3, 1990, a complete ice cover period. Ice and snow thicknesses were intermittently measured.

Numerical simulations of (water and sediment) temperature dynamics and ice formation and decay were performed. Material properties such as density, specific heat and thermal conductivity or diffusivity were assumed homogeneous in the semi–infinite sediment below the lake bottom. The thermal diffusivity of sediment used in the simulation was 0.0225 m^2/day. The molecular diffusivity coefficient of water was considered as the lower bound of diffusivity of water in the lake. The upper bound was set by HKMAX. A HKMAX value of 0.1 m^2/day was used for the simulation period, i.e. the ice cover period from Nov. 15, 1989 to Apr. 3, 1990. Surface absorption coefficients, surface reflectivity and attenuation coefficients of snow and ice used in the simulation were 0.32, 0.7, 38 (m^{-1}), 0.18, 0.45 and 1.7 (m^{-1}), respectively. The water reflected fraction was computed from a function of the solar radiation entering the water surface and concentration of suspended sediments (Stefan, et al., 1982). The absorption coefficient and attenuation coefficient of water were equal to 0.3 and 0.5 (m^{-1}) respectively.

Predicted and observed ice thicknesses during the winter of 1989–1990 are shown in Fig. 5.10. The measured ice thickness includes data from Island Lake and the Harris Wastewater Ponds, for comparison. Statistical analysis of error between field data and simulated ice thickness gave a regression slope of 0.99, a regression coefficient of 0.91 and a standard error of 0.05 m (Appendix A). Measured and modeled ice and snow thicknesses in Ryan Lake for the winter of 1988–1989 are shown in Fig. 5.11. It can be seen that the model predicted the snow thickness as well as the ice thickness reasonably well.

Sediment temperatures were recorded only to a depth of 1.5 m below the bottom of Ryan Lake. The Lake Calhoun simulation showed, however, that the temperature waves of the annual period propagating from the sediment surface downward penetrated to a depth of 6 m. Beneath this depth the temperature remains constant and approximately equal to the long–term mean water temperature. Therefore the same computation domain extending to 10 m below the sediment surface and a boundary condition T_1 = 6.5 °C as in the Lake Calhoun simulation were used in the Ryan Lake simulation. Model simulations and field temperatures measured with three probes in the bottom sediments are shown in Fig. 5.12 in the form of time series. Measurements were interrupted in April. Fig. 5.13 presents field recorded and model predicted sediment temperature profiles on three different Julian days in water. Temperatures follow the typical behavior described in

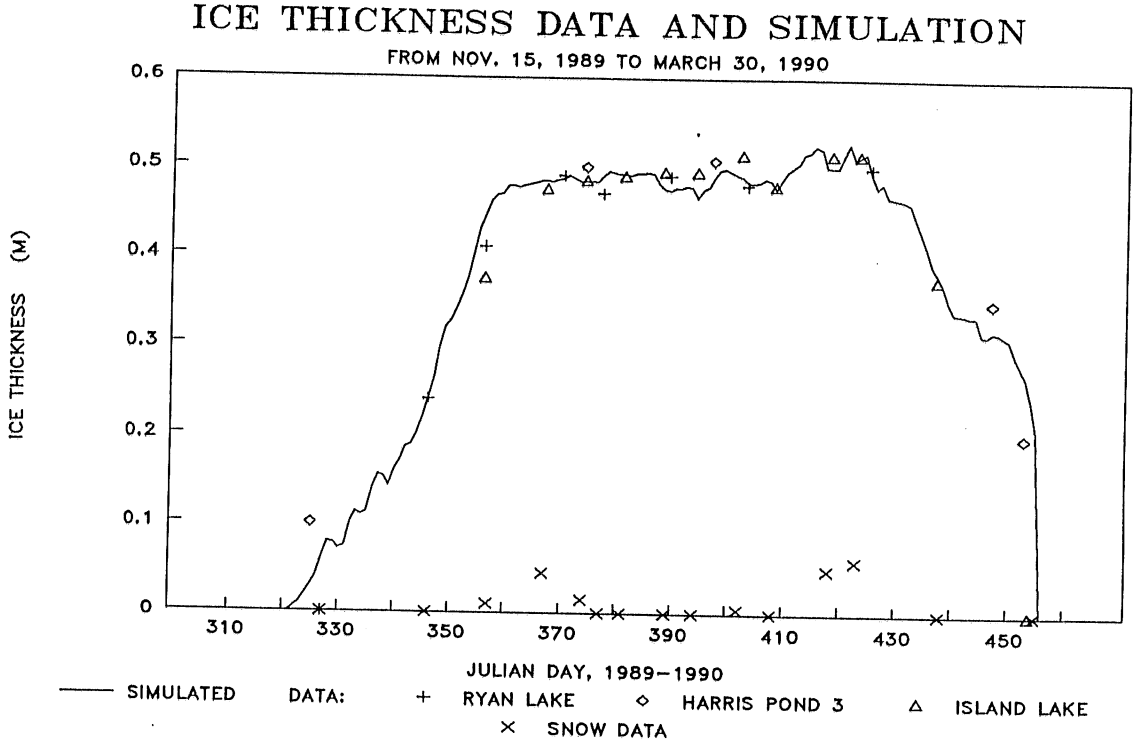

Fig. 5.10 Observed and simulated ice thickness: Ryan lake, 1989–1990

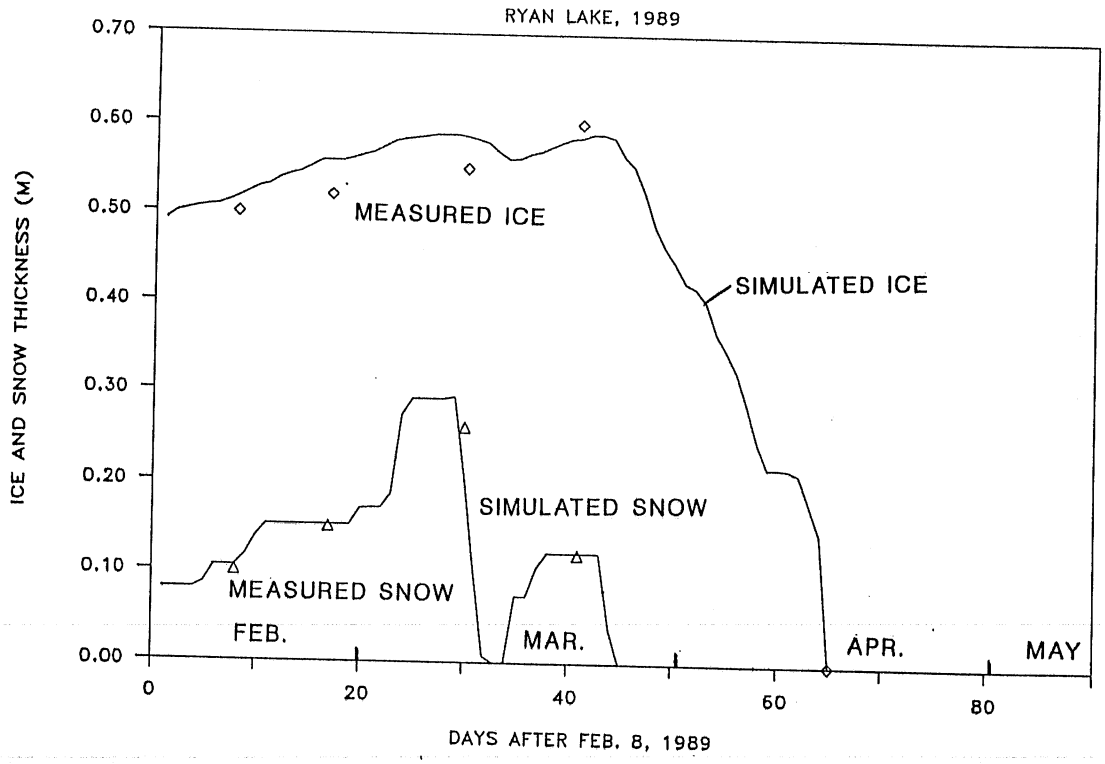

Fig. 5.11 Observed and simulated ice thickness and snow thickness: Ryan lake, 1989

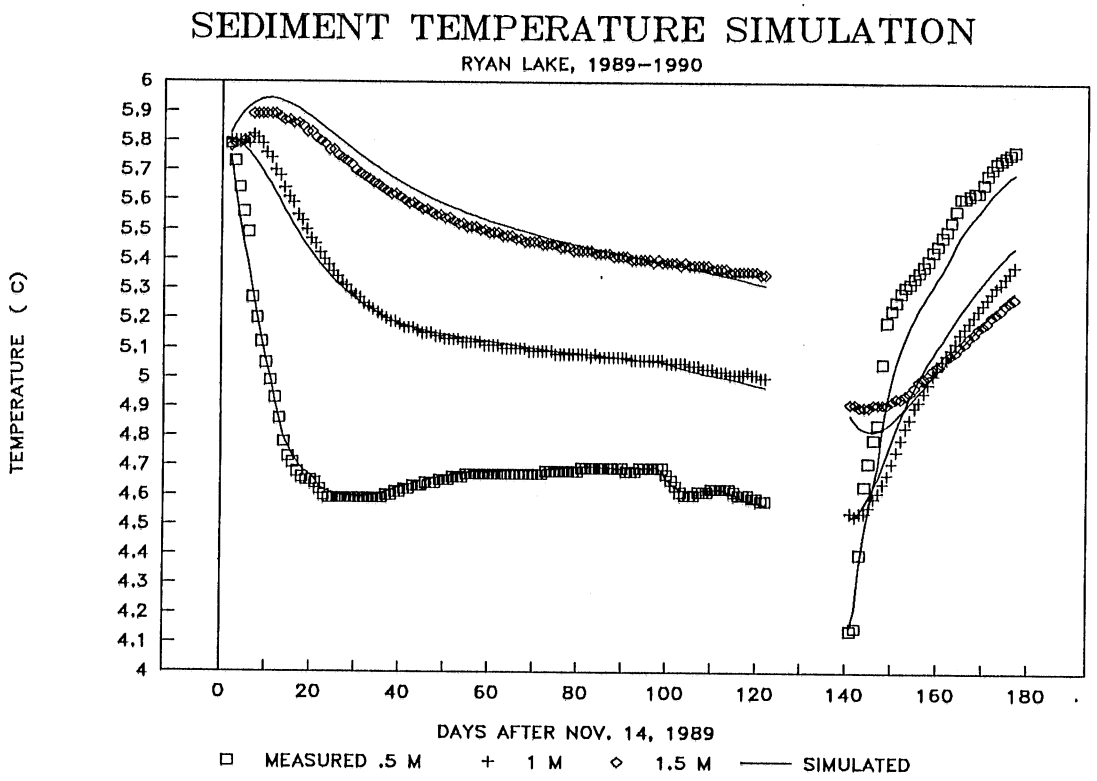

Fig. 5.12 Measured and predicted temperatures in sediments: Ryan lake, 1989–1990

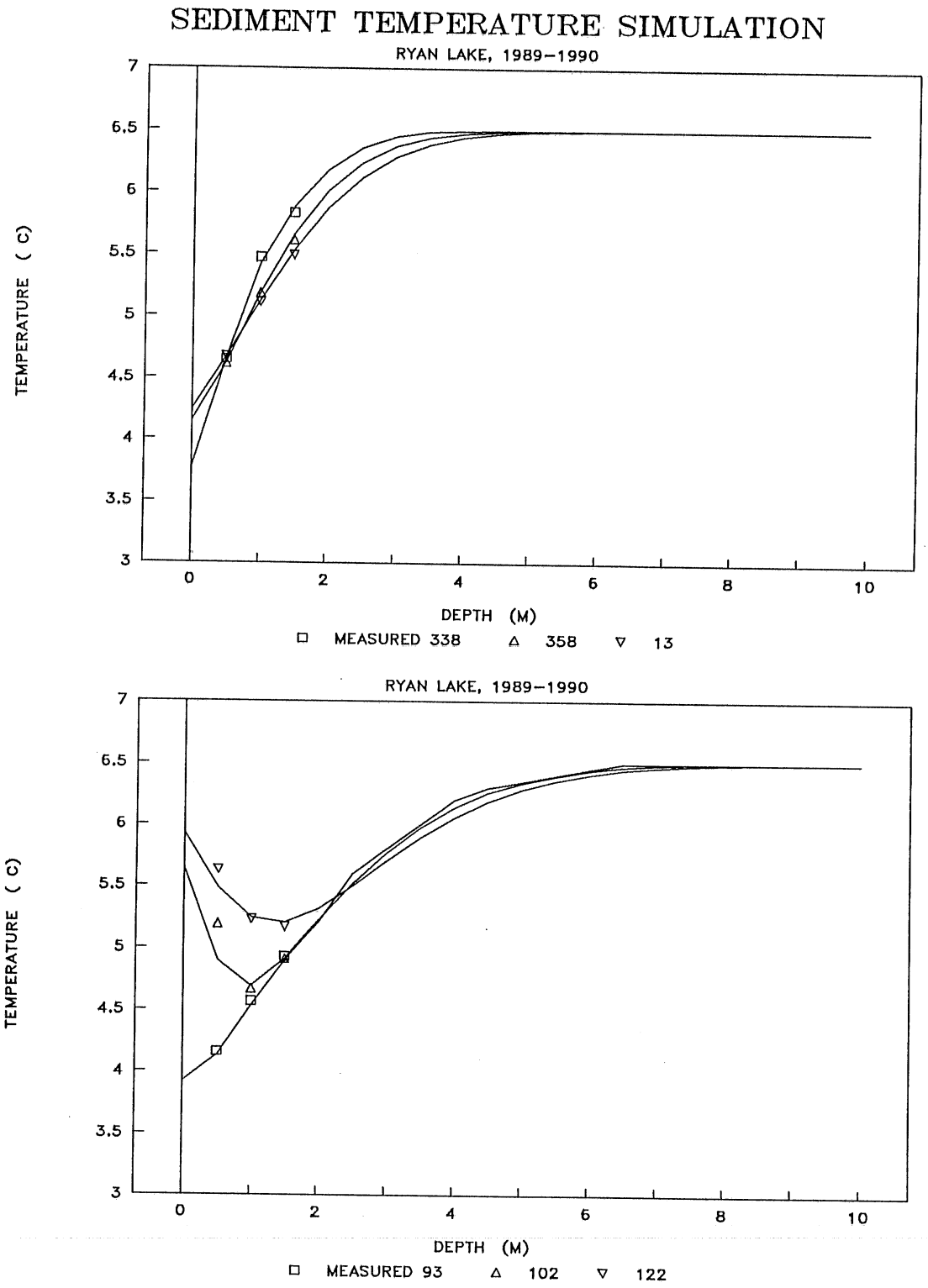

Fig. 5.13 Measured and predicted sediment temperature profiles: Ryan lake, 1989–1990

Fig. 5.8. Statistical analysis (Appendix A) indicates good agreement between data and model with a regression slope of 1.0, a regression coefficient of 0.98 and a standard error of 0.05 °C, based on 444 data points.

Good simulations of energy exchanges through the boundaries (snow and ice covers and bottom) resulted in consistent measured and predicted water temperatures in Ryan Lake. The validity of the year–round simulation model is demonstrated by the statistical analysis of error (Appendix A) based on 1936 data points, giving a regression slope of 0.97, a regression coefficient of 0.74 and a standard error of 0.33 °C. The measured and simulated water temperatures at different elevations above the lake bottom and their variation with time are presented in Fig. 5.14. It can be seen that heat flux from the sediment into the water contributed to an increase, from 3°C to 4°C, in the water temperature near the lake bottom. It is also obvious that water temperatures in the upper layers are mainly dependant on solar radiation entering the water surface after penetrating through snow and ice covers. As shown in Fig. 5.14. there are two significant drops in surface water temperatures corresponding to two major snow events in late December, 1989 and early March, 1990. Disagreement occurs during the ice melting period when the hydrological, hydraulic and thermal features are complicated. Partial breaking of the ice cover, inflows and unknown currents are examples of this complexity.

5.6 Summary

A seasonal dynamic lake water temperature simulation model (MINLAKE) has been extended to year–round conditions by adding submodels for the winter cover and lake sediments. The model has been applied to Lake Calhoun and validated indirectly by examining the effects of the winter cover on the water temperature for which field data are available. In particular, the insulating nature of the snow layer is clearly evident. The rate of change in ice thickness depends strongly on the inverse of the snow thickness. The model is directly validated against Ryan Lake data with respects to water temperatures, ice and snow thicknesses and sediment temperatures.

There are important differences between the thermal structures of the water in the summer period and during the ice–covered period. These physical processes responsible for these differences are parameterized by the mixing coefficients (HKMAX, WSTR and WCOEF) used in the year–round simulation for different seasons (summer and winter).

There is a significant heat flux between the water and the bottom sediments throughout a year. The major role of the sediments is to store heat in summer and deliver it to the water in winter. The numerical simulation of sediment temperatures with the appropriate selected boundary and initial conditions displays well the behavior described by field data. The significance of heat fluxes between sediments and water on the water temperature stratification in the lake depends on lake depth and meteorological conditions.

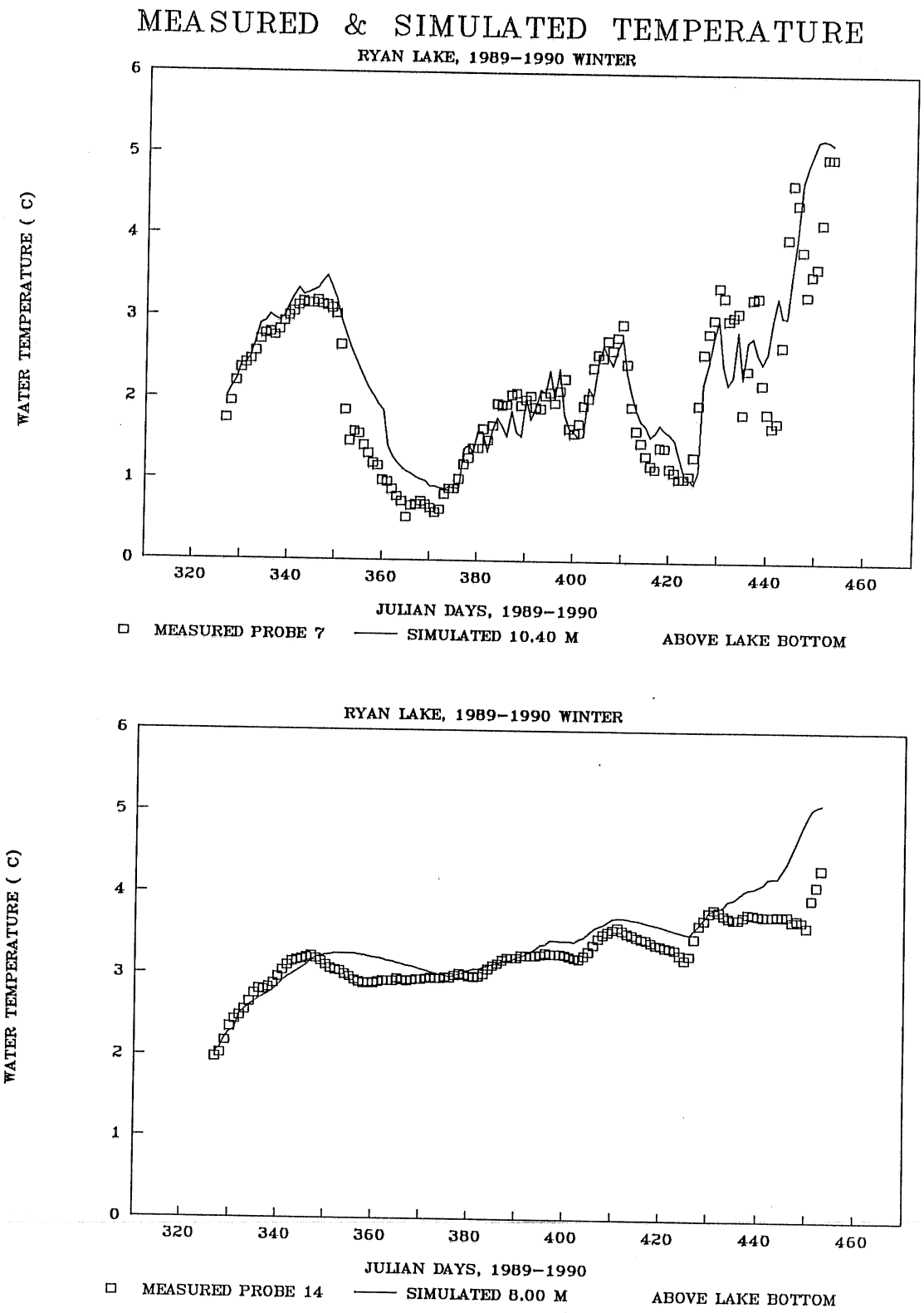

Fig. 5.14 Measured and simulated water temperatures: Ryan lake, 1989–1990

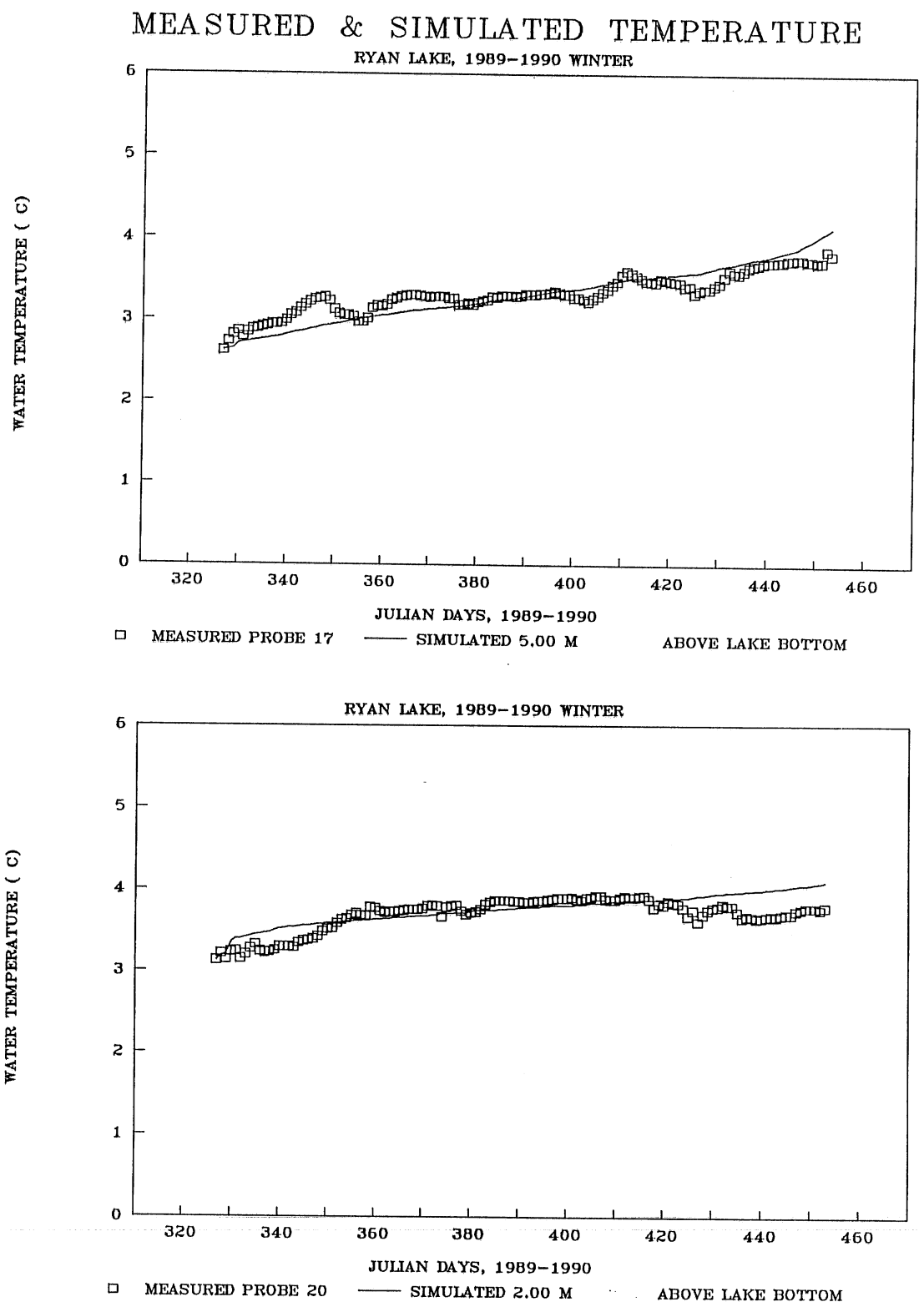

Fig. 5.14 (Continued)

The thermal structure of the water is also affected by the winter cover through attenuation of solar radiation. Particularly the snow cover has an important effect on water temperatures in the upper water layers because of its high attenuation of light as clearly shown by the Ryan Lake data.

The freeze–up date is determined by taking account of the effect of wind and ice thickness which must be sufficient to resist breakup. The rate of ice growth and decay depends strongly on heat conduction in the ice and snow cover and on the heat flux from the water to the ice cover.

Chapter 6 Simulations of Jet Mixing in a Stratified Lake or Pond

6.1 Submerged jets in a stratified lake

6.1.1 Introduction

Water column mixing by a hydraulic system consisting of withdrawal, pump and jet reinjection (Fig. 6.1a) is a form of reservoir water quality manipulation (Irwin et al., 1966; Dortch, 1979; Dortch and Holland, 1980; Steichen, 1974). The system withdraws water from one elevation and discharges it to another, typically in the form of a (horizontal or vertical) jet. This method can break down temperature stratification in a lake completely and/or create a deeper surface mixed layer. This artificial destratification is of interest during the summer growth season. There are several options for the placement of a destratification system with respect to jet orientation and location of withdrawal and discharge (Dortch, 1979; Dortch and Holland, 1980).

One method for the disposal of waste and heat from industrial processing is to discharge the warm water into large bodies of water such as reservoirs. The submerged outlets or multiport diffuser systems for thermal discharges are usually designed for summer conditions. Few studies have been conducted for winter conditions (Fig. 6.1b). Concern has been expressed on the effect of warm water jet discharges on ice–covers as well as on the ecology of ice–covered lakes during winter (Jain and Pena, 1975; Robillard and Vasseur, 1978). Of particular interest is the modification or suppression of the ice cover.

To simulate water quality with jet mixing effects a submodel for the water jet and the mixing produced by the jet (JETMIX) was developed in chapter 3. The jet–mixing submodel is a combination of nearfield jet model and farfield mixing model. It has now been linked to the existing unsteady, one–dimensional dynamic lake water quality model for a natural field (artificially undisturbed region) which simulates the effect of weather, in particular solar radiation, wind etc., and hydrological processes on stratification. Several such models are available. The one used herein is the dynamic lake water quality simulation model MINLAKE (Riley and Stefan, 1987 and 1988). Its most recent version has been described by Riley (1989). Governing equations, model assumptions, input requirements and model capacities for both models (MINLAKE and JETMIX) are summarized in Table 6.1. The MINLAKE model has been developed to simulate some important physical, biological, and other dynamic relationships in a lake on a daily time scale. Parameters such as water temperature, dissolved oxygen, phosphate, chlorophyll–a, and suspended solids among others are simulated as

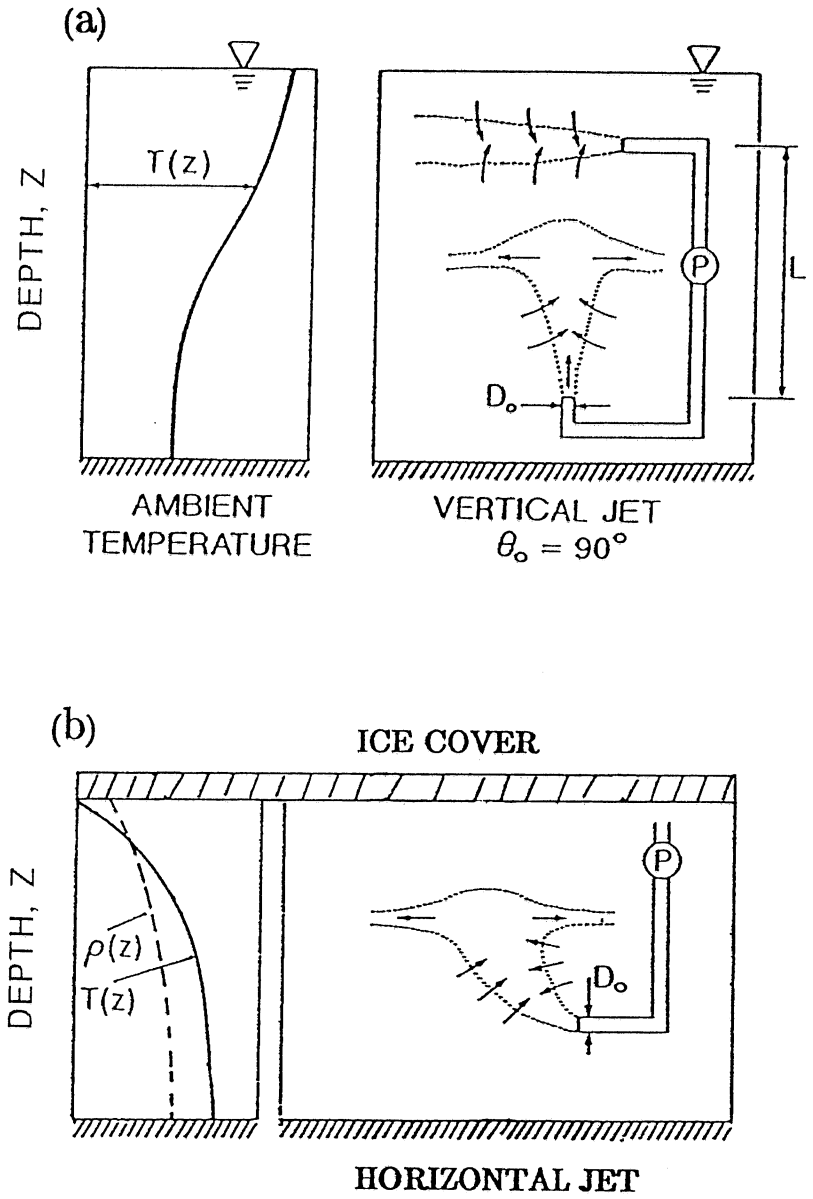

Fig. 6.1 Schematic illustration of buoyant water jets in a stratified lake: (a) a hydraulic jet–mixing system for summer destratification and (b) jet discharge system for winter waste water disposal

Table 6.1 Summary of models

Models	MINLAKE	JETMIX
Governing Equations	Conservation of mass, heat: 1–D advection–diffusion equations	Conservation of mass, momentum and energy: 2–D Eqs. of continuity, momentum and energy for jet flow; 1–D continuity Eqs. and advection Eqs. for jet mixing
Dependant Variables	Temperature or concentrations	Jet parameters; Temperature or concentrations
Independent Variables	Depth and time	Natural coordinates: jet center–line and normal; Depth and time
Assumptions	1–D lake in depth treated as series of horizontally homoge–neous layers (hori–zontally well mixed)	Similarity hypothesis for velocity and temperature profiles, steady and turbulent flow; 1–D lake closed to external factors, submerged jet
Input Requirements	Coefficients, initial conditions, (field data), inflow data, and weather data	Turbulence coefficient and dispersion ratio, jet parameters: angle, diameter (width), velocity; Locations of withdrawal and jet, discharge temperature, timestep
Capacities	Simulating existing conditions of a lake, testing lake manage–ment alternations and generating fluctu–ations in temperature, D.O., and other bio–chemical components	Calculating jet trajectories, variations of jet parameters along the jet centerline and jet entrainment; Predicting processes of jet mixing reflected by changes in temperature (or concentrations) depth profiles with time

a function of depth and time over an entire summer season (several months). The MINLAKE simulation model is process oriented and simulates heat transfer, light penetration, mixing by wind and natural convection, and biological and chemical processes related to primary productivity (Riley, 1989). The output of MINLAKE consists of daily vertical distribution of water temperature, dissolved oxygen, suspended solids, up to three forms of phytoplankton, and up to three forms of phosphorus. The water quality parameter profiles given with MINLAKE represent changes due to the natural effects. The timestep is one day, and the lake is subdivided into layers of variable thickness.

The temperature simulation of MINLAKE was, as described in chapter 5, expanded to include winter conditions so that a year–round simulation is possible (Gu and Stefan, 1990a). The incorporation of the jet model into the year–round MINLAKE model can serve to model not only the summer destratification but also the submerged water discharge and mixing effects on the thermal fields of lake water at low temperatures and the ice cover in winter.

The physical aspects of the water jet mixing processes were previously investigated in chapter 2 and 3 (see also Gu and Stefan, 1988a), and a one–dimensional simulation model was developed in chapter 3 (see also Gu and Stefan, 1988b). This simulation model for water jet mixing predicts the effect of mixing on the variability of water quality parameters with respect to lake depth. The jet mixing model (JETMIX) was coupled with the MINLAKE model by alternating changes in the water quality parameter profiles due to natural effects (results from MINLAKE) with changes due to the mixing by the water jet (Gu and Stefan, 1990b).

This section summarizes the incorporation of the water jet submodel into the year–round MINLAKE simulation model and presents sample results of numerical simulations. The extended model simulates the continuous change of lake stratification in response to artificially induced water jet mixing simultaneously with natural conditions. This model is verified against laboratory experimental data. The combined model can also be used to investigate effects of a warm water discharge on winter thermal conditions and the ice cover of a lake. The versatility of this revised MINLAKE simulation model is shown by applying the model to Lake Calhoun (Minneapolis, Minnesota). The numerical simulation results of a hypothetical summer destratification with water jets in the lake and a planned submerged winter water discharge into the quiescent water near freezing temperature (0° C to 4° C) in the lake are presented to illustrate the capacity and applicability of the combined model. The lake has a surface area of 1.71×10^6 m^2, a volume of 1.71×10^7 m^3 and a mean depth of 10 m. Maximum depth is 27 m. The results can be used to design a hydraulic jet–mixing system for a lake or reservoir in summer and a submerged thermal outfall for year–round conditions.

6.1.2 Incorporation of the jet mixing submodel JETMIX into MINLAKE

The JETMIX model, which simulates changes in the vertical profiles of water quality parameters with time due to mixing by a circular horizontal or vertical jet, was incorporated into the MINLAKE model which predicts the water quality in response to natural effects particularly atmospheric inputs. The water quality parameter profiles given with each simulation of JETMIX are different from those given with MINLAKE alone. The problem was assumed quasi–steady. Calculations in JETMIX and calculations in MINLAKE are alternated. The jet mixing subroutine is linked to the main program by the "lake specific subroutine" in MINLAKE. This subroutine allows the user to adapt the program to a specific lake and specific treatment circumstance without modifying the main program. Shown in Fig. 6.2 is a flowchart to illustrate the incorporation of the jet mixing subroutine JETMIX into the main program MINLAKE. The combined simulation model predicts vertical distribution profiles of water quality parameters at successive time steps during the mixing process. The state variables are temperature, dissolved oxygen, suspended solid, phytoplankton and phosphorus. For computations initial conditions are specified, e.g. the temperature profile at time $t = 0$, and information on the lake (area and depth) and the jet mixing system (jet diameter, flowrate and location). Jet densimetric Froude number and the stratification number, as defined in chapter 2, are specified.

There are two lines of communication between the MINLAKE and JETMIX models. One is through the state variables (water quality parameters). The profile of each state variable at the end of each time step as calculated by the main program (MINLAKE) is taken as the initial condition (input) of the jet mixing calculation carried out by the subroutine (JETMIX) for that time step. The profile calculated by JETMIX is stored in MINLAKE for the next time step.

The other line of model communication consists of entrainment from ambient layers by the jet. The entrainment is defined as the volume received from (negative) or added to (positive) each ambient layer by the jet. Each entrainment layer is computed first for each time step in the jet mixing subroutine with the initial state variable profile taken from the output of MINLAKE. The vertical distribution of entrainment is sent to the MINLAKE program to determine the new layer thicknesses and water quality distribution at the end of the time step.

The jet mixing subroutine has the same time step as the main program if the time required for full mixing is much larger than the time step used in MINLAKE (1 day). Otherwise the time step used in JETMIX is smaller than one day. Lake destratification results from changes in the thickness of lake water layers and the position of the layers. The center of each layer may move up or down, depending on the change in the thickness of the layer and the neighboring layers.

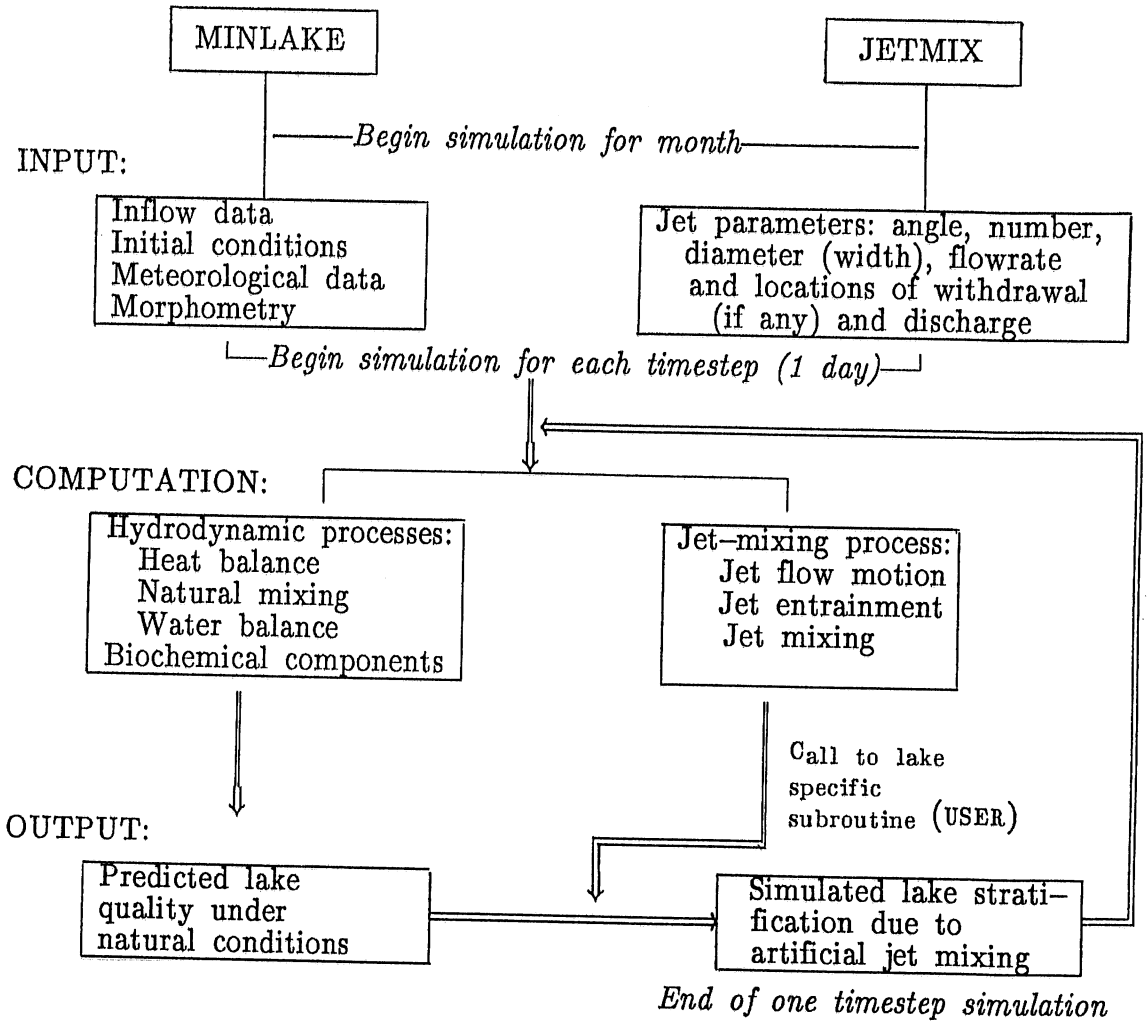

Fig. 6.2 Flowchart illustrating the incorporation of the jet mixing model (JETMIX) into the dynamic lake water quality model (MINLAKE)

6.1.3 Application to modeling of summer destratification

Validation of the simulation model with laboratory data

The MINLAKE model has been applied to Lake Chicot, Ark., Long Lake, Round Lake and Lake Riley, Minn. Several other lakes are currently under study. The calibration and verification of the model were discussed by Riley and Stefan (1987, 1988) and Riley (1989). The 1–D jet–mixing model (JETMIX) was verified in chapter 4 against experimental data for both horizontal and vertical jets in a stratified laboratory tank and applied to the mixing of Vesuvius Lake, Ohio (Gu and Stefan, 1988b). The integral jet model was previously validated and calibrated in chapter 3 with data from Fan (Hirst, 1971), Wright and Walance (1979), Lee and Cheung (1986). Presented here are the results of the simulations with the combined JETMIX and MINLAKE model verified against experimental data for vertical jets. Experiments on the mixing of stratified water by buoyant jets were described in chapter 4.

Since MINLAKE was designed for a natural lake, modifications in the input data files and the main program were made so that a laboratory tank could be simulated. The main difference between the tank and a real lake included the absence of external effects due to solar radiation and wind at the water surface, time scales and space scales.

Fig. 6.3 illustrates selected measured vertical temperature profiles and numerical simulations for two of the experiments (see Table 4.1). The computed and measured vertical temperature profiles agree well. The temperature discrepancies in the surface layers are due to a small rate of heat loss through the water surface during the laboratory experiments, where the simulations assume a zero heat loss rate. Standard error between predicted and measured values in water temperatures was 0.15° C for profiles shown in Fig. 6.3a and 0.25° C for profiles shown in Fig. 6.3b. Both experiments used vertical jets but had different densimetric Froude numbers (10 and 2) and stratification numbers (32 and 48). Profiles of water temperatures are shown at different dimensionless time t*. t* is defined as tQ/V, where t = time, Q = jet flow rate, and V = total lake volume.

Application to Lake Calhoun

In the application of the combined model to modeling of summer destratification in the lake, the input data consist of an initial water quality parameter profile (temperature or dissolved oxygen, etc.), hypothetical jet performance parameters, lake morphometry characteristics and meteorological conditions, followed by a simulation of the response of stratification to the jet and the weather respectively.

The simulation results presented in this section for hydraulic summer destratification of a lake is an example to show the capacity of the combined model and to illustrate the applicability of the model to a practical case. Thermal profile data for Lake Calhoun recorded in 1971 were selected since data had already been well organized. The sensitivity of the model to jet

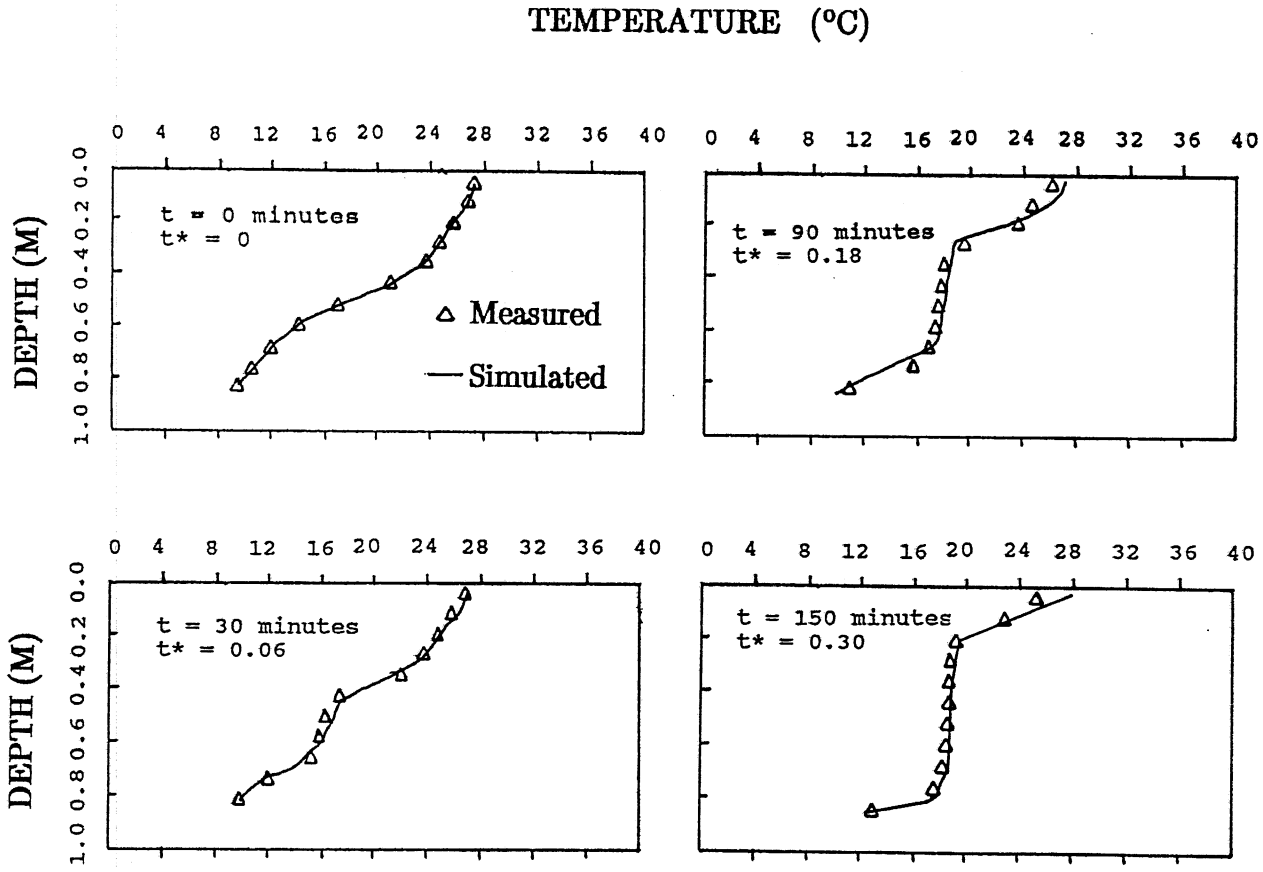

Fig. 6.3a Vertical temperature profiles using data from laboratory Exp. No. 4 and the numerical simulation with a mean standard error of 0.15 °C: Fr = 2, St = 32, $\theta = 90^{o}$

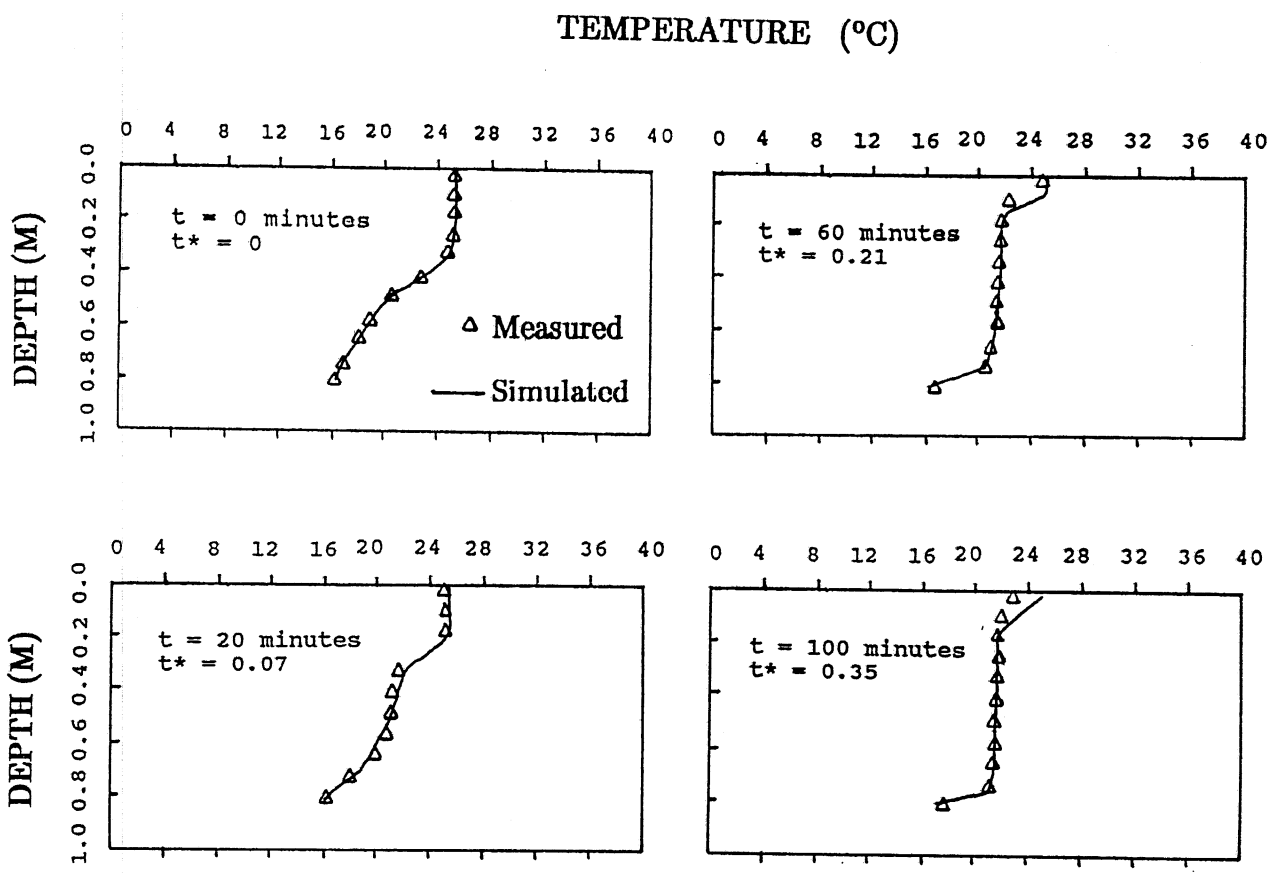

Fig. 6.3b Vertical temperature profiles using data from laboratory Exp. No. 8 and the numerical simulation with a mean standard error of 0.25 °C: Fr = 10, St = 48, $\theta = 90^{o}$

parameter values is also examined. There are no field measurements of water quality profiles with jet mixing available to compare with the simulated ones.

Sample results are presented in Figs. 6.4 and 6.5 in the form of temperature and dissolved oxygen profiles vs. depth at various times after the beginning of mixing. Horizontal and vertical jets are simulated. Other state variables characterizing water quality, such as phosphorus and chlorophyll, can be simulated by the same procedures. Chemical or biological kinetics are not included in these results but can be taken from the MINLAKE model. Physical characteristics of the systems simulated are listed in Table 6.2. In the simulations leading to Fig. 6.4 and Fig. 6.5, operation of the system is initiated on May 19, 1971. Water is withdrawn from a depth of 2 m below the lake water surface and discharged at a depth of 12 m. The mixing effects of horizontal jets are not very dependent on the densimetric Froude number Fr but significant differences are shown between vertical and horizontal jets. More mixing is generated by horizontal jets than vertical jets during the first month of operation. Vertical jets bring more heat and dissolved oxygen to the mixed layer than horizontal jets bring during the latter period of operation.

Table 6.2 Characteristics of hydraulic mixing systems for summer destratification

System	Injection angle	Jet diameter	Number of jets	Jet flow rate	Densimetric Froude number
	(°)	(m)		(m^3/s)	
1	90	0.23	20	0.05	6.7
2	0	0.23	10	0.10	13.3
3	0	0.23	20	0.05	6.7
4	0	0.23	40	0.025	3.3

It can be seen in Figs. 6.4 and 6.5 that the lake is not truly destratified, but transferred into a three–layer system in terms of temperature and dissolved oxygen. Jet mixing by the pumping system produces a new and nearly uniform layer in place of the previous thermocline. The circulation also creates two new sharper thermoclines at the top and bottom of the new layer. Water quality in the previous thermocline region or below is improved with the transport of heat and dissolved oxygen from upper layers of the lake where temperatures and the concentration of dissolved oxygen are higher.

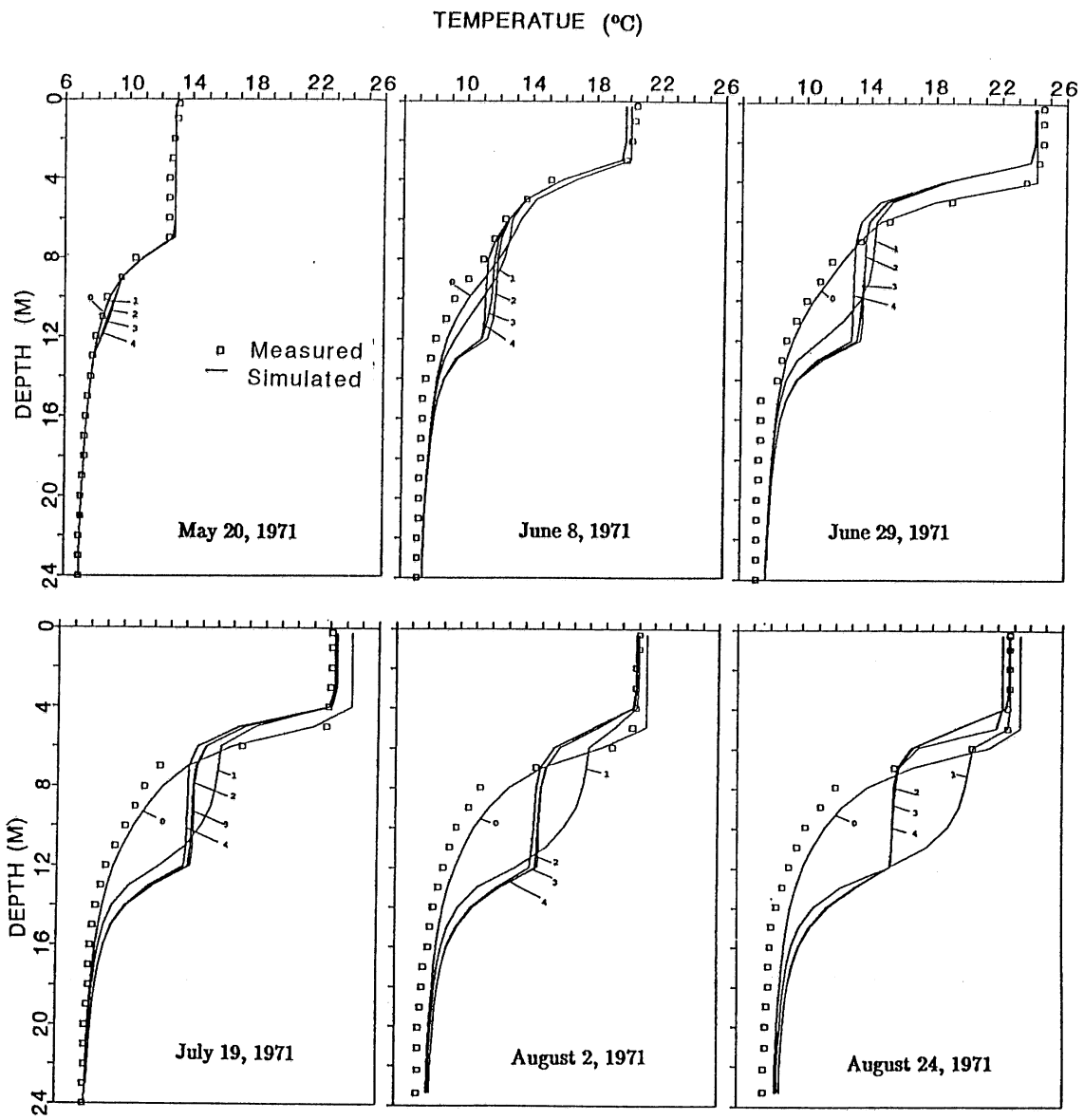

Fig. 6.4 Temperature profiles in Lake Calhoun (1971): field data (symbols) and simulations (solid lines) without jet mixing (0) and for hydraulic systems 1, 2, 3 and 4

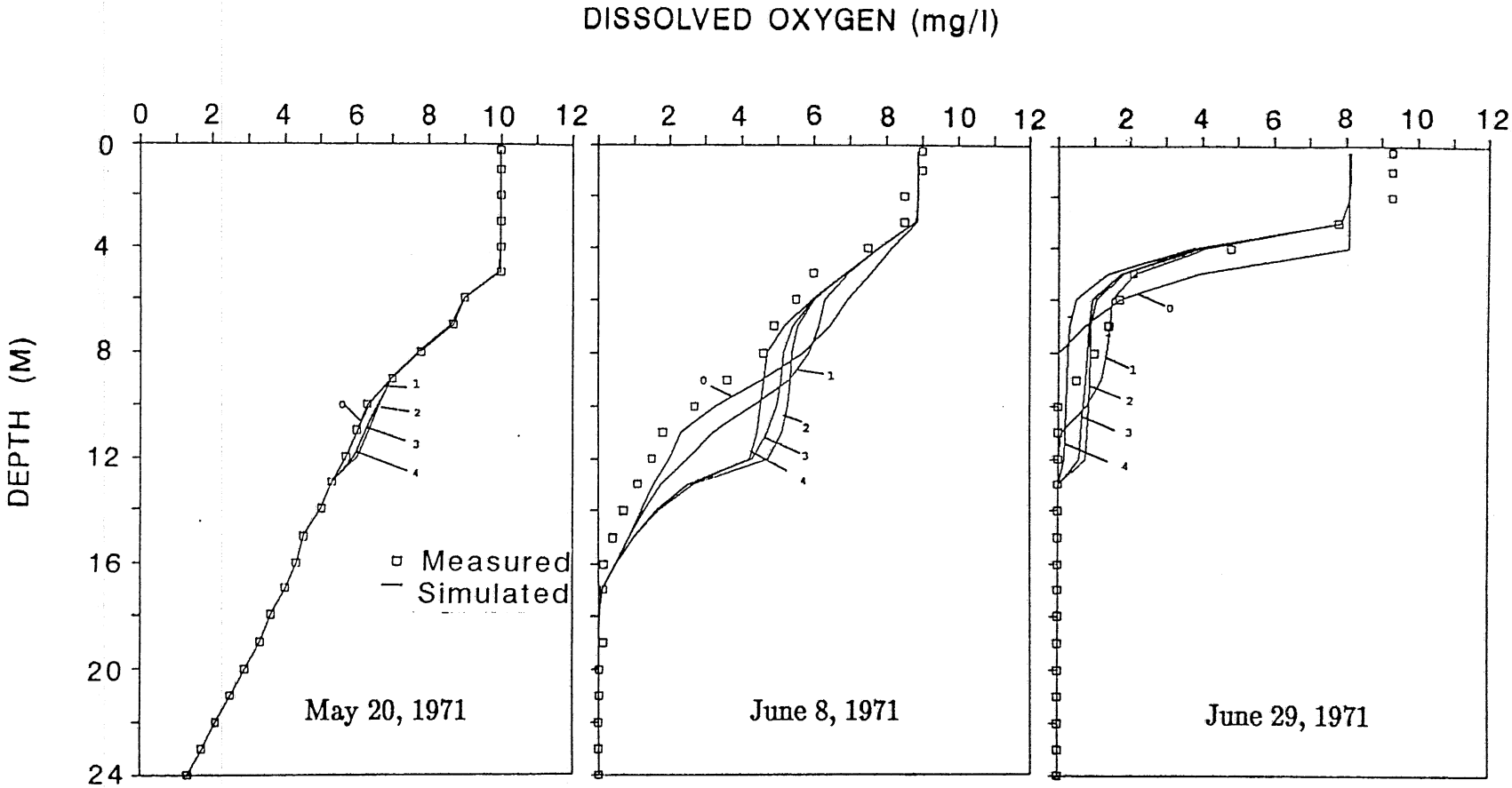

Fig. 6.5 Dissolved oxygen profiles in Lake Calhoun (1971): field data (symbols) and simulations (solid lines) without jet mixing (0) and for hydraulic systems 1, 2, 3 and 4

When the densimetric Froude number is very large, the vertical jet collapses on the water surface forming a horizontal spreading layer. In this case the typical jet flow pattern is lost. The model does not simulate the surface impingement and possible plunging flow as similarity assumptions do not hold in this region. However, the limitation $Fr < Fr_c$ does not make the model less practical since jets with low Froude numbers are preferable because of higher energy efficiencies. If the vertical jet reaches the water surface of the lake, a separate simulation model which was developed in chapter 3 (section 3.4) has to be used to handle surface impingement and plunging flow.

6.1.4 Application to warm water discharge into ice–covered lake

The jet mixing submodel was also applied to the simulation of a planned submerged water discharge into Lake Calhoun in winter. This simulation analyzes the hypothetical response of lake water temperature to jet mixing under the ice cover. In adapting the existing numerical models, the presence of an ice cover at the free surface and of low ambient water temperature (0° C to 4° C) has to be considered. The presence of an ice cover modifies the surface heat transfer.

A typical water temperature structure of a north central U.S. lake in winter is 0° C at the ice/water interface and 3° to 4° C at the lake bottom. The temperature of the entire mixing layer produced by the discharge is increased by the gain of heat from the warm water injection. Due to the density anomaly of water at low temperatures (maximum density at 4° C), a density instability may be encountered. The density of the mixing layers may be larger than that of the layers below the injection elevation. Under this condition the jet is negatively buoyant. The heavier water in the upper layers will therefore sink downward to mix with the lighter water in the lower layers until the density instability disappears. This convective mixing process was incorporated into the model of the warm water discharge in winter. Ice thickness and heat transfer through the ice cover and snow cover were contained in the original model.

Fig. 6.6 shows, as an example of simulated results, the effects of a warm water discharge (10° C) on the thermal structure in Lake Calhoun in winter. Such a discharge was proposed in 1988 for the disposal of groundwater. The lake has a typical winter temperature profile (0° C to 4° C). The warm water is discharged at a depth of 15 m in horizontal direction from a submerged circular pipe with a radius of 0.23 m. The discharge rate is 0.063 m^3/s. The densimetric Froude number Fr = 8.4. With these conditions the rise of the warm water jet due to buoyancy is limited by the presence of the stable stratification in the ambient water. The simulated warm water jet did not reach the ice cover even after four months of continuous injection (as shown in Fig. 6.6). The mixing of the jet with the ambient water is weak and occurs within a layer between 8 m and 15 m depth below the surface. Therefore effects of the warm water discharge on the ice cover are predicted to be negligible. The proposed discharge was not implemented and the prediction could therefore not be verified.

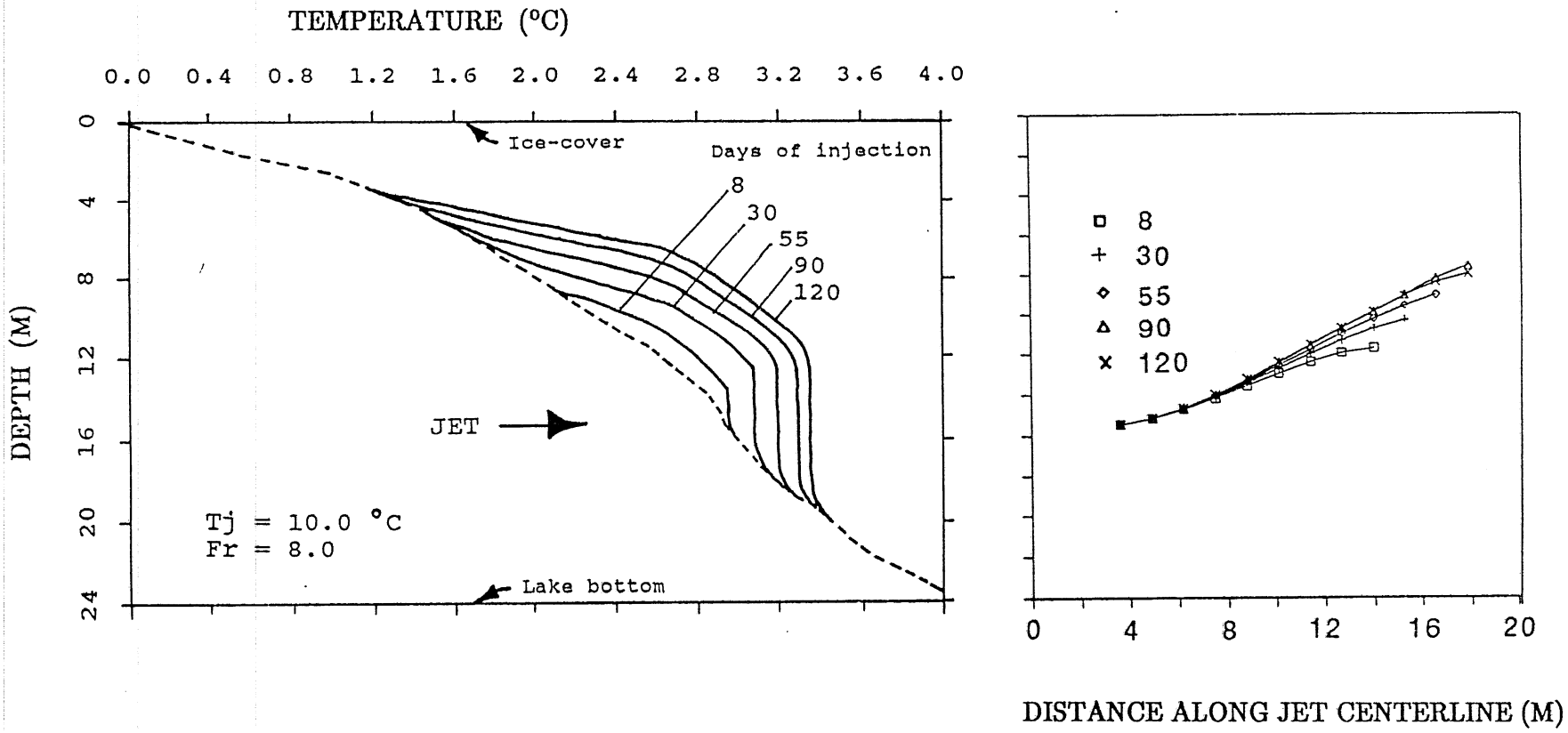

Fig. 6.6 Simulation of temperature distribution produced by a warm water discharge into a ice-covered lake and variation of jet centerline trajectories with time (Tj = 10°C)

The behavior of a jet in the temperature range where the density variation is nonlinear will be quite different from that of a buoyant jet in which the density can be assumed to be a linear function of the temperature. When the water jet simulation model is applied to the winter situation, another complex phenomenon is encountered. Due to the peculiar variation of the density of water at low temperatures, a heated jet discharging into quiescent water near freezing temperature (0° C to 4° C) can either sink due to negative buoyancy or rise due to positive buoyancy. Because of inertial effects, it can overshoot its depth of neutral buoyancy and an oscillation, as simulated in Fig. 6.7, may result. Such an oscillation has impacts on stability of stratification and turbulent mixing in the flow field. Turbulence is largely enhanced by the instability of stratification. The shear at the interface of the intruding layer and the ambient water at the oscillation level will induce re–entrainment and enhance the turbulent mixing. Fig. 6.7 also shows the non–linear effects for various discharge temperatures. It is found that the jet trajectory is very sensitive to temperatures around 4° C.

6.2 Vertical jet discharge into a shallow wastewater stabilization pond

In this section a simplified integral mixing model for a vertical jet discharge into a shallow water developed in chapter 3 is incorporated into the MINLAKE model. Simulations of the jet entrainment from ambient water, depth of flow intrusion (spreading) and forced mixing of the pond water due to the vertical inflow jet are performed for Harris wastewater stabilization ponds. Useful knowledge is obtained for the prediction of the temperature stratification dynamics and for the study of physical limnology and management of ponds (Gu and Stefan, 1991).

At the Harris wastewater treatment facility wastewater is pumped underground through a 4 inch diameter pipe and discharged vertically at the bottom in the center of pond 1 (Fig. 3.20). The inflow rate and the inflow water temperature were continuously measured at the pumping station during operation for about 1 year (Luck and Stefan, 1990). The average inflowrate was 185 gallons per minute (0.0167 m^3/s). The inflow was intermittent. Typically one of two pumps would kick in at roughly 20 minute intervals and run for 2–3 minutes. This form of wastewater inflow produces a forced jet which upwells on the surface and a surface spreading flow. Due to differences in densities between the incoming and the ambient pond water the surface spreading flow tends to sink during the summer (Fig. 3.20).

Fig. 3.20 illustrates schematically the flow pattern produced by the wastewater discharge in pond 1 during the summer. The jet entrains much ambient water from the bottom portion of the pond. The jet reaches and overshoots the water surface due to shallow water depth (0.6–1.8 m) and high initial momentum. The condition for overshooting is the exceedance of a critical densimetric Froude number for the round jet, Fr_c (Eqs. 3.28 and 3.29). With D_j = 0.1016 m and H = 1.8 m for the wastewater discharge in Harris Pond 1, one obtains Fr_c = 6.5. A typical inflow temperature is 17° C in late summer when the pond temperature is approximately 10° C. For a

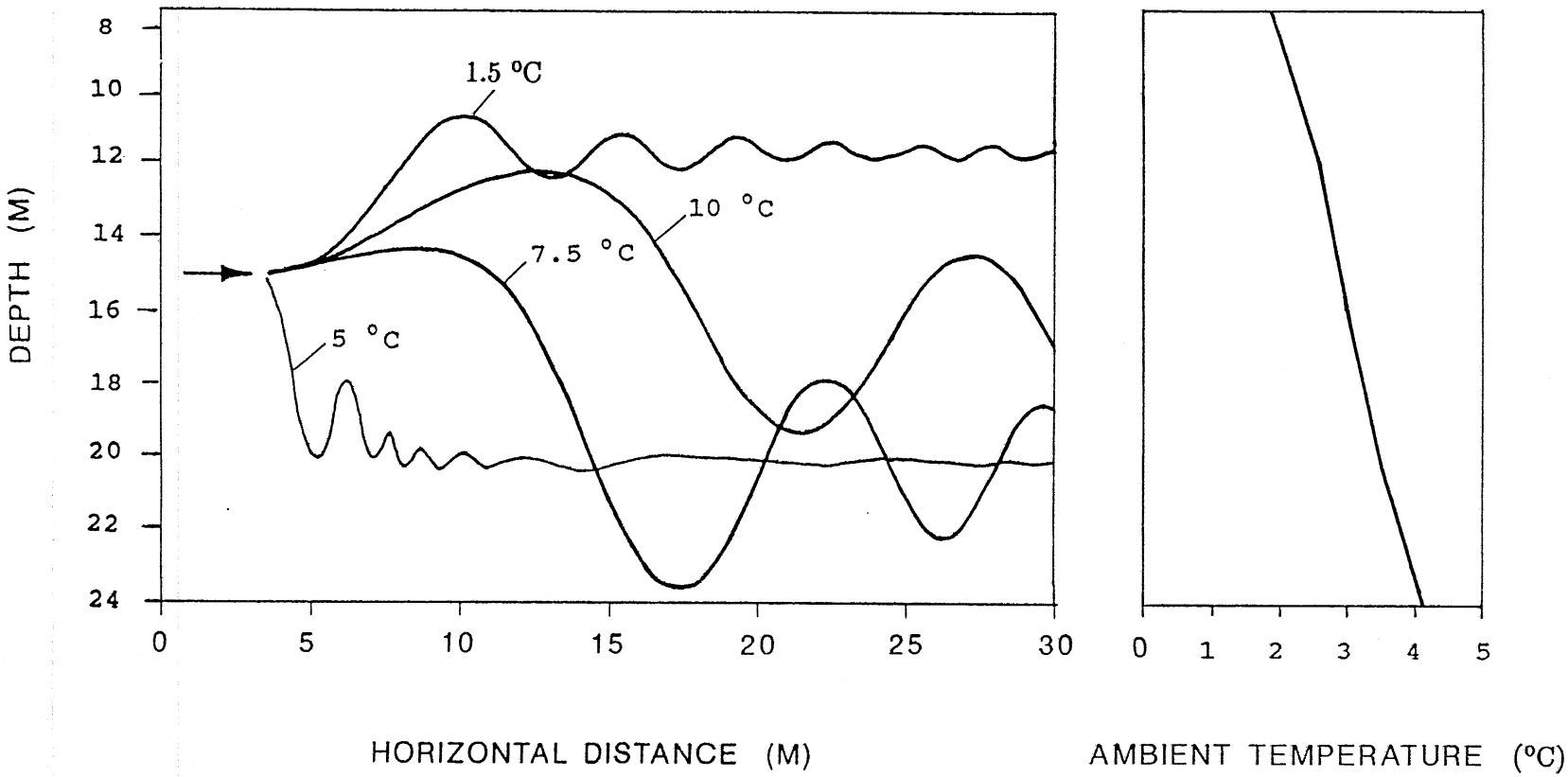

Fig. 6.7 Centerline trajectories of horizontal jets with different discharge temperatures

temperature difference of 7° C, the density difference is about 0.9 kg/m^3. With U_j = 1.44 m/s (discharge flowrate Q_j = 0.0167 m^3/s) the densimetric jet Froude number Fr = 48 using Eq. 2.12. Since this value is much larger than Fr_c (= 6.5) the discharge jet will emerge on the water surface. With H = 1.8 m and D_j = 0.1016, one gets the stability parameter for this discharge is Fr_s = 82 (Eq. 3.30). The jet flow in pond 1 satisfies the stability criterion (Lee, 1980).

It is assumed that there is no entrainment into the plunging–intruding–spreading flow beyond the jet region (nearfield). Flowrate and temperature of the interflow are therefore approximated by Eqs. 3.36 and 3.37, respectively. A density–temperature function ρ(T) (Gu and Stefan, 1988a) is used to determine the depth of the interflow layer by neutral buoyancy. If information on suspended and dissolved solids available, density due to total solids should be considered for the density calculation. The volume of each layer in the pond is modified in each timestep by subtracting the water entrained from the layer and adding the interflow to the equilibrium layer. The temperature in the equilibrium layer is modified using temperature of the incoming water weighted by its volume over a computational timestep (typically 12 hours).

Entrainment of ambient water by the vertical water jet is a function of the total pond water depth as described in Eq. 3.33 and shown in Fig. 6.8 to 6.11. Calculated results show that the ratio of entrainment, Q_e, to the inflow, Q_j, is in the range of 4 to 9 for 1989 and 6 to 10 for 1990. The temperature in the intruding–spreading layer depends on both inflow and ambient water temperature. Temperature in the spreading water is mainly determined by the ambient water temperature, which is between the injected water temperature and ambient temperature but much closer to the latter (Fig. 6.12). If entrainment is small due to shallow depth, inflow temperature is of importance. Figs. 6.13 and 6.15 show the locations where the interflow intrudes and spreads, i.e. the equilibrium layer. It can be seen (Figs. 6.12 and 6.14) that the inflow spreads closer to the bottom when the injected water is heavier (colder) than ambient water. The role of vertical jet entrainment and mixing in the temperature stratification simulation of Harris pond 1 can be seen in the comparison of temperature–depth profiles simulated with and without the jet model (Figs. 6.16 and 6.17).

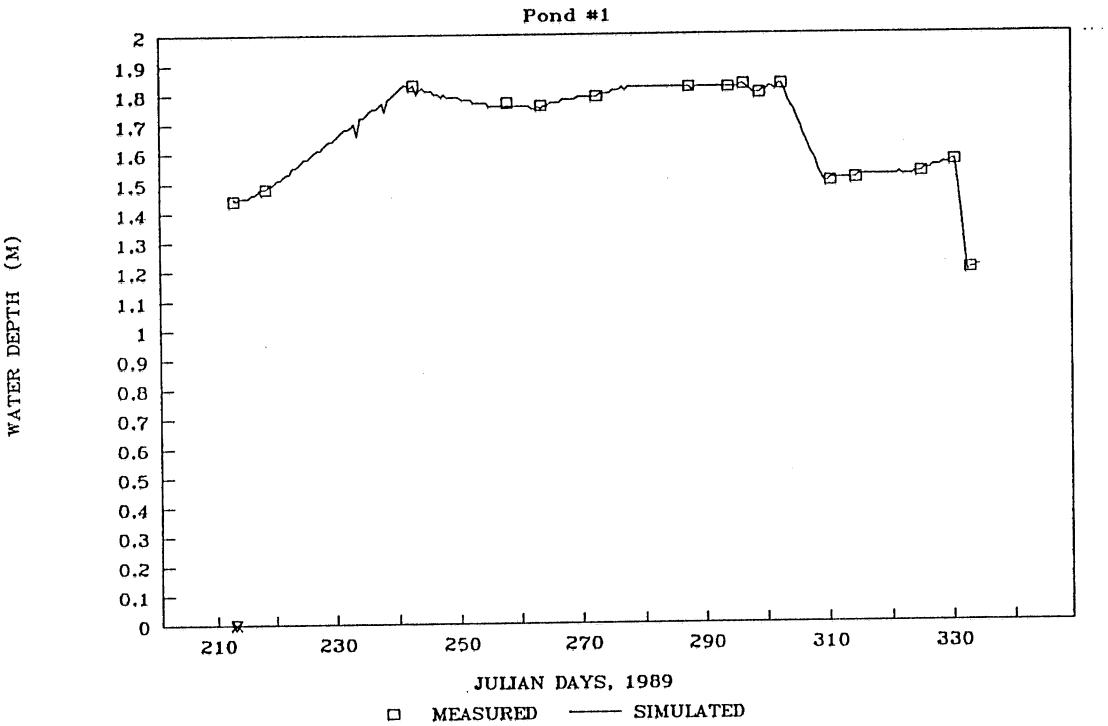

Fig. 6.8 Measured and calculated water depth: pond 1, 8/1–11/30, 1989

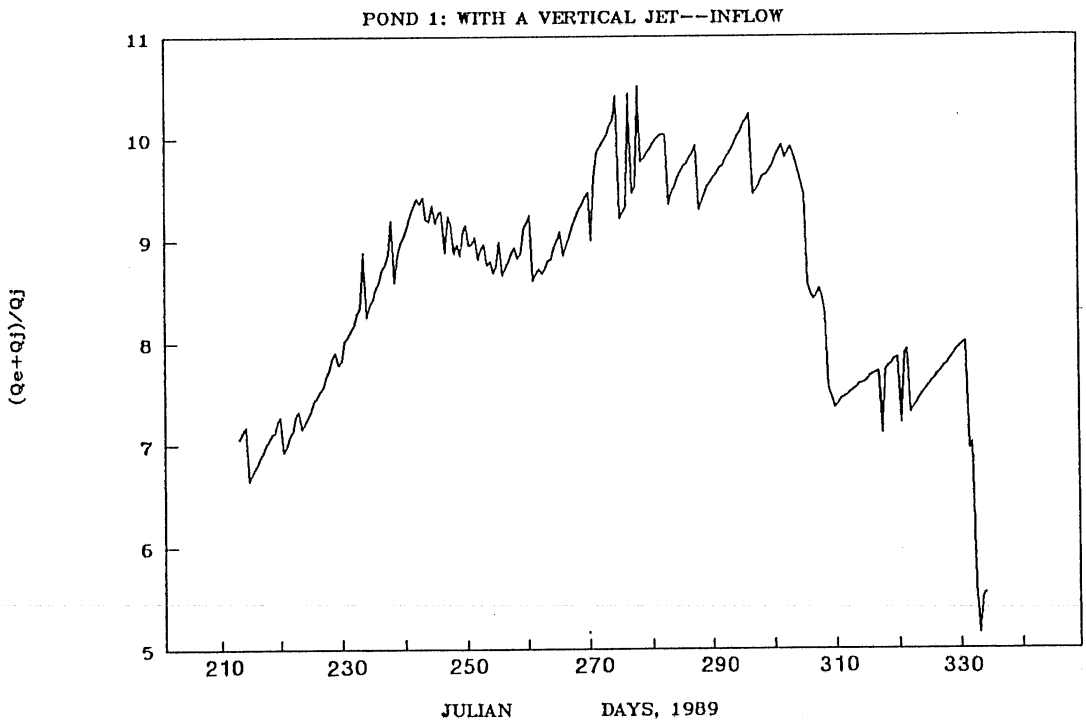

Fig. 6.9 Calculated flowrate of entrainment by inflow jet: pond 1, 1989

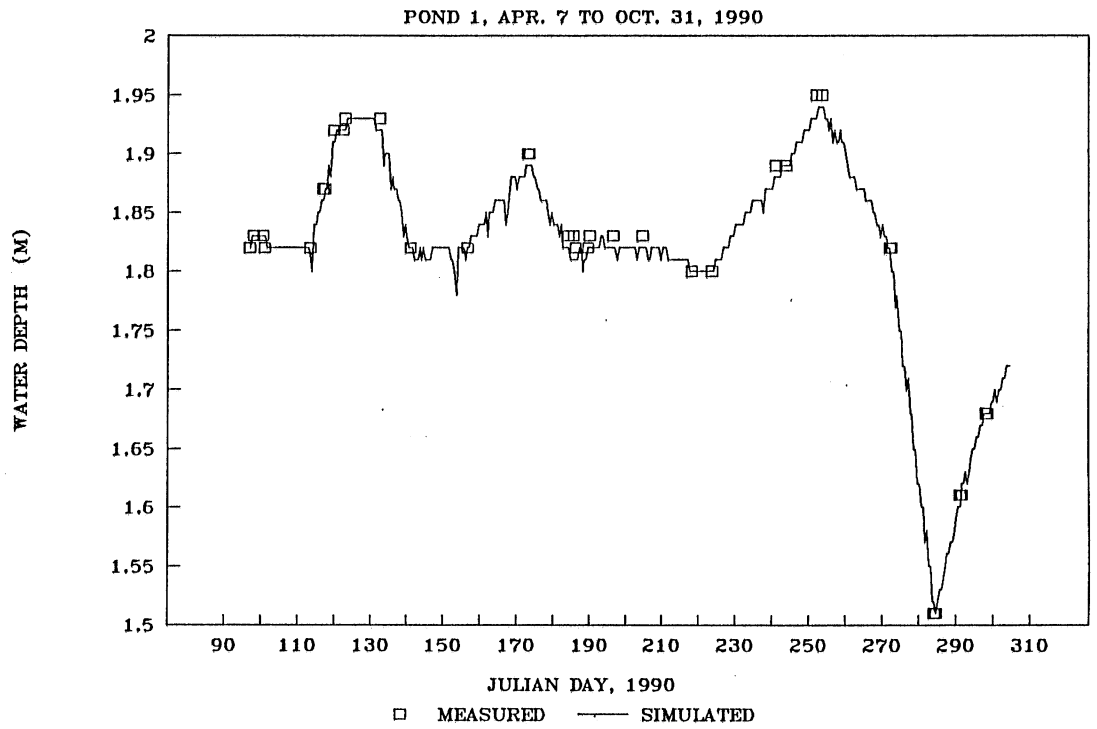

Fig. 6.10 Measured and calculated water depth, pond 1, 4/7–10/31, 1990

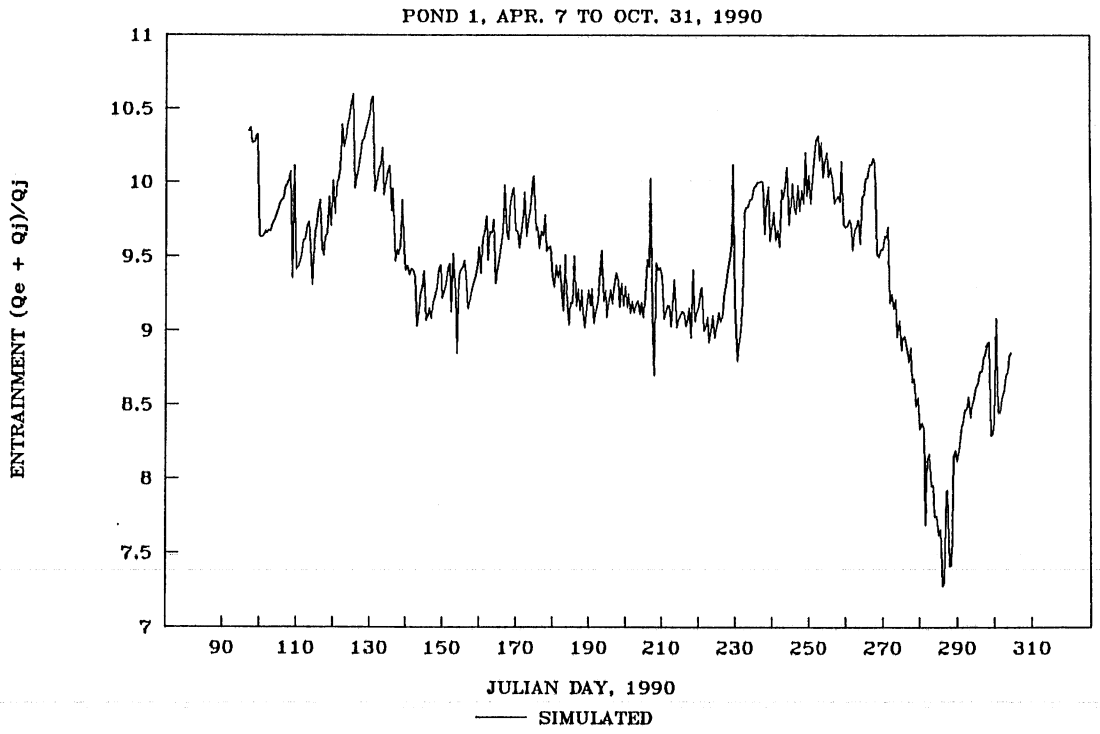

Fig. 6.11 Calculated flowrate of entrainment by inflow jet: pond 1, 1990

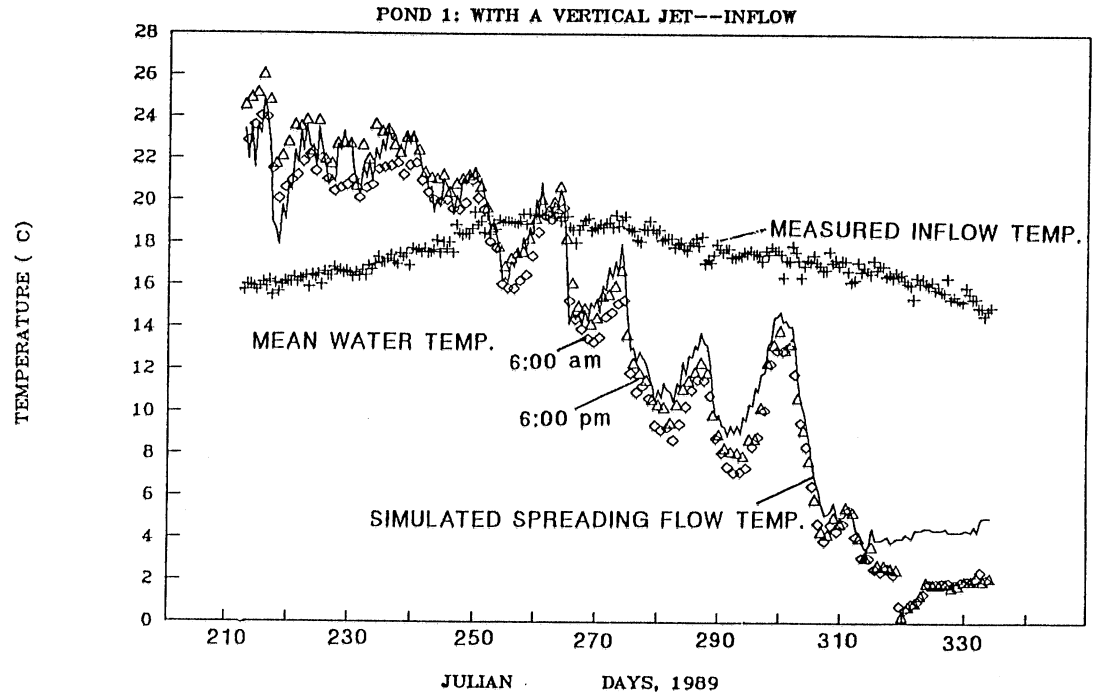

Fig. 6.12 Measured inflow temperature and simulated spreading flow temperature: pond 1, 8/1–11/30, 1989

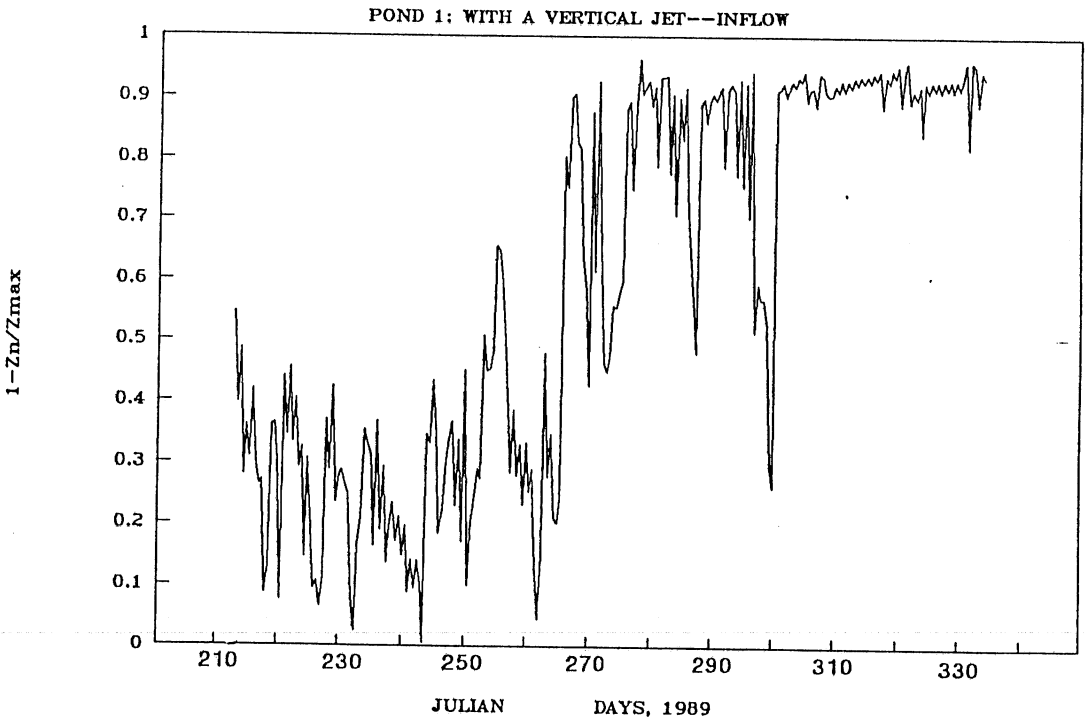

Fig. 6.13 Calculated depth of intruding interflow: pond 1, 1989

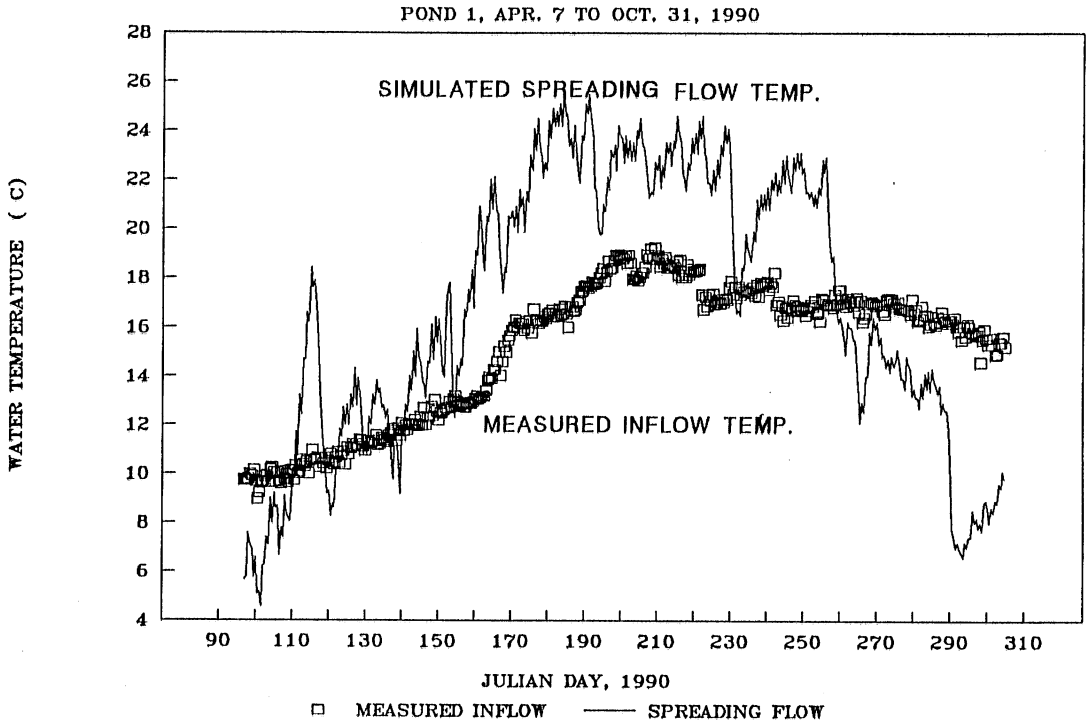

Fig. 6.14 Measured inflow temperature and simulated spreading flow temperature: pond 1, 4/7–10/31, 1990

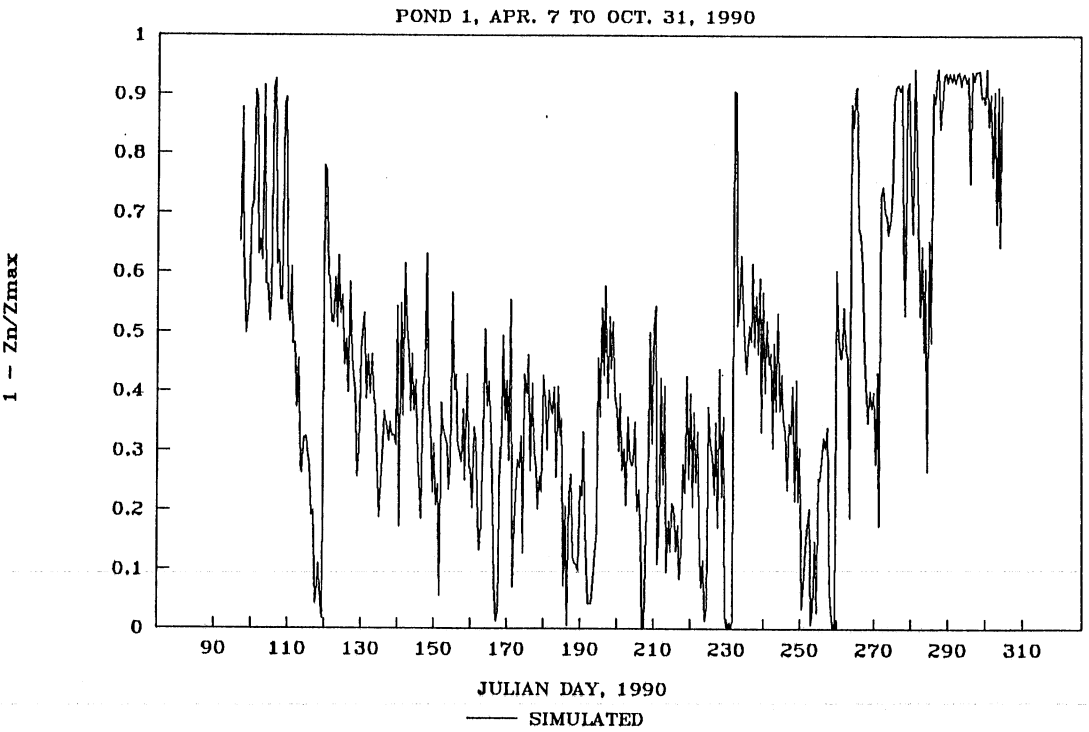

Fig. 6.15 Calculated depth of intruding interflow, pond 1, 1990

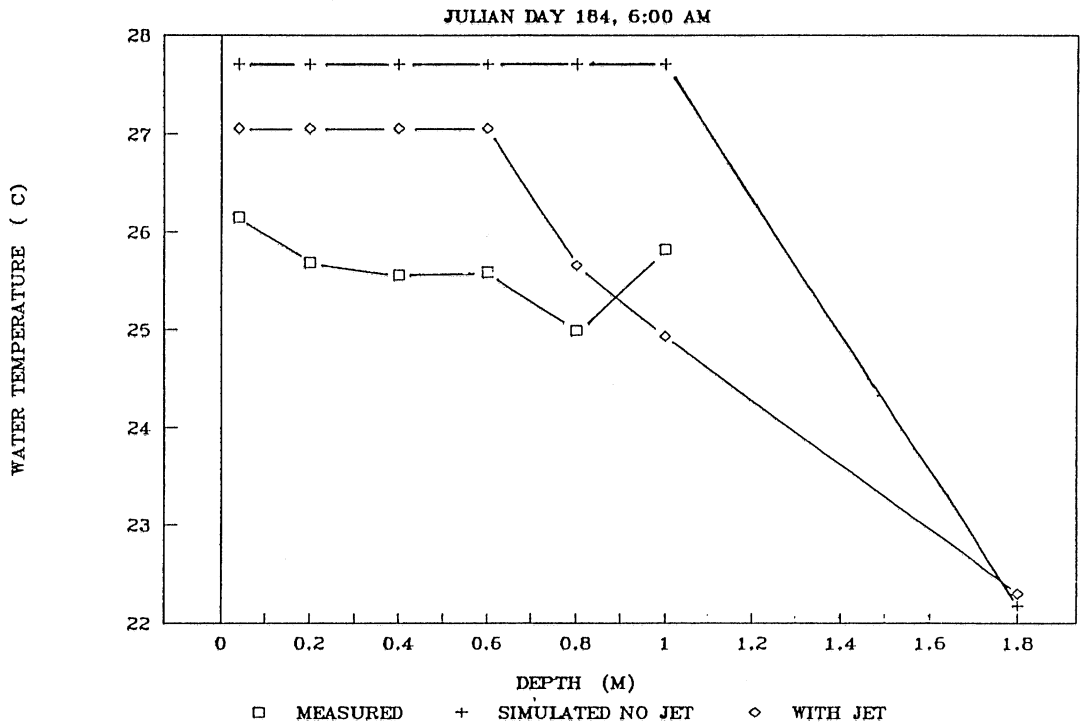

Fig. 6.16 Comparison of water temperature profiles simulated with jet and without jet, pond 1, 6:00 pm, July 3, 1990

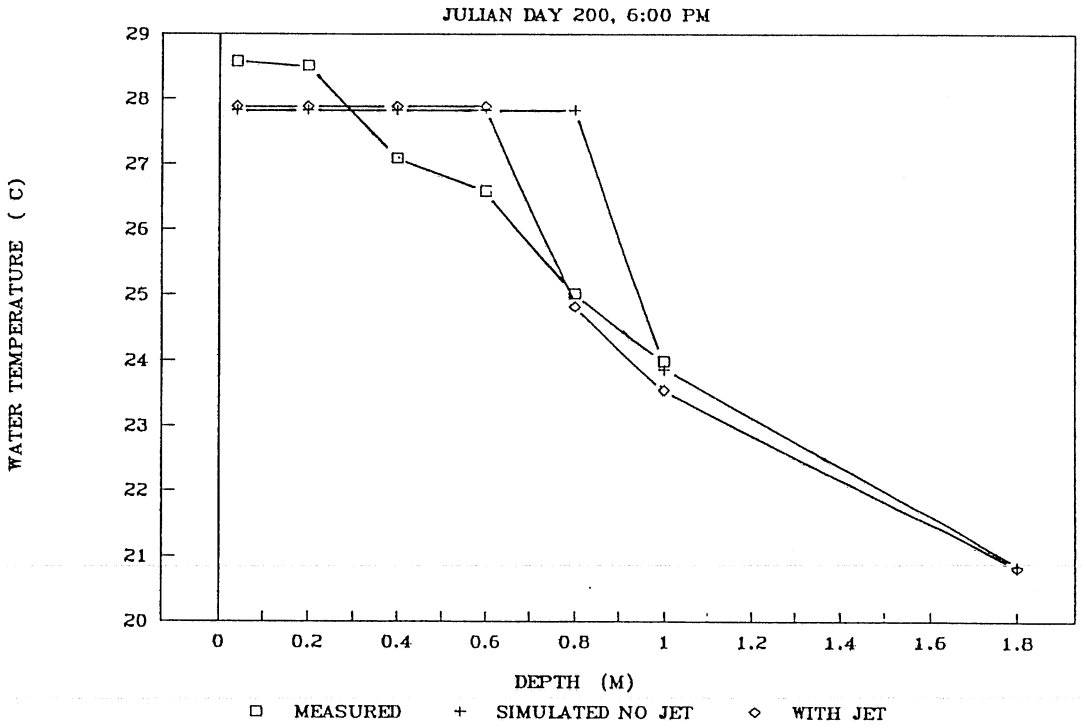

Fig. 6.17 Comparison of temperature–depth profiles simulated with jet and without jet, pond 1, 6:00 pm, Aug. 29, 1990

Chapter 7 Analysis and Design of Water Jet Destratification Systems

7.1 Introduction

An economical solution to water quality problems which are linked to thermal stratification can be to forcibly modify or break up the stratification pattern, especially in ponds or small lakes or reservoirs (Burns and Powling, 1981; Price, 1990)). Two groups of methods are in use to achieve artificially forced water column mixing: pneumatic (using air) and hydraulic (using water jets). Pneumatic destratification uses compressed air injected through a submerged diffuser. The buoyant air–water plume rises to the surface and the associated entrainment, redistribution and mixing of water eliminates thermal stratification (Lorenzen and Fast, 1977; Johnson, 1980, Maruyama, 1983; Zic, et al, 1990). Hydraulic destratification involves a water jet generated by a mechanical recirculating pump system (direct drive mixer) as discussed in earlier chapters. This system withdraws water from one elevation and discharges it vertically or horizontally at another elevation in the form of a buoyant jet flow (Fig. 7.1). It moves water from top to bottom or vice versa and produces mixing of water at various levels in the lake. Besides the recirculating pump system, a Garton pump system (Fig. 7.1) has been used for local mixing as a means of improving quality of water discharged from reservoirs rather than total lake destratification (Garton and Punnett, 1982, Garton, 1976, Steinchen, 1974). The Garton pump mainly consists of a large propeller with vertical axis installed near the water surface (axial flow pump) producing a downward directed low velocity and large volume jet with a smaller distance of jet penetration than the recirculating pump.

It has been indicated that hydraulic destratification is more efficient than pneumatic destratification (Dortch, 1979, Dortch and Holland, 1980, Holland, 1984, Holland and Dortch, 1984). Destratification efficiencies for different systems listed in Table 7.1 give a range from 1% to 35% for hydraulic recirculating pump systems (water jets) and from 0.1% to 12% for diffused–air pumping systems (air plumes).

Pneumatic methods produce only some or little direct aeration of the hypolimnion while hydraulic methods pump epilimnetic water to the bottom (Henderson–Seller, 1984). Although the hydraulic method has been less tested in the field than the pneumatic method, its use deserves more attention because of its potential higher efficiency.

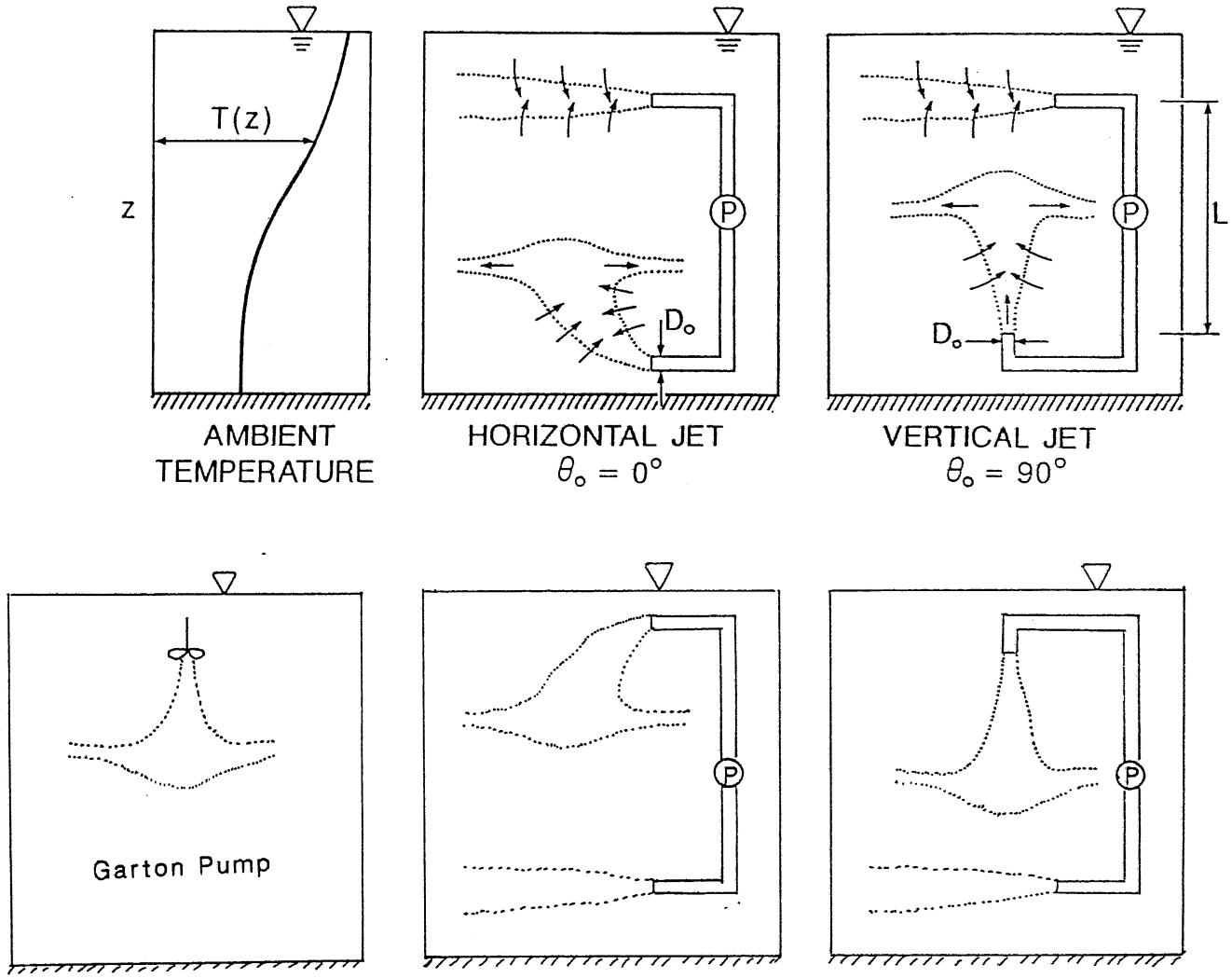

Fig. 7.1 Schematic diagram of hydraulic mixing systems in a temperature–stratified water body

Table 7.1 Destratification efficiencies for different systems

Method	System	Efficiency (%)	Type of data	Reference
Pneumatic	Diffused–air pumping systems Air bubble plumes	0.3–0.7	Field	Almquist, 1987
		0.03–1.5	Field	Steichen, 1974
		0.1–1.3	Laboratory	Dortch, 1979
		1.0–2.5	Laboratory	Zic, 1990
		4.0–12.0	Laboratory	Asaeda & Imberger, 1988
Hydraulic	Garton pump	0.2–6.0	Field, swirl jet	Steichen, 1974
	Recirculating–pump systems Water jets	1.0–16.0	Lab., multi–port	Dortch, 1979 (Fr = 30–1000)
		10.0–35.0	Lab., single jet	Gu & Stefan, 1988 (Fr = 2–10)
		2.3	Field, single jet	Irwin, 1966, Fr = 25

In this chapter a conceptual procedure for the design of hydraulic destratification systems is outlined. Emphasis is on mechanical recirculating pump systems which withdraw water at one depth, discharge a water jet at another depth and thereby redistribute and mix a stratified lake or reservoir. The effects of jet discharge angle (orientation) and jet momentum on mixing are investigated and discussed. In particular horizontal and vertical low momentum jets are compared. Destratification is measured by a stability parameter. Efficiency was measured in terms of energy demand relative to change in potential energy. This chapter also discusses simplifications in the basic design theory for application in practical situations of lakes or reservoirs. Effects of initial stratification, lake shape and boundary conditions on the destratification process are examined. An example is presented to illustrate an application of the design method to a case study.

7.2 Review of previous studies

With the exception of the Garton pump, hydraulic destratification has been investigated mostly in laboratory experiments (Dortch, 1979, Ditmars, 1970, Gu and Stefan, 1987). A field study was conducted by Irwin, et al (1966). Dortch (1979) performed experiments with buoyant jets for high densimetric Froude numbers (30 to 1000) with variations of orientation (vertical or horizontal) and injection location (bottom or surface). His experimental results suggested that vertical jets were more efficient than horizontal jets. The physical aspects of the mixing process were studied and a simulation model by the integral method was developed in chapter 3. The model was verified against laboratory data for both horizontal and vertical jets of low densimetric Froude number, Fr, from 2 to 10 in chapter 4 (also see Gu and Stefan, 1988b; Stefan and Gu, 1991).

Price (1989) evaluated commercially available destratification devices, i.e. hydraulic mixers: axial (Garton) pumps and direct drive mixers. The current concept to determine pumping requirements includes the following steps: 1) to determine lake or reservoir characteristics, 2) to determine the required depth of penetration of the hydraulic jet, 3) to evaluate the volume flux and 4) finally to determine the number and horsepower of pumps.

If destratification is feasible (Holland, 1984) and a device has been selected (Price, 1989), a system can be designed based on jet analysis, numerical simulations and laboratory results (Gu and Stefan, 1991). In this chapter the governing parameters and a conceptual design and evaluation method are presented.

7.3 Conceptual background—governing parameters

The rate of mixing produced by a hydraulic destratification system is related to its input power and the lake or reservoir geometry and the initial stratification of the lake or reservoir. The variables affecting artificial destratification can be grouped into several dimensionless parameters.

The water jet is characterized by the initial jet Reynolds number, Re, and an initial jet densimetric Froude number, Fr, as defined in chapter 2. The initial stratification of a lake or reservoir (the ambient water) is expressed by the stratification number, St (chapter 2).

The lake geometry is characterized by a shape factor, S, defined as

$$S = \frac{V_t}{H^3} \tag{7.1}$$

where V_t and H are total volume and mean depth of the lake, respectively.

The progression of the mixing process can be related to a dimensionless time t*, defined as

$$t^* = tQ/V \tag{7.2}$$

where t = real time, i.e. elapsed pumping time, Q = jet discharge rate, V = volume between the elevations of withdrawal and discharge. V/Q is the characteristic time for the destratification system. The dimensionless time, t*, can be interpreted as the fraction of total lake volume which has been pumped.

To quantify "mixing", the concept of potential energy was used. Progressive mixing is reflected in the changes of the temperature–depth profiles with time. The increase in potential energy required for complete mixing of a prismatic volume of water with initially linear density stratification is

$$\Delta E_{max} = \frac{\Delta\rho_0 g V L}{12} \tag{7.3}$$

where L, $\Delta\rho_0$ and V are the distance, density difference, and volume between withdrawal and discharge, respectively. The increase in potential energy at any time is

$$\Delta E = \Delta\rho_0 g\ V(Y - Y_i) \tag{7.4}$$

where $Y = \left[\int_0^L A(z)\rho(z)z\,dz\right]\left[\int_0^L A(z)\rho(z)\,dz\right]^{-1}$, A = horizontal area at elevation z, and Y_i = initial value of Y. The ratio of the potential energy increase achieved at a given time during the mixing process to the total potential energy increase required for complete mixing is $\Delta E/\Delta E_{max}$ and is referred to as "percent mixed" (ratio given in percent)

$$m = \frac{\Delta E}{\Delta E_{max}} \tag{7.5}$$

Experimental results for high Fr ($30 < Fr < 1000$) by Dortch (1979) suggest that the dimensionless time, $t^*_{80\%}$, for 80% mixed state ($m = 0.80$), is equal to 0.02 to 0.16. Laboratory studies for low Fr ($2 < Fr < 10$) showed the same number $t^*_{80\%}$ to be in the range of 0.20 to 0.35 . Data by Ditmars (1970) for horizontal jets with Fr = 1 to 24 gave $t^*_{80\%} = 0.19$ to 0.24. The data also indicate that $t^*_{80\%}$ varied with jet orientation (vertical or horizontal) and initial ambient stratification (strong or weak).

The efficiency of a hydraulic destratification system can be defined as

$$\eta = \frac{m\Delta E_{max}}{P \cdot t} \tag{7.6}$$

where P = power input by the jet.

The total energy per unit time required is the sum of the energy necessary to overcome the pressure difference caused by the temperature stratification between the intake and the discharge ($\frac{QLg\ \Delta\rho_o}{2}$) and the kinetic energy per unit time of the jet ($\frac{Q\rho_o U_o^2}{2}$). The term $\frac{QLg\ \Delta\rho_o}{2}$ is small and decreases as the mixing proceeds.

$$P = \frac{1}{2}\, Q\, (\rho_o\, U_o^2 + \Delta\rho_o Lg) \tag{7.7}$$

$$\eta = \frac{2\ m\Delta E_{max}}{Q(\rho_o\, U_o^2 + \Delta\rho_o Lg)t} \tag{7.8}$$

For a prismatic water volume, ΔE_{max} is given by Eq. 7.3 and with the dimensionless time t^* defined in Eq. 7.2 efficiency becomes

$$\eta = \frac{m}{6\ t^*(Fr_L^2 + 1)} \tag{7.9}$$

where

$$Fr_L^2 = Fr^2\, \frac{D_o}{L} \tag{7.10}$$

Fr_L is a densimetric Froude number for the "system," whereas Fr is one for the jet. In a linearly stratified basin, $St = \frac{L}{D_o}$ and hence

$$Fr_L^2 = \frac{Fr^2}{St} \tag{7.11}$$

For basins of nonprismatic shape, a similar expression can be developed. Only the coefficient 1/6 in Eq. 7.9 will be changed.

It can be seen that efficiency is inversely proportional to the square of the system densimetric Froude number plus one, and therefore low discharge Froude numbers are desirable.

Eq. 7.9 combined with Eq. 7.11 indicates that a desired percentage of mixing (m) is achieved at any dimensionless time t^* with maximum efficiency when $Fr_L = Fr^2/St$, is minimized (Fig. 7.2). Experimental data show that the variation of m/t^* with time t^* (Fig. 7.3) is moderate and average values are on the order of 2.5 for vertical jets and 2.0 for horizontal jets for times up to $t^* = 0.32$.

7.4 Analysis of mixing systems

7.4.1 Jet trajectories

A method for the calculation of low momentum jet trajectories in infinite stratified water was presented in Chapter 3. Fig. 7.4 shows examples of calculated jet centerline trajectories for round buoyant jets discharged at three different angles into a linearly stratified ambient. It is obvious that the vertical jet penetrates higher regions in the ambient water than the horizontal jet at a given time. Fig. 7.4 gives computed terminal heights when the discharge angle is varied, provided that independent parameters, such as Fr and St are constant. In case of very weak stratification (large St and small Fr), the maximum rise does not appear to depend much on the discharge angle. The simulated influence of Fr and St on the terminal (maximum) rise of horizontally discharged jets is clearly shown in Fig. 7.5. For a constant St, an increase in Fr can result in a decrease in the maximum height if the jet is horizontal, but not if the jet is vertical (Fig. 7.6). The same statement applies to the "neutral height," i.e. the elevation at which the buoyant jet is eventually absorbed as a stratified lateral flow (Fig. 7.6). The height by which the vertical jet "overshoots" its neutral density elevation can be estimated from Fig. 7.6, where both maximum elevation and neutral elevation of the jet are given.

In the above examples of jet trajectories, the jet flow is considered to be steady and the ambient is assumed to be infinite and linearly stratified. In the thermal destratification of a finite lake or pond volume, jet trajectories vary with time because of the variation of the ambient condition during the mixing processes. Fig. 7.7 shows simulated successive positions of the jet centerline trajectories of horizontal discharges during the mixing process. At

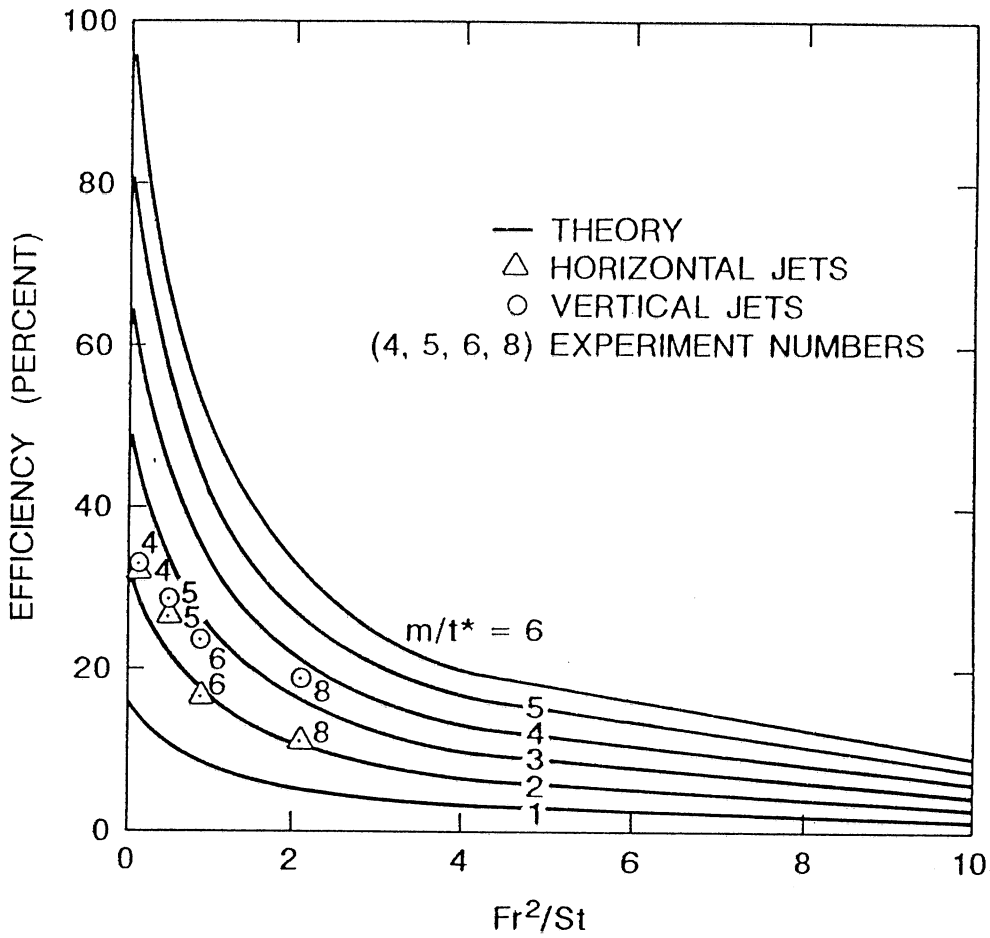

Fig. 7.2 **Efficiency as a function of parameters m/t^* and Fr^2/St: theory and experimental data.**

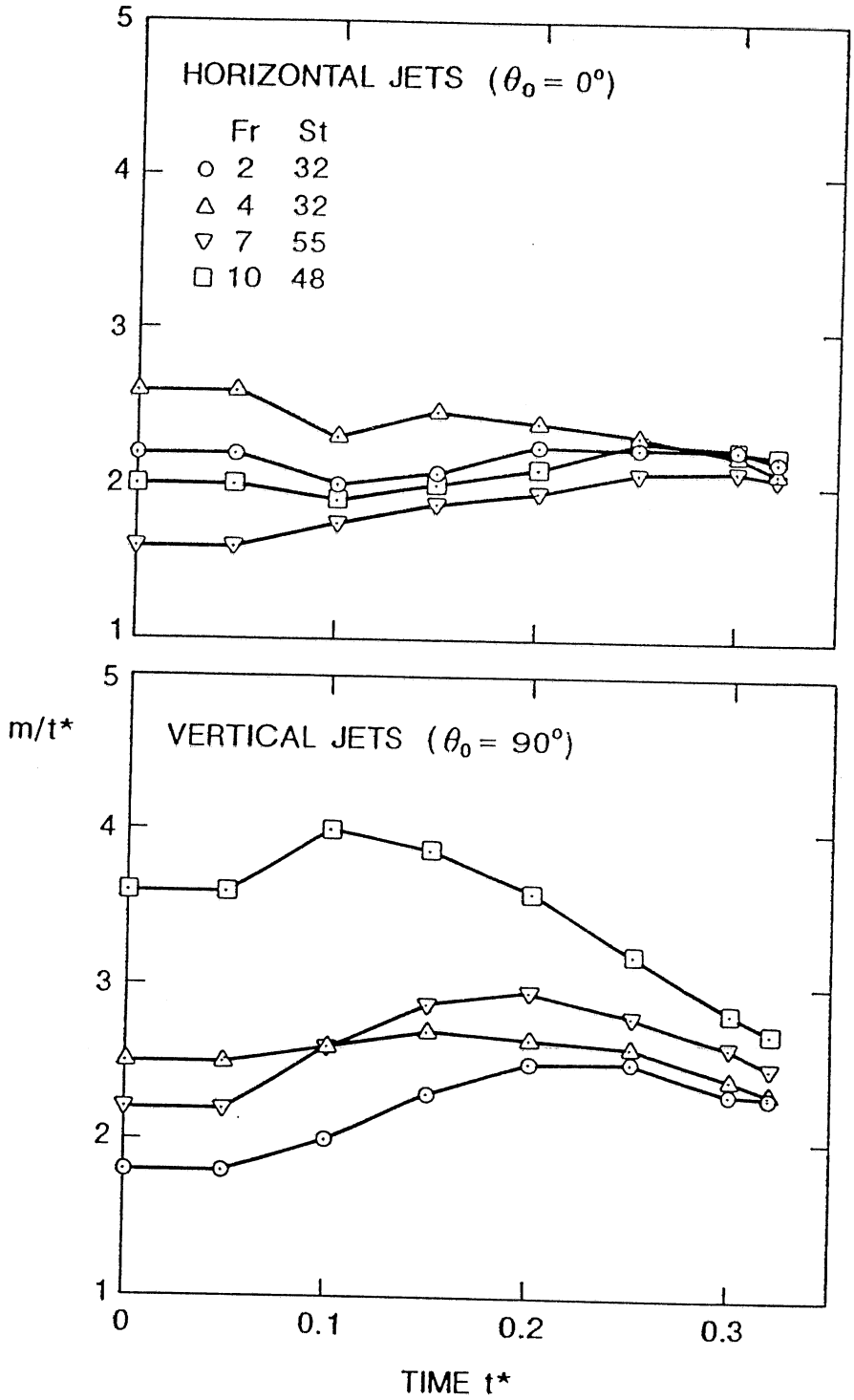

Fig. 7.3 Variation of parameter m/t* with time t* in experiments.

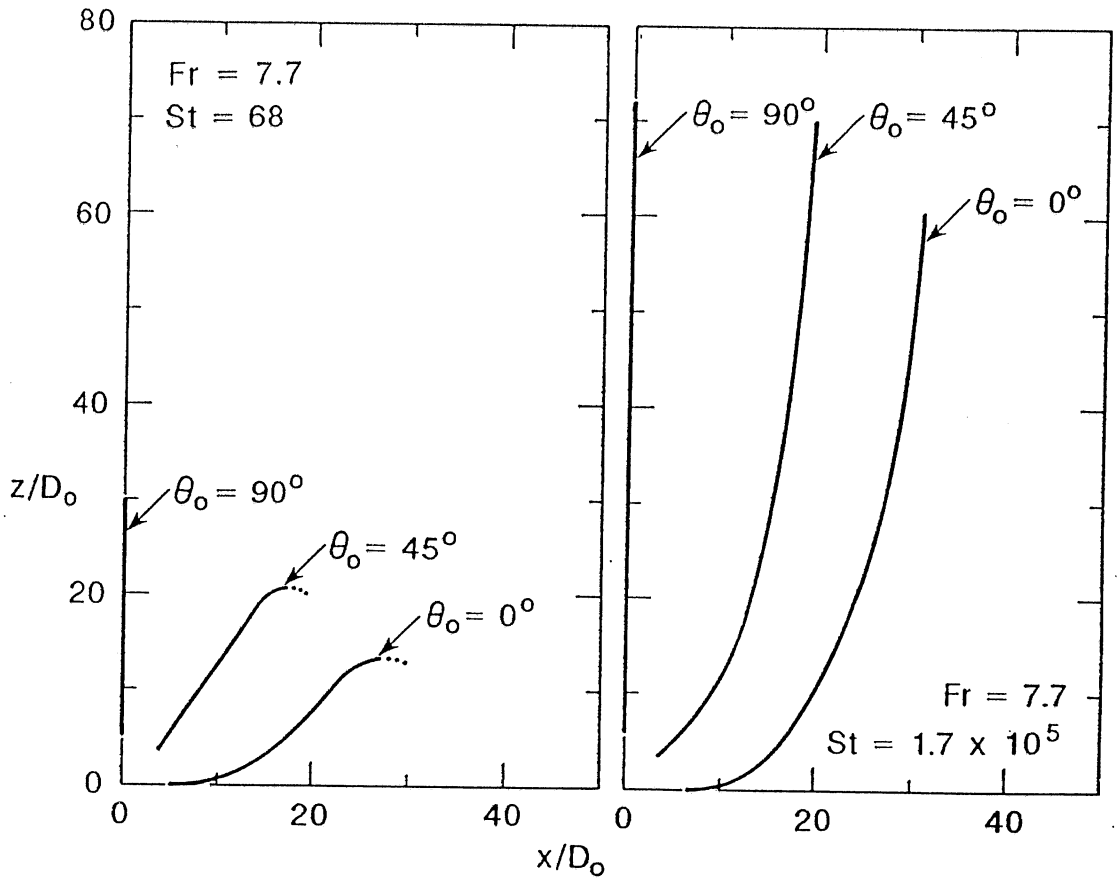

Fig. 7.4 Trajectories of round jets discharged at three angles θ_o into linearly density—stratified ambients: strong stratification (left); weak stratification (right).

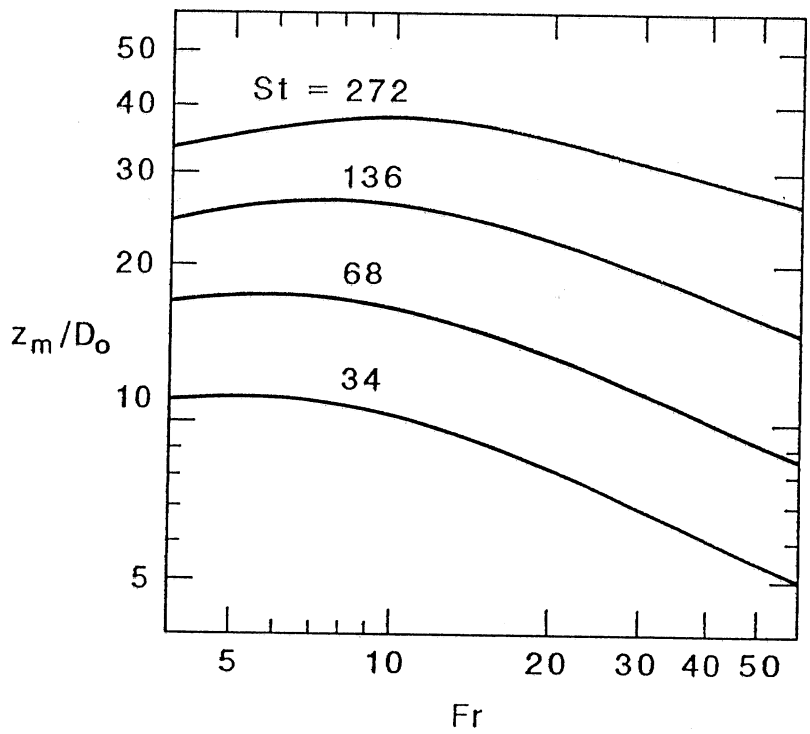

Fig. 7.5 Variation of maximum height of horizontal round jets, z_m , with initial densimetric Froude number, Fr, and stratification number, S_t, in a linearly density–stratified ambient.

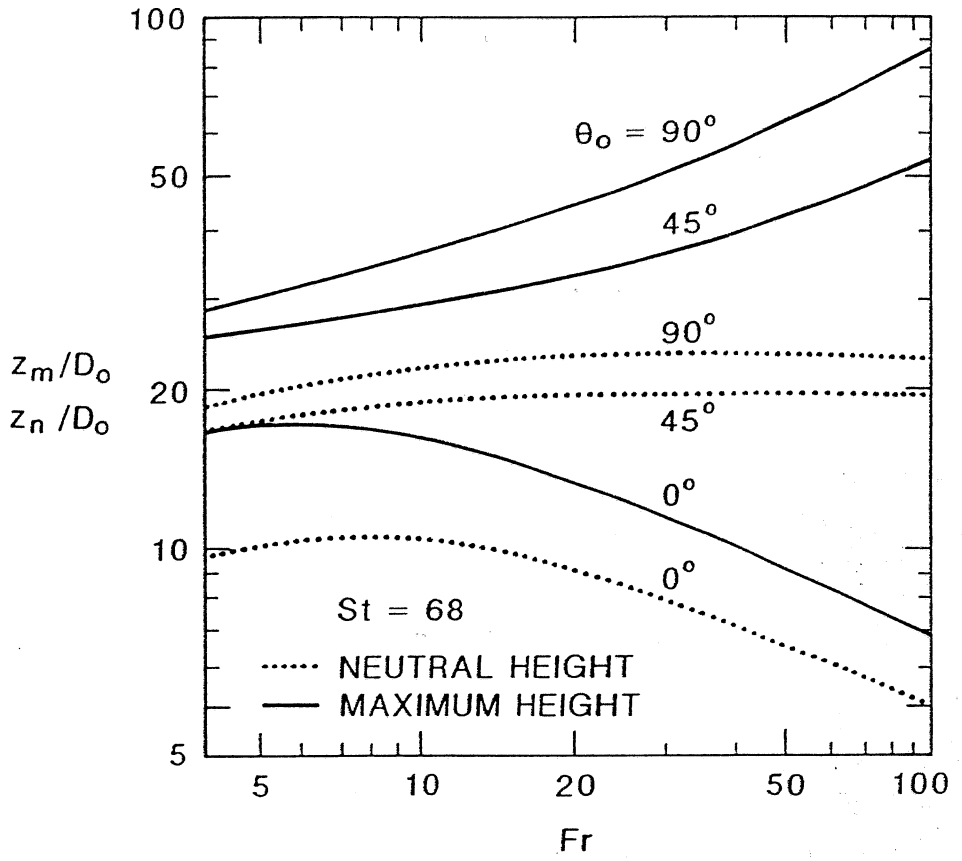

Fig. 7.6 Variation of maximum height, Z_m, and neutral height, Z_n, with initial densimetric Froude number, Fr, and jet angle θ_o.

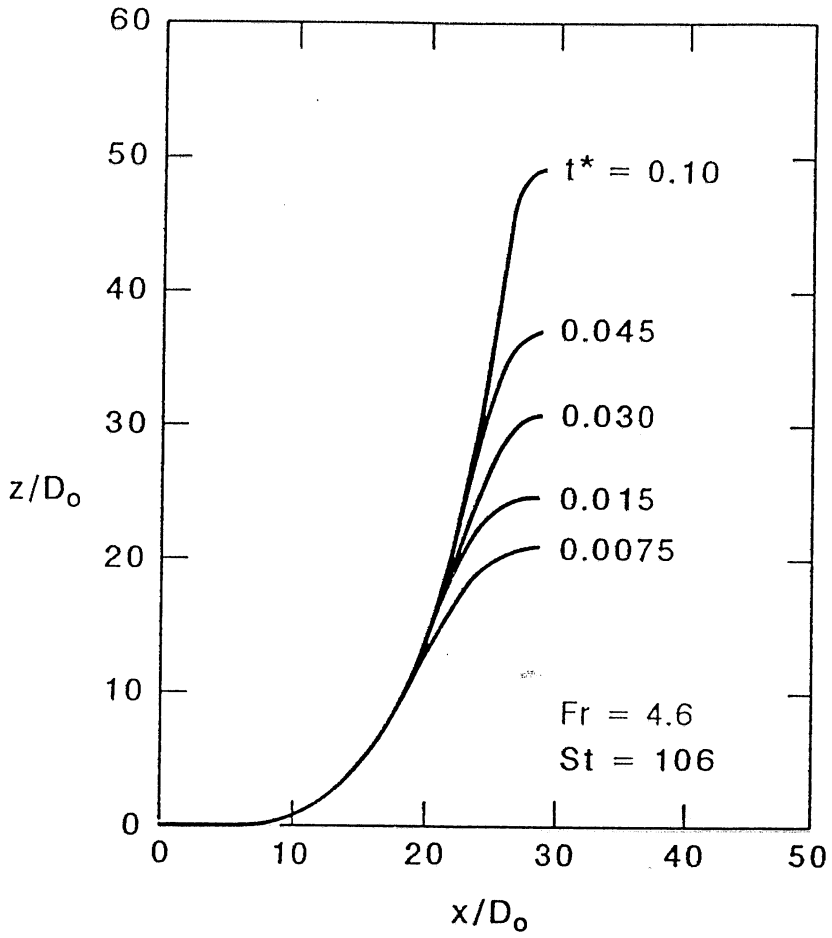

Fig. 7.7 Centerline trajectories of horizontal jets discharged into a linearly density–stratified ambient as a function of time t*.

the beginning, the surrounding water is linearly stratified, and the horizontal jet has a small terminal height of rise. As time progresses, the water through which the jet passed is well mixed, and the jet rises to higher and higher levels. At the terminal level of the jet, a density gradient of increasing strength is formed.

7.4.2 Mixing effectiveness and efficiency

The process of mixing, as reflected by changes in the temperature–depth profiles of finite volume basins, was simulated for various types of jets using the model developed in Chapter 3. The total heat content of the water was conserved, i.e. no heat exchange through the water surface was permitted.

Fig. 7.8 shows examples of simulated temperature profiles created by a pumping system with vertical or horizontal low momentum discharges. The horizontal jet mixes the basin more slowly. The mixing simulated in Fig. 7.8 was for a basin with a constant horizontal area (prismatic). The size of the basin was incorporated in the dimensionless time t^*. Fig. 7.9 shows similar simulated mixing results for a parabolic basin (linear relation between horizontal area A and depth z). In that case, the lower region of the ambient water responded to the mixing more rapidly than the upper region because of its smaller volume.

Fig. 7.10 shows a simulated progression of the mixing in a prismatic basin for various values of Fr. Fig. 7.11 shows the simulated mixing in a parabolic basin. In both cases, initial stratification is linear. It can be seen that mixing by the horizontal jet progresses more slowly than with the vertical jet. If t^*_{80} is defined as the time required for an 80% mixed state, t^*_{80} is equal to about 0.2 for the vertical jet compared to 0.3 for the horizontal jet in a prismatic basin. Comparison of results in Figs. 7.10 and 7.11 show that the shape of a basin and initial jet densimetric Froude number Fr do affect the mixing process appreciably. In a parabolic basin, t^*_{80} is about 0.3 for the vertical jet and about 0.4 for the horizontal jet. These results confirm that vertical jets are more efficient than horizontal jets for lake destratification as concluded also by Dortch and Holland (1980) on the basis of experimental laboratory results alone.

In the preceding examples, the injection point is below the withdrawal point and the discharge is a rising buoyant jet. It is possible to reverse this arrangement. For a prismatic lake with a linear initial stratification of temperature, reversal of the location of intake and discharge (bottom or surface) does not change the mixing characteristics since only the sign of buoyancy is inverted.

The progression of measured and simulated mixing by vertical and horizontal jets is indicated in Figs. 7.12 and 7.13, respectively, for various values of Fr. These figures confirm that (a) vertical jets produce more rapid mixing than horizontal jets and (b) densimetric Froude number, Fr, has more influence on mixing by vertical jets than by horizontal jets.

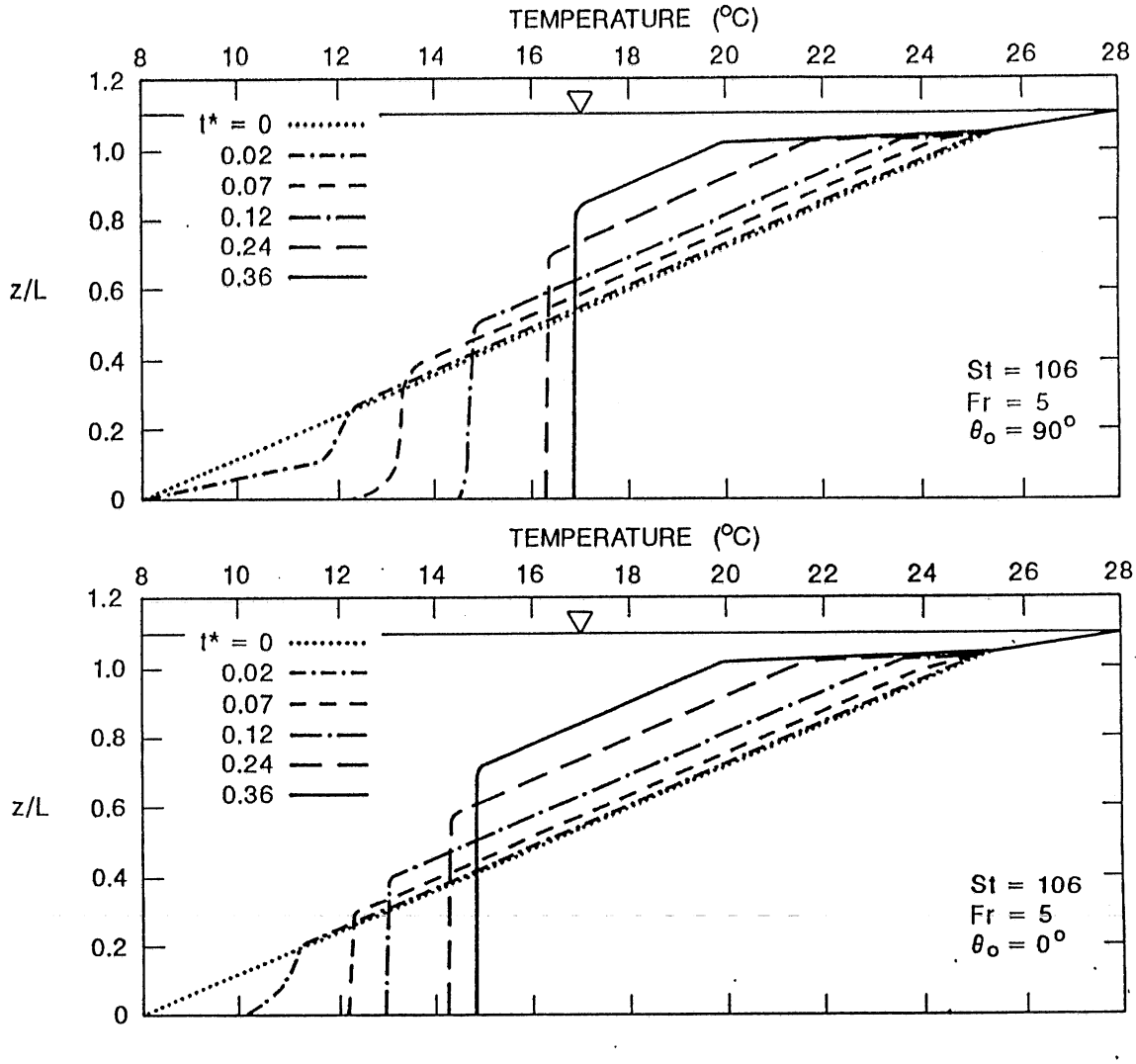

Fig. 7.8 **Temperature profiles during the hydraulic destratification of a linearly stratified prismatic basin**

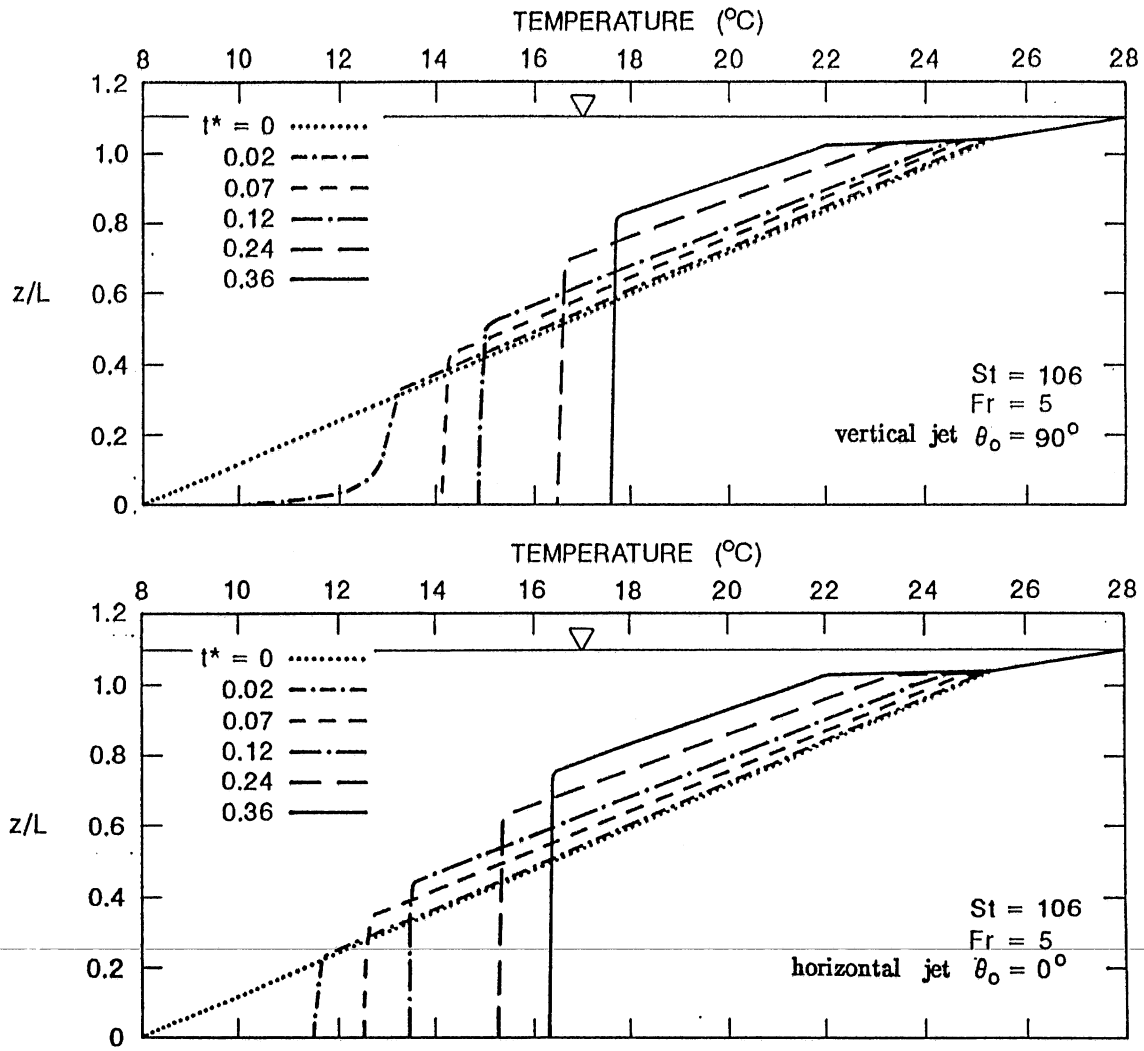

Fig. 7.9 **Temperature profiles during the hydraulic destratification of a linearly stratified parabolic basin**

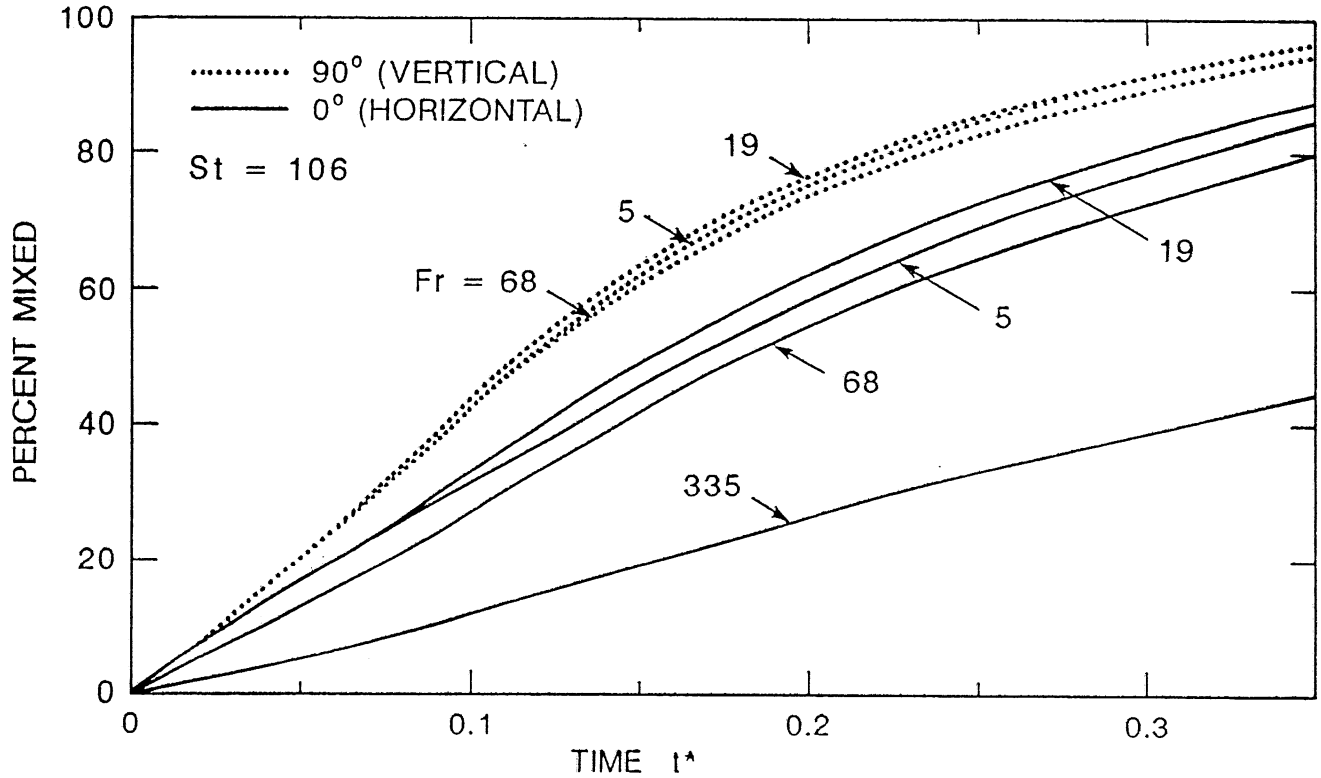

Fig. 7.10 Effect of jet orientation on hydraulic destratification of a linearly stratified prismatic basin (A = constant).

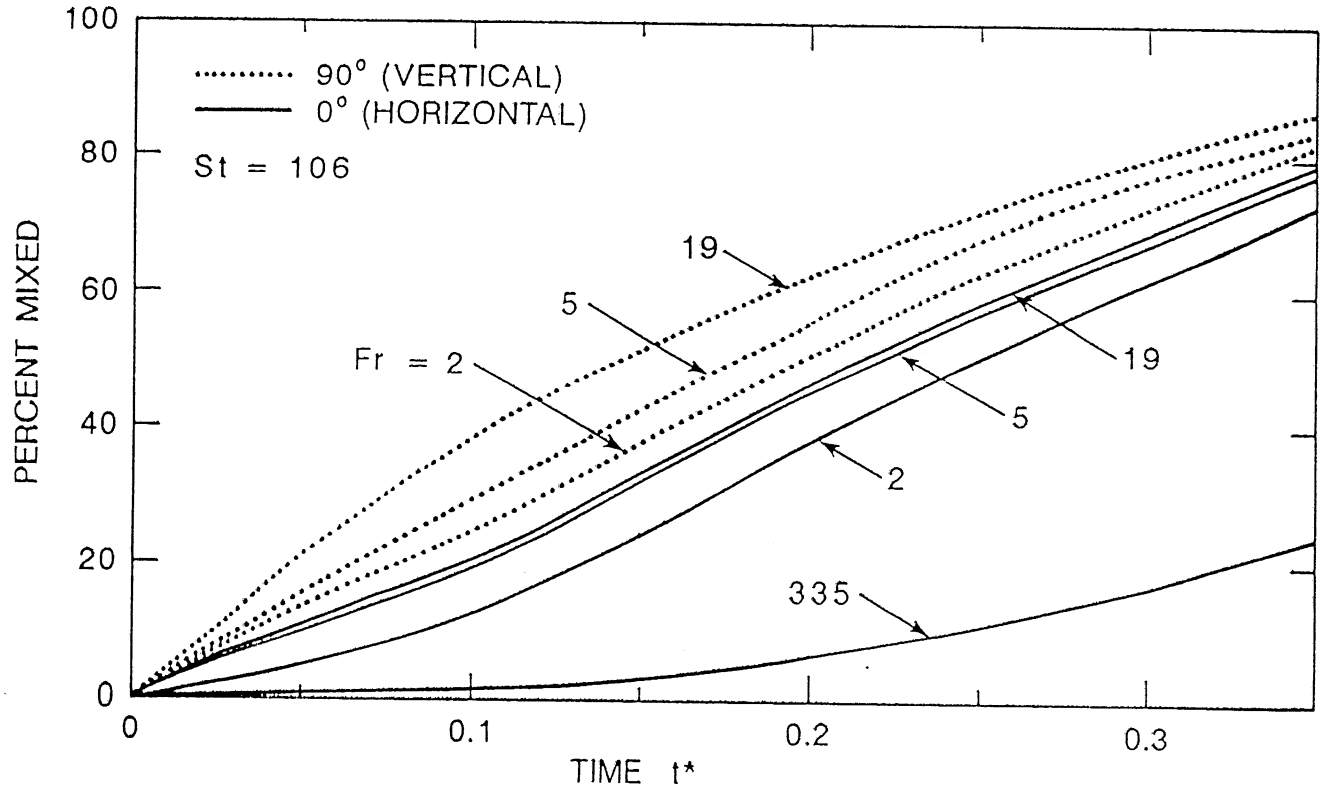

Fig. 7.11 Effect of jet orientation on hydraulic destratification of a linearly stratified parabolic basin.

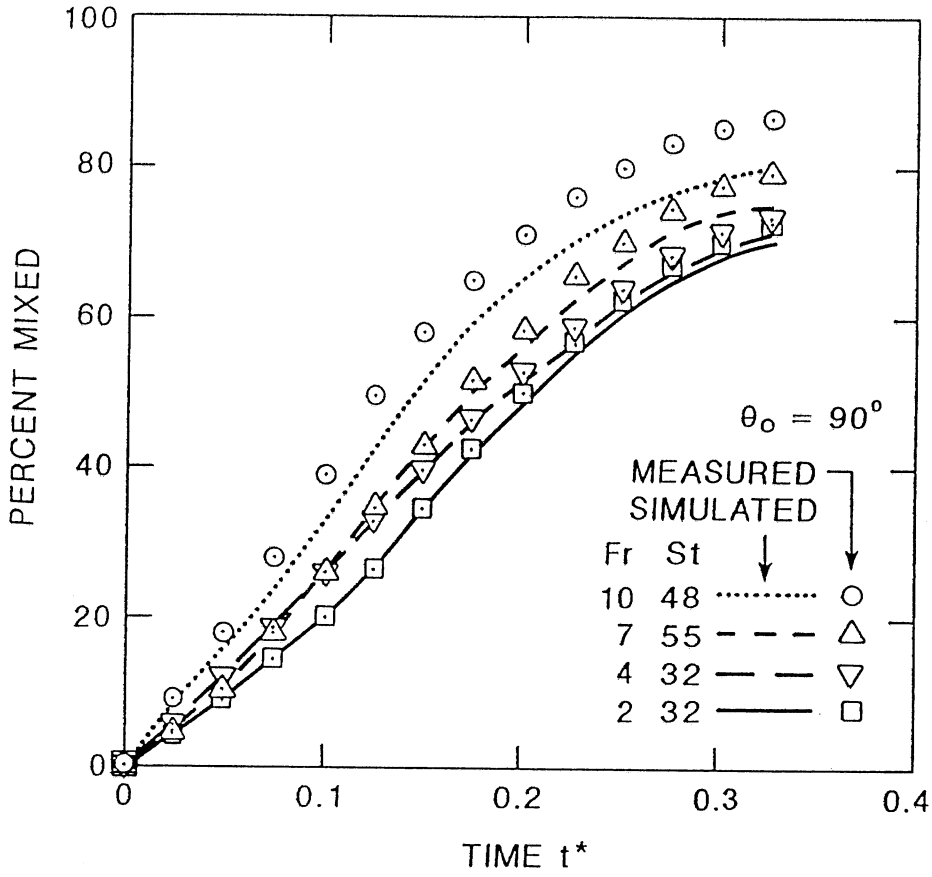

Fig. 7.12 Measured and simulated mixing by vertical jets: Exp. No. 4, 5, 6, and 8.

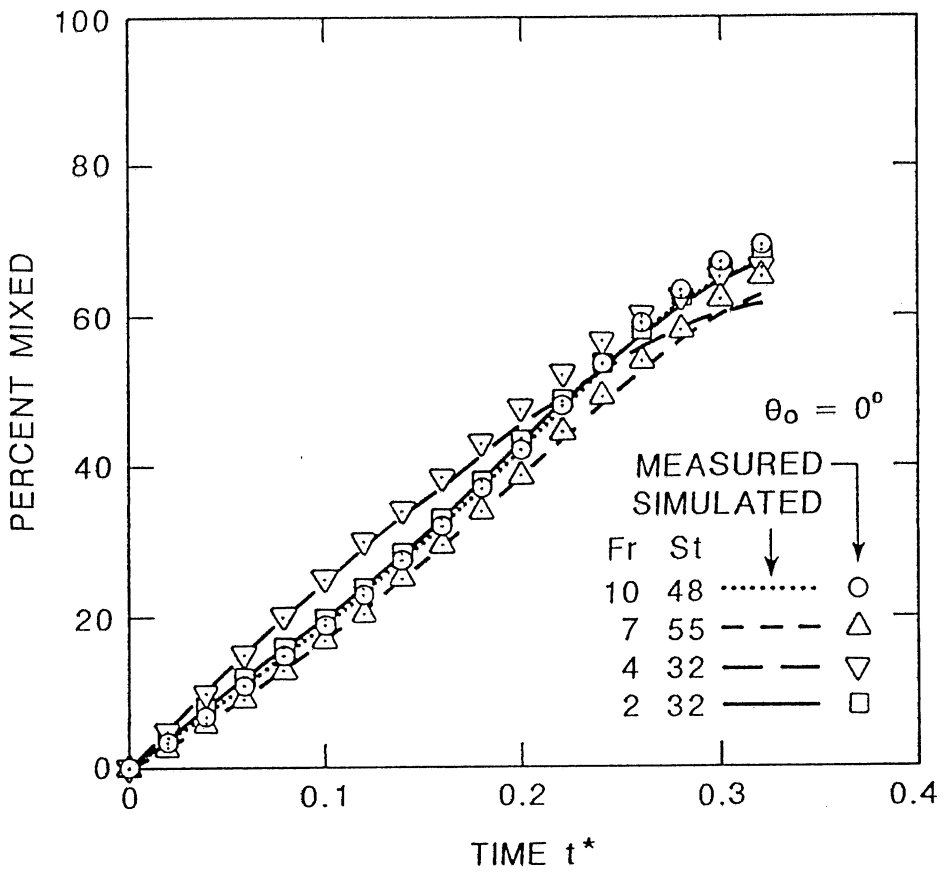

Fig. 7.13 Measured and simulated mixing by horizontal jets: Exp. No. 4, 5, 6, and 8.

It was shown that efficiency is inversely proportional to the square of the system densimetric Froude number plus one, and therefore low discharge Froude numbers are desirable. Maximum efficiency is achieved when Fr_L, which is equal to Fr^2/St, is minimized for a desired percentage of destratification m at dimensionless time t^* (Fig. 7.2). The variation of m/t^* with time t^* (Fig. 7.3) is moderate and average values are on the order of 2.5 for vertical jets and 2.0 for horizontal jets for time up to $t^* = 0.32$. Experimental results for efficiency as a function of m/t^* and Fr^2/St are also shown in Fig. 7.2. Values range from 12% to 33%. Jets with lower densimetric Froude numbers, Fr, were also seen to be more efficient in these laboratory investigations. Fig. 7.14 shows very good agreement between the efficiencies calculated from simulated and measured temperature profiles.

The above findings lead to the following conclusions. A system which creates a vertical jet produces more rapid mixing of a stratified lake than a horizontal jet. The difference in mixing effects is small in the case of small jet densimetric Froude numbers, Fr, but may be much larger in the case of large Fr. The dimensionless time required for an 80% mixed state (t^*_{80}), is in the range of 0.2 – 0.4 for all cases examined, provided Fr is small enough so that surface and bottom interference are avoided. A vertical jet of high Fr may overshoot the water surface, spread at the surface and plunge into deeper layers, causing excessive energy loss. A horizontal jet with high Fr may impinge on the bottom, disturb sediments and produce mixing only over a layer of small vertical thickness.

The model simulations and laboratory experiments analyzed herein suggest that hydraulic destratification systems using selective withdrawal and jet reinjection have the potential to destratify sections of temperature stratified water bodies or entire water bodies very efficiently. Both the shape of a basin and the relative location of diffuser and intake affect the mixing processes. A prismatic basin is more rapidly mixed than a non–prismatic one when the diffuser is located at the bottom. The inversion of diffuser and intake location does not change the mixing characteristics in the prismatic basin.

Energy requirements for hydraulic destratification are extremely reasonable and make the method appear very attractive. Highest operational energy efficiencies are achieved when discharge densimetric Froude numbers are virtually kept as low as possible ($2 < Fr < 10$).

7.5 Proposed design procedure

Parameters characterizing the operation of the device such as η, m, t^*_m, and t_m are called operation parameters. Parameters which describe the device, including pumping capacity, Q, pipe size, D, and the distance between withdrawal and injection, are termed system parameters. For a lake of specific characteristics, two paths are followed during the design procedure.

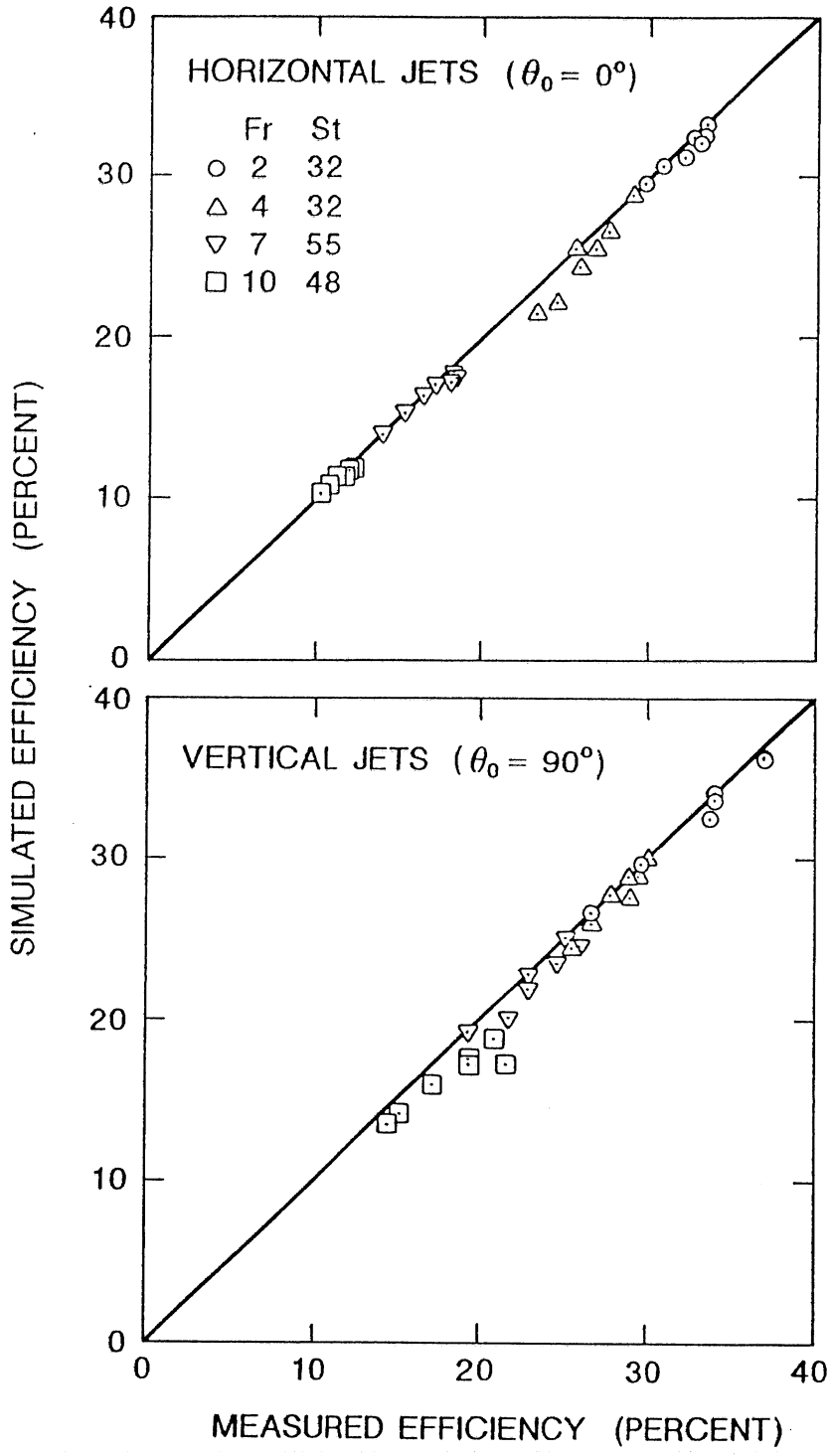

Fig. 7.14 Measured and simulated efficiencies.

One is from the selection of operational parameters to the determination of system parameters for a destratification device. The other is from selection of system parameters to determination of operational parameters. The former can be considered as the first step of design and a single jet system will be given as an example. The latter will be illustrated for multiple jet systems.

(1) Specification of lake characteristics

Lake characteristics are specified by lake morphometry and stratification. Total lake volume, V_t, surface area, A_s, mean depth, H, maximum depth, H_{max}, and density difference, $\Delta\rho_a$, between hypolimnetic and epilimnetic water before destratification are necessary basic parameters. In addition more detailed information is necessary in form of volume–depth function, V(z), area–depth function, A(z), and lake stratification in the form of density (or temperature) distribution with depth at the start of the destratification process.

(2) Selection of operational parameters

Destratification systems are frequently needed during summer when the hypolimnion becomes anoxic. The initiation date and the desired pumping period to mix the lake, t_m, e.g. one month, have to be chosen. An 80% mixed state, i.e. m = 0.80, is suggested because a 100% mixed state is very difficult to obtain because of continuous restratification due to heat input from atmosphere. To make a lake thoroughly homogeneous requires pumping rates which are usually impracticably large (Gu and Stefan, 1987, Dortch, 1979). The 80% mixed state represents a compromise for practical purposes.

The value of t_m^*, i.e. volume of water which will be pumped as a fraction of lake volume, needs to be selected. $t^*_{80\%}$ is in the range of 0.02 to 0.16 for high Fr ($30 < Fr < 1000$, Dortch, 1979) and 0.2 to 0.3 for low Fr ($1 < Fr < 30$, Gu and Stefan, 1987, Ditmars, 1970). If quick mixing of a lake is required, a large Fr can be selected to reduce the mixing time at the expense of efficiency.

A destratification efficiency for the system, η, is chosen according to the range of Fr preferred. Fig. 7.2 and Table 7.1 can provide some guidance. Low Fr for both vertical and horizontal jets are recommended because of high efficiency. A vertical jet of low Fr avoids energy loss due to surface overshooting. Horizontal jets with low Fr can avoid disturbing sediments and may produce mixing over a larger vertical layer than high Fr. Efficiency, η, is recalculated after evaluation of multiple systems, after examination for vertical jets.

(3) Determination of system parameters

System parameters for a single pump mainly include discharge flowrate, Q, pipe diameter, D_0 and jet velocity, U_0. They are determined from the operational parameters, Fr and St (Eq. 2.12 and Eq. 2.15), and the η relationship (Eq. 7.9).

Selection of withdrawal and discharge elevation and distance between them, L, can be based on lake depth and accessibility. Surface withdrawal and bottom discharge are advantageous as mentioned before. For total lake mixing, withdrawal close to the surface and discharge close to the bottom, are recommended for two reasons. The first reason is that a vertical jet is more efficient than a horizontal one (Dortch, 1979; Gu and Stefan, 1991; Stefan and Gu, 1991). The second reason is that epilimnetic water with higher dissolved oxygen is discharged into the hypolimnion in which D.O. may need to be improved. The initial density difference between jet and surrounding water, $\Delta\rho_o$, is calculated from, $\rho(z)$.

The flowrate, Q, is determined from the volume to be mixed, V, the desired pumping period, $t_{80\%}$, and the dimensionless time required for 80% mixing, $t^*_{80\%}$,

$$Q = \frac{V\, t^*_{80\%}}{t_{80\%}} \tag{7.12}$$

The pipe diameter is derived from Eqs. 7.2, 7.3, 7.13, and 7.15 and continuity equation

$$Q = U_o \pi \frac{1}{4} D_o^2 \tag{7.13}$$

which leads to

$$D_o = \left[\frac{96 Q^2 \eta\, t^*_m \frac{d\rho_a}{dz}}{\pi^2 g' \Delta\rho_o (m - 6\eta t^*_m)} \right]^{\frac{1}{4}} \tag{7.14}$$

where $g' = g\frac{\Delta\rho_o}{\rho_o}$, and η and m were selected in section 7.5.2.

The jet velocity is obtained by solving Eq. 7.13 for U_o. The turbulence level of the flow field generated by the mixing system with the jet can be estimated by Reynolds number, Re (Eq. 2.11). Flow fields with a jet Reynolds number, Re > 2,000, can be considered as turbulent (Gu and Stefan, 1987). Since turbulence enhances the mixing of ambient water by jet flows a value of Re larger than 10,000 should be a goal.

(4) Adjustment to multiple systems

The single jet system for destratification examined above with respect to flowrate, pipe diameter and lake characteristics needs to be reexamined for multiple jet systems if any of the parameters, assumed or calculated, is not suitable. For example the required flowrate for a single jet, Q, or the pipe diameter, D_o, might be impracticably large, make the installation difficult and the cost too high.

If either D_o or Q or S are considered too large, e.g. $S > 1000$ or $D_o > 1.0$ m, the single jet system has to be replaced by multiple jet systems with smaller D and Q per jet. In that case the lake is divided into a number of smaller sections. If n sections are chosen to meet the practical limitations for pump capacity and pipe diameter, each section with a volume $V_n = \frac{V}{n}$, is provided with a pumping system characterized by Q_n and D_n, where

$$Q_n = \frac{Q}{n} \tag{7.15}$$

and

$$D_n = \frac{D_o}{n^{1/2}} \tag{7.16}$$

A multiple jet system may also be advantageous because a single jet mixing system may, in practice, not be able to cover the full horizontal extent of a lake which is large and shallow. Q and D_o are the values previously found for the single jet.

The vertical distance between withdrawal and jet discharge, L_n, may vary from one section to another, depending on lake depth in each section. The governing parameters, Fr, Re and St, and efficiency, η, are recalculated for multiple systems based on the flow rates, Q_n, and diameters, D_n, for further consideration below.

(5) Examination for vertical jets

One requirement for the application of numerical and experimental results for jet mixing such as given in Figs. 7.2 and 7.3 is that the jet remain submerged. To aviod jet overshooting at the water surface each vertical jet generated by the destratification system is examined. If the Fr number of a jet exceeds a critical densimetric Froude number, Fr_c introduced in chapter 3, it will overshoot. If it is found that $Fr > Fr_c$, the jet velocity is reduced to $U_v = U_o \frac{Fr_c}{Fr}$. Flow rate is adjusted to $Q_v = U_v \frac{\pi}{4} D_n$, provided that pipe diameter is not changed. Reduction in flow rate per jet is compensated by a larger number of jets. Assume that $t_{80\%}$, and $t^*_{80\%}$ are still kept as initially chosen, the number of sections of the lake, n, is replaced by

$$n_v = \frac{Q}{Q_v} \tag{7.17}$$

Each section has a volume $V_v = \frac{V}{n_v}$, and is provided with a single jet characterized by U_v, Q_v and D_n. Governing parameters are recalculated.

7.6 Significance of assumptions

The theory and laboratory results of jet mixing and design information are presented for ideal jet conditions. A lake was assumed to be prismatic in shape with linearly stratified water before destratification and without heat or energy exchanges through the water surface surface and bottom. The design approach outlined in this paper should be applied with caution because of these simplifications and assumptions.

Thermal stratification is usually nonlinear. The assumption of linear stratification may lead to a mixing time different from the real one. The difference depends on how the center of mass in the ideal lake differs from that in the real lake. The difference may be not significant in many practical cases because the density difference between the nonlinear and the linear stratification is often more or less symmetric about the mass center but with opposite signs.

The projected horizontal area of a real lake is usually a function of depth with smaller volumes in the lower regions and larger volumes in the upper layers. In previous numerical and experimental simulations as in this design analysis a prismatic lake was assumed. Hydraulic destratification with a jet at the bottom and withdrawal at the top was recommended. A real lake is probably mixed faster in a greater vertical extent than the assumed prismatic lake.

Another difference between theory and reality is in the boundary conditions. The assumption of zero heat exchanges through lake boundaries has been made for analysis and design of jet mixing. However these exchanges do exist in a real lake because of addition of heat by solar radiation and heat loss to the cold bottom sediments. A lake usually restratifies after pumping stops. Effects of exchange through boundaries on the mixing process over a pumping period could be significant and should be taken into consideration if the pumping period is longer than a week. In general, periodic or continuous mixing is required to maintain continuous destratification through a summer.

On the other hand, natural mixing occurs in the real lake due to wind disturbance on the surface water and convection of surface cooling water. A decline in the thermal stability of a lake resulting from wind mixing and nighttime surface cooling help to mix the lake. Omission of these processes in the simulation and design leads to an overestimated mixing time. However they are counteracted by an underestimated mixing time due to the assumption of an adiabatic water surface.

Numerical models are available to simulate the synoptic effects of destratification by jet and restratification by heat input from the atmosphere. The changes in temperature (density) stratification in a real lake of specified geometry and exposed to variable real weather can be followed in these models continuously over an entire summer season at timesteps of one day. The description and application of these models is beyond the scope of this study.

7.7 Summary

The artificial mixing of temperature–stratified ponds, or small lakes or reservoirs improves water quality. Mixing by vertical liquid jets was found potentially more efficient than other systems currently in use. Based on studies of jet mixing mechanics of stratified water bodies a conceptual design approach was presented. The main design parameters including "operational" and "system" parameters were considered in the proposed method.

Chapter 8 2–D Model for Buoyant Jet Flows in a Lake or Pond with an Ice Cover

8.1 Introduction

The integral method discussed above and the 1–D jet–mixing model developed in chapter 3 are suitable mainly when the flow retains its jet–type characteristics. The 1–D lake stratification simulation model, coupled with the integral jet model can give a good prediction of the effect of the mixing processes in the lake or reservoir due to the water jet. This model does not describe two–dimensional or three–dimensional details of the flow field and is difficult to extend it to more complex flows situations, e.g. unsteady turbulent buoyant jet flow in a stratified lake with an ice cover. In particular jet impingement on solid or free surfaces is difficult to describe with the integral method because the similarity hypothesis does not hold in the vicinity of a wall. The reason is that in such cases the flow is not a boundary–layer type flow, the velocity profiles are neither similar nor symmetric and difficult to prescribe empirically. Entrainment from the region below the injection level is also beyond the computational capability of a 1–D model, and so is entrainment through the boundaries of the spreading layer as observed in flow visualization experiments (Wong, 1987).

The differential method and a two–dimensional approach is used in this study to gain insight into flows (large–scale convective circulation) and mixing in a lake or reservoir induced by the jets. A 2–D model introduced by Patankar (1972, 1980, 1981, 1982) based on Rodi's work (1984) is modified for flows considered. The buoyancy–extended k–ϵ turbulence model is used as a closure of the problem following Hossain and Rodi's work (1986). The 2–D model is capable of simulating a plane (slot) horizontally or vertically discharged water jet and an axisymmetric (round) vertically discharged jet. A horizontally discharged round jet would require a 3–D simulation. Only plane jets are investigated and simulated. The evolution of flow and thermal fields as a result of mixing created by the jet including the effects of buoyancy and stratification on flow patterns and heat transfer from water to ice were investigated by the 2–D simulation. Effects of jet flows on the water quality and ice cover in the lake or pond were not explicitly investigated. The 2–D numerical solutions can also be used for the evaluation of the integral method and the 1–D simulation models, e.g. the assumption of Gaussian distributions of velocity.

The 2–D numerical simulation model developed in this study for unsteady turbulent buoyant jet flows in stratified basins with ice cover serves two main objectives: (1) to simulate in detail the flow and thermal fields and

jet mixing effects to evaluate the integral methods and assumptions, and (2) to study the trajectories of horizontally discharged jet in low temperature ambients (0°–4°C) and effects on an ice cover which is of concern in winter aeration and waste water discharges.

The winter situation selected for simulation is physically more complex than the summer case but easier to deal with in numerical simulation because the ice cover makes it unnecessary to deal with the boundary conditions for a free water surface. A free surface can be approximated, as will be further discussed in Sec. 8.3, by a plane of symmetry or a moving plane. In order to have the boundary conditions closer to the real case for a jet in summer lake with free surface, it is suggested that an outflow boundary should remain and the free surface could be replaced by a solid boundary. This approximation is permitted by the theoretically and experimentally supported existence of similarity between the effect of a free surface and the effect of a rigid wall on the behavior and trajectory of a jet.

The jet impingement on the free surface causes a small superelevation which in turn leads to an excess hydrostatic pressure that drives the fluid sideways away from the impingement region. This impingement process is very similar to that on a solid wall, except that there is no deformation of the surface but a rise in the static pressure which drives the flow sideway . This similarity hypothesis is supported by experimental data of Andreopoulos et al. (1986) for a vertical plane jet impinging on a solid wall and data of Gutmark et al. (1978) for free the surface case (to be discussed in Sec. 8.5). It is also supported by data of Stoy and Stenhouse (1975), Sawyer (1960) and Ali and Salehi–Neyshaboury (1989) for horizontal plane offset jets, showing the similar effects of two bounding surfaces, a free surface and a rigid wall, on jet deflection, attachment and impingement.

8.2 Governing equations and closure of the problem

The differential method solves the Reynolds mean flow equations for the unsteady turbulent buoyant jet flow velocity components, temperature (or density) at each point in the flow field (field method). The mean flow equations do not form a closed set due to the non–linearity of the original Navier–Stokes equations. The averaging process introduces unknown correlations between velocity fluctuations and between velocity and scalar fluctuations which represent the transport of momentum, and heat/mass due

($\rho \overline{U_i' U_j'}$ and $\rho \overline{U_j' \varphi'}$). Adopting the eddy viscosity concept, the turbulent (Reynolds) stresses and the turbulent diffusion fluxes are modeled by the turbulent momentum and heat/mass transport equations

$$-\rho\overline{U_i' U_j'} = \mu_t\left[\left(\frac{\partial U_i}{\partial x_j} + \frac{\partial U_j}{\partial x_i}\right) - \frac{2}{3}\,\delta_{ij}\frac{\partial U_k}{\partial x_k}\right] - \frac{2}{3}\,\delta_{ij}\rho k \tag{8.1}$$

$$-\rho\overline{U_j' \varphi'} = \frac{\mu_t}{\sigma_t}\frac{\partial \varphi}{\partial x_j} \tag{8.2}$$

where μ_t = eddy (turbulent) viscosity, k = turbulent kinetic energy of fluctuation ($k = \frac{1}{2}\,\overline{U_i' U_i'}$), $\frac{\mu_t}{\sigma_t}$ = eddy (turbulent) diffusivity and σ_t = turbulent Prandtl number if $\varphi = T$ = the temperature or Schmidt number if $\varphi = C$ = the species of mass.

The closure of the problem is made by relating the mean flow (Reynolds) equations and the turbulent momentum and heat/mass transport equations. However, the introduction of the eddy–viscosity concept shifts the main problem to the distribution of μ_t, i.e., a turbulence model is required.

The turbulence model used in this study is the buoyancy–extended k–ϵ model (Rodi, 1984). The k–ϵ turbulence model is one of the most widely used two–equation model in which ϵ is the rate of turbulent energy dissipation and $\epsilon = C_\mu k^{1.5}/L$, where C_μ is a constant and L is the mixing length (dissipation length scale). Eddy viscosity is calculated from

$$\mu_t = \rho k^{1/2}/L \tag{8.3}$$

i.e.

$$\mu_t = \rho C_\mu k^2/\epsilon \tag{8.4}$$

The values of k and ϵ are represented by transport equations which incorporate the effects of convection, diffusion, shear and buoyancy in flows (Rodi, 1984).

The differential (field) method does not require the division of the jet–mixing field into nearfield and farfield nor the Boussinesq approximation, or the similarity hypothesis, entrainment functions (coefficients) introduced in the integral method. Density variations, velocity and temperature profiles and entrainment rates are obtained as part of the solution.

To deal with the pressure term in the mean flow equations an approach similar to the integral method is employed. The only difference is in the definition of ρ_a which is defined as the density of stagnant water undisturbed ambient by the jet (the natural field). The governing equations for the

numerical simulation of unsteady turbulent buoyant jet flows, based on the Reynolds mean flow equations and the turbulent transport equations and the k–ϵ turbulence model, in a two–dimensional (Cartesian) coordinate system or an axisymmetric (cylindrical) coordinate system are written as:

$$\frac{\partial \rho}{\partial t} + \frac{\partial(\rho u)}{\partial x} + \frac{1}{y^{\ell}} \frac{\partial(y^{\ell} \rho v)}{\partial y} = 0 \tag{8.5}$$

$$\frac{\partial(\rho u)}{\partial t} + \frac{\partial(\rho u^2)}{\partial x} + \frac{1}{y^{\ell}} \frac{\partial(y^{\ell} \rho uv)}{\partial y} = - \frac{\partial p}{\partial x} + (\rho_a - \rho) g + 2 \frac{\partial}{\partial x} \mu_e \frac{\partial u}{\partial x} + \frac{1}{y^{\ell}} \frac{\partial}{\partial y} y^{\ell} \mu_e \left(\frac{\partial u}{\partial y} + \frac{\partial v}{\partial x}\right) \tag{8.6}$$

$$\frac{\partial(\rho v)}{\partial t} + \frac{\partial(\rho uv)}{\partial x} + \frac{1}{y^{\ell}} \frac{\partial(y^{\ell} \rho v^2)}{\partial y} = - \frac{\partial p}{\partial y} + 2 \frac{1}{y^{\ell}} \frac{\partial}{\partial y} y^{\ell} \mu_e \frac{\partial v}{\partial y} + \frac{\partial}{\partial x} \mu_e \left(\frac{\partial u}{\partial y} + \frac{\partial v}{\partial x}\right) - \ell \frac{\mu_e + \mu}{y^2} v \tag{8.7}$$

$$\frac{\partial(\rho \varphi)}{\partial t} + \frac{\partial(\rho u \varphi)}{\partial x} + \frac{1}{y^{\ell}} \frac{\partial(y^{\ell} \rho v \varphi)}{\partial y} = \frac{1}{y^{\ell}} \frac{\partial}{\partial y} y^{\ell} \alpha_e \frac{\partial \varphi}{\partial y} + \frac{\partial}{\partial x} \alpha_e \frac{\partial \varphi}{\partial x} + S_{\varphi} \tag{8.8}$$

$$\frac{\partial(\rho k)}{\partial t} + \frac{\partial(\rho u k)}{\partial x} + \frac{1}{y^{\ell}} \frac{\partial(y^{\ell} \rho v k)}{\partial y} = \frac{1}{y^{\ell}} \frac{\partial}{\partial y} y^{\ell} \left(\mu + \frac{\mu_t}{\sigma_k}\right) \frac{\partial k}{\partial y} + \frac{\partial}{\partial x} \left(\mu + \frac{\mu_t}{\sigma_k}\right) \frac{\partial k}{\partial x} + P - \rho \epsilon + B \tag{8.9}$$

$$\frac{\partial(\rho \epsilon)}{\partial t} + \frac{\partial(\rho u \epsilon)}{\partial x} + \frac{1}{y^{\ell}} \frac{\partial(y^{\ell} \rho v \epsilon)}{\partial y} = \frac{1}{y^{\ell}} \frac{\partial}{\partial y} y^{\ell} \left(\mu + \frac{\mu_t}{\sigma_{\epsilon}}\right) \frac{\partial \epsilon}{\partial y} + \frac{\partial}{\partial x} \left(\mu + \frac{\mu_t}{\sigma_{\epsilon}}\right) \frac{\partial \epsilon}{\partial x} + \left(C_1 (P + B) - C_2 \rho \epsilon\right) \frac{\epsilon}{k} \tag{8.10}$$

$$\rho = \rho(T, C) \tag{8.11}$$

where p is a new pressure redefined as

$$p = p_d + \frac{2}{3} \mu_e \left(\frac{\partial u}{\partial y} + \frac{\partial v}{\partial x}\right) + \frac{2}{3} \rho k \tag{8.12}$$

μ_e and α_e are effective viscosity and diffusivity respectively.

$$\mu_e = \mu + \mu_t \tag{8.13}$$

$$\alpha_e = \frac{\mu_t}{\sigma_t} + k_\varphi \tag{8.14}$$

in which σ_t is turbulent Prandtle number (φ = T) or Schmidt number (φ = C), u and v are mean velocity components in x and y direction respectively, P is production by shear, B is buoyancy production/destruction

$$P = \mu_t\left[2(\frac{\partial v}{\partial y})^2 + 2(\frac{v}{y})^2\ell + 2(\frac{\partial u}{\partial x})^2 + (\frac{\partial v}{\partial x} + \frac{\partial u}{\partial y})^2\right] \tag{8.15}$$

$$B = -\frac{g}{\rho}\frac{\mu_t}{\sigma_t}\frac{\partial \rho}{\partial x} \tag{8.16}$$

and ℓ is equal to 0 for plane flows in Cartesian coordinates and is equal to 1 for axisymmetric flows in cylindrical coordinates.

C_1, C_2, C_μ, σ_k, and σ_ϵ are empirical constants and coefficients. The values used in this study are listed in the following table 8.1. C_μ is modified to take account of the effect of buoyancy (Sini and Deceyser, 1986) with

$$C_\mu = 0.09 + 0.04[1 + \tanh(2\log Fr^{-2} + 3)] \tag{8.17}$$

The value of σ_t = 0.9 is for wall jet flows, i.e. wall boundary layers. For the situation of free jets (free boundary layers) σ_t = 0.5. Modifications of C_2 and C_μ for axisymmetric jets were introduced by Rodi (1984) with a deceleration parameter, f, as

$$C_2 = 1.92 - 0.04f \tag{8.18}$$

and

$$C_\mu = 0.09 - 0.04f. \tag{8.19}$$

where f is defined as

$$f = \left| \frac{\delta}{\Delta U_m} \left[\frac{\partial U_m}{\partial s} - \left| \frac{\partial U_m}{\partial s} \right| \right] \right|^{0.2}$$

in which U_m = velocity along the axis of the jet (s), ΔU_m = maximum velocity difference across the jet and δ = distance from symmetric axis (s) to the point of 1% of ΔU_m at the outer edge.

Table 8.1 Constants in the turbulence model

C_1	C_2	C_μ	σ_k	σ_ϵ	σ_t	Pr
1.44	1.92	0.09	1.0	1.3	0.9	0.7

The equations are normalized (non–dimensionalized) by initially known quantities such as jet velocity U_o, jet diameter or width D_o, reference density ρ_r and reference temperature or concentration φ_r. Dependant variables, velocity components u, v, pressure p, kinetic energy k, dissipation rate ϵ, density ρ, and φ (temperature or concentration), are normalized by U_o, ρU_o^2, U_o^2, $\frac{U_o^2}{D_o}$, ρ_r, and φ_r respectively. Independent variables, coordinates x and y and time t, are normalized by D_o and D_o/U_o respectively. Dimensionless parameters are

$$Re = \frac{\rho_r U_o D_o}{\mu} \tag{8.20}$$

$$R\mu_e = \frac{\rho_r U_o D_o}{\mu_e} \tag{8.21}$$

$$R\mu_t = \frac{\rho_r U_o D_o}{\mu_t} \tag{8.22}$$

and

$$Fr = \frac{U_o}{\left[\frac{\rho_r - \rho}{\rho} g D_o\right]^{1/2}} \tag{8.23}$$

If the same symbols as previous ones are used, for convenience, the dimensionless equations are obtained from Eq. 8.5–8.11 with Re, $R\mu_e$, and $R\mu_t$ in places of μ_e, μ and μ_t, and with Fr^{-2} replacing the buoyancy term $(\rho_r - \rho)g$.

8.3 Boundary and initial conditions

Boundary conditions

Boundary conditions have to be specified on all surfaces of the computational domain. Boundaries presented in this study are a solid wall, a free boundary, a symmetric plane (line), a free surface, an outflow boundary and an inflow boundary. Boundary conditions for a horizontal jet and a vertical jet in a lake with an ice cover in winter are shown in Fig.8.1 and Fig. 8.2, respectively.

A free boundary is defined as the location where velocity and a scalar quantity is nearly equal to its free–stream ambient value. Often, the ambient fluid is assumed to be entirely free of turbulence so that all turbulent stresses and fluxes and the dissipation rate are zero at the free boundary.

On fluid surfaces of inflow and outflow, the values of all variables are specified at locations where the flow enters the domain, and zero gradients are specified on outflow surfaces.

On the free water surface, the normal velocity is assumed to be zero. In the absence of wind–induced shear stress and of heat exchange with the atmosphere, a free water surface can be approximately considered as a plane of symmetry or otherwise as a moving wall. For a free surface driven by wind, the surface stress in the direction of wind is obtained from either an empirical relation or from a wall functions if it is considered as a moving wall. Where an ice cover existed the wall treatment is applied.

At solid surfaces such as the ice cover and the lake sediment bottom, the no–slip condition is applied, i.e. both mean and fluctuating velocities are zero. The boundary condition for k is proposed as an approximate zero gradient. There is some difficulty for ϵ since it tends to be infinite and requires fixing of a value of ϵ at a near–wall point according to an empirical relation.

In the region near a wall, μ_t and μ are of similar magnitude, but $\mu_t >> \mu$ in most of the flow field, and the boundary layer is not resolved but rather bridged using wall functions. The dependent variables at the near–wall point are connected to the wall conditions (e.g. wall shear stress, heat fluxes and wall temperature) by applying a linear function for the viscous sublayer and the log–law of the wall just outside the region. The ice

ICE COVER: $u = v = 0$; $T = 0^{o}C$; $\frac{\partial k}{\partial x} = 0$; $\epsilon = \frac{C_{\mu}^{3/4} k^{3/2}}{0.4\delta x}$

OUTFLOW: $\frac{\partial u}{\partial y} = \frac{\partial v}{\partial y} = \frac{\partial T}{\partial y} = \frac{\partial k}{\partial y} = \frac{\partial \epsilon}{\partial y} = 0$; $Q_o = Q_i$

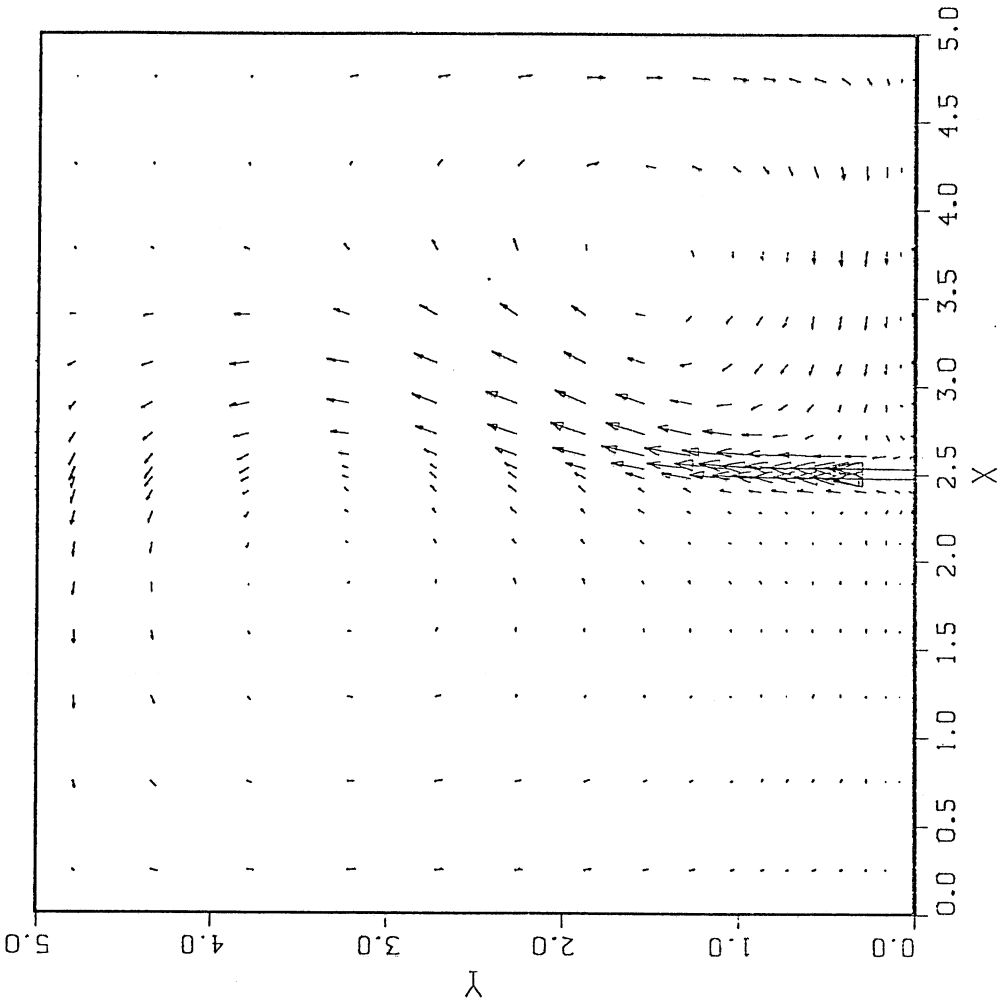

FREE BOUNDARY: $u = v = k = \epsilon = 0$; $T = T_a$

INFLOW: U_o, D_o, Q_i

LAKE BOTTOM: $u = v = 0$; $\frac{\partial T}{\partial x} = \frac{\partial k}{\partial x} = 0$; $\epsilon = \frac{C_{\mu}^{3/4} k^{3/2}}{0.4\delta x}$

Fig. 8.1 Boundary conditions for a horizontal jet

ICE COVER: $u = v = 0$; $T = 0^{o}C$; $\frac{\partial k}{\partial x} = 0$; $\epsilon = \frac{C_{\mu}^{3/4} k^{3/2}}{0.4\delta x}$

OUTFLOW: $\frac{\partial u}{\partial y} = \frac{\partial v}{\partial y} = \frac{\partial T}{\partial y} = \frac{\partial k}{\partial y} = \frac{\partial \epsilon}{\partial y} = 0$; $Q_o = Q_i$

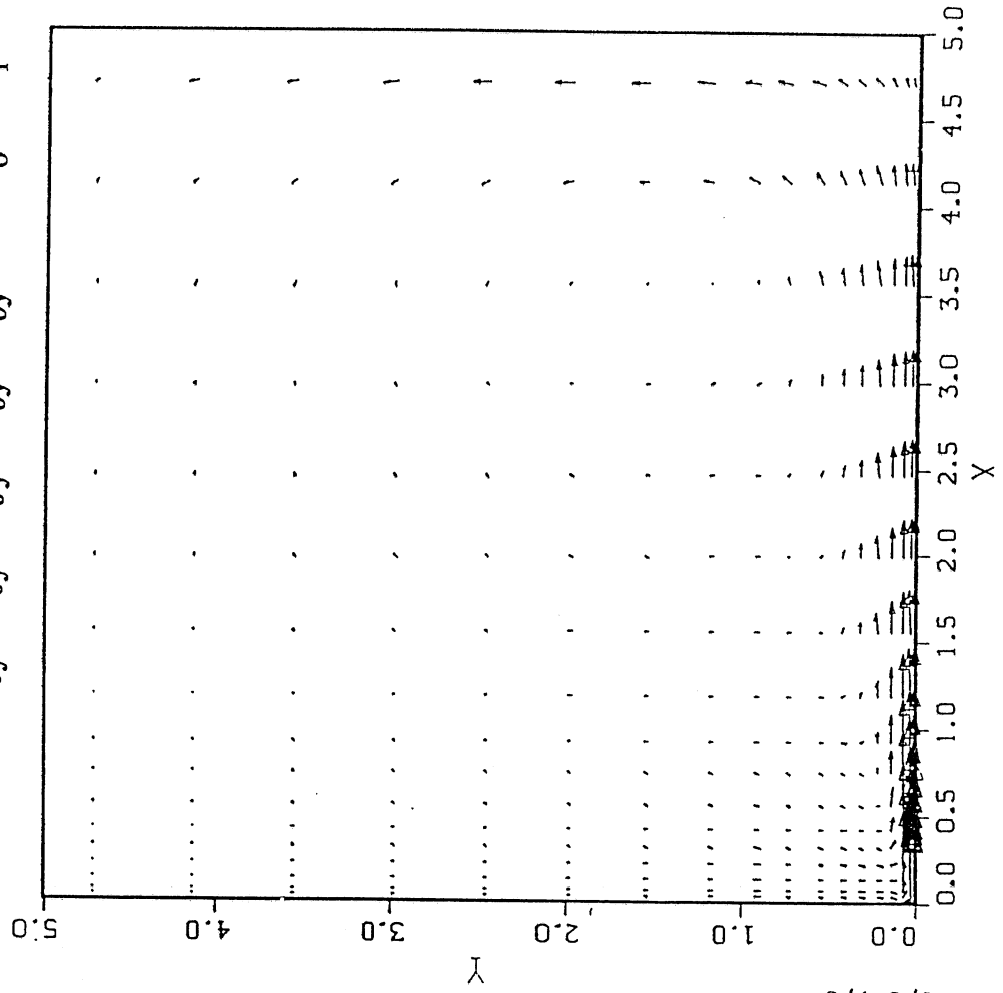

AXIS OF SYMMETRY: $\frac{\partial u}{\partial y} = \frac{\partial T}{\partial y} = \frac{\partial k}{\partial y} = \frac{\partial \epsilon}{\partial y} = 0$; $v = 0$

LAKE BOTTOM: $u = v = 0$; $\frac{\partial T}{\partial x} = \frac{\partial k}{\partial x} = 0$; $\epsilon = \frac{C_{\mu}^{3/4} k^{3/2}}{0.4\delta x}$

INFLOW: U_o, D_o, Q_i

Fig. 8.2 Boundary conditions for a vertical jet

cover may be considered as smooth wall and the lake bottom sediment as a rough wall and then corresponding wall functions are adopted for each of them (Patankar, 1982).

For the solution of the problem, the following boundary conditions are specified: (1) Temperature at the ice/water interface is 0° C, (2) lake bottom is adiabatic, i.e. no heat transfer between water and sediment, and (3) the ambient water (natural field) is calm with a given temperature field.

Initial conditions

The flow field is initially a quiescent fluid with a given thermal (or temperature) field throughout the basin (lake or reservoir). The initial temperature field has constant temperatures in horizontal planes and a linear or non–linear variation of temperatures along the vertical distance between the bottom, typically 4° C, and the top (0° C at the ice cover) of the basin. The initial flow velocity components u and v are given as $u = v = 0$ for the stationary ambient water. Initial k and ϵ are set to be as $k = \epsilon = 0$.

8.4 Numerical method and procedure of solution

The governing equations are based on the mean flow equations of momentum, thermal energy and chemical species transport and the turbulent energy transport equations (k–ϵ). They can be written in the general form:

$$\frac{\partial(\rho\phi)}{\partial t} + \frac{\partial(\rho u\phi)}{\partial x} + \frac{1}{y^{\ell}}\frac{\partial(y^{\ell}\rho v\phi)}{\partial y} = -\frac{\partial p}{\partial x_{\phi}} + \frac{\partial}{\partial x}\Gamma_{\phi}\frac{\partial\phi}{\partial x} + \frac{1}{y^{\ell}}\frac{\partial}{\partial y}y^{\ell}\Gamma_{\phi}\frac{\partial\phi}{\partial y} + S_{\phi} \qquad (8.24)$$

where $x_{\phi} = x$ for the u–equation and y for the v–equation, $\phi = u, v, T, C, k$ and ϵ, and Γ_{ϕ} and S_{ϕ} = diffusion coefficients and sources or sinks in the governing equations as listed in Table 8.2.

In the 2–D simulation model a set of eight equations, which consists of six transport equations of the general form (Eq. 8.24), one continuity equation and one state equation, are solved for the eight dependent variables u, v, p, k, ϵ, ρ, T and C. The independent variables are time t and coordinates x and y.

Equations governing the flow field and thermal field are solved numerically by the method and procedure given by Patankar (1972, 1980, 1981). The computer code (program) of Patankar (1982) with the SIMPLER algorithm is employed with little change. Modifications were made to the original code to extend it so that solutions of the unsteady nonlinear flow problem within a finite time step could be obtained and to incorporate and implement the terms due to buoyancy in the program.

Table 8.2 Diffusion coefficients and source terms in the governing equations

Variable ϕ	Diff. Coeff. Γ_ϕ	Source term S_ϕ
u	μ_e	$\frac{\partial}{\partial x}\mu_e\frac{\partial u}{\partial x} + \frac{1}{y^\ell}\frac{\partial}{\partial y}y^\ell\mu_e\frac{\partial v}{\partial x} + (\rho_a - \rho)g$
v	μ_e	$\frac{1}{y^\ell}\frac{\partial}{\partial y}y^\ell\mu_e\frac{\partial v}{\partial y} + \frac{\partial}{\partial x}\mu_e\frac{\partial u}{\partial y} - \ell\frac{\mu_e + \mu}{y^2}v$
T or C	α_e	S(T) or S(C)
k	$\mu + \frac{\mu_t}{\sigma_k}$	$P - \rho\epsilon + B$
ϵ	$\mu + \frac{\mu_t}{\sigma_\epsilon}$	$(C_1(P + B) - C_2\rho\epsilon)\frac{\epsilon}{k}$

The finite–volume method, which is based on the control–volume formulation over a regular grid, was used to derive the (algebraic) discretization equations from the governing differential equations. The physical conservation of mass, energy and momentum in the control volume is mathematically expressed by integration of the governing differential equations over the control volume. The power–law scheme which is a computationally efficient and close approximation of the (exact) exponential scheme was adopted for the convection–diffusion terms. The stagged grid is used with the SIMPLER procedure and the velocity components are computed and stored at the points on faces of the main control volume.

Solutions to the simultaneous linear algebraic equations are obtained by the line–by–line iterative method which is the combination of the TriDiagonal–Matrix–Algorithm (TDMA) for one–dimensional situations and the iterative Gauss–Seidel method.

The fully–implicit scheme for the unsteady term gives stable solutions even at large time steps. The nonlinearity of the convection, diffusion and source terms in the governing equations is handled by iteration.

The pressure and velocity correction is made during the computation so that the continuity equation is closely satisfied by the velocity components. The error in the continuity equation is one of the criteria for converged solutions or the convergence of iteration. The other criterion for convergence is that the relative error with respect to velocities and temperatures in an iteration is smaller than 1%, i.e.

$$\left| \frac{\phi_{new} - \phi_{old}}{\phi_{old}} \right| \leq 10^{-2} \tag{8.25}$$

where ϕ_{new} = new value of ϕ after the current iteration and ϕ_{old} = old value of ϕ after the previous iteration. The time step is variable and based on the speed of convergence in previous timesteps.

A selected size of the computational domain is characterized by a ratio of length to depth, y_1/x_1, with a constant ratio of depth to jet width, x_1/B_o, typically in the range 50 to 100 for a jet in a lake. A non–uniform grid system is used with finer grids for the jet region and boundary layers and coarser grids for other regions. Sensitivity of the 2–D model to the domain size and grid points was studied by examining simulated results for horizontal buoyant jets in stratified ambients from numerical experiments with various space steps and different y_1/x_1, respectively. Based on the numerical sensitivity analysis for the jet with T_j = 10° C, U_j = 0.175 m/s, T_a = 1–4° C, and B_o = 0.2 M, it was shown (Figs. 8.3–8.8) that the numerically predicted jet (centerline) velocities, temperatures and trajectories were quite insensitive to the number of grid points in the range 26 x 34 to 48 x 63 and y_1/x_1 = 2.5 to 4.0. In general these ranges of values are appropriate for economical computational time and good results. The 26 x 34 mesh and the ratio y_1/x_1 = 3.0 were used in the following numerical simulations.

8.5 Model validation with data for vertical jets

Validation of the 2–D model was first made by comparing simulated results with existing data for a vertical plane impinging jet in a uniform ambient. Gutmark and Wygnanski (1976) conducted an experimental investigation of the two–dimensional turbulent jet impinging on a plate (wall). The jet was numerically simulated using the unsteady 2–D model developed in this study.

In the experiment for a non–buoyant jet (Gutmark and Wygnanski, 1976) in homogeneous water, the jet emerged from a nozzle 1.3 cm wide and 50 cm long. The Reynolds number based on the nozzle width was 30,000. The plate on which the jet impinged was installed 100 slot widths downstream of the nozzle, H_o/B_o, at right angle to the jet. H_o is the distance from the nozzle to the plate. The mean longitudinal velocity component, W, was measured.

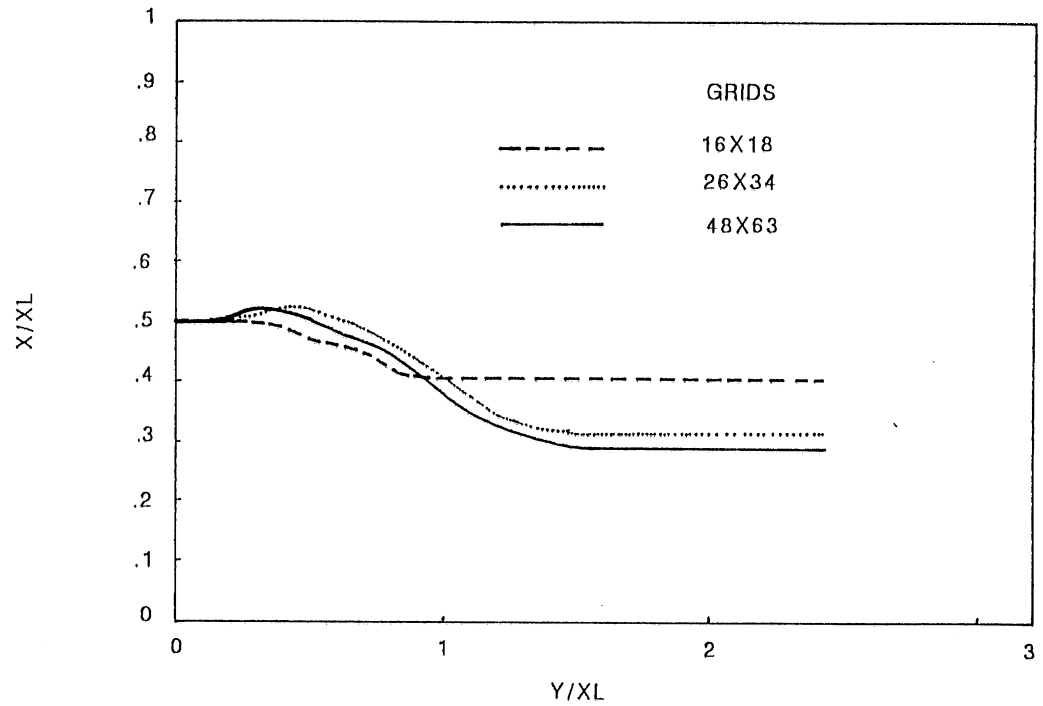

Fig. 8.3 Jet centerline trajectories in three grid systems: $t^* = 0.02$

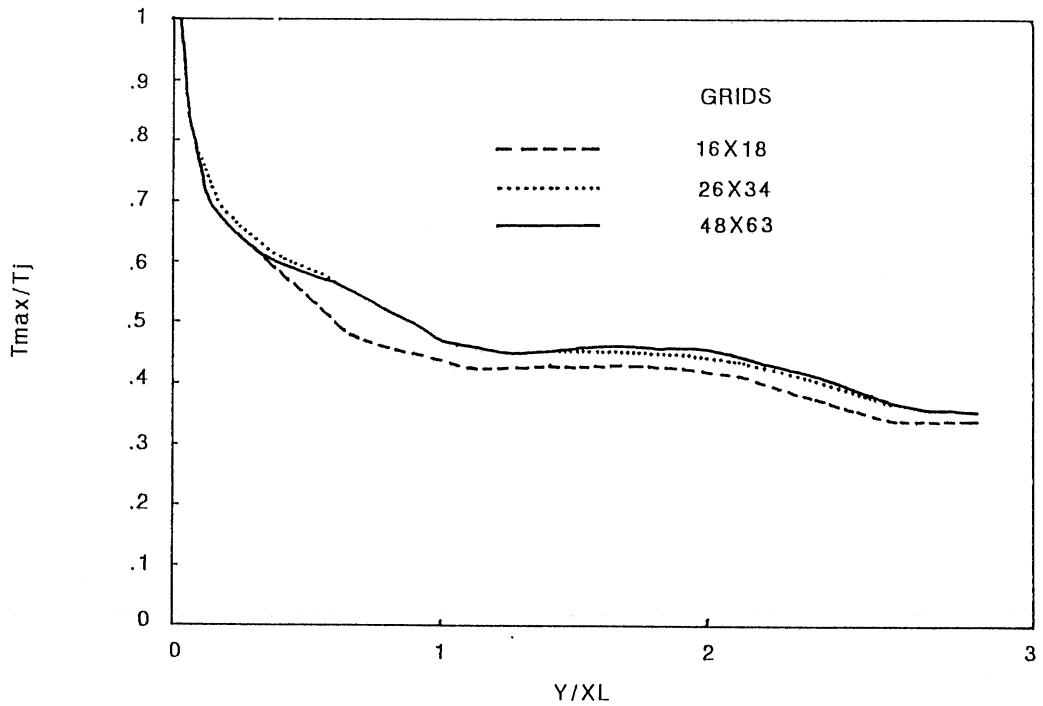

Fig. 8.4 Decay of centerline temperatures in three grid systems: $t^* = 0.02$

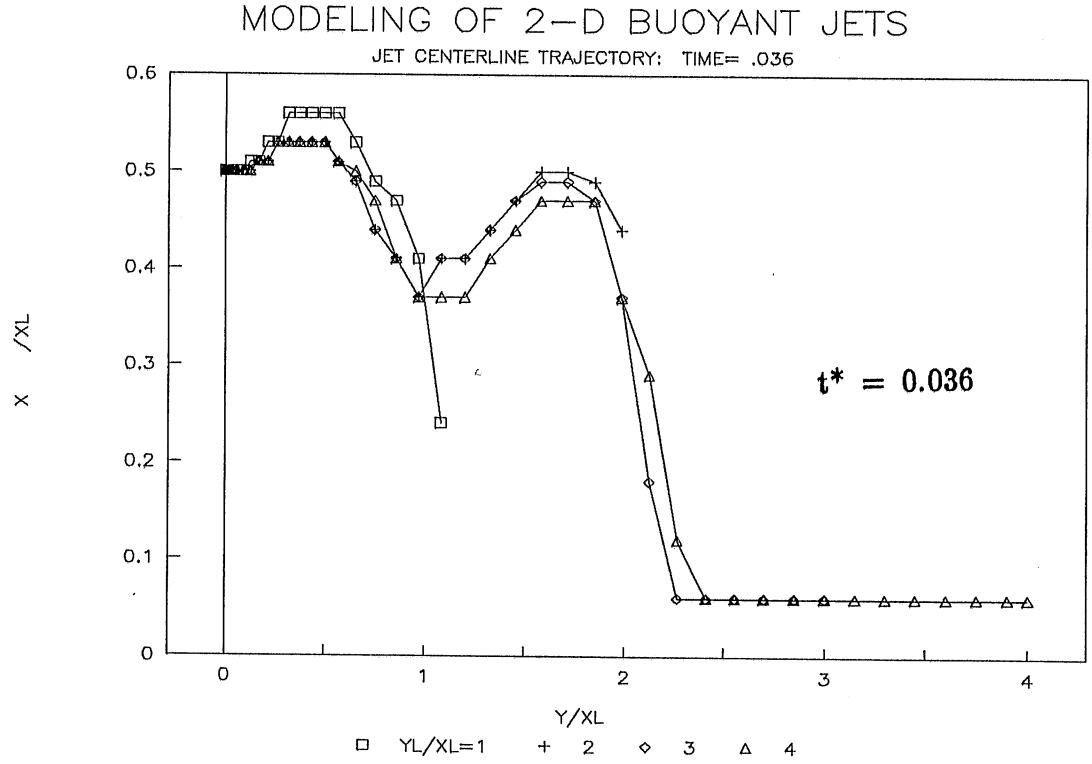

Fig. 8.5 Jet centerline trajectories in four computational domains

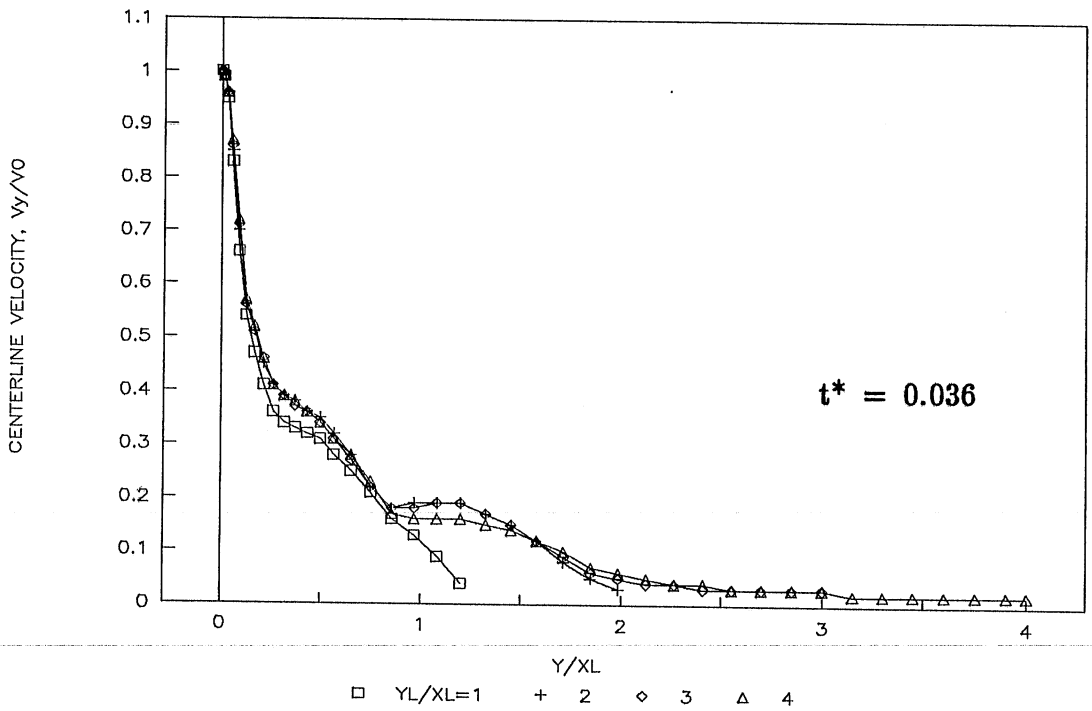

Fig. 8.6 Decay of centerline velocity in four computational domains

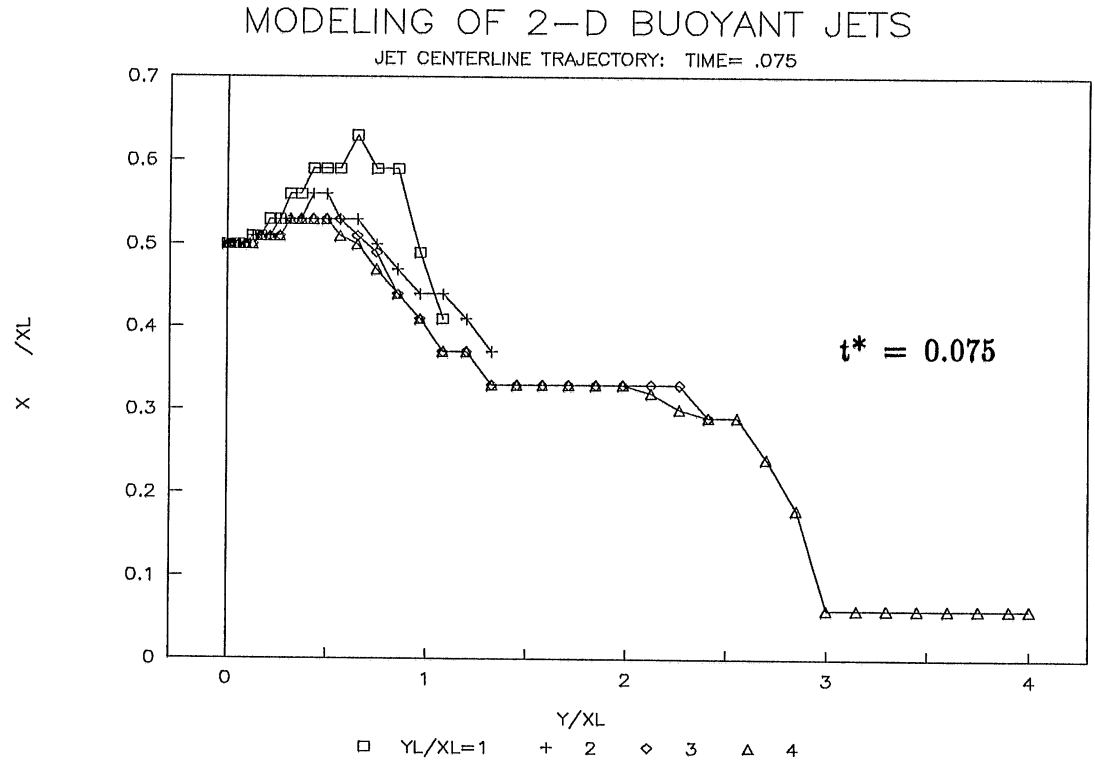

Fig. 8.7 Jet centerline trajectories in four computational domains

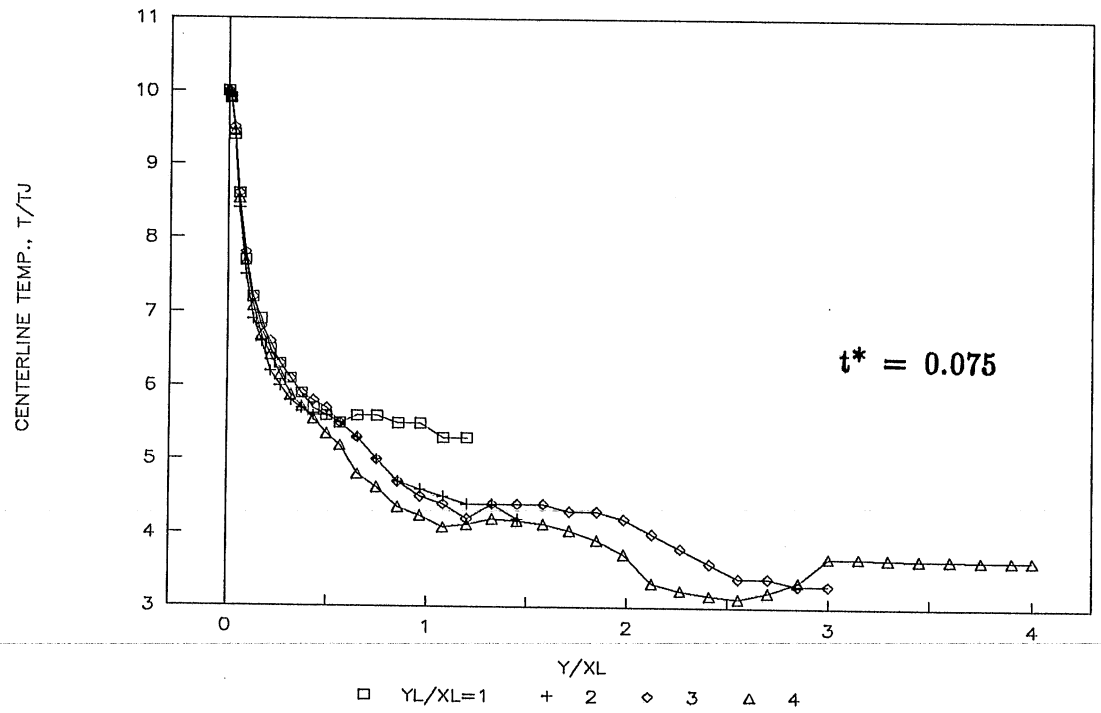

Fig. 8.8 Decay of centerline velocity in four computational domains

The measured and simulated mean longitudinal velocity along the non–buoyant jet centerline, W_m, are presented in Fig. 8.9 in dimensionless form, W_m/W_o vs. z/H_o, where W_o is the jet velocity at the exit of the nozzle. Experimental data of Andreopoulos et al. (1986) for a vertical plane jet impinging on the free surface of shallow water are also presented in Fig. 8.9 to supported the consideration that there is similarity between cases of a free surface and a rigid wall (plate). Fig. 8.10 shows simulated flow fields in the form of velocity vectors.

If the jet has strong buoyancy, e.g. Fr = 12, the numerically predicted centerline velocity appears to have a slower decay in the jet region and a sharper decay close to the plate in the impingement region than the non–buoyant case does (Fig. 8.11). The buoyancy effect was also described by Andreopoulos, et al. (1986) based on experimental data for vertical plane buoyant and non–buoyant jets in shallow water with a free surface.

8.6 Simulation of a plane offset jet

Experiments were performed by some investigators to study the flow characteristics of a plane offset jet discharging parallel to a flat plate (Sawyer, 1960, Ali and Salehi–Neyshaboury, 1989, and Rajaratnam and Subramanya, 1968) or a free surface (Stoy and Stenhouse, 1975). Flow fields, velocity profiles, jet trajectories and attachment length (cavity length) were investigated through detailed velocity measurements. These laboratory data are also used to validate the 2–D model, developed in this study, for wall–affected flows. Numerical simulations were carried out for plane offset jets which had been experimentally examined.

A slot jet is discharged near a solid wall boundary or a free surface as shown in Fig. 8.12. After leaving the nozzle, the jet curves towards the boundary and attaches to it enclosing an eddying region of separated flow. This phenomenon known as the Coanda effect (Rajaratnam and Subramanya, 1968) is caused by the reduction of pressure on the inner side of the jet. It was suggested by Stoy and Stenhouse (1975) that a slot jet might be used to contain a pool of heated water near a jet outlet because of the entrapped vortex or to retard the rise of a jet by locating the discharge close to the bottom surface. The submerged offshore type of outfalls is considered to be pretty effective in reducing temperature rise in the water surface due to waste heat disposal (Hino, et al, 1975).

The essential feature of the flow is the entrainment of fluid by the jet, which enables a stable flow pattern to be attained. When the jet efflux is close to a solid boundary or a free surface there is only a finite volume of fluid which is available to be entrained between the jet and the boundary. Therefore, the surrounding fluid being entrained must be replenished by a back flow near the boundary where a vortex forms. The pressure in the recirculation region is reduced (less than hydrostatic pressure). The jet deflects towards the boundary. This flow is typical of cavity flows. The entrainment of a curved plane jet is reduced along the inner edge and

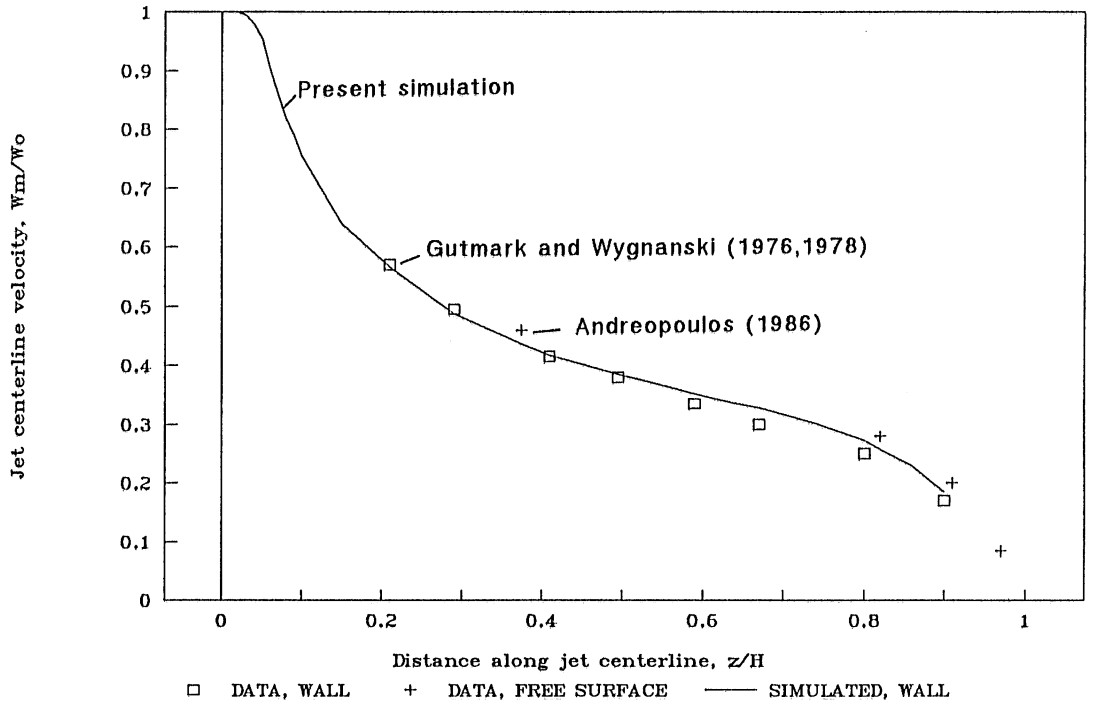

Fig. 8.9 Measured and simulated mean longitudinal velocity along the vertical non–buoyant jet centerline

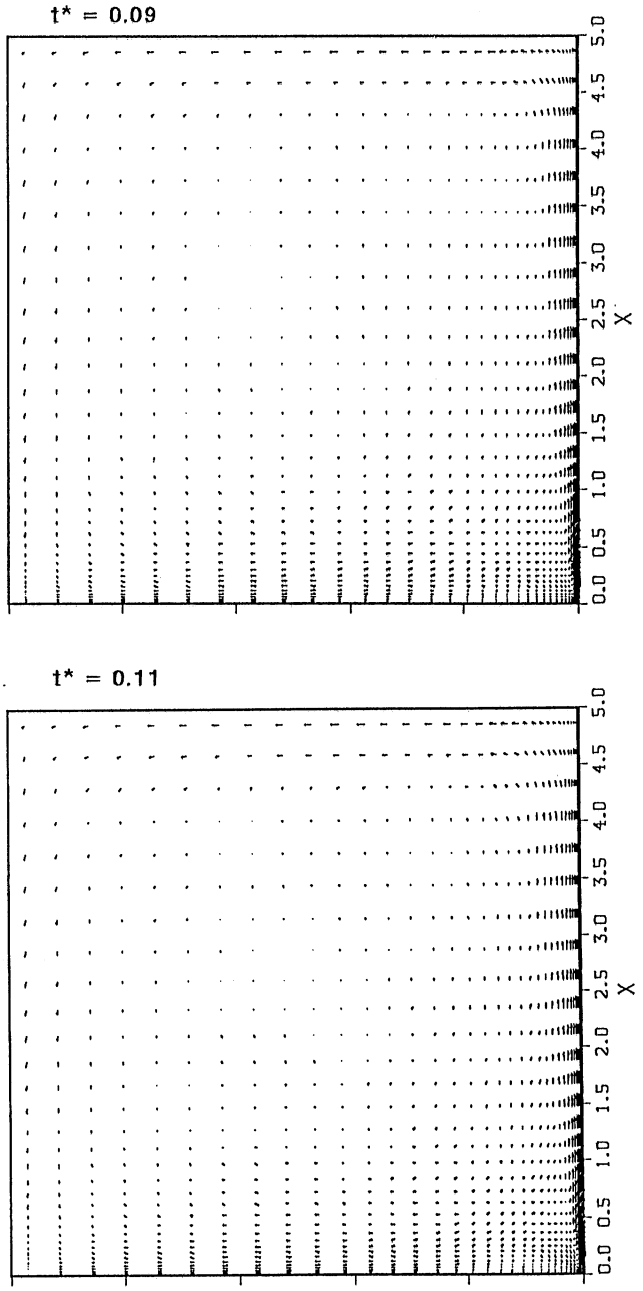

Fig. 8.10 Calculated flow fields of a vertical jet in the form of velocity vectors at $t^* = 0.09$ and $t^* = 0.11$

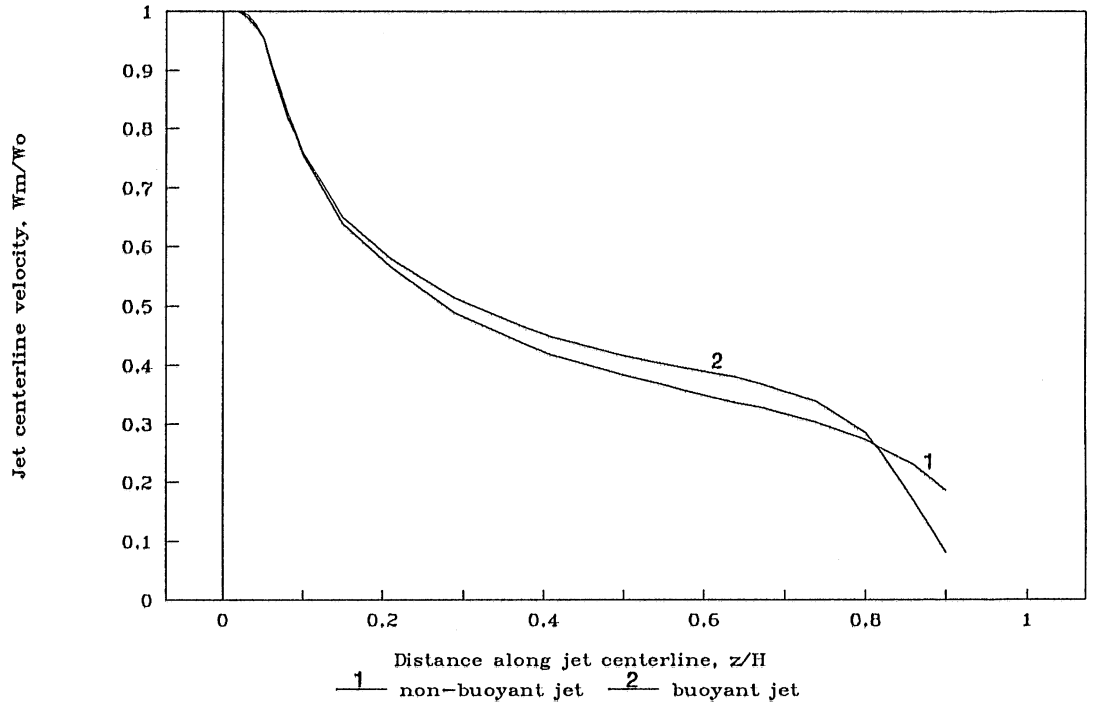

Fig. 8.11 Comparison of jet centerline velocities of (vertical) buoyant and non–buoyant jets

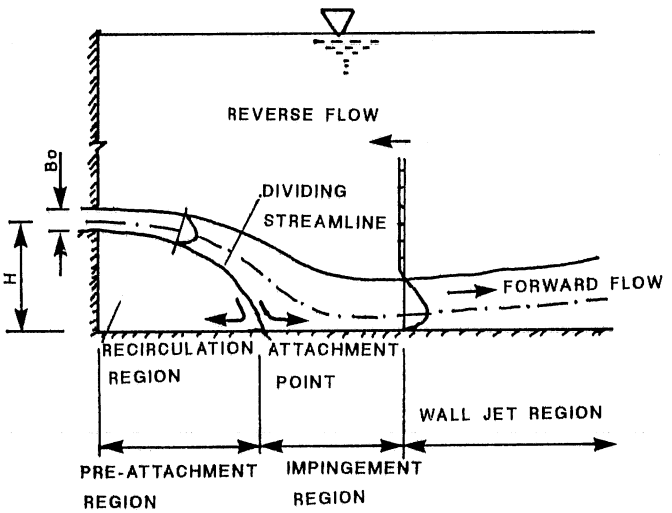

Fig. 8.12 Definition sketch for an offset jet

enhanced along the outer edge. For a round axisymmetric jet discharge no significant attachment to boundaries was observed because of the absence of vortex formation (Stoy and Stenhouse, 1975).

If the discharge is located close to two (top and bottom) boundary surfaces, attachment of the jet to either boundary is possible. Generally, the jet will attach to the nearer surface but external forces such as ambient turbulence, surface turbulence, jet buoyancy, and slope of the bottom can alter the jet trajectory. For symmetric geometry and external forces about the jet centerline (axis), the jet remains straight and attachment does not occur as seen in Fig. 8.13.

Velocity vectors simulated by the 2–D model for an offset jet are presented in Fig. 8.14. As shown in Fig. 8.14 the initial action of the offset jet which enters the the stationary ambient water is similar to that of a free jet, entraining fluid from the ambient. At a later stage a vortex or eddy contained by the lower portion of the jet, the bottom, and the vertical wall is formed by the entraining effect of the jet. An offset ratio, defined as H/B_o, is used to characterize the jet, where H is the distance of the slot centerline from the boundary (Fig. 8.12). For a free surface, H/B_o is called submergence ratio and H is the submergence depth.

The jet centerline trajectory is defined as the locus of the position of the maximum velocity. Fig. 8.15 shows the jet trajectory measured by Ali and Salehi–Neyshaboury (1989) and the centerline simulated by the 2–D model. The agreement is fairly good.

The attachment point is the exact location of the intersection of the dividing streamline. The attachment length (or cavity length or standing eddy length) was obtained by considering mean velocity in the y direction in the impingement region. In Fig. 8.16 attachment lengths predicted by the 2–D model are plotted along with measurements of various investigators. The numerical simulation agrees well with the experimental data. Stoy and Stenhouse's experimental results for a submerged slot jet near a free surface support the notion that jets impinging on a free surface and on a rigid wall do indeed behave rather similarly.

A typical velocity distribution at different sections, y/B_o, simulated by the 2–D model is plotted in Fig. 8.17 along with velocity profiles experimentally observed by Rajaratnam and Subramanya (1968) for a jet with $H/B_o = 3.8$. In this figure x = vertical distance form bottom, y = longitudinal (horizontal) distance from the nozzle, and v = the horizontal velocity. Agreement of model results with the laboratory data was reasonably good.

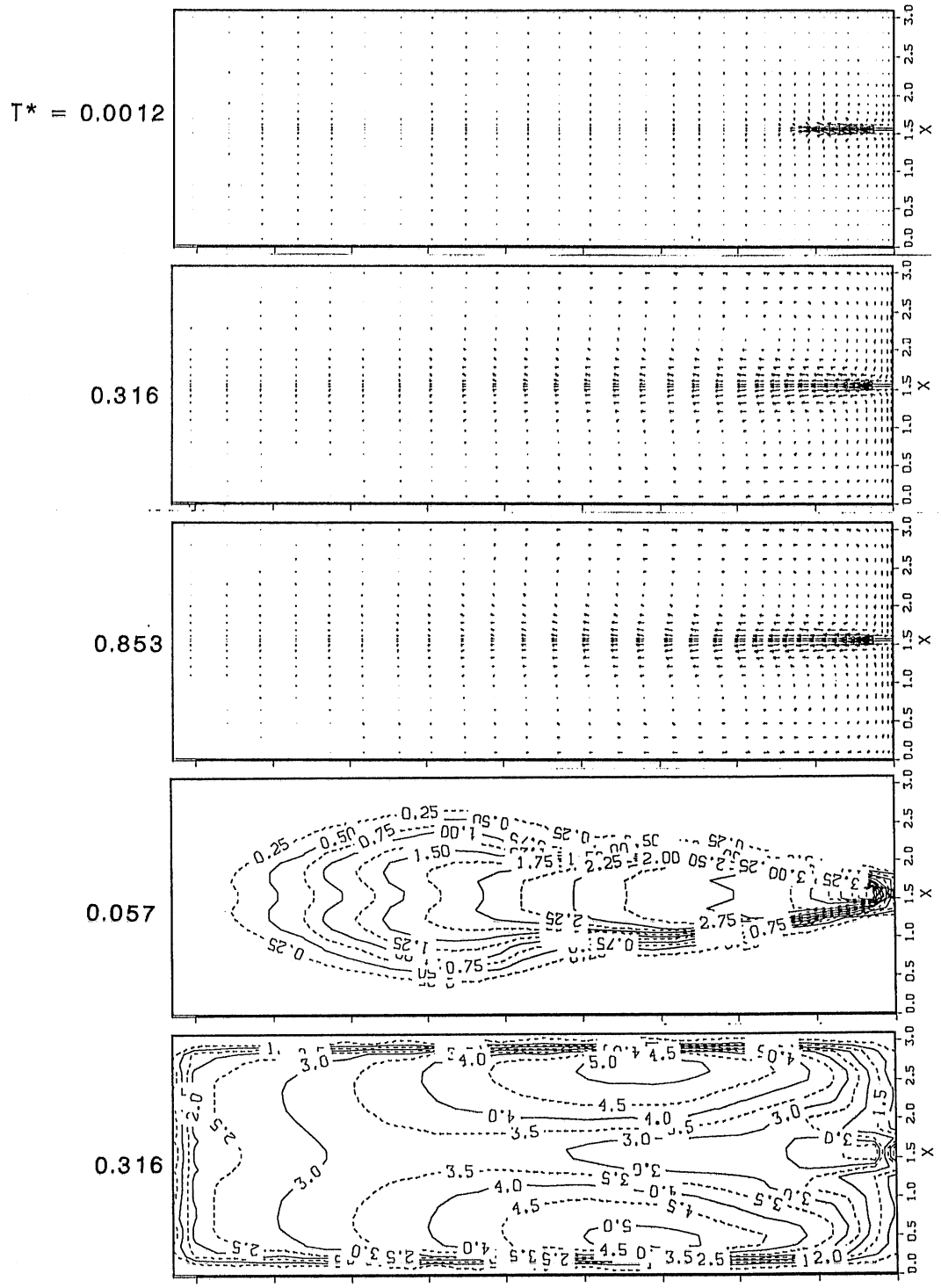

Fig. 8.13 Computed flow fields (velocity vectors) and μ_t contours of an offset jet in a symmetric situation

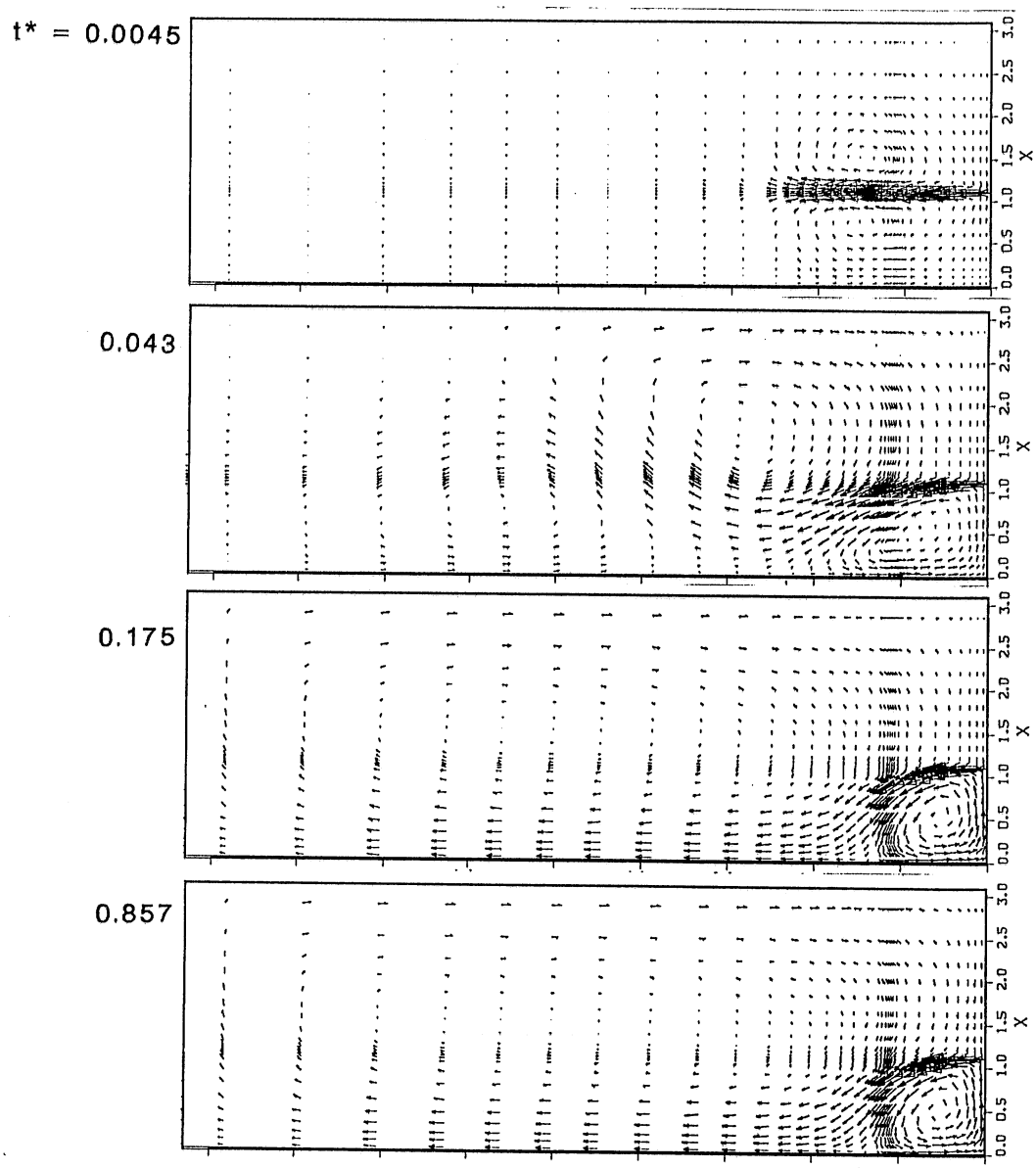

Fig. 8.14 Simulated velocity fields of an offset jet: $H/B_o = 25$, $B_o = 0.014$ m, $U_j = 3.33$ m/s

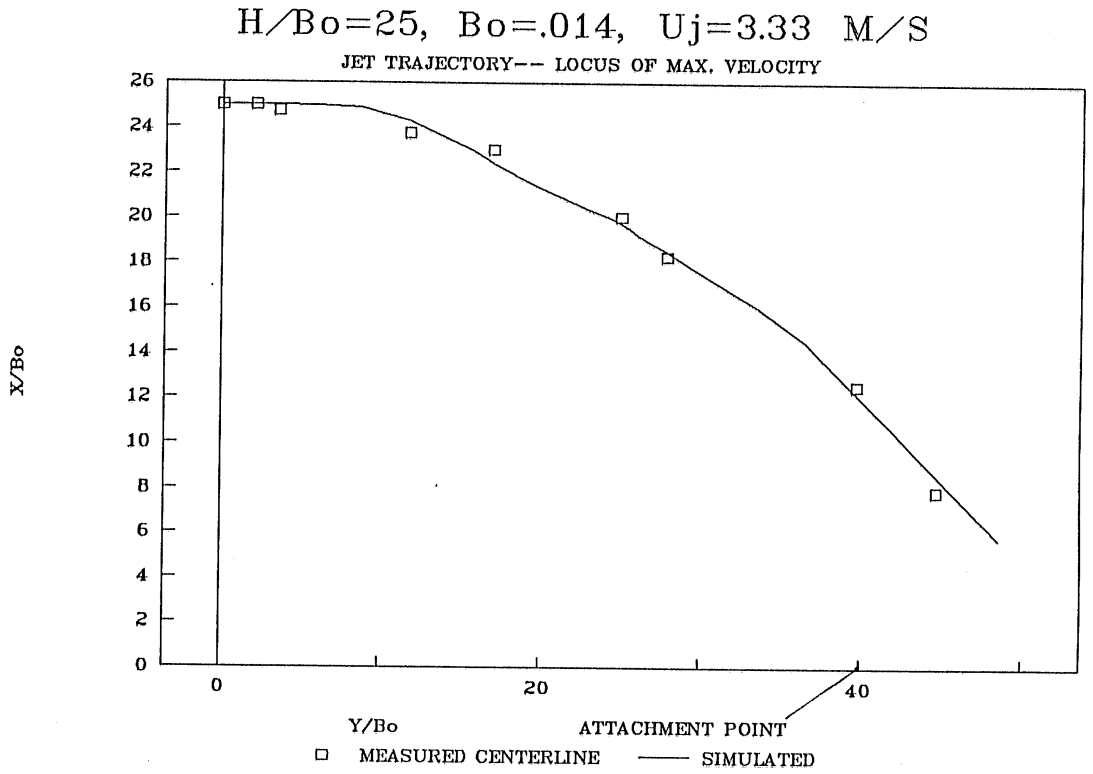

Fig. 8.15 Centerline trajectory of an offset jet measured by Ali and Salehi–Neyshaboury (1989) and presently simulated with the 2–D model: $H/B_o = 25$, $B_o = 0.014$ m, $U_j = 3.33$ m/s

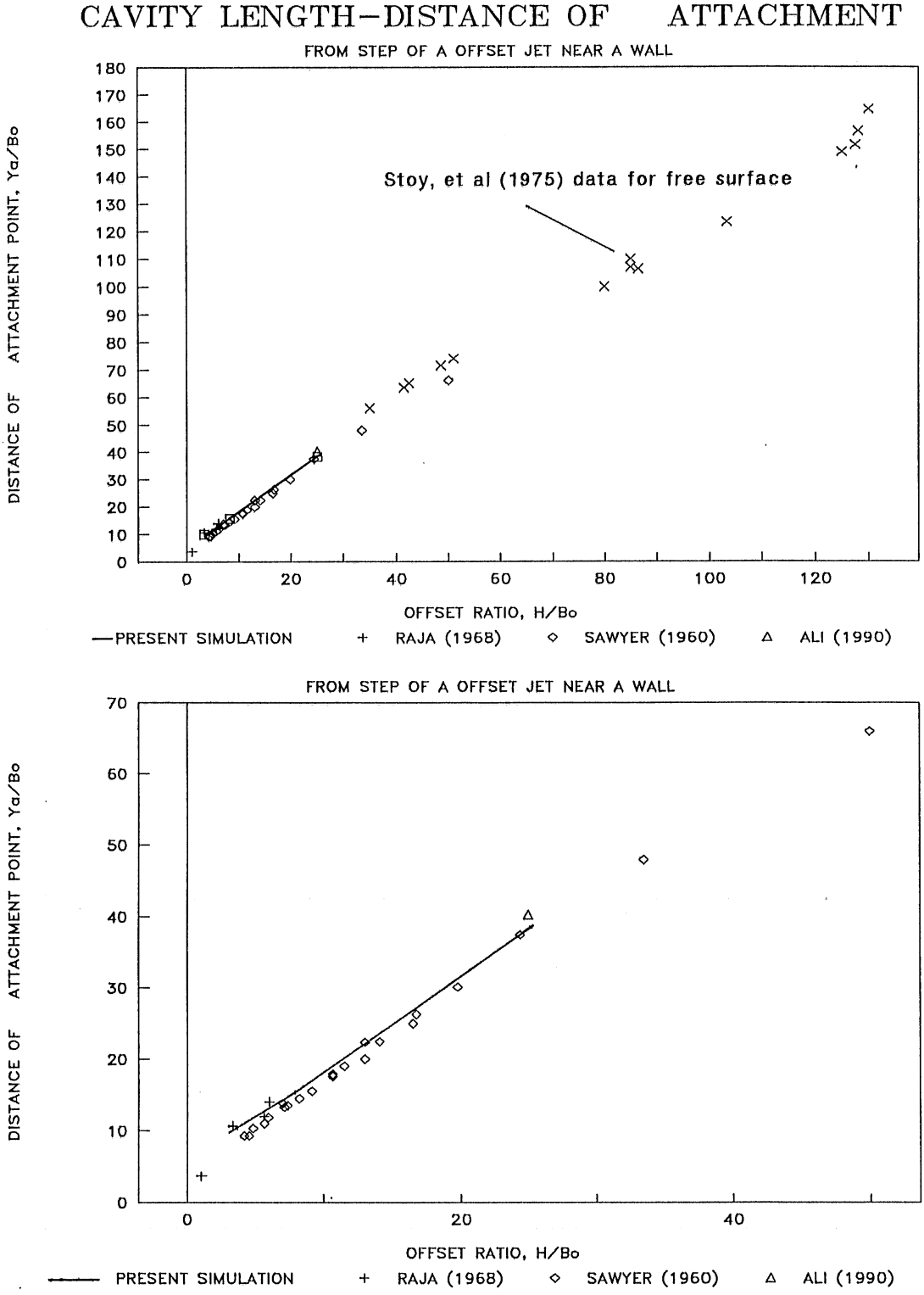

Fig. 8.16 Measured and predicted attachment lengths

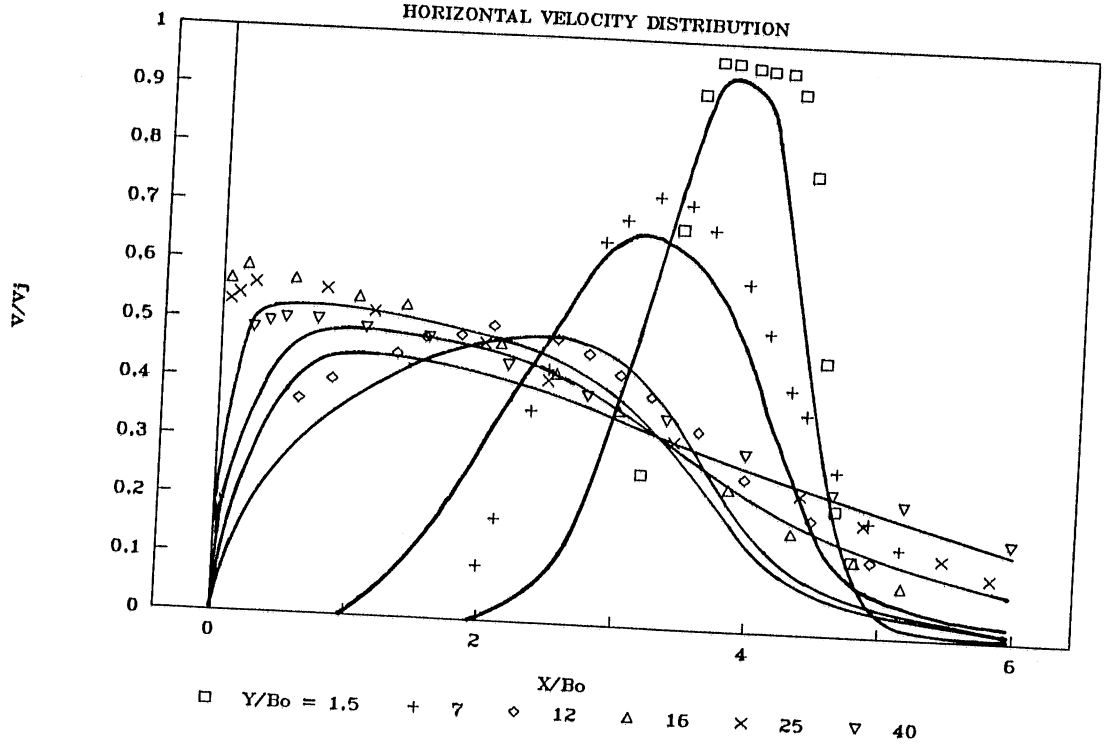

Fig. 8.17 Velocity profiles of an offset jet ($H/B_o = 3.8$) measured by Rajaratnam and Subramanya (1968) and presently simulated with the 2–D model

8.7 Numerical investigation of horizontal jets in stratified ambients

Numerical simulations of horizontal jets in stratified water of low temperatures (0 – 4 °C) with the integral analysis approach were described in Chapter 6. Robillard and Vasseur (1978) and Jain and Pena (1975) also studied trajectories of a horizontally discharged jet into uniform ambients with the integral method. No numerical results from 2–D modeling were found in the literature. In this section numerical results for horizontal jets in a winter lake with an ice cover are presented. The effects of injection temperature and stratification on the jet flow behavior and mixing feature are studied. Because of the difficulty in creating low temperature water (0 – 4° C) and ice cover under laboratory conditions, no experimental data are available for the validation of the 2–D simulation results to be presened.

A free boundary with $u = v = u_a = v_a = 0$ and $T = T_a$ was assumed for the right side of the computational domain (Sec. 8.3). In practical situations there is no such boundary between the jet flow and the ambient water. Flows into or out of the computational domain may exist. With the stationary free boundary the jet becomes an offset jet as described in Sec. 8.6. In order to investigate the effects of buoyancy and stratification on the jet behavior and mixing process, the offset jet phenomena such as the deflection of the jet due to a wall, need to be eliminated from the numerical simulation. This can be done by setting the jet centerline at the mid–point between the top boundary (ice cover) and the bottom boundary (sediment). This arrangement produces a symmetrical situation in which the effects of both bounding surfaces are identical. As discussed in Sec. 8.6, no deflection occurs to a non–buoyant offset jet with symmetric boundaries and external forces (Fig. 8.13). This is because the reduced pressures caused by the presence of confined vortices on both sides of the jet are also symmetrical. Therefore, any deflection of a horizontal jet, rising to the top or falling to the bottom, seen in a stratified environment is caused only by the buoyant force.

One of the advantages of the numerical model simulation is the ability to investigate a variety of cases interested by changing inputs for various conditions. In the problem of a horizontal jet discharged into low temperature ambient water (0 – 4° C), the major parameters characterizing flow patterns are the temperature of injected water which determines the sign of the buoyancy, jet densimetric Froude number describing the strength of buoyancy, and Reynolds number representing turbulence level. Cases with different injection (discharge) temperatures, $0° C \leq T_j \leq 20° C$, will be investigated. Two groups of runs were carried out. One group is for jets with different Reynolds numbers, Re, but constant Froude number, Fr = 6, as listed in Table 8.3. For the second group of simulations (Table 8.3) Reynolds number, Re, is fixed but Froude number, Fr, is variable. Ambient water stratification in all cases is vertically linear and temporally constant, i.e. $T_a = 0° C$ on the top (ice cover) and $T_a = 4° C$ on the bottom (sediment). Only one value (0.2 m) for jet width was used. Velocity and

Table 8.3 Summary of numerical simulation conditions

Run No.	Jet temp.	Jet velocity	Stratifi –cation number	Reynolds number	Froude number	Richard –son number
	T_j	U_j	St	Re	Fr	Ri
	(°C)	(m/s)				
A0	0.05	0.081	38.0	16,000	6.0	0.0278
A4	4.0	0.044	12.0	8,000	6.0	–0.0278
A8	8.0	0.082	40.0	16,000	6.0	0.0278
A10	10.0	0.131	101.0	26,200	6.0	0.0278
A15	15.0	0.243	351.0	48,000	6.0	0.0278
A20	20.0	0.350	727.0	70,000	6.0	0.0278
B0	0.05	0.175	38.0	35,000	13.3	0.00565
B2	2.0	0.175	0.0	35,000	∞	0.0
B4	4.0	0.175	12.0	35,000	24.0	–0.0017
B6	6.0	0.175	1.7	35,000	60.0	0.00028
B8	8.0	0.175	40.0	35,000	12.8	0.00610
B10	10.0	0.175	101.0	35,000	8.0	0.01563
B15	15.0	0.175	351.0	35,000	4.3	0.05408
B20	20.0	0.175	727.0	35,000	3.0	0.11111

x_1 = 10 m and y_1 = 30 m; Grid points, 26 x 34;

ambient temperature T_a = 0 to 4 °C and jet width B_o = 0.2 m

temperature distributions were simulated for each set of conditions. A great variety of flow patterns and mixing processes were obtained based on the 2–D numerical simulations.

Due to the peculiar variation (nonlinearity between density and temperature of water at low temperatures (0 – 10° C) and maximum water density at 4° C (Fig. 8.18), the buoyancy effects on the jet in winter are complicated. A heated jet discharged with a temperature $T_j > 4°C$ into ambient water at temperature of 0 – 4° C may rise up during a initial time period and but sink down in a later time period. The spatial and temporal reversal of flow direction is a unique feature of the situation. In summer ($T_j > 4°C$ and $T_a > 4°C$) a jet always rises due to positive buoyancy (Fig. 7.7) or sinks all the time due to negative buoyancy (Fig. 8.19).

The behavior of a horizontal plane warm water jet discharged into an ice–covered lake (0 – 4° C) is illustrated by two typical cases in which T_j = 8 and 10° C, respectively, Fr = 6 and Re = 35,000. In order to give a general idea of the flow situations and their evolution, flow fields in the form of velocity vectors, thermal fields in the form of isotherms at different times are presented in Fig. 8.20 and Fig. 8.21. Significant buoyancy and stratification effects on flow patterns and development can be seen quite clearly. The reversible buoyancy in water with temperatures of 0 to 8° C becomes very evident.

Generally, the movement of a jet flow can be characterized as rising, falling or neutral. At the very beginning of the discharge (Fig. 8.20 (a) and Fig. 8.21 (a)), the heated warm water jet (8 or 10° C) exits into stagnant surrounding water of about 2° C, and rises slightly under the positive buoyancy near the nozzle outlet of discharge. As it is cooled quickly by dilution down to 4° C it achieves maximum density by entrainment ambient cold water. Once the buoyancy becomes negative because of dilution to lower temperature and heavier density, the jet is deflected downward. In the region of deflection, the buoyancy force always works against the flow. Together with ambient stratification the buoyant force locally acts to bring the jet back to its equilibrium level (layer of neutral buoyancy).

As time progresses (Fig. 8.20 (b)and 8.21 (b)) more mixing between the jet and the ambient occurs. The ambient water becomes warmer and more uniform in the region near the jet origin. Consequently cooling of the jet is slowed down. Stronger positive buoyancy drives the jet upwards over a longer distance. The change in flow direction still exists since water in the middle region has not been heated up by the jet and continues to cool the flow to reverse buoyancy.

When the ambient water is close to a well mixed situation (Fig. 8.20 (c) and 8.21 (c)) or close to a steady state (completely mixed situation), the jet is driven up to the top surface by positive buoyancy. As the process continues, the jet impinges on the ice–cover surface, becoming a wall jet, and plunges after some distance downwards to deeper layers (Fig. 8.21 (c)) as the ambient water in the remote area has been only slightly disturbed and

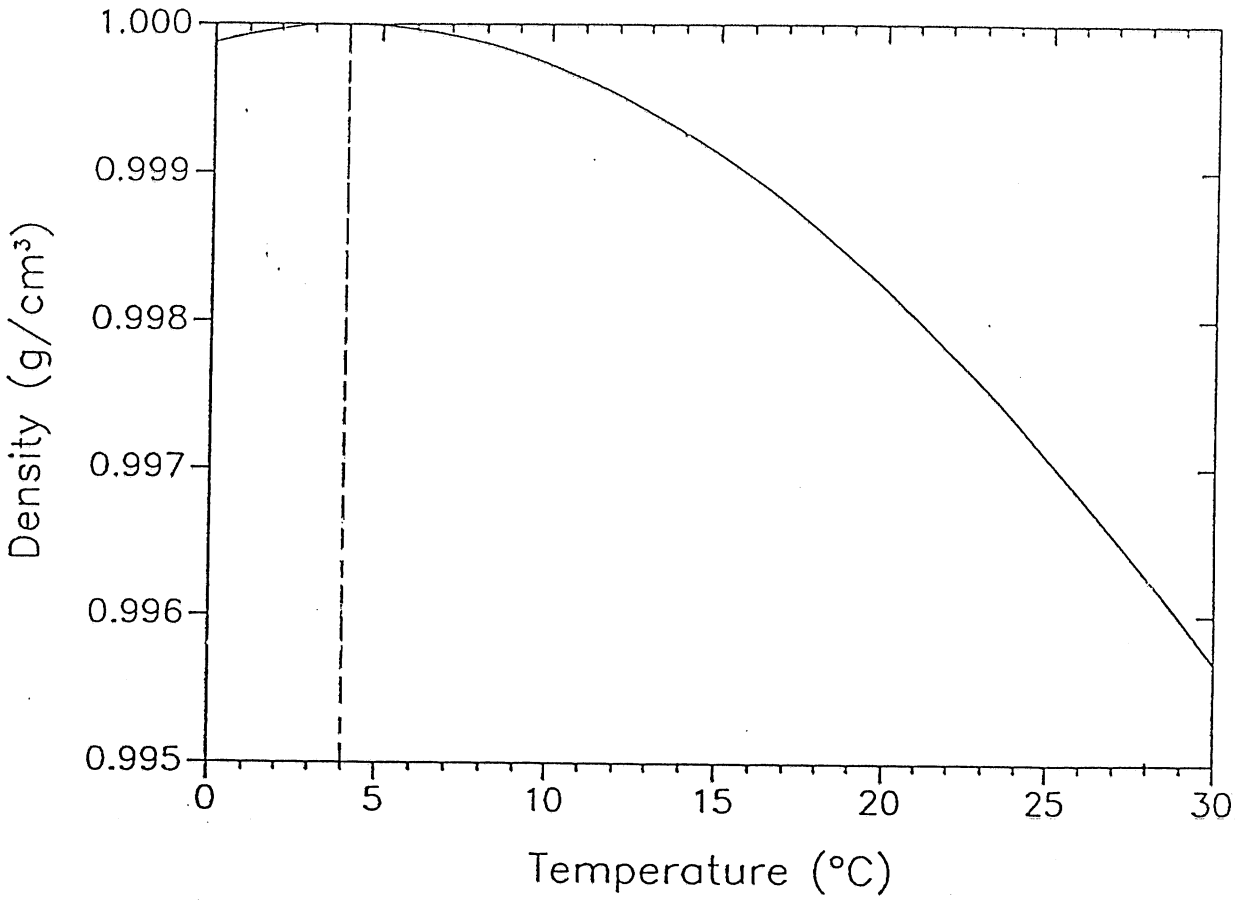

Fig. 8.18 Density of water as function of temperature

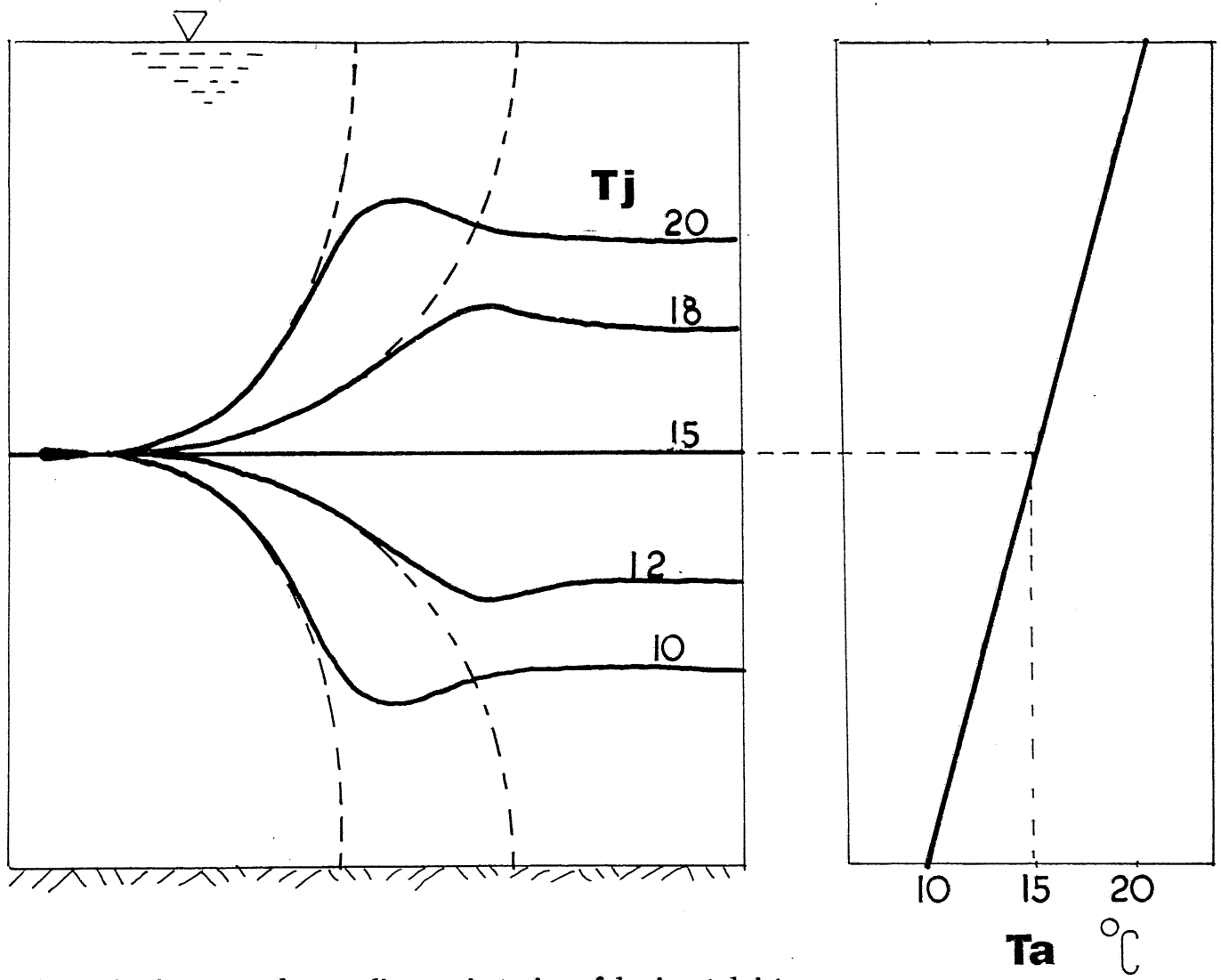

Fig. 8.19 Schematic diagram of centerline trajectories of horizontal jets with different discharge temperatures in a summer lake

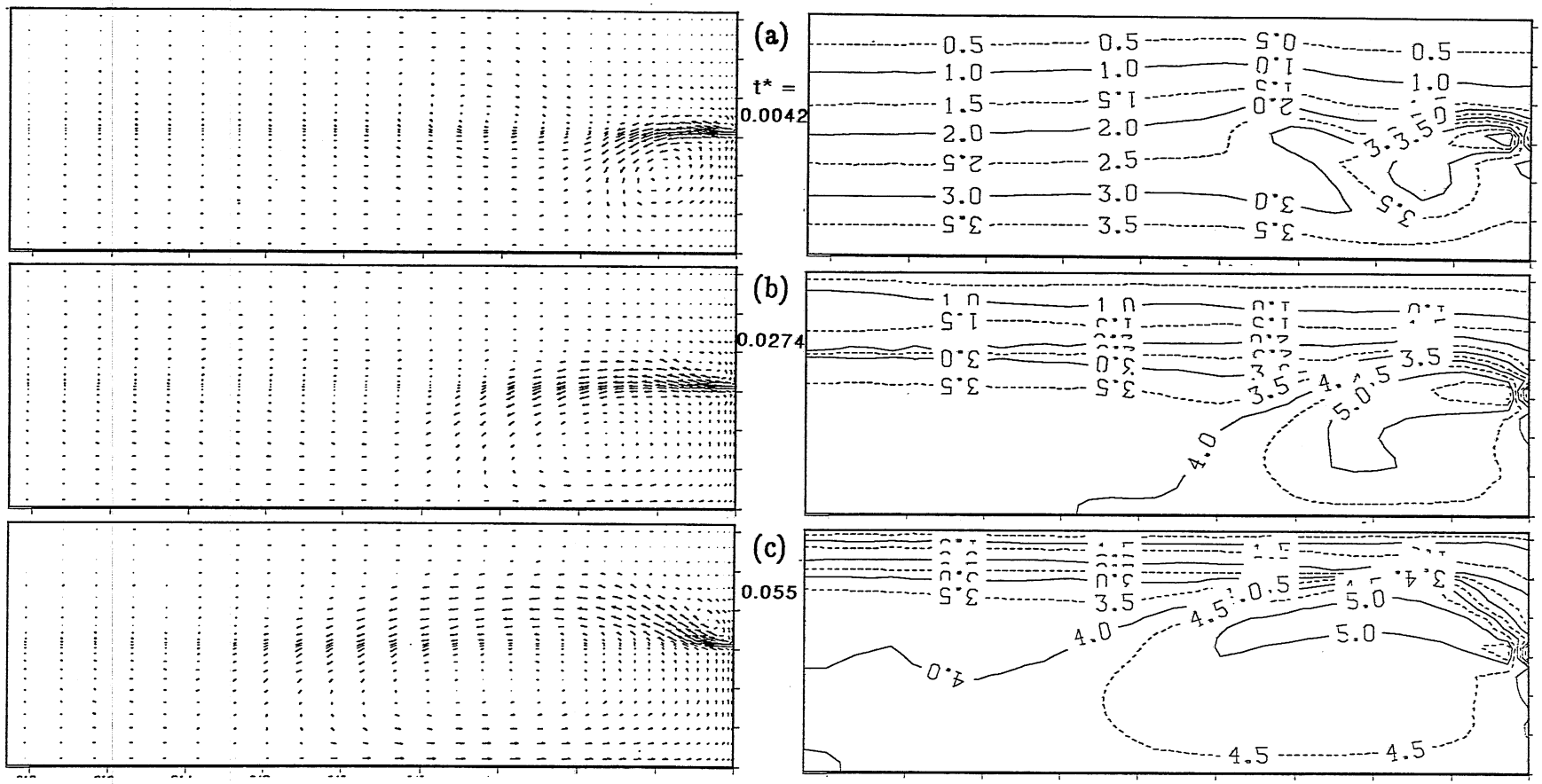

Fig. 8.20 Velocity vectors and temperature contour: Run No. A8, T_j= 8°C

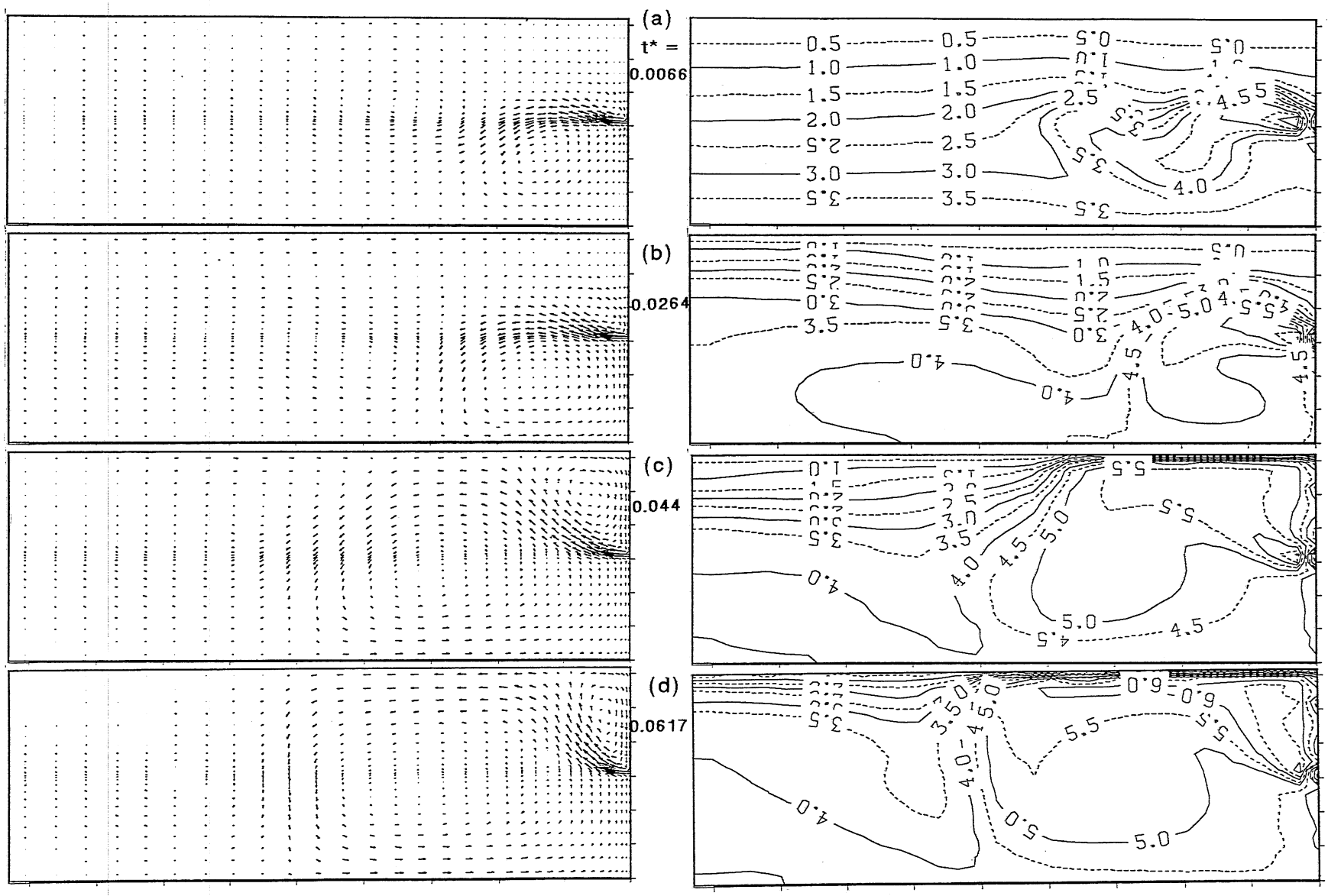

Fig. 8.21 Flow fields and thermal patterns: Run No. A10, T_j= 10°C

warmed. The plunging flow spreads in two directions near the bottom, going towards the outflow boundary as an interflow, and returning back to the jet to produce a re–circulation zone containing a large eddy (vortex). It can be seen in Fig. 8.21 (c) and (d) that the plunging point (stagnation point) moves downstream as time progresses.

A pair of large turbulent vortices remains on both sides of the jet as can be observed in Fig. 8.22. The vorticity is controlled by the direction of flow.

Fig. 8.23 to 8.34 present the predicted dynamical (velocity vectors) and thermal (isotherm) patterns of jet flows for other sets of conditions, T_j = 0, 2, 4, 6, 8, 10, 15 and 20 °C, from the two groups of runs. It can be seen that the flow patterns and mixing processes are quite complex and very sensitive to the jet temperature, T_j, due to the reversible buoyant force. Since all jets are highly turbulent (8,000 < Re < 70,000), the flow patterns are not sensitive to Re. The flows may be considered as buoyancy–dominated. Low values of Froude number (3 < Fr < 24.0) were used for the jets except in two special cases (T_j = 2° C with Fr = ∞ and 6° C with Fr = 60). As time is extended, the jet flows approach situations similar to summer cases (T_j > 4° C and T_a > 4° C) because the ambient is warming up. Typical flow features of a jet in a summer lake were seen in Fig. 7.7 for the positively buoyant case. Eventually both high and low temperature jet flows become steady state associated with a completely isothermal flowfield.

To analyze and characterize the jet flow development with time, variation of each jet trajectory with time (Fig. 8.35) and trajectories at specific time for discharges of different temperatures (Figs. 8.36 and 8.37) are compared. It can be seen that variation of winter jet trajectories of 0° C ≤ T_j, T_a ≤ 4° C is similar to the summer cases. The 0° C and 4° C jets behave similarly since both do not face the reversible buoyancy. The former is driven to the top by positive buoyancy and the latter to the bottom by negative buoyant force. The jet with T_j = 2° C is neutrally buoyant (Fr = ∞) and flows horizontally, keeping its straight centerline (axis) with slight oscillation. Behavior of jets of 6° C is similar to jets between 2° C and 4° C, but it is affected by the reversible buoyancy slightly. This is because at 6° C temperature the density is very close to that at 2° C but it falls on a different side of the maximum density point (4° C). The strong effect of reversible buoyancy on jet centerline trajectory can be seen in flows with T_j ≥ 8° C. The centerlines of these jets shift widely in vertical direction over the entire depth and change rapidly with time. The flows are deflected and reversed from rising to falling or from falling to rising. The buoyancy effect varies with T_j for cases of T_j > 4° C. Positive buoyancy has more influence on jets of higher injection temperatures, e.g. 15 to 20° C. Negative buoyancy plays a more important role in determining the trajectory patterns at lower injection temperatures (4 to 6° C). The reversal of buoyancy in time and space dominates the flow features of jets discharged at 8° C and 10° C, e.g. widely shifting centerline trajectories of jet flows.

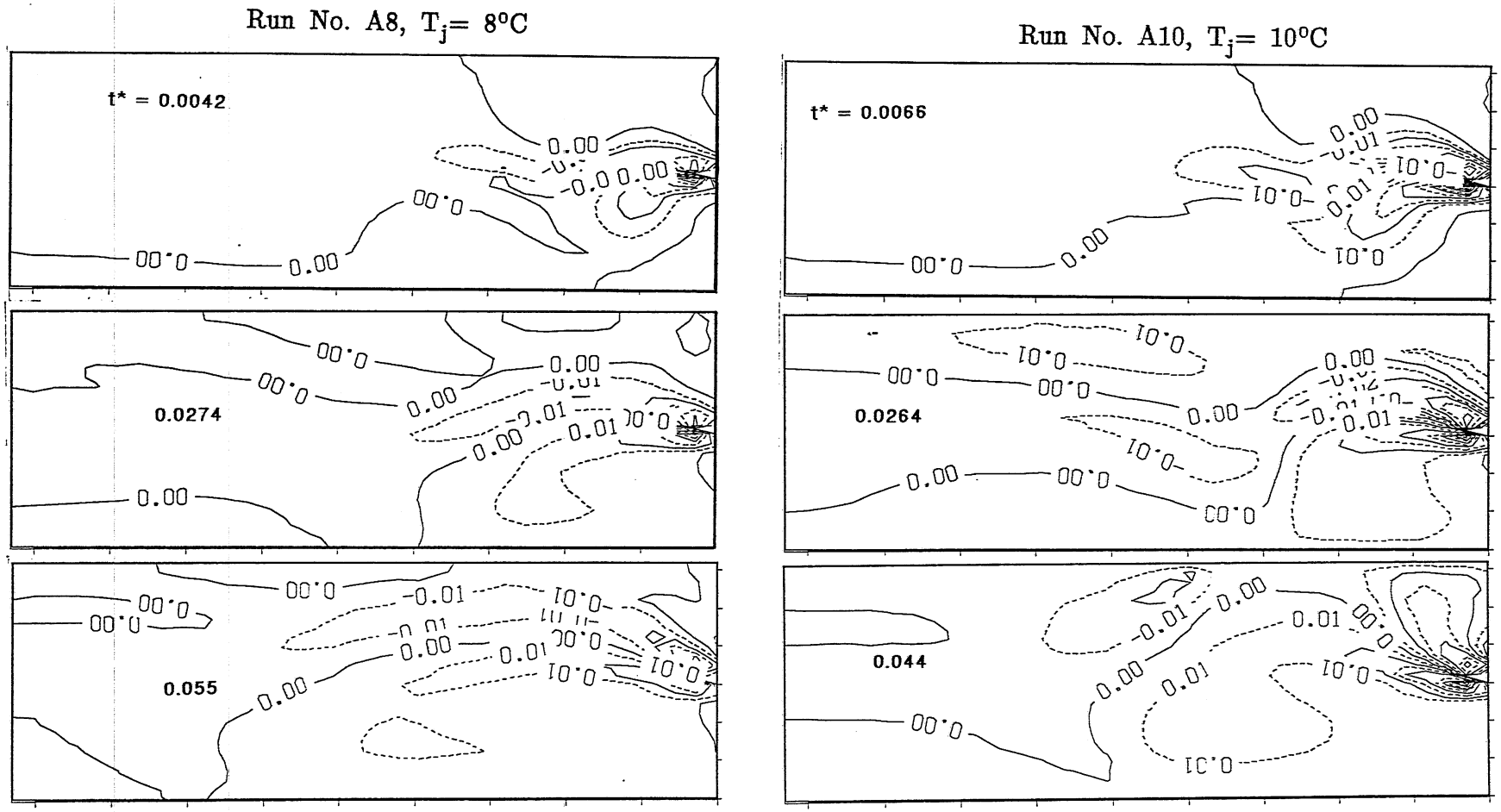

Fig. 8.22 Vorticity: computer Run No. A8, T_j = 8°C and A10, T_j= 10°C

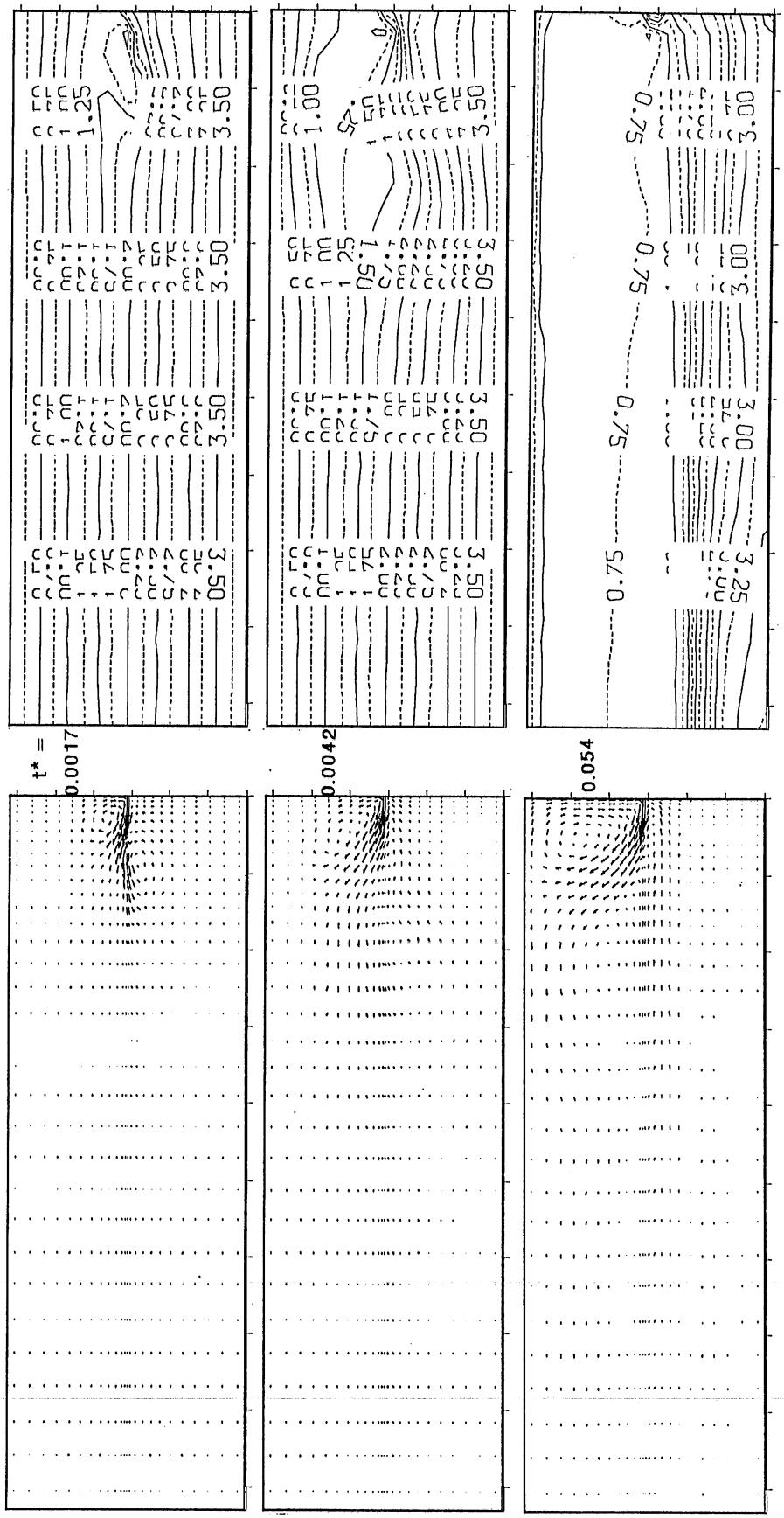

Fig. 8.23 Computed velocities and temperatures: Run No. A0, T_j= 0.05°C

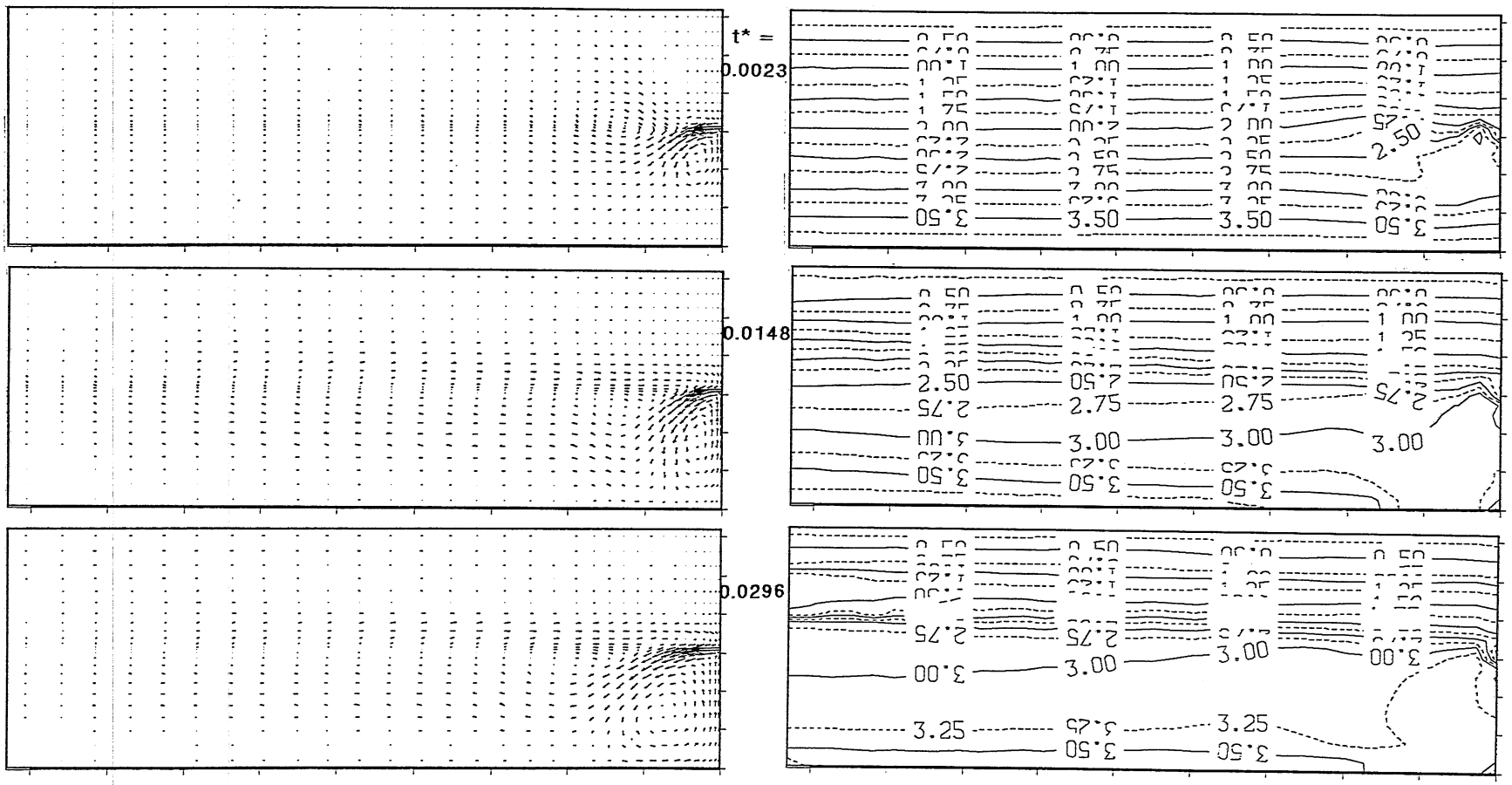

Fig. 8.24 Computed velocities and temperatures: Run No. A4, T_j= 4°C

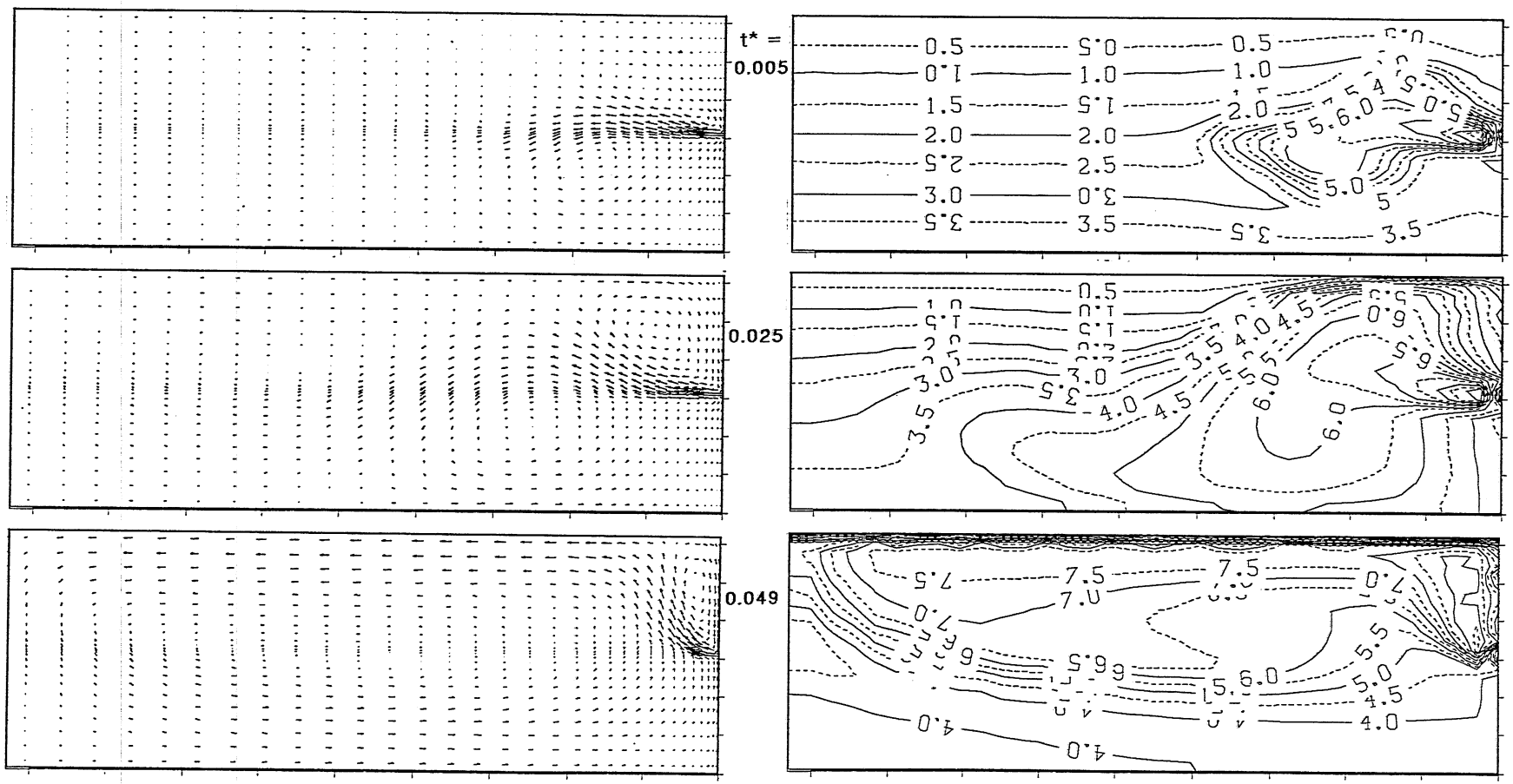

Fig. 8.25 Computed velocities and temperatures: Run No. A15, T_j= 15°C

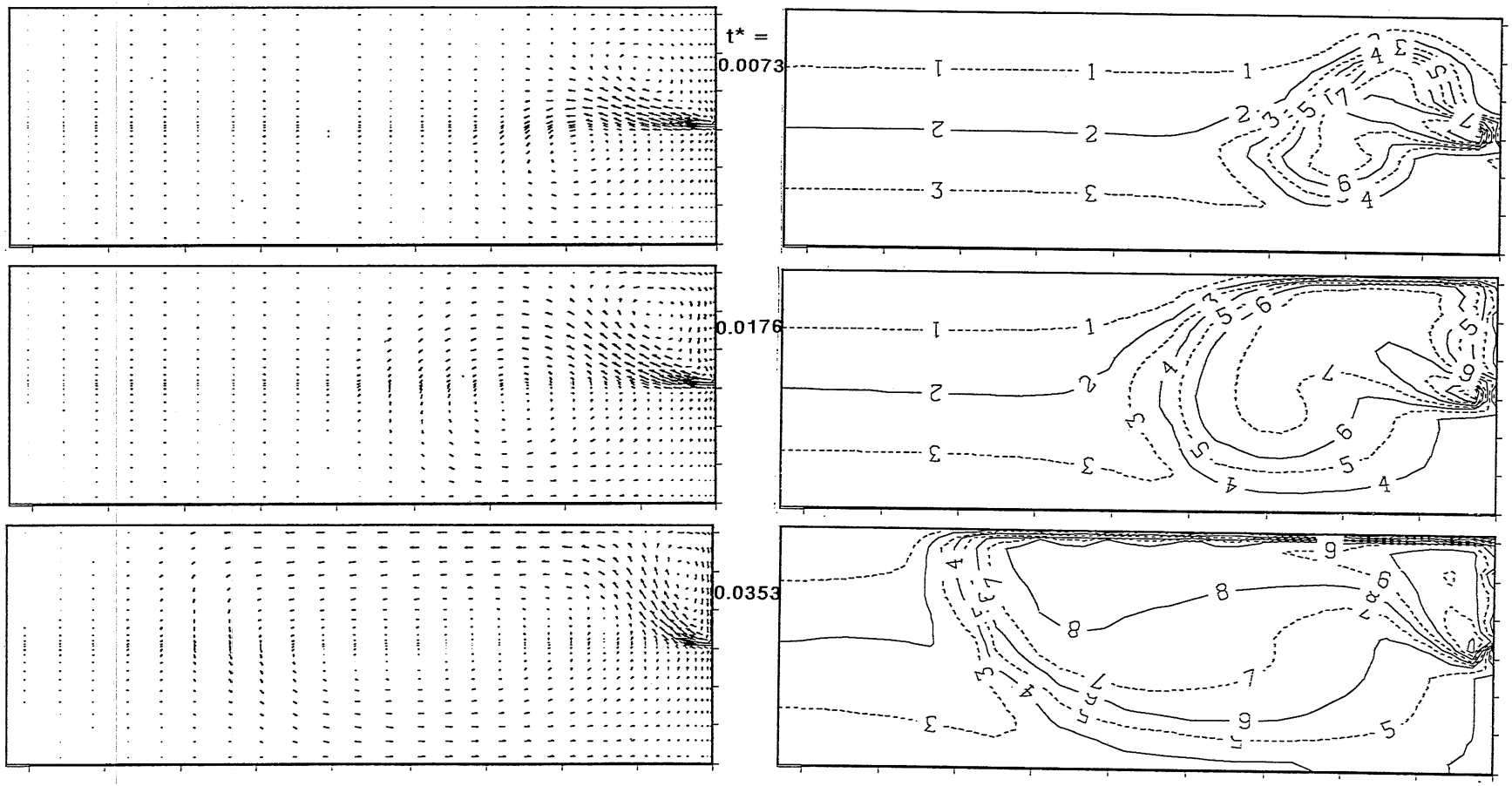

Fig. 8.26 Computed velocities and temperatures: Run No. A20, T_j= 20°C

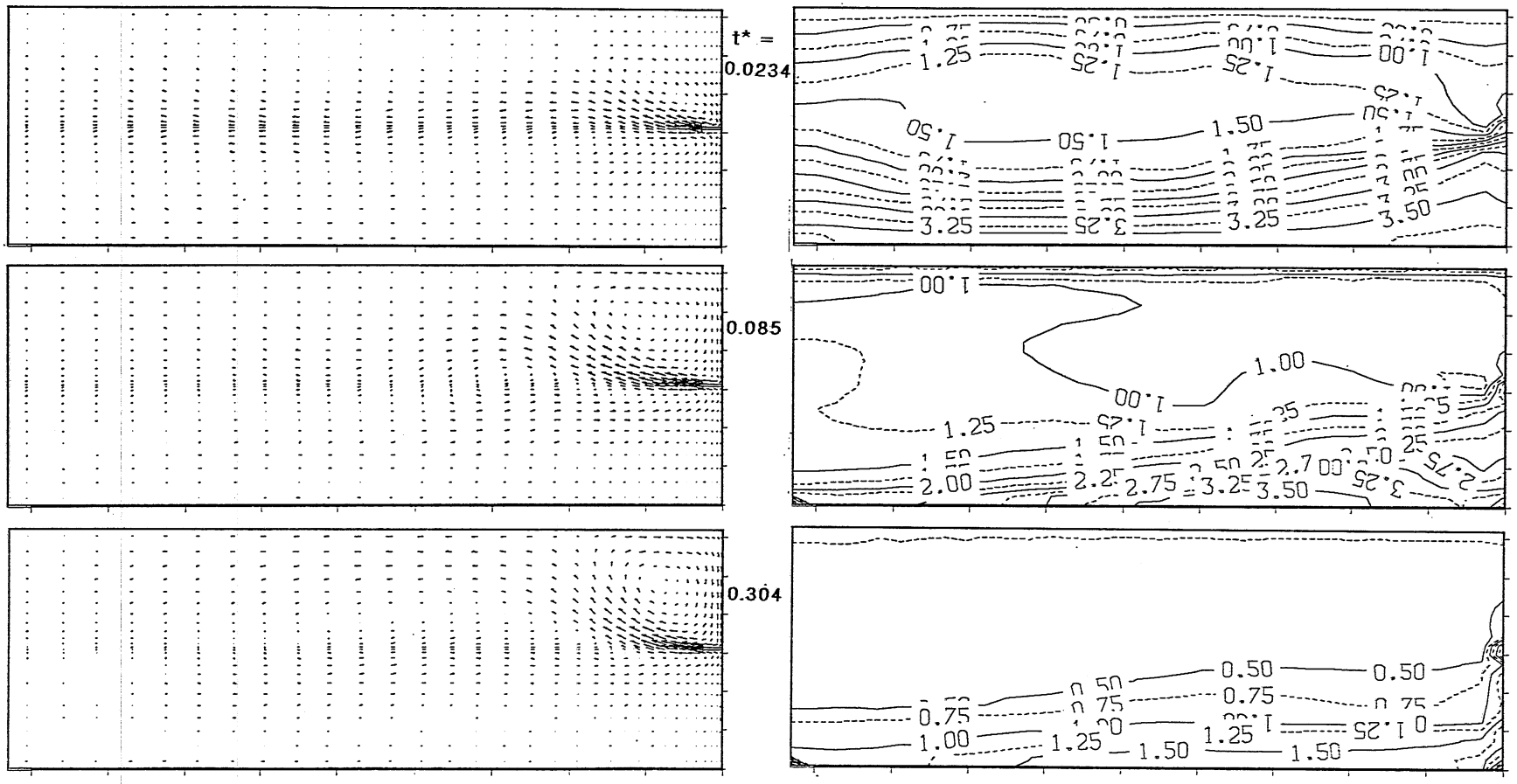

Fig. 8.27 Computed velocities and temperatures: Run No. B0, T_j= 0.05°C

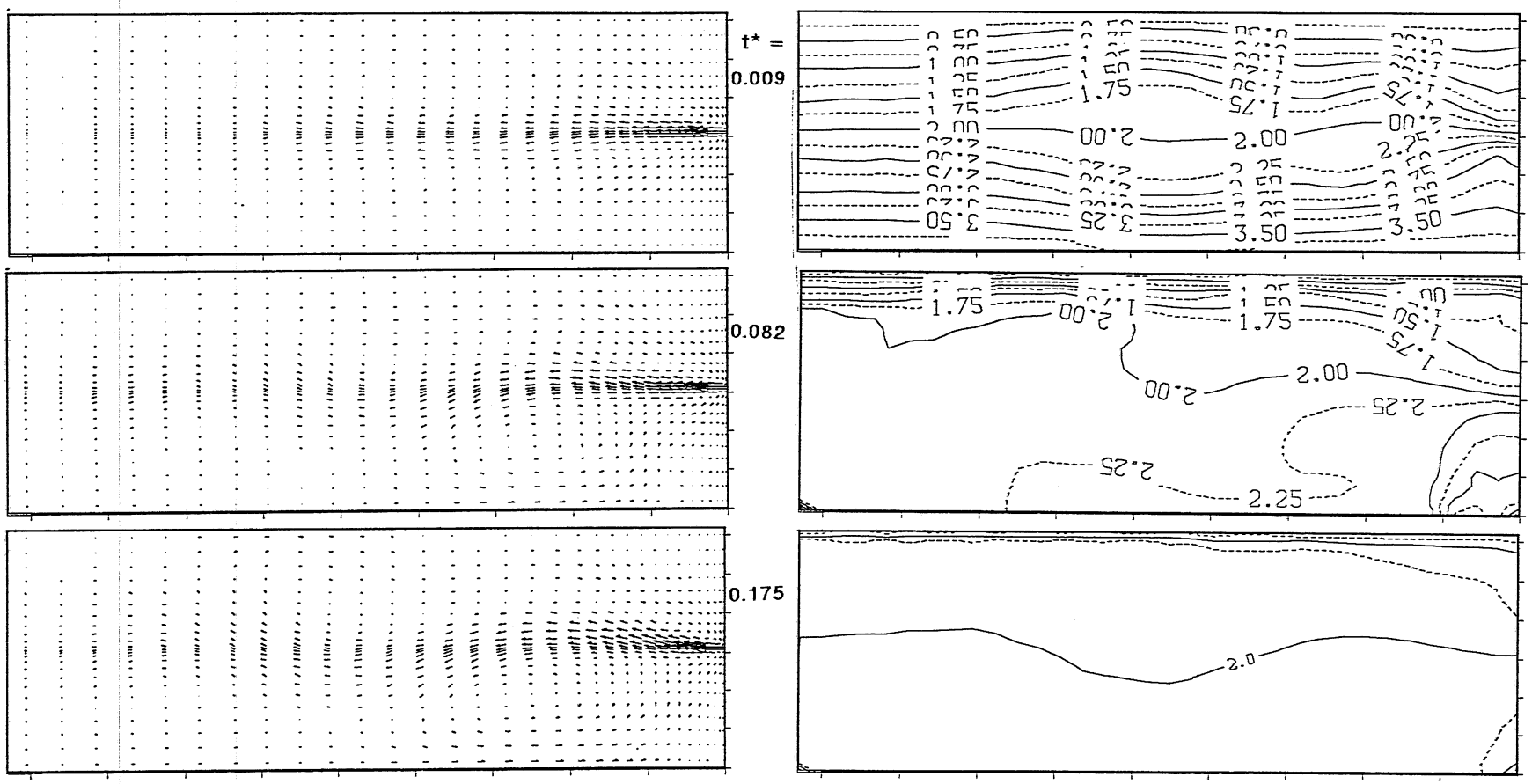

Fig. 8.28 Computed velocities and temperatures: Run No. B2, T_j= 2°C

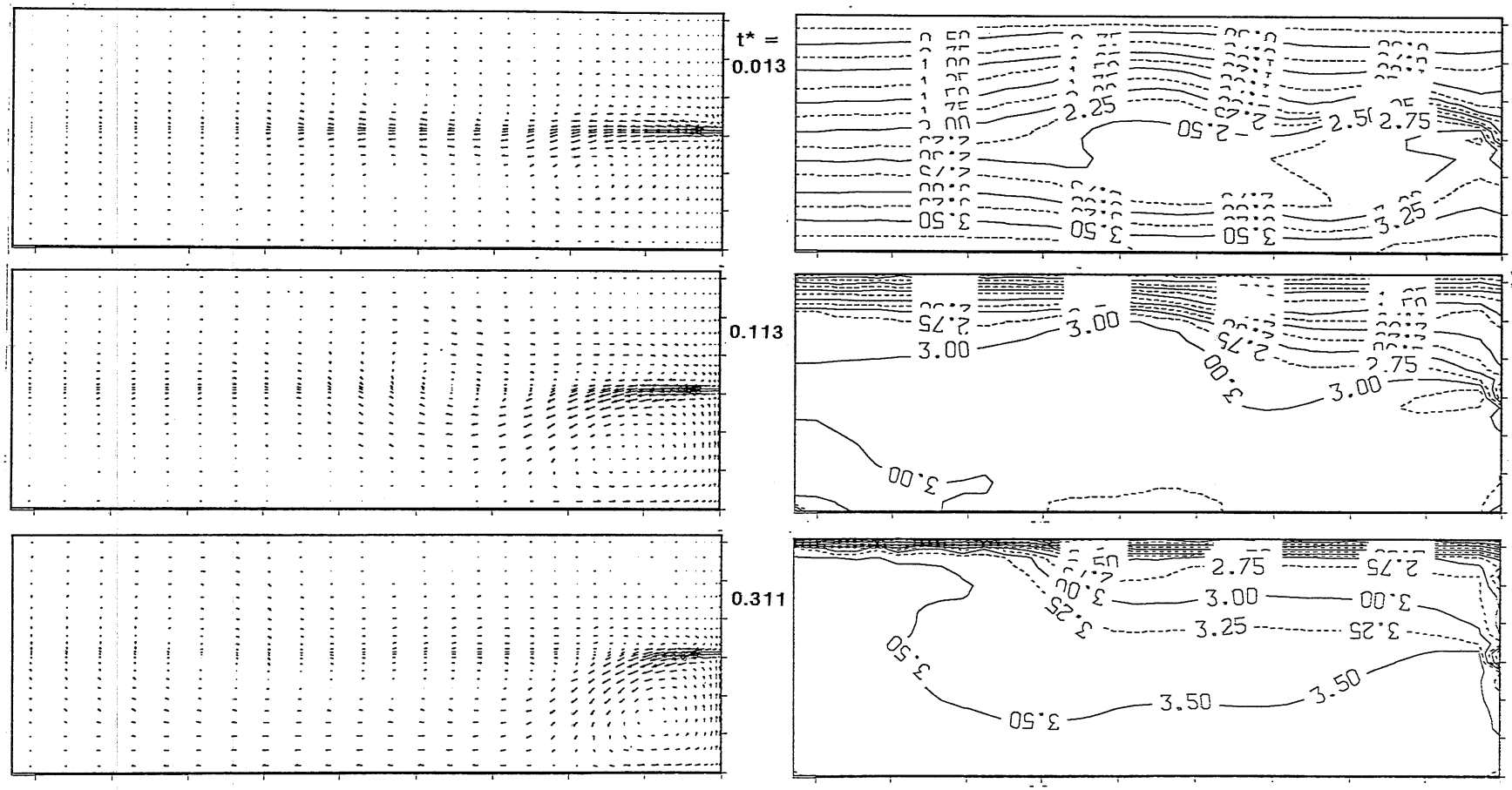

Fig. 8.29 Computed velocities and temperatures: Run No. B4, T_j= 4°C

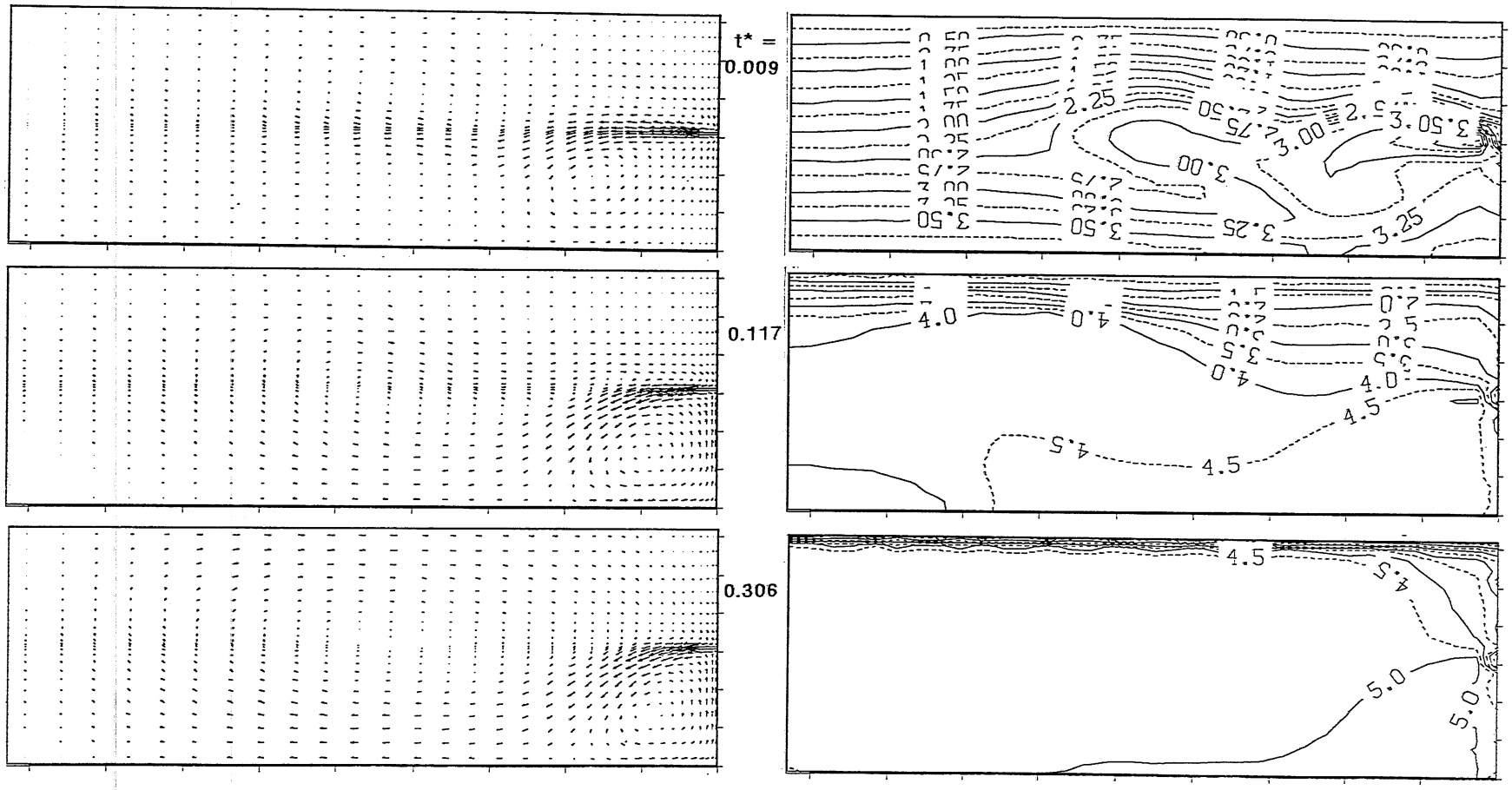

Fig. 8.30 Computed velocities and temperatures: Run No. B6, T_j= 6°C

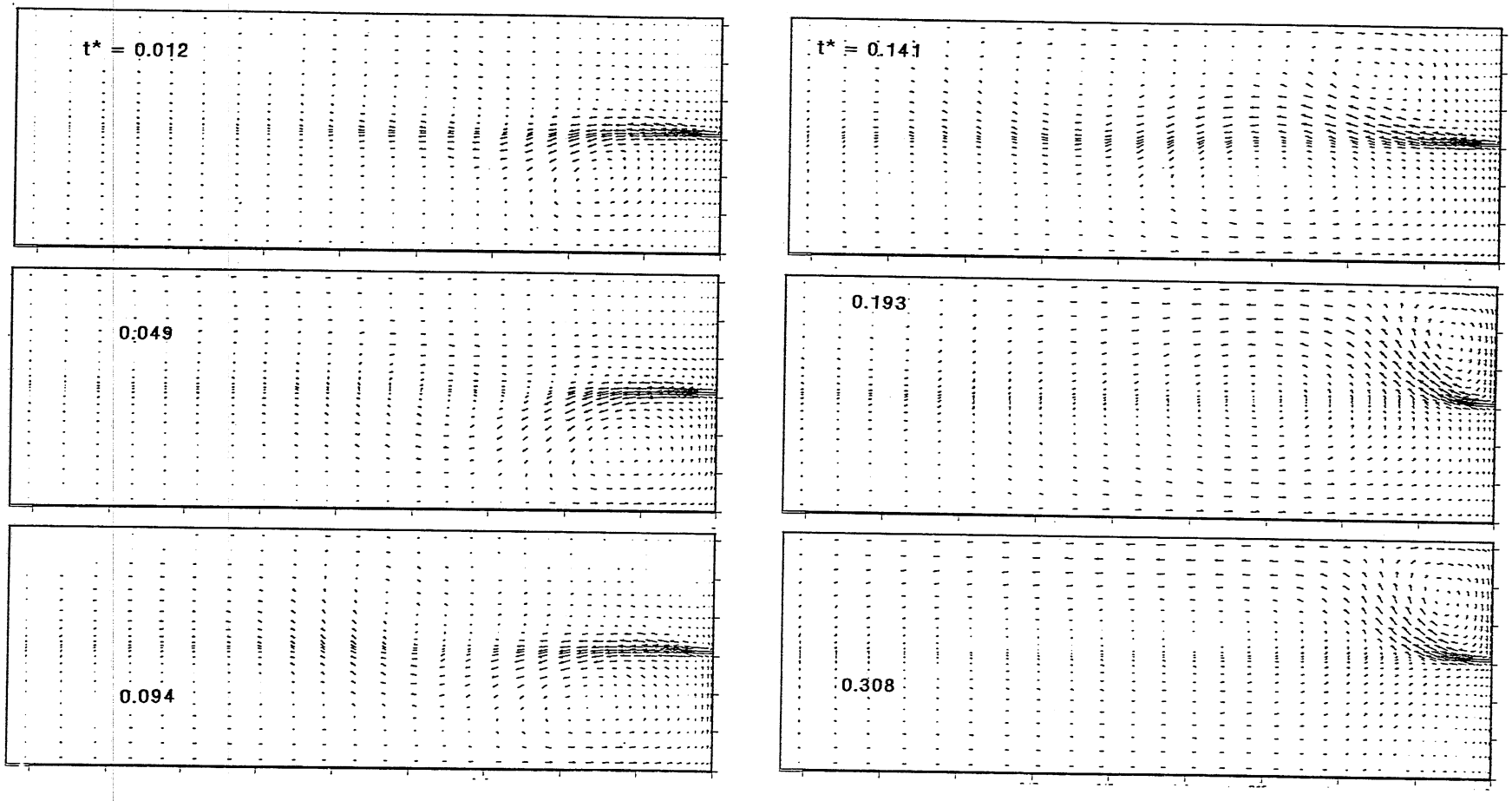

Fig. 8.31 Computed velocities: Run No. B8, T_j= 8°C

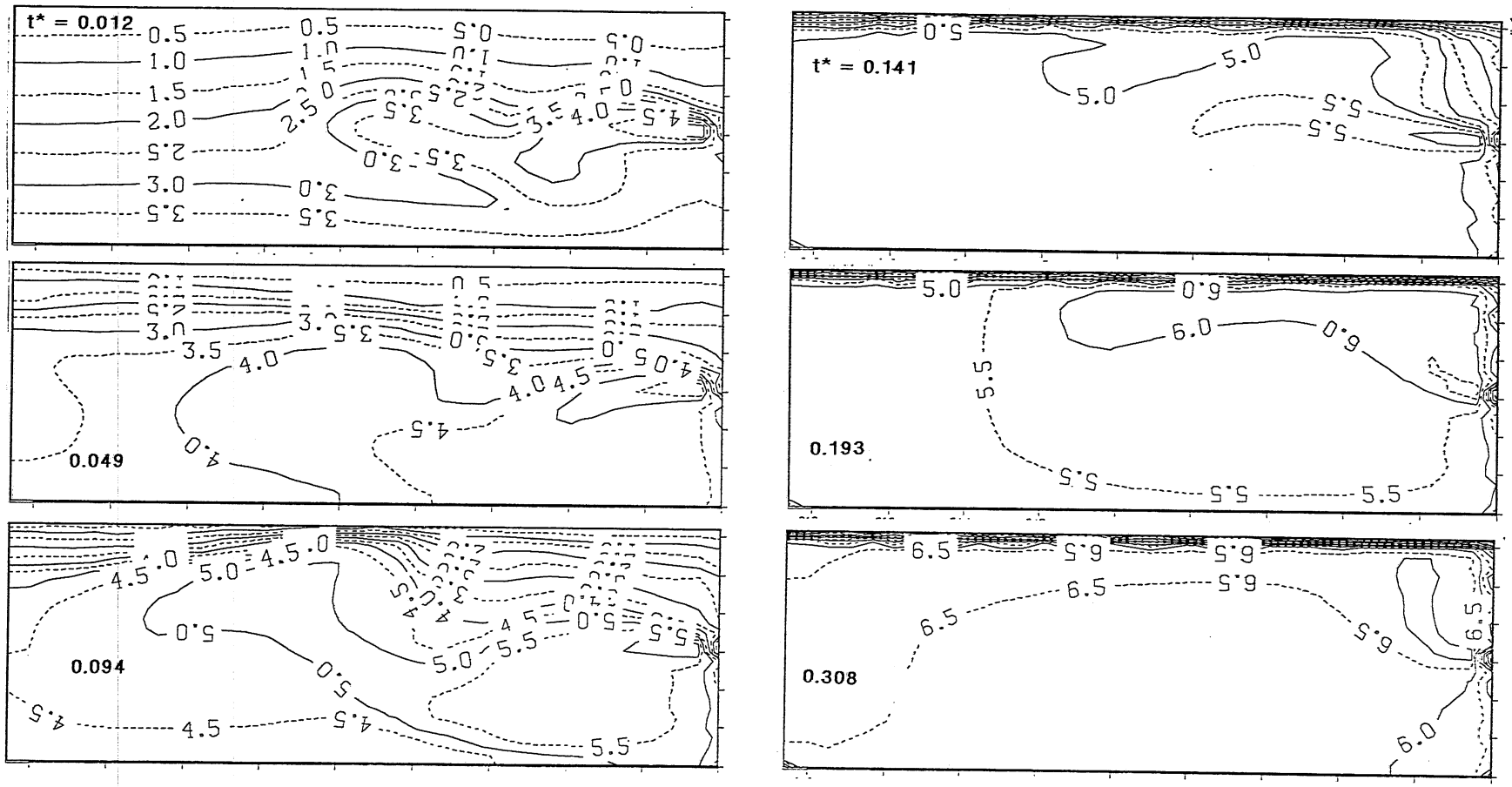

Fig. 8.32 Computed temperatures: Run No. B8, T_j= 8°C

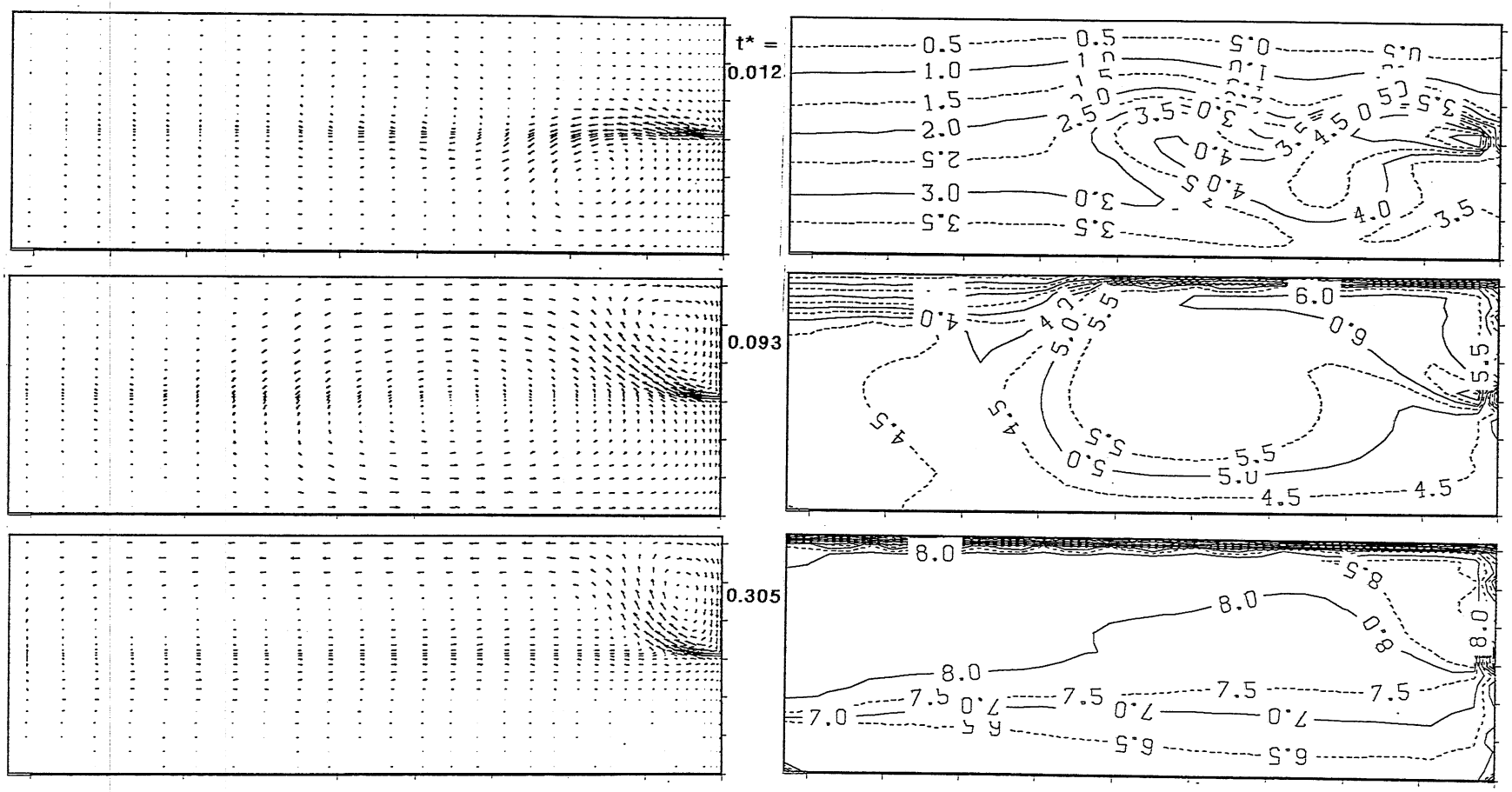

Fig. 8.33 Computed velocities and temperatures: Run No. B10, T_j= 10°C

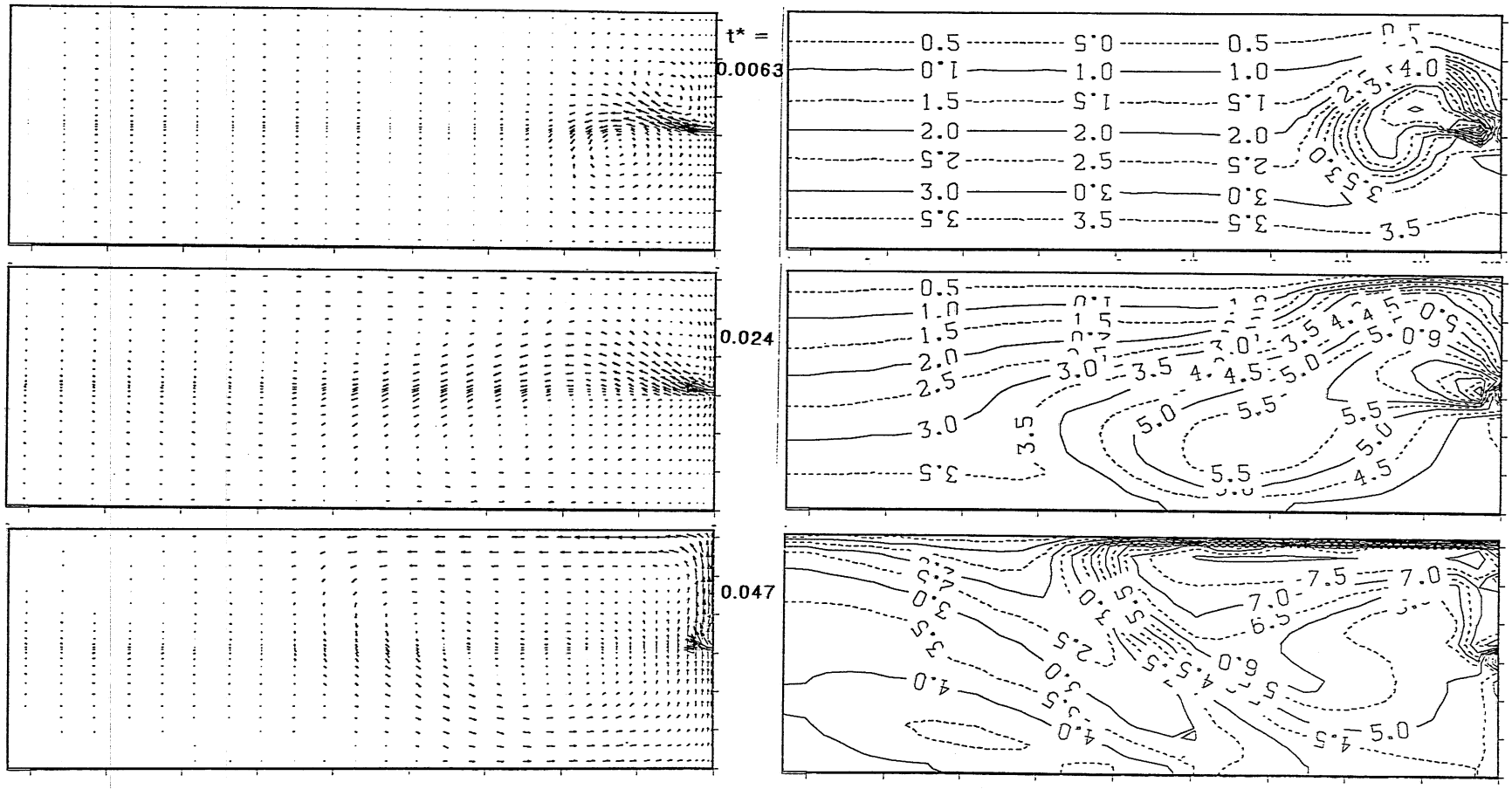

Fig. 8.34 Computed velocities and temperatures: Run No. B15, T_j= 15°C

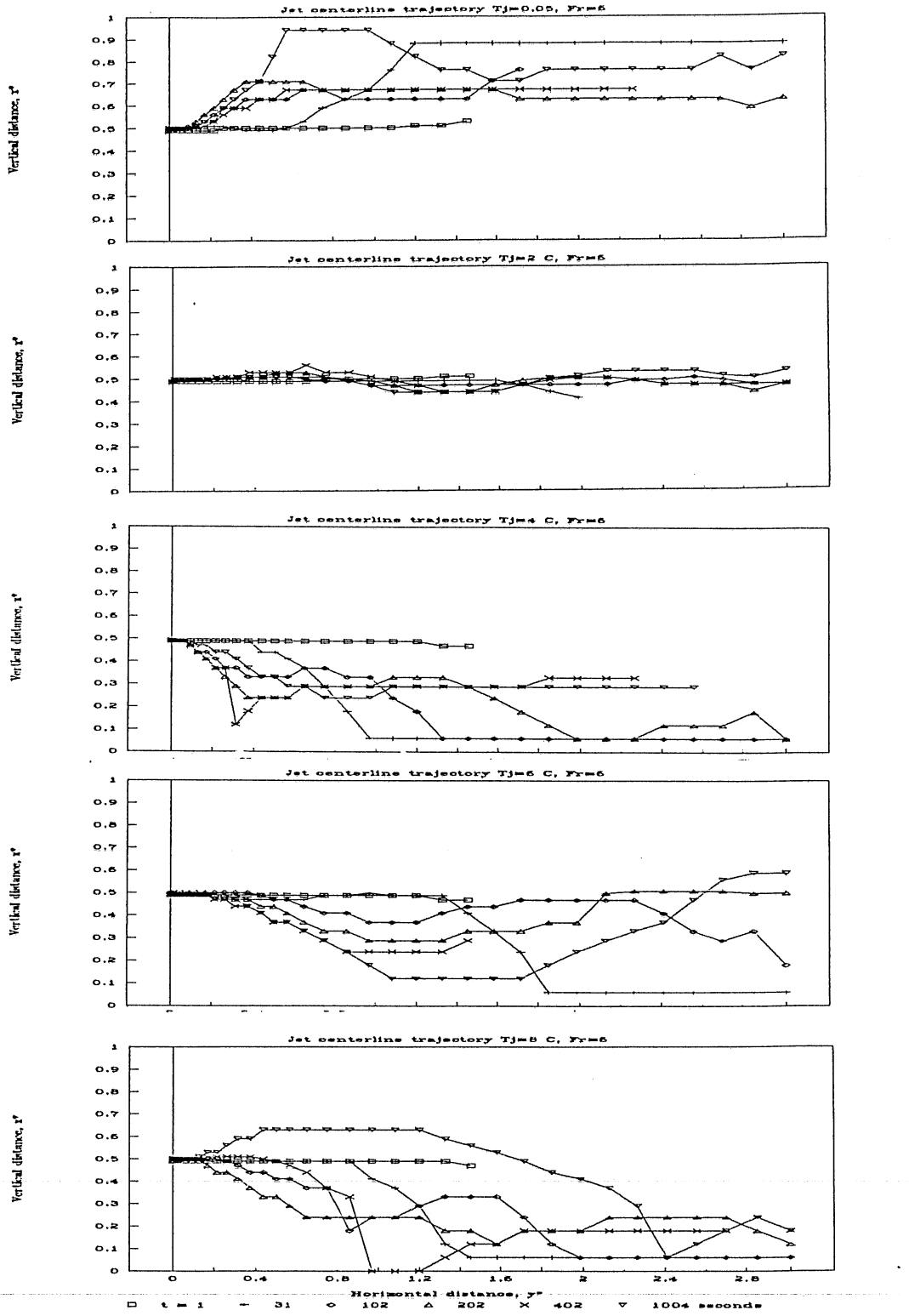

Fig. 8.35 Variation of jet trajectory with time: Run No. A0–A20

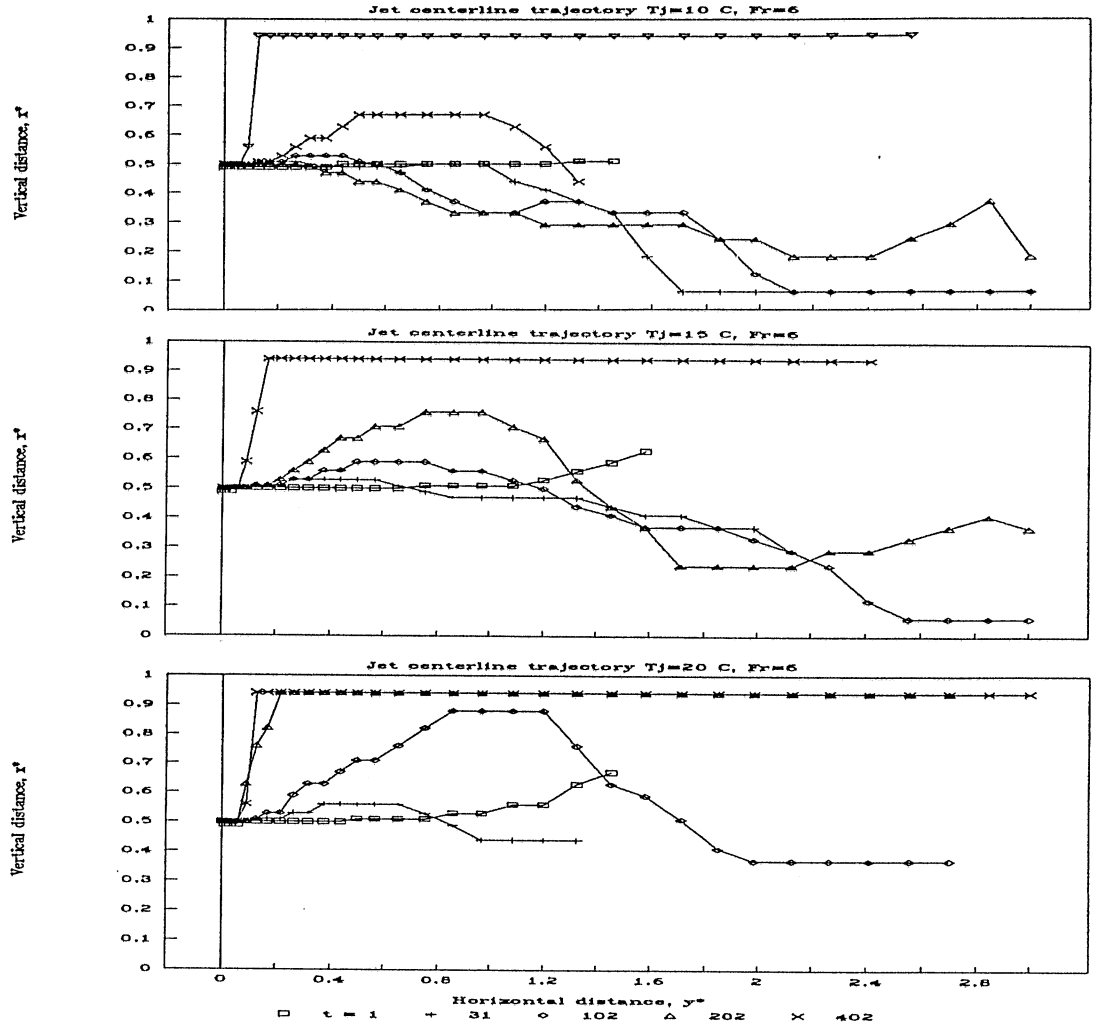

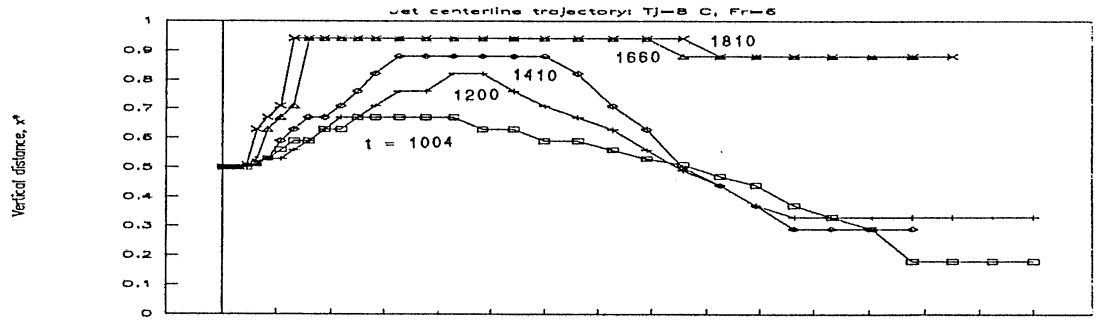

Fig. 8.35 Variation of jet trajectory with time: Run No. A0–A20 (Continued)

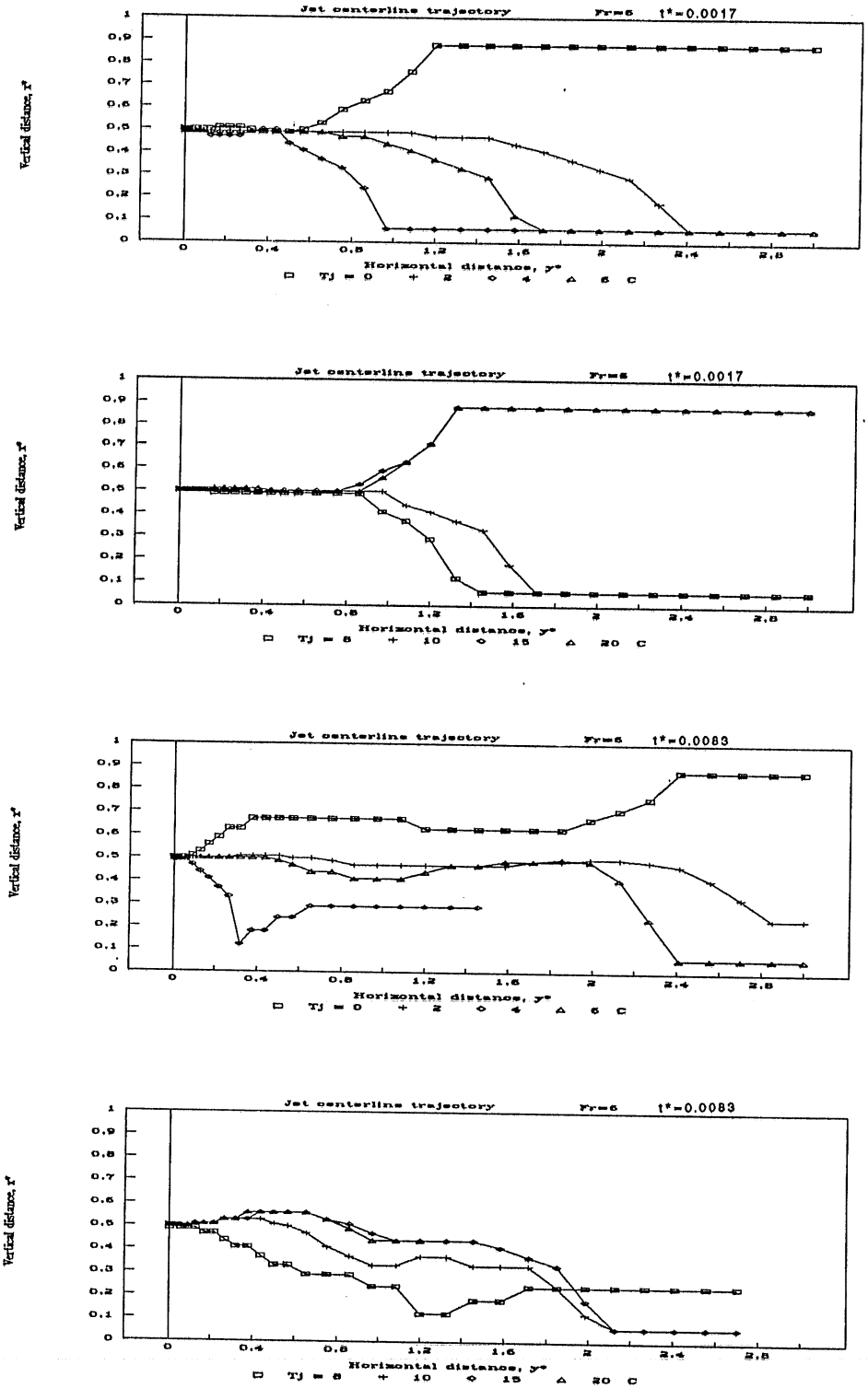

Fig. 8.36 Variation of jet trajectory with T_j: Run No. A0–A20

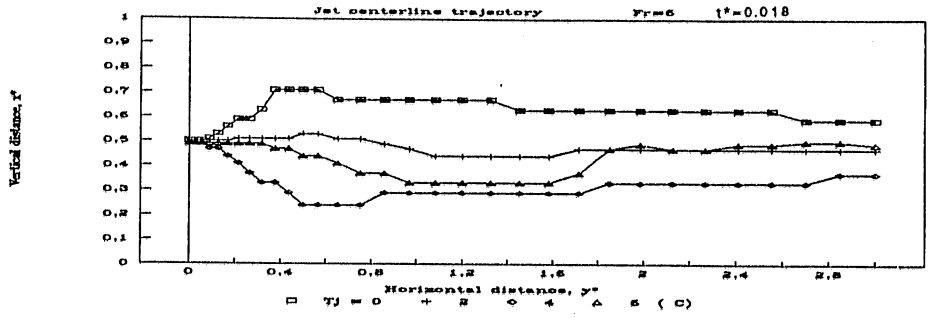

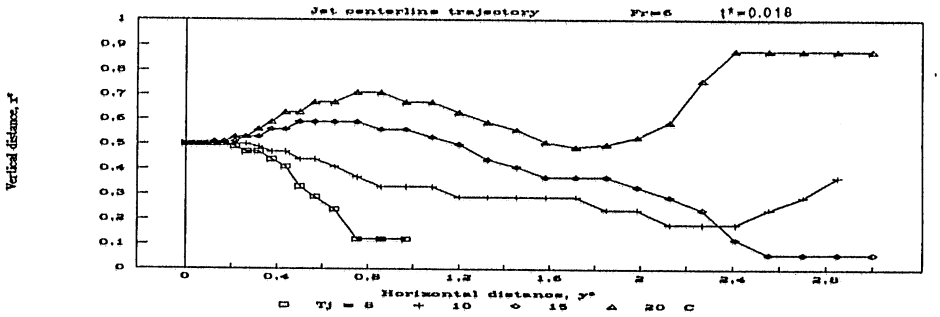

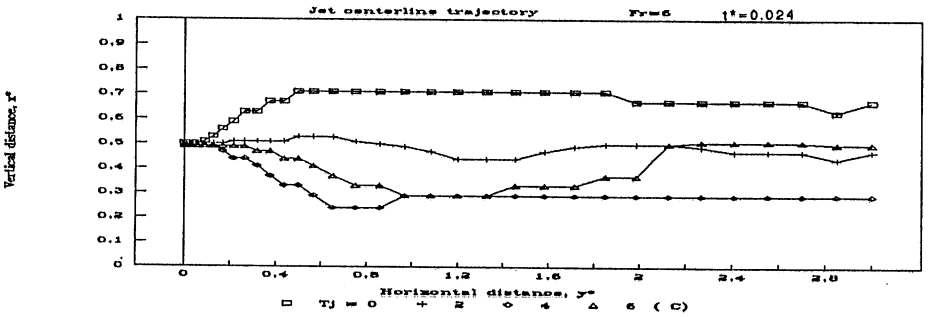

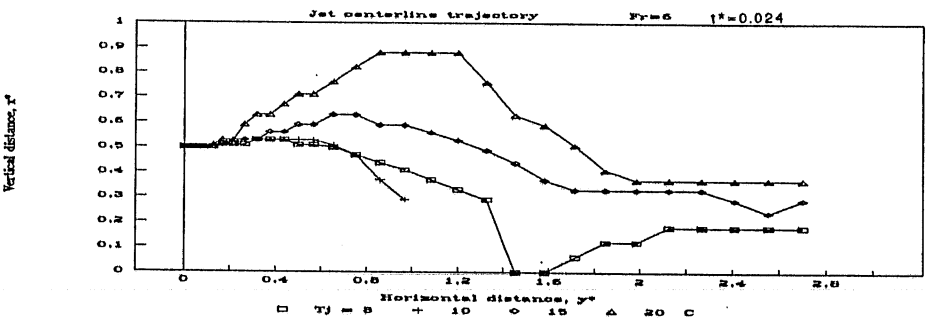

Fig. 8.36 (Continued)

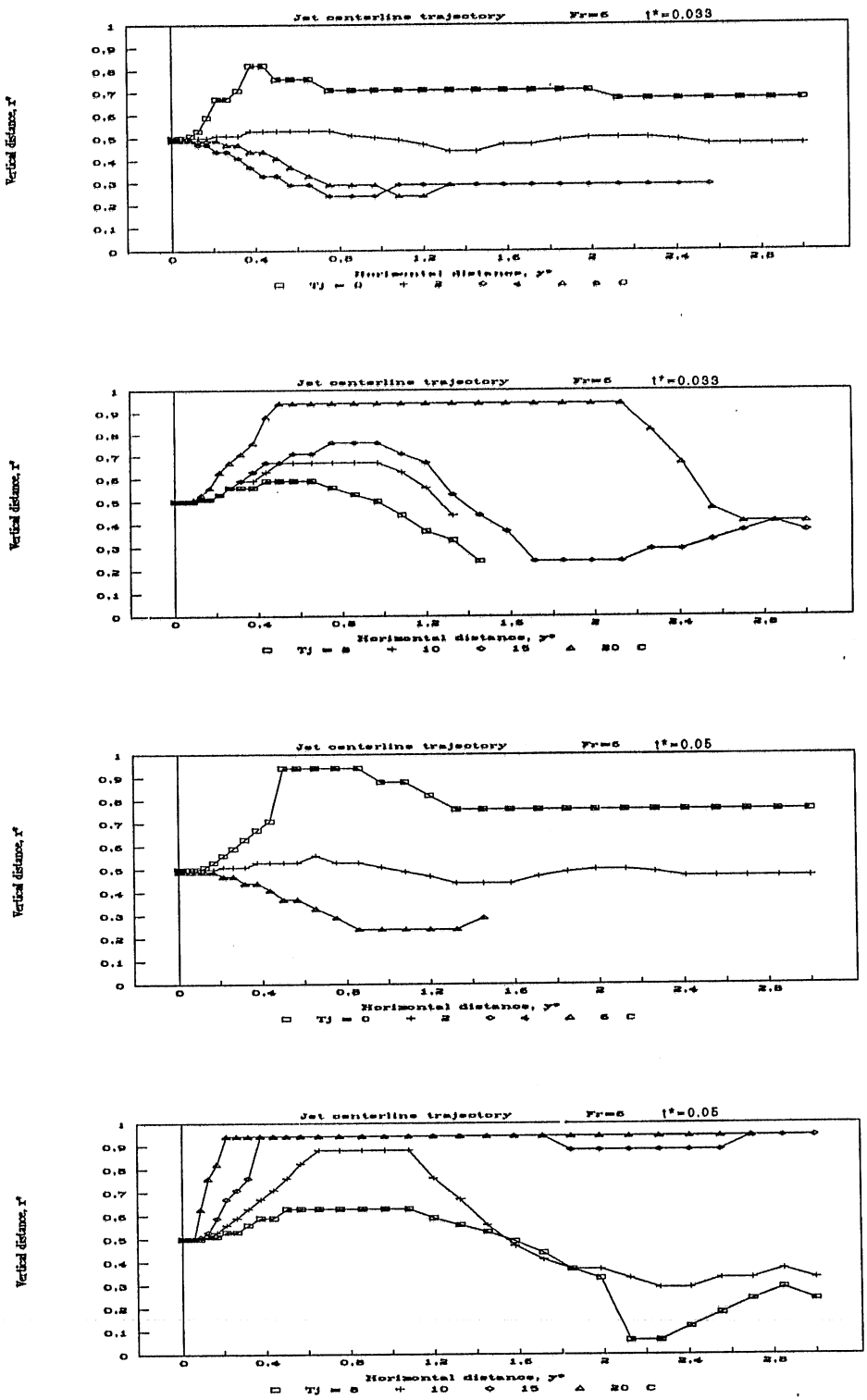

Fig. 8.36 (Continued)

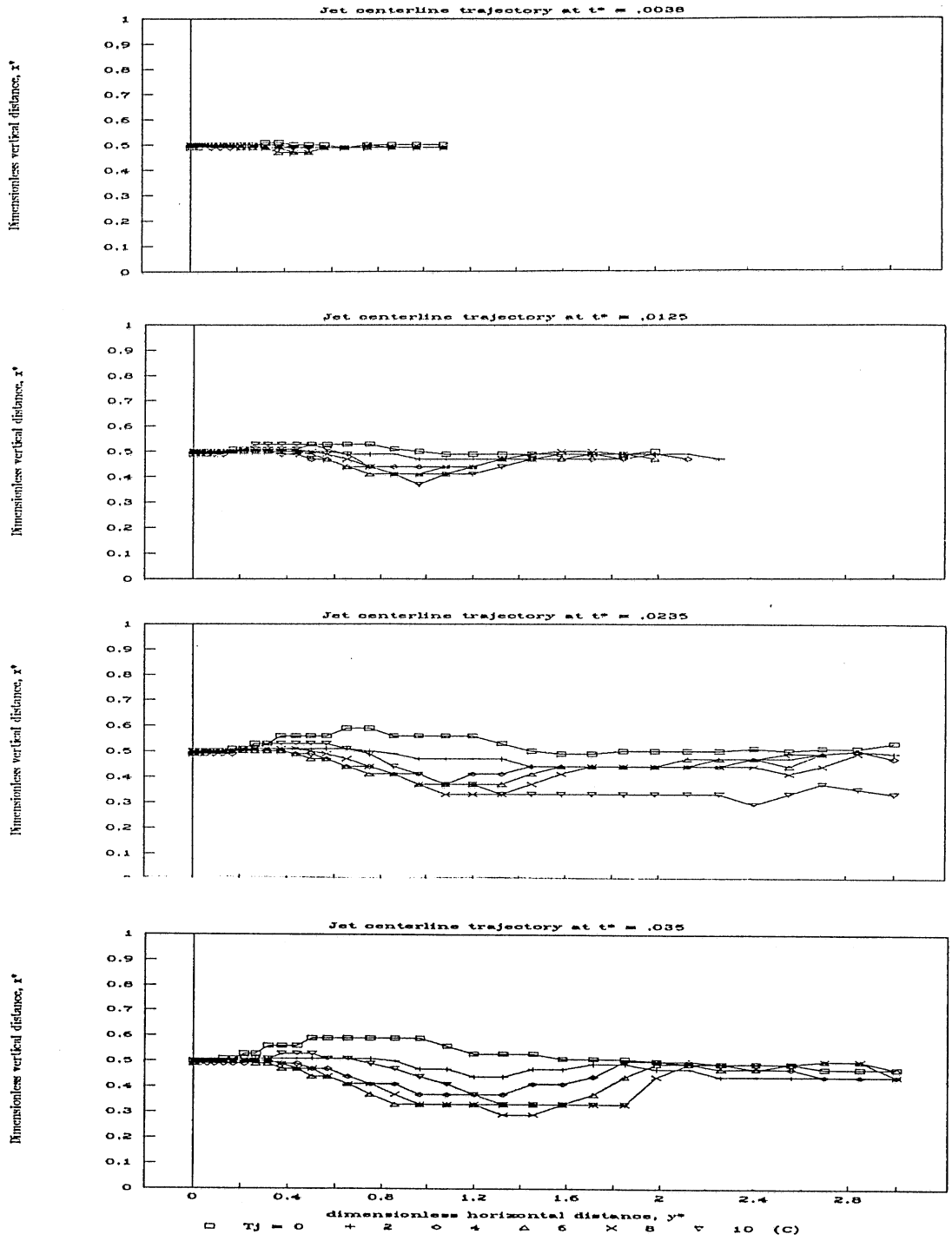

Fig. 8.37 Variation of jet trajectory with T_j: Run No. B0–B10

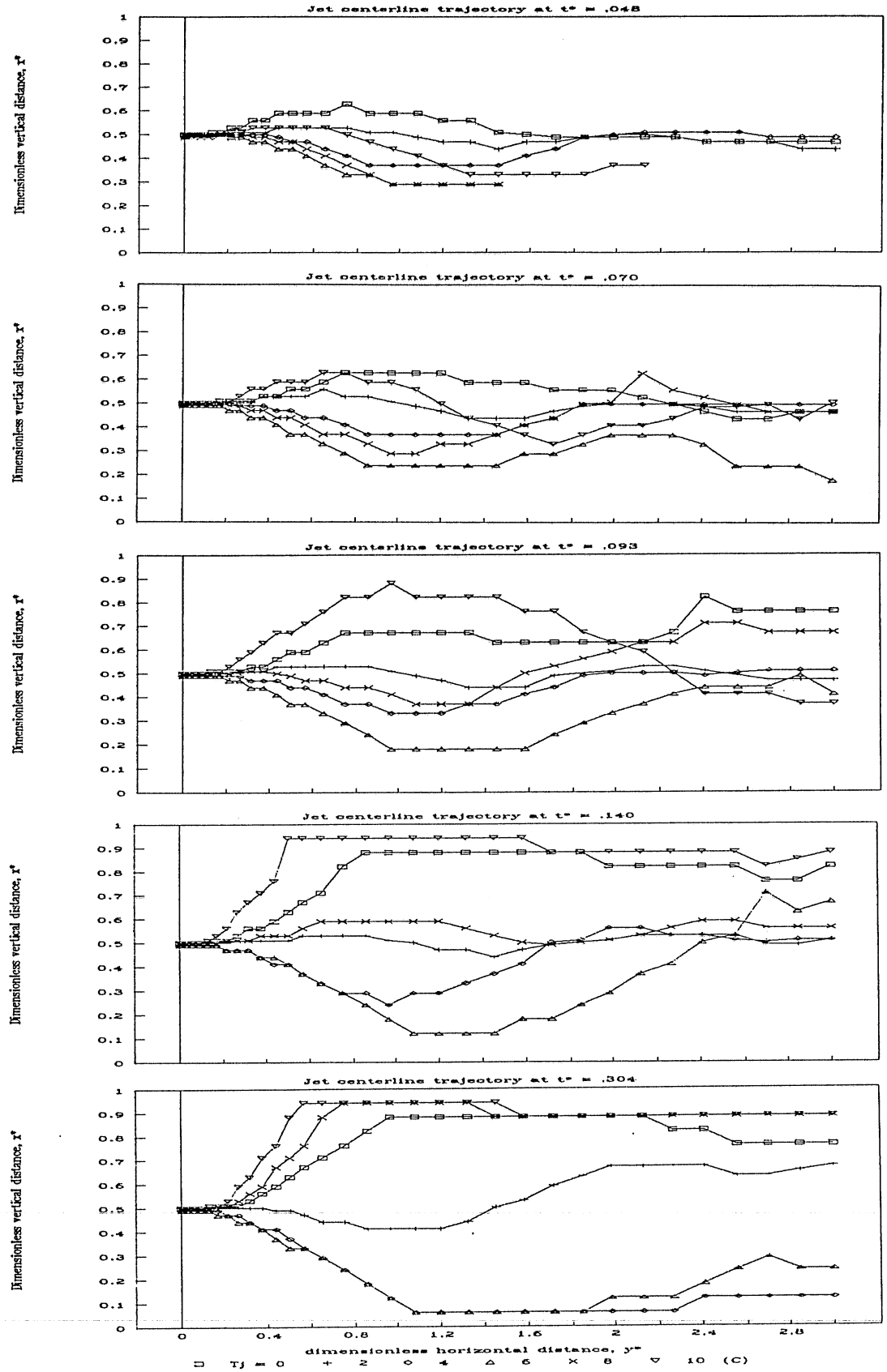

Fig. 8.37 (Continued)

Samples of simulated jet centerline velocities and temperatures are shown in Fig. 8.38. The decay of velocity and temperature along the jet axis slows with time.

Heat flux, Q_{wi}, from water to ice cover is also of concern because of reduced ice thickness. Figs. 8.39 and 8.40 show some numerical results from the 2–D model. Direct simulation of heat transfer from water to ice, Q_{wi}, enhances the applicability of the winter cover simulation model developed in Chapter 5 since Q_{wi} is essential in the calculation of ice thickness of a lake where flows and mixing exists near the ice cover. An empirical constant heat flux was assumed in previous investigations for a lake under the natural condition. The assumption of constant heat flux, Q_{wi}, is not suitable for the situation with highly unsteady and dynamic jet flows. The available results for Q_{wi} presented in Fig. 8.39 and 8.40 provide useful information which can be used for the calculation of ice thickness and its variation with time and horizontal distance.

8.8 Summary

A 2–D model was presented for unsteady buoyant jet flows an mixing in a stratified basin. Modifications to the existing computer program were made to incorporate the effect of buoyancy and to obtain solutions for the unsteady nonlinear flow problem by iteration within a finite time step. The buoyancy–extended k–ϵ turbulence model has been found to be applicable to the prediction of flows considered here, especially horizontal warm water jets into a stratified water body in low temperatures (0 to 4° C) with an ice cover and a sediment bottom. The validation of the 2–D model was verified against existing data for two special cases: (a) a vertical plane jet impinging on solid wall and (b) an (non–buoyant) offset jet discharging parallel to a flat plate or free surface in uniform ambients.

Based on numerical experiments on model sensitivity it has been seen that solutions were quite insensitive to meshes greater than 26 x 34 for a grid system and length to depth ratio larger than 2.5 in the computational domain. In the investigation of effects of buoyancy and stratification on the horizontal jets a symmetric situation was arranged to avoid the Coanda effect (offset jet phenomena).

Systematic investigation of horizontally discharged warm water jets into a stratified water body in low temperatures with an ice cover were carried out through numerical simulations with the 2–D model. New knowledge on jet trajectories, flow fields, thermal patterns, mixing process and heat transfer from the water to the ice were obtained. The process of evolution from an unsteady flow to a steady state and from a stratified ambient to a well mixed situation were simulated. The unique feature of reverse buoyancy was examined and was shown to have the essential effect on the jet flows. It has been found that the jet pattern is very sensitive to the temperature of discharge (T_j) due to the reverse buoyancy, especially warm water in

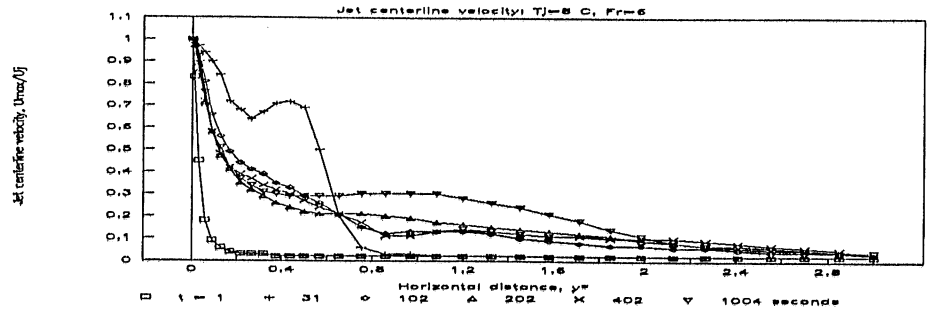

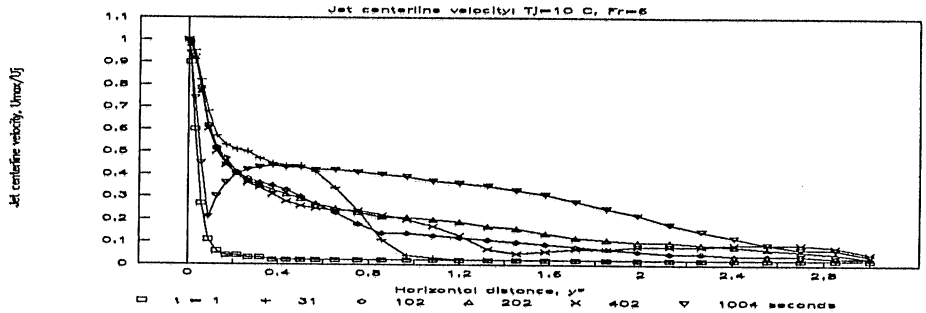

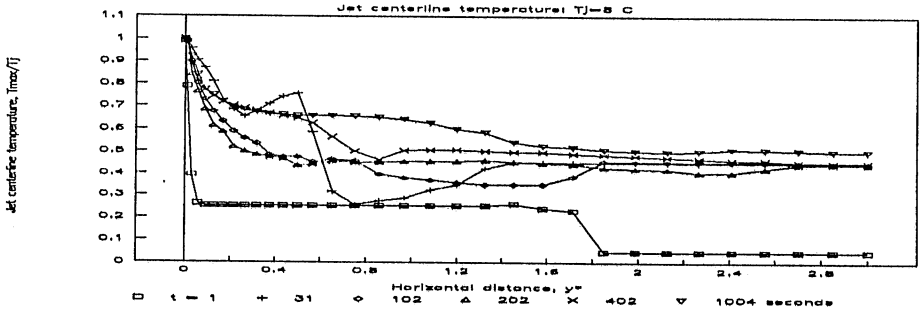

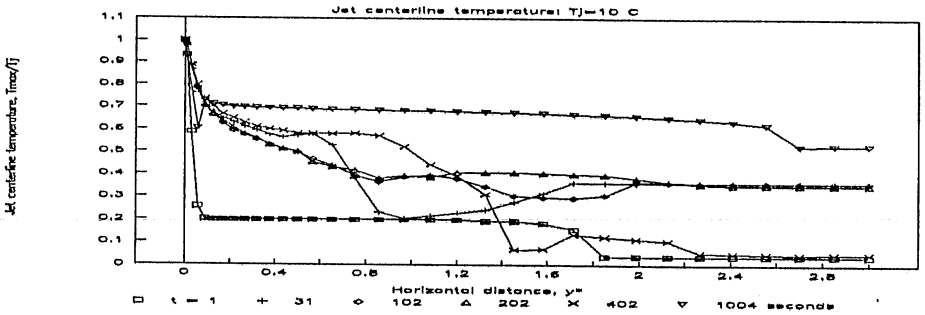

Fig. 8.38 Jet centerline velocities and temperatures

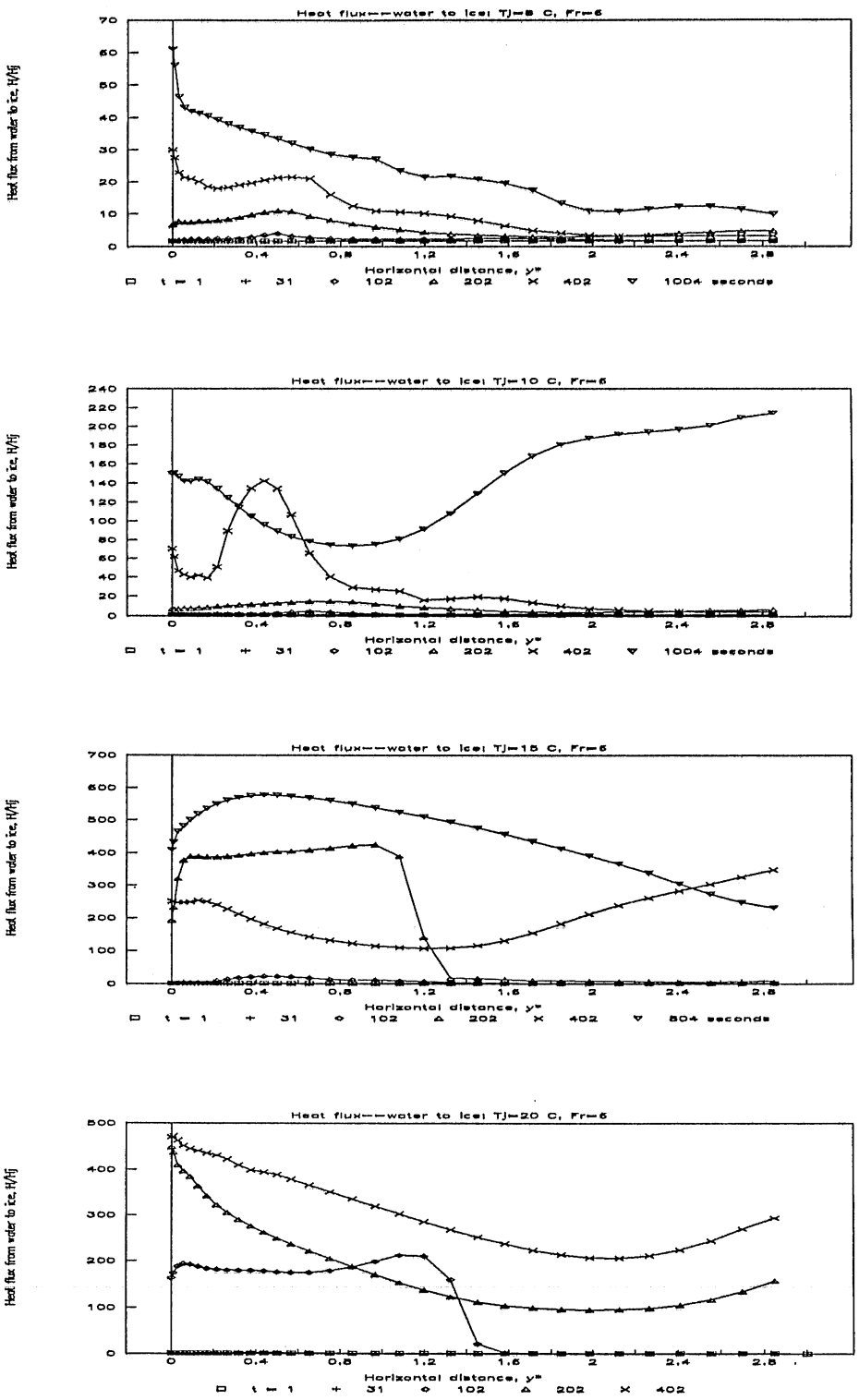

Fig. 8.39 Distribution of heat flux to ice along horizontal distance

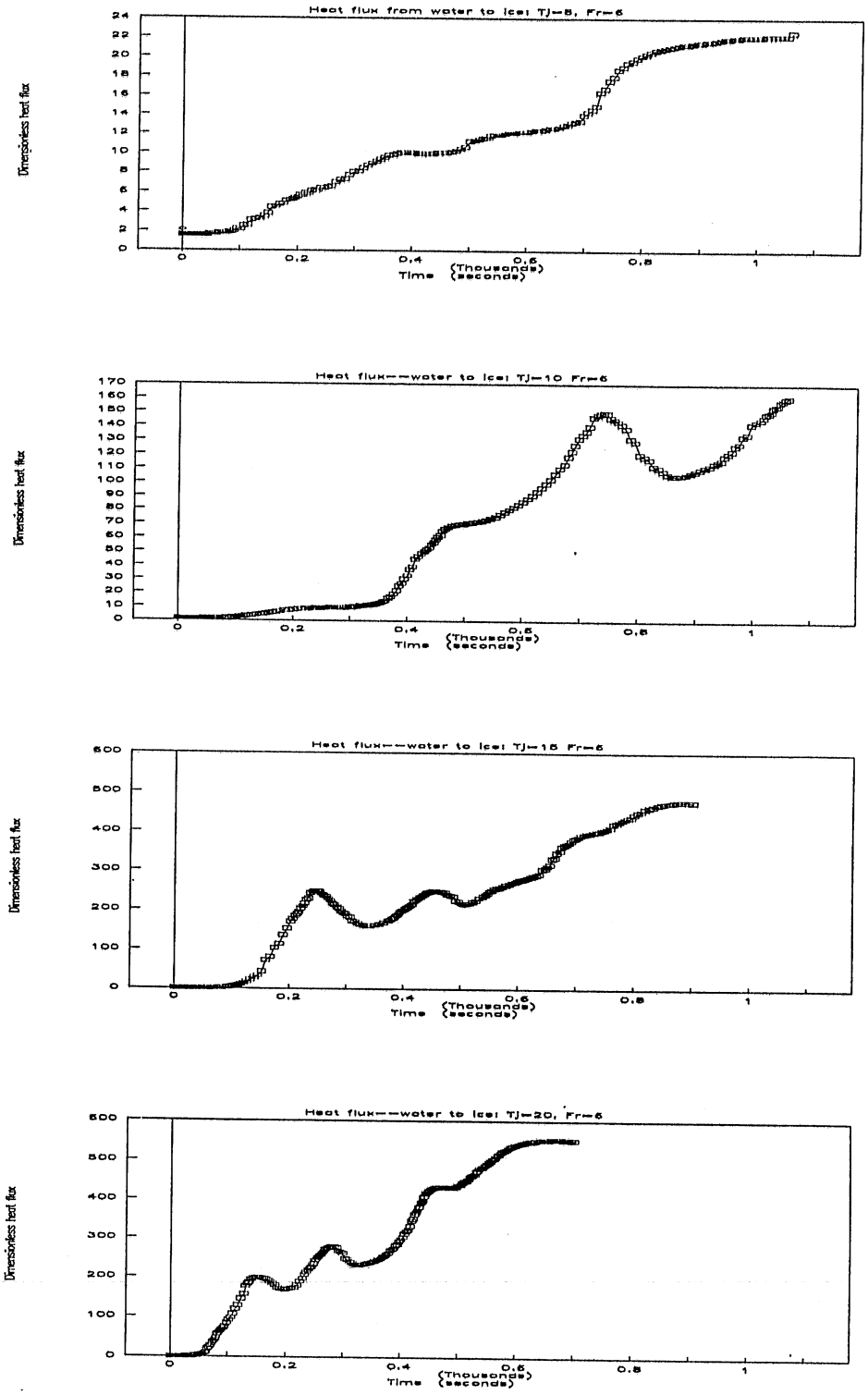

Fig. 8.40 Variation of heat flux from water to ice with time

temperatures 8 – 15° C which are commonly generated from aeration or waste water and heat disposal. Preliminary comparison of the results presented in this chapter for horizontal jets with the 1–D simulations showed that the 1–D model underpredicted the mixing of the ambient water and overpredicted the oscillation of the jet centerline trajectories.

Chapter 9 Conclusions

Mixing of stratified natural water bodies by jets and characteristics of buoyant jet flows in stratified basins have been investigated by theoretical analysis, numerical simulations and laboratory experiments. Of practical interest are applications to ponds, reservoirs and lakes which may improve in water quality when they are being mixed. Also of interest are jet discharges, e.g. of wastewater into impoundments, their dilution, and effects on ice covers in winter. It is believed that the understanding of the jet behavior and mixing process have been advanced through this study, and that as a result the design of mixing systems for destratification and discharge systems for disposal can be improved. New tools for analysis and design have been developed or improved specially for the following aspects:

(A) intergral jet flow model for a buoyant single horizontal or vertical, turbulent jet in stratified ambients and progressive mixing simulation of a natural water body under the effect of a single vertical or horizontal jet;

(B) practical applications of the 1–D jet–mixing model to artificially forced summer destratification with a pump/jet system, including natural energy exchange at the water surface;

(C) conceptual design method and procedure for selection of single and multiple jet systems for hydraulic destratification of ponds/reservoirs/lakes/ including efficiency and cost;

(D) extension of the natural water temperature stratification simulation of a water body from summer to winter conditions, including ice cover, snow cover and heat transfer from/to bottom sediments; and

(E) both 1–D and 2–D jet flow simulations in stratified water bodies under winter conditions (0 – 4° C water temperature) including special effects of buoyancy reversal.

Referring to the above five points, the following more detailed conclusions were reached.

(A) A turbulent buoyant jet discharge into infinite, density–stratified, stagnant ambient water was studied by the integral–analysis approach. The theoretical analysis using the integral–conservation equations was extended in several ways: (1) dynamic pressure was considered; (2) a new entrainment function was derived; (3) a non–linear $\rho(T)$ relationship was used and (4) the conservation equation for heat was used in place of the conservation equation for buoyancy. A nearfield jet model applicable to round jets, slot jets, horizontal, incline or vertical discharges was developed. The physical features of mixing due to entrainment and deliverance which lead to thermal destratification were analyzed. A 1–D convection model was devised for the farfield (or mixing region). The integral jet model was coupled with the 1–D convection model to develop a 1–D jet–mixing simulation model. The coupled model predicts changes in the temperature (or density) stratification of an adiabatic basin due to mixing by a submerged jet. The main physical features of jet trajectories and mixing processes were investigated experimentally in the laboratory. The experimental results for both horizontal and vertical jets were compared with those simulated by the 1–D numerical model. The followings conclusions are reached:

1. A sensitivity analysis on the empirical coefficients used in the model gave solution deviations of the model results for entrainment, maximum height and "percent mixed" of less than twenty–five percent, when the coefficients were varied over the widest conceivable range.

2. Jet trajectories and dilution predicted with the integral jet model were compared with experimental data obtained by other investigators and found to be good.

3. Simulated temperature profiles during the process of destratification showed good overall agreement with measurements in a stratified tank. The validity of the 1–D jet–mixing simulation model was thus verified.

4. Phenomena which could not be simulated by the 1–D jet–mixing model, e.g., entrainment from the region below the injection level were observed in laboratory experiments. Analysis of data indicated that horizontal jets entrained more water from the below–diffuser region than vertical jets. It was seen that the entrainment coefficient, C_k, did not vary significantly with time.

5. The integral jet model has been found very useful but has its limitation in the analysis of mixing effects since the jet trajectories and flow patterns were determined using a similarity assumption for jet velocity and temperature profiles.

6. The 1–D mixing model is valid for a closed system excluding the region below the jet origin.

7. Further improvement of the integral method requires more accurate expressions of jet velocity and temperature profiles that become nonsymmetric about the jet axis.

(B) In practical applications of the 1–D jet–mixing model to artificially forced summer lake destratification with a recirculating pump/jet discharge system natural energy exchange at the water/air interface leading to restratification has to be included. For this purpose the dynamic lake water stratification simulation model (MINLAKE) was used and linked to the water jet mixing submodel. As a special case the vertical jet in shallow water was also investigated. The following conclusions are reached:

1. The incorporation of one model into the other enables simulations of artificially induced jet mixing phenomena simultaneously with natural restratification phenomena. The combined model was found to be an efficient tool to evaluate the effect of buoyant jet flows and mixing in stratified lakes, reservoirs or ponds.

2. The results from the combined model can be used to design a hydraulic jet–mixing system or a submerged thermal outfall for summer conditions.

3. A critical Froude number for determining overshooting of the vertical jet was given. Information on flow behavior, entrainment and mixing by a vertical jet in shallow water was obtained for a study of wastewater stabilization ponds.

(C) Based on laboratory experiments and numerical simulations of jet mixing mechanics of stratified water bodies a conceptual design method for hydraulic destratification systems of temperature–stratified ponds or small reservoirs was developed. The effects of jet discharge angle and jet momentum on mixing were investigated. In particular horizontal and vertical low momentum jets were compared. With respect to the design of jet destratification systems the following inferences are made:

1. It has been seen that mixing by water jets is potentially more energy efficient than other systems currently in use, e.g. pneumatic methods.

2. The experimental results indicated that vertical jets were more effective mixing devices than horizontal jets.

3. It was found that destratification by low momentum jets was more efficient than by high momentum jets.

4. More than eighty percent mixing could be achieved when twenty to forty percent of the water volume between the withdrawal and reinjection level is recycled, provided the jet densimetric Froude number is small enough so that surface and bottom interference are avoided.

5. The analytical results can be used to guide the selection and operation of hydraulic destratification devices according to their energy efficiency.

(D) The need of solving practical winter lake problems, e.g., the warm water discharge into an ice–covered lake, including effects of jet mixing on the ice cover, is the main reason for extension of the seasonal MINLAKE model to a year–round cycle. The effort was made also because of interest in the winter thermal regime of lakes in a cold climate. Submodels for the winter cover and lake sediments were developed and added into the main model. The model is validated against data from Ryan Lake and Lake Calhoun. Important differences between the thermal structures in the summer period and the ice–covered period have been analyzed. This extension enhanced the applicability and versatility of the MINLAKE model.

(E) A 2–D mathematical model was presented for simulating the flow and thermal fields of jet flow situations where buoyancy plays an important role. Systematic investigation of the horizontally discharged warm water plane jets (0 – 20° C) into a winter lake (0 – 4° C) with an ice cover have been performed for two–dimensional unsteady flows. The following conclusions are drawn from the 2–D simulations:

1. The k–ϵ turbulence model is judged to be appropriate for prediction of a buoyant jet in a stratified lake or pond.

2. Numerical simulations for the vertical jet and the horizontal offset jet in steady state agree fairly well with laboratory experimental data.

3. These numerical simulations provided new knowledge and valuable information on flow fields, thermal structures, jet trajectories, mixing processes and heat flux from water to ice. It was found that reversible buoyancy occurs in certain areas of the flow field when jet discharge temperature $T_j > 4°C$ and ambient temperature $T_a = 0 - 4°C$. The jet trajectory is very sensitive to T_j.

The 1–D model is suitable for the simulation of winter conditions mainly when the flow retains its jet–type character. It does not describe the strongly deflected flow (or reversed flow) due to reverse buoyancy and jet impingement on solid or free surfaces. These phenomena have only been seen in the unsteady, two–dimensional jet flows in winter situations.

References

Abraham, G., Jets and plumes issuing into stratified fluid, Proceedings, Inter. Symposium on Stratified Flows, Inter. Assoc. for Hyd. Res., Novosibirsk, 1972.

Adams, W. P., 1981. "Snow and ice on lake." Chapter 10 of *Handbook of Snow,* Gary, D. M. and Male, D. H. eds., Pergmon Press.

Albertson, M. L., Dai, Y. B., Jensen, R. A. and Rouse, H. (1948). "Diffusion of submerged jets." Transaction of ASCE, 115: 639–664.

Ali, K. H. M. and Salehi–Neyshaboury, A. A. (1989). "Application of the strip integral method turbulent offset jets." XXIII Congress of IAHR, Ottawa, Canada, pp. A–339 to A–346.

Almquist, C. W. (1987). Minimum power required to destratify a stratified flow. Tennessee Valley Authority, Office of National Resources and Economic Development, Division of Air and Water Resources, Engineering Laboratory, Report No. WR28–2–590–137.

Andreopoulos, J., Praturi, A. and Rodi, W. (1986). "Experiments on vertical plane buoyant jets in shallow water." *J. Fluid Mech.,* Vol. 168, pp. 305–336

Asaeda, T. and Imberger, J. (1988). "Structure of a bubble plume in stratified environments." Environmental Dynamics Report ED–88–250, Center for Water Research, University of Western Australia, Nedlands, WA 6009.

Ashton, G. D. (1986). *River and Lake Ice Engineering.* Water Resources Publications, Littleton, CO.

Ashton, G. D. (1983). "First–generation model of ice deterioration." *Proceedings of The Conference on Frontiers in Hydraulic Engineering,* ASCE, Edited by Shen, H. T., pp. 273–278.

Awar, H. O., Behavior of buoyant jet in calm fluid, *J. Hyd. Div.*, ASCE, Vol. 95, No. HY4, 1289–1303, 1969.

Bates, R. E. (1980). "Winter thermal structure, ice conditions and climate of lake champlain." U. S. Army Cold Regions Research and Engineering Lab., Hanover, N. H. Report 80–2

Bender, M. D., and Stefan, H. G. (1986), Engineering analysis of lake aerators and design of a metalimnetic aerator, SAFHL, Project Report No. 247.

Bilello, M. A. (1968). "Water temperature in a shallow lake during ice formation, growth and decay." *Water Resources Research,* Vol. 4, No. 4, pp. 749–760.

Bolsenga, S. J. (1977). "Preliminary observations of the daily variation of ice albedo." *J. Glaciology,* 18:517–521.

Brooks, N. H. (1980). "Synthesis of stratified flow phenomena for design of outfalls." *Proceedings of Second International Symposium on Stratified Flows*, Norway, June 24–27, 1980

Brooks, N. H. and Koh, R. C. Y., Selective withdrawal from density–stratified reservoirs, *J. Hyd. Div.*, ASCE, Vol. 95, No. HY4, July, 1969.

Burns, F. L. and Powling, I. J. (1981). Destratification of lakes and reservoirs to improve water quality. *Proceedings of Joint United States/Australia Seminar and Workshop,* Melbourne, Australia, Feb. 19–24, 1979, Australia Government Publishing Service.

Carslaw, H. S. and Jaeger, J. C. (1971). *Conduction of Heat in Solids.* Oxford University Press.

Dake, J. M. K., and Harleman, D. R. F. (1969). "Thermal stratification in lakes: analytical and laboratory studies." *Water Resources Research*, Vol. 5, No. 2, pp. 484–495.

Debler, W. R., Stratified flow into a line sink, *J. Eng. Mech. Div.*, ASCE, Vol. 85, No. EM3, July, 1959, pp. 51–65

Ditmars, J. D. (1970). "Mixing of density stratified impoundments with buoyant jets." Report No. KH–R–22, W. M. Kech Lab., Pasadena, California.

Dortch, M. S. (1979). Artificial destratification of reservoirs—hydraulic laboratory investigation. U.S. Army of Engineering Waterways Experiment Station, Hydraulic Laboratory, Technical Report E–79–1.

Dortch, M. S., and Holland, J. P., Methods of total lake destratification, *Proceedings of the Symposium on Surface Water Impoundments,* ASCE, H. Stefan, ed., Minneapolis, Minnesota, June 1980, pp. 913–922.

Ellis, C. and Stefan. H. G. (1989). Hydraulic design of a winter lake aeration system. University of Minnesota, St. Anthony Falls Hydraulic Laboratory Project Report.

Ellis, C., Stefan, H. G. and Gu, R. (1990). "Temperature measurements in an ice covered lake." To be printed in *Limnology and Oceanography.*

Fertuck, L. J., Spyker, J. W., and Husband, W. H. W. (1971). "Numerical estimation of ice growth as a function of air temperature, wind speed and snow cover." *Transactions of the Canadian Society for Mechanical Engineering,* EIC, Vol. 14, No. B–9.

Fischer, H. B., List, E. J., Koh, R. C. Y., Imberger, J., and Brooks, N. H. (1979), *Mixing in Inland and Coastal Waters*, Academic Press

Ford, D. E. and Stefan, H. G. (1980). "Thermal predictions using integral energy model." *Journal Hydraulics Division,* ASCE, Vol. 106, No. 1, pp. 39–55.

Fox, D. B., forced plume in a stratified fluid, *J. Geophys. Res.*, 75(33), 6818–6835, 1970.

Garton, J. E. (1976). "Evaluation of effectiveness of reservoir destratification." Oklahoma Water Resources Research Institute, Oklahoma State University. Project No. A–052.

Garton, J. E. and Punnett, R. E. (1980). "Quality improvement of release from reservoirs." in *Proceedings on Surface Water Impoundments,* ASCE, H. G. Stefan, ed., pp. 782–791.

Gebhart, B. et al. (1988). *Buoyancy Induced Flows and Transport.* Hemisphere Publishing Corporation.

Glekas, G. B. and Athanassiadis, N. (1986). "Accuracy tests of the k–ϵ model of turbulence for negative buoyant axisymmetric jets." *Proceedings of International Symposium on Buoyant Flows*, Athens–Greece.

Goossens, L. H. J., *Reservoir Destratification with Bubble Column,* Delft University Press, 1979.

Greene, G. M. (1981). "Simulation of ice–cover growth and decay in one dimension on the upper St. Lawrence River." NOAA Technical Memorandum Erl GLERL–36.

Gu, R. and Stefan, H. G. (1987). "Buoyant jets in temperature stratified ambient and application to mixing of lakes and reservoirs." University of Minnesota, St. Anthony Falls Hydraulic Laboratory Project Report No. 264.

Gu, R. and Stefan, H. G. (1991a). "Numerical simulation of stratification dynamics in the Harris wastewater stabilization ponds." University of Minnesota, St. Anthony Falls Hydraulic Laboratory Project Report No. 309b.

Gu, R. and Stefan, H. G. (1991b). "Design of hydraulic water jet destratification systems." Submitted to *Journal of Water Resources Bulletin*, AWRA

Gu, R. and Stefan, H. G., Analysis of turbulent buoyant jet in density–stratified water, *J. of Environmental Engineering,* ASCE, Vol. 114, No. 4, Aug. 1988a, pp. 878–897.

Gu, R. and Stefan, H. G., Mixing of temperature stratified lakes and reservoirs by buoyant jets, *J. of Environmental Engineering*, ASCE, Vol. 114, No. 4, Aug. 1988b, pp. 898–914.

Gu, R. and Stefan, H., 1990a. "Year–round temperature simulation of cold climate lakes." *Journal of Cold Regions Science and Technology*, Volume 18, No. 2, pp. 147–160

Gu, R.and Stefan, H., 1990b. "Jet mixing in lake or reservoir stratification simulations." *Journal of Lake and Reservoir Management*, Vol. 6, No. 2.

Gutmark, E., Wolfshtein, M. and Wygnanski, I. (1978). "The plane turbulent impinging jet." *J Fluid Mech.* 88, 737–756.

Gutmark, E. and Wygnanski, I. (1976). "The two–dimensional turbulent jet." *J Fluid Mech.* 73, 465–495.

Harleman, D. R. F. (1986). "Hydrothermal modeling of reservoirs in cold regions: status and research needs." *Proceedings of the Cold Regions Hydrology Symposium*, AWRA, pp. 39–49

Hart, W. E. (1961). "Jet discharge into a fluid with a density gradient." *Jour. of Hydr. Div.*, ASCE, Vol. 87, No. HY6.

Henderson–Seller, B. (1984). *Engineering Limnology.* Pitman Publishing Inc., Massachusetts.

Hill, H. (1967). "A note on temperature and water conditions beneath lake ice in spring." *Limnology and Oceanography*, Vol. 12, pp. 550–552.

Hino, M., Onishi, S. and Hanyu, M. (1975). "Numerical experiment on waste heat disposal into stratified flow." *Proceedings of 16th Conference, IAHR*, Vol. 5.

Hirst, E., Buoyant jets discharged into quiescent stratified ambients, *J of Geophysical Research*, 76 (1971), No. 30, Oct., pp. 7375–7384.

Holland, J. P. (1984). "Parametric investigation of localized mixing in reservoirs." US Army Corps of Engineers, Waterways Experiment Station, Environmental and Water Quality Operational Studies, Vol. E–84–7.

Holland, J. P. and Dortch, M. S. (1984). "Design guidance on hydraulic destratification." US Army Corps of Engineers, Waterways Experiment Station, Environmental and Water Quality Operational Studies, Vol. E–84–4.

Hooper, F. F., Ball, R. C., and Tanner, H. A., An experimentation in artificial circulation of a small Michigan Lake, *Transactions, Amer. Fisherias Soc.*, Vol. 82, 1952, p. 222.

Hossain, M. S. and Rodi, W. (1986). "A turbulent model for buoaynt flows and its application to vertical buoyant jets." HMT, Pergamon Press.

Irwin, W. H., Symons, J. M. and Robeck, G. G. (1966). "Impoundment destratification by mechanical pumping." *Journal of the Sanitary Engineering Division*, ASCE. Vol. 92, No. SA6, pp. 21–40.

Jain, S. C. and Pena, J. M., 1975. "Turbulent jets with reservoirs buoyancy." *Jour. of Hydr. Div.*, ASCE, Vol. 101, No. HY9, pp 1221–1223.

Jassby, A. and Powell, T. (1975). "Vertical pattern of eddy diffusion during stratification in Castle Lake, California." *Limnology and Oceanography*, Vol. 20, No. 4, pp. 530–543.

Johnson, P. L. (1980). The influence of air flow rate on line diffuser efficiency and impoundments impact." *Proc. Symp. of Surface Water Impoundments,* Minneapolis, ASCE, H. G. Stefan, ed., pp. 900–912.

Kotsovinos, N. E. and List, E. J (1977), Plane turbulent jets, Part 1, Integarl properties, *J. Fluid Mech.*, 81: 25–44.

Lee, J. H. W. (1980). "Stability and mixing of a round buoyant discharge in shallow water." *Proceedings of Second International Symposium on Stratified Flows,* Norway.

Lee, J. H. W., and Cheung, V. W. L., Inclined plane buoyant jet in stratified fluid, *J. Hyd. Div.*, ASCE, Vol. 112, No. 7, July, 1986.

Lee, J. H. W. and Jirka, G. H. (1981). "Vertical round buoyant jet in shallow water." *J. of Hydraulic Division*, ASCE, Vol. 107, No. HY12, 1651–1675.

Li, W. and Chen, C. J. (1984). "Vertical plane buoyant jets in stratified environment." Proc. ASCE, *J. of Eng. Mechanics*, Vol. 110, No. 2, pp. 224–237.

Light, P. (1941). "Analysis of high rate of snow melting." Trans., *American Geophysical Union,* Vol. 22, pp. 195–205.

List, E. J. and Imberger, J.(1973), Turbulent entrainment in buoyant jets and plumes, *J. Hyd. Div.,* ASCE, Vol. 99, No. HY9: 1461–1474.

Lorenzen, M. and A. Fast, 1977. A Guide to Aeration/circulation Techniques for lake management, US EPA, EPA–600/3–77–004.

Luck, F. and Stefan, H. G. (1990). Physical limnology of the Harris wastewater stabilization ponds: July 1989 to Oct. 1990. University of Minnesota, St. Anthony Falls Hydraulic Laboratory Project Report No. 309.

Margeta, J., Fontane, D. and Ko, S. (1990). "Multicriteria ranking wastewater disposal alternatives for coastal towns." *Water International,* IWRA, Vol. 15, No. 2.

Maruyama, T., Kamishima, N. and Mizushina, T. (1983). "An investigation of bubble plume mixing by comparison with liquid jet mixing." *Journal of Chemical Engineering of Japan*, Vol. 17, No. 2. pp. 120–126.

Michel, B. (1971). *Winter regimes of rivers and lakes.* U.S. Army Cold Regions Research and Engineering Lab., Hanover, N. H., Monograph 3–B1a.

O'Neill, K., and Ashton G. D. (1981). "Bottom heat transfer to water bodies in winter." U. S. Army Cold Regions Research and Engineering Lab., Hanover, N. H., Special Report 81–18.

Patankar, S. V. (1981). A calculation procedure for two–dimensional elliptic simulations, *Numerical Heat Transfer*, Vol. 4, pp. 409–442.

Patankar, S. V. (1980). *Numerical Heat Transfer and Fluid Flow.* Hemisphere Publishing Corporation, McGraw–Hill, New York.

Patankar, S. V. (1982). Computation of heat transfer and fluid flow—a general–purpose computer program for two–dimensional elliptic situations. University of Minnesota, Minneapolis, MN.

Patankar, S. V. and Spalding, D. B. (1972). "A calculation procedure for heat, mass and momentum transfer in three–dimensional parabolic flows." Int. *J. Heat and Mass Transfer*, Vol. 15, pp. 1787–1794.

Patterson, J. C. and Hamblin, P. F. (1988). "Thermal simulation of a lake with winter ice cover." *Limnology & Oceanography*, 33(3), 323–338.

Pivovarov, A. A. (1972). *Thermal Conditions in Freezing Lakes and Rivers.* Wiley, New York.

Price, R. E., Water Quality Enhancement Techniques used within the Corps of Engineers, Misc. Paper w–90–1, Hydr. Lab., Waterways Experiment Station, Corps of Engineers, Oct. 1990, 39pp.

Price, R. E. (1989). "Application of mechanical pumps mixers to improve water quality." Lake Line, North America Lake Management Society, 1989.

Rajaratnam, N. and Subramanya, N. (1968). "Plane turbulent reattached wall jets." ASCE, *J of Hydr. Div.*, Vol. 94, HY1, pp. 95–112.

Riley, J. M. and Stefan, H. G. (1988). "MINLAKE: a dynamic lake water quality simulation model." *Ecological Modeling,* 43: 155–182.

Riley, M., 1989. User's manual for the dynamic lake water quality simulation program "MINLAKE". External Memorandum No. 213, Univ. of Minnesota, St. Anthony Falls Hydr. Lab., Minneapolis, Minn.

Riley, M. and Stefan, H., 1987. "Dynamic lake water quality simulation model 'MINLAKE'." Report No. 263, Univ. of Minnesota, St. Anthony Falls Hydr. Lab., Minneapolis, Minn.

Riley, M., and Stefan, H. G. (1985), Formulation of the Minnesota Lake water quality model I, SAFHL, Internal Memorandum. No. 111.

Robillard, L. and Vasseur, P., 1978. "Thermal discharges in winter conditions interaction with the ice covers." *Symposium on Ice Problem, International Association for Hydraulic Research,* Lulea, Sweden.

Rodi, W. (1982). *Turbulent Buoyant Jets and Plumes.* HMT, The Science and Application of heat and Mass Transfer—Reports, Reviews and Computer Programs, Volume 6, Pergamon Press.

Rodi, W. (1984). Turbulent models and their application in hydraulics —A State of the Art Review, Book Publication of International Association for Hydraulic Research, Delft, Netherlands.

Rouse, H., Yih, C. S., and Humphreys, H. W., Gravitational convection from a boundary source, *Tellus*, 4, 1952, No. 3, Aug., pp. 201–210.

Rumer, P. R. (1983). "Simulation of lake ice dynamics." ASCE, *Proceeding of The Conference on Frontiers in Hydraulic Engineering,* Edited by Shen, H. T., pp. 236–241.

Sawyer, R. A. (1960). "The flow due to a two–dimensional jet issuing parallel to a flat plate." *J. of Fluid Mech.*, Vol. 9, pp. 543–560.
Scott, J. T. (1964). "A comparison of the heat balance of lakes in winter," Tech. Report 13, Univ. Wisconsin, Dept. of Meteorology, Madison, WI.
Shen, H. T., and Chiang, L.–A. (1984). "Simulation of growth and decay of river ice cover." *Journal Hydraulic Engineering*, ASCE, 110(7), pp. 958–971.
Shen, H. T., and Yapa, P. D. (1983). "Simulation of the St. Lawrence river ice cover thickness and breakup." Report No. 83–1. Department of Civil and Environment Engineering, Clarkson College, Potsdam, NY, p. 57.
Shirazi, M. A., and Davis, L. R., Workbook of thermal plume prediction, Volume ——submerged discharge, EPA–R2–72–005a, Aug., 1972.
Singh, R. A., A study of submerged and surface horizontal buoyant jets, PhD. dissertation, 1976.
Sini, J. F., and Dekeyser, I., Numerical prediction of 2–D turbulent forced plumes in stratified fluid, *Proceedings, Third International Symposium on Stratified Flows*, Pasadena, Feb., 1987.
Smith, D. R., et al. (1987), "Improved Description of Selective Withdrawal Through Point Sinks", Technical Report E–87–2, US Army Engineer Waterways Experiment Station, Vicksburg, Miss.
Sotil, C. A., Computer program for slot buoyant jets into stratified ambient environments, W. M. Keck Lab., Technical memorandum 71–2, June, 1971.
Spigel, R. H., Farrant, B., Selective withdrawal through a point sink and pycnocline formation in a linearly stratified flow, *J. Hyd. Div.*, ASCE, Vol. 22, 1984, No. 1.
Stefan, H. G. and Ford, D. E. (1975). "Temperature dynamics in dimictic lakes." *Journal Hydraulics Division,* ASCE, Vol. 101, No. 1, pp. 97–113.
Stefan, H. and Gu, R., 1990. "Jet–mixing of temperature stratified basins." To be printed in *Journal of Environmental Engineering,* ASCE.
Steichen, J. M., 1974. The effect of lake destratification on water quality parameters. Ph.D. thesis, Oklahoma State University, Stillwater, 103 pp.
Stoy, R. L. and Stenhouse, M. H. (1975). "Vortex containment of a submerged jet discharge." Project Report of Depart. of Mechanical Engineering, University of Connecticut, Storrs, Connecticut.
Tatom, F. B., Errors from using conservation of buoyancy concept in plume computations, *J. Hyd. Div.*, ASCE, Vol. 111, No. 6, June, 1985, 1005–1009.
Wake, A. and Rumer, R. R., Jr. (1979). "Modeling ice regime of Lake Erie." *Journal of Hydraulics Division,* ASCE, Vol. 105, No. HY7, pp. 827–844.
Wei, C. Y. and Hamblin, P. F. (1986). "Reservoir water quality simulation in cold regions." *Proceedings of the Cold Regions Hydrology Symposium,* AWRA.
Wirth, T. L. (1970). "Mixing and aeration systems in Wisconsin lakes." Pages 31–46 in E. Schneberger, ed. A symposium on the management of midwestern winterkill lakes. North Cent. Div. Am. Fish. Soc. Sp. Publ.
Wong, D. R. (1987). Buoyant jet entrainment in stratified fluids. PhD dissertation, University of Michigan.

Wong, D. R. and Wright, S. J., Submerged turbulent jets in stagnant linearly stratified fluids, IAHR, *Journal of Hydraulic Research,* Vol. 26, No. 2, 1988, pp. 199–223.

Wright, S. J., and Wallace, R. B. (1979), Two–dimensional jets in stratified fluid, *J. Hyd. Div.*, ASCE, Vol. 105, HY11: 1393–1406.

Yannopoulos, P. C., Momentum and energy equations in round turbulent buoyant jets, *Proceedings, International Symposium on Buoyant Flows,* Athens–Greece, 1–5, Sept., 1986.

Yih, S.–S., On the flow of a stratified fluid, *Proceedings Third National Congress of Applied Mechanics*, 1958, pp. 857–861

Zic, K. and Stefan, H., 1988. "Lake aerator effect on temperature stratification analyzed by "MINLAKE model" Lake and Reservoir Management 4(2), 85–90, North American Lake Management Society.

Zic, K. and H. Stefan (1990). "Analysis and simulation of mixing of stratified lakes or reservoirs by air bubble plumes". University of Minnesota, St. Anthony Falls Hydraulic Laboratory Project Report No. 305.

Appendix A Statistical parameters of error analysis

Several statistics were considered in the simulations for calibration and/or verification purposes. All parameters measure agreement or disagreement between (laboratory or field) data and simulated model results. A constrained regression was chosen as providing the most useful information. The goodness of fit in the calibration and/or verification was primarily measured by the regression. The regression is constrained through the origin to provide a direction regression of data to model results.

The slope of the regression, which indicates if the model is overpredicting (slope < 1.0) or underpredicting the data, is defined as

$$s_r = \frac{\sum_{i=1}^{n}(y_i x_i)}{\sum_{i=1}^{n}(x_i)} \tag{A.1}$$

where y_i, x_i and n are data, prediction and number of pairs of data, i.e. data points (y_i, x_i), respectively. The objective value of this parameter for calibration is 1.0.

The regression coefficient is the ratio of variance in the data explained by the regression to the total variance in the field data. It is expressed as

$$r^2 = 1 - \frac{s_e^2}{\sigma^2} \tag{A.2}$$

where s_e and σ are standard error of estimate and standard deviation of the mean of data, respectively, given as

$$s_e^2 = \frac{\sum_{i=1}^{n}(y_i - x_i)^2}{n} \tag{A.3}$$

and

$$\sigma^2 = \frac{\sum_{i=1}^{n}(y_i - \bar{y})^2}{n} \tag{A.4}$$

where $\bar{y}$ is the mean of data

$$\bar{y} = \frac{\sum_{i=1}^{n} y_i}{n} \tag{A.5}$$

The calibration objective is that r^2 approaches 1.0 and s_e goes to 0.0.